

# Evaluating Uncertainty in Hygrothermal Modelling of Heritage Masonry Buildings

by

Michael Gutland

A thesis submitted to the Faculty of Graduate and Postdoctoral Affairs  
in partial fulfillment of the requirements for the degree of

Doctor of Philosophy

in

Civil Engineering

Carleton University

Ottawa, Ontario

© 2022, Michael Gutland

## **Abstract**

Hygrothermal models are important tools for assessing durability risks in building envelopes, such as biological growth (mould and wood rot fungi), corrosion and freeze-thaw action in masonry. Hygrothermal modelling of mass masonry wall assemblies are known to have numerous weaknesses and gaps in our understanding. First, there are significant uncertainties relating to model inputs including material properties and boundary conditions. Second, it is difficult to calibrate model results against data measured in the field. Third, two and three-dimensional interactions between adjacent materials in masonry assemblies are poorly understood and are rarely modelled in practice. And fourth, geometric irregularities, imperfections and the effects of decay are rarely considered by modellers. Combined, these uncertainties can lead to reduced confidence in the model's conclusion and alter our opinions on the durability risks and whether retrofits such as interior insulation are appropriate or not.

This doctoral thesis examines how uncertainty factors into hygrothermal modelling of heritage masonry, and how it can be reduced, and or, acknowledged in practice. This is demonstrated using a combination of simulation studies and on-site monitoring work. Three peer-reviewed papers which demonstrate examples of uncertainty in hygrothermal modelling are presented.

The first paper presents a methodology for integrating calibrated hygrothermal and energy models of the Southwest Tower of the East Block for the purpose of assessing durability. This project consisted of in-situ monitoring of the masonry and

interior climate of the Southwest Tower for over a year. The calibrated energy model was used as basis for estimating the net benefit of interior climate retrofits on the durability of the masonry. The calibrated hygrothermal model was not as successful, but the lessons learned were transferable to the third paper.

The second paper examines the imperfect nature of the mortar-unit interface in masonry and how this affects moisture transfer into and out of the wall. Simulations showed that modelling this interface explicitly as a fracture will increase water absorption during wetting periods, but also help slightly with releasing moisture under drying conditions.

The third paper examines the uncertainty in geometry and construction of the rubble core walls of the East Block. The wall's stack pattern is highly irregular and the core of the walls are known to have significant levels of voids which can act like insulating layers, or act as mini-rainscreens slowing moisture transfer into the wall. A Python script was developed to stochastically-generate sections of walls with and without voids. A significant variation in state variables, and heat and moisture fluxes was found between stochastically generated geometries in the mortar joints and in the rubble core. This variation increased with the number of voids.

Overall, this research contributes to efforts make hygrothermal modelling of masonry more accurate and more intuitive for practitioners to use. Establishing sound baseline models and uncertainty windows is key to confidently estimating the deterioration risk. Underestimating the deterioration risk can lead to accelerated and irrecoverable deterioration. Or conversely, overestimating the durability risk can lead

to being overly conservative if considering thermal retrofits, or overly reactionary and considering unnecessary interventions being taken.

## **Preface**

This integrated article thesis consists of three journal papers and one conference paper, that have been published. The articles are listed below in the same order as they appear in the thesis:

**Article 1 (Chapter 3.):** Gutland, M., Bucking, S., & Santana Quintero, M. (2019). Assessing Durability of Historic Masonry Walls with Calibrated Energy Models and Hygrothermal Modeling. *International Journal of Architectural Heritage*, 1–17.  
<https://doi.org/10.1080/15583058.2019.1618976>

**Article 2 (Chapter 4.):** Gutland, M., Santana Quintero, M., & Bucking, S. (2019, September). Calibration of an historic masonry building using measured temperature and heat flux data. *Proceedings of Building Simulation 2019: 16th Conference of IBPSA. Building Simulation 2019, Rome, Italy.*

**Article 3 (Chapter 5.):** Gutland, M., Bucking, S., & Santana Quintero, M. (2021). A methodology for hygrothermal modelling of imperfect masonry interfaces. *Journal of Building Physics*, 44(6), 485–509. <https://doi.org/10.1177/1744259121989388>

**Article 4 (Chapter 6.)** Gutland, M., Bucking, S., & Santana Quintero, M. (2022). Hygrothermal modelling of historic rubble masonry walls: Accounting for geometric and compositional variability. *Journal of Building Engineering*, 48, 103929.  
<https://doi.org/10.1016/j.jobbe.2021.103929>

The journal and conference papers have not been edited from the final versions unless noted in the preface of each chapter, and the addition of a preface section to provide additional context to the work that was done.

In the co-authored articles, Michael Gutland was the principal contributor to the research methodology, concept, design, experimental set-up, data acquisition and interpretation, and preparing and writing the material presented in the articles under the supervision of Scott Bucking and Mario Santana Quintero.

## **Acknowledgements**

I would like to thank many people for their support in my graduate studies. I would first like to thank my two supervisors Mario Santana Quintero and Scott Bucking for their support and guidance throughout my studies.

At Carleton, I would like to thank my colleagues in the NSERC CREATE Heritage Engineering Program, the Building Performance Research Group and the many excellent professors involved with the Architectural Conservation and Sustainability program.

I would also like to thank the many people within the Ottawa heritage community who provided mentorship and opportunity. From Public Works and Heritage Conservation Services I would like to thank Myles McDevitt, Doug Stephenson, Ann De Mey, Jack Vandenberg and Rob Melanson. From my time at Robertson Martin Architects, I would like to thank Robert Martin, Danica Robertson and James Maddigan. I would also like to thank Michael Petrescu-Comnene and Damian De Krom (Department of Foreign Affairs), Bruce Fournier (WSP), and Sarah Gray and Randy Van Straaten (RDH) for helping at various points of my engineering career.

I would like to also acknowledge the support provided by NSERC through their CREATE and Engage grants and the Carleton University Ontario Graduate Scholarship.

# Table of Contents

Abstract.....	ii
Preface.....	v
Acknowledgements.....	vii
List of Tables.....	xvi
List of Figures.....	xvii
1. Introduction.....	1
1.1 Motivations.....	3
1.1.1 Limit States Approach.....	6
1.1.2 Validation.....	11
1.2 Research Objectives and Questions.....	13
2. Background.....	15
2.1 Heritage Conservation Principles.....	15
2.1.1 Preservation, Restoration and Rehabilitation.....	17
2.2 Heritage Masonry.....	20
2.2.1 Heritage Masonry in Standards.....	22
2.2.2 Energy Retrofits of Masonry Walls.....	25

2.3 Hygrothermal Modelling.....	28
2.3.1 Theory.....	30
2.3.2 Tools.....	32
2.3.2.1 Glaser Method.....	34
2.3.2.2 Numerical Methods.....	35
2.3.2.3 Coupled Hygrothermal – Building Energy Models.....	36
2.3.2.4 Software Validation.....	38
2.3.3 Material Properties.....	39
2.3.3.1 Porosity.....	39
2.3.3.2 Moisture Retention Curve.....	41
2.3.3.3 Liquid Conductivity.....	46
2.3.3.4 Vapour Permeability.....	51
2.3.3.5 Thermal Conductivity and Heat Capacity.....	53
2.3.4 Boundary Conditions.....	55
2.3.4.1 Exterior Climate.....	55
2.3.4.2 Wind-Driven Rain.....	58
2.3.4.3 Exterior Transfer Coefficients.....	62
2.3.4.4 Interior Climate.....	63

2.3.4.5 Interior Transfer Coefficients.....	64
2.4 Masonry Pathologies.....	64
2.4.1 Freeze-Thaw.....	65
2.4.2 Biological Growth.....	69
2.4.3 Corrosion.....	71
2.4.4 Efflorescence.....	73
2.4.5 Other Pathologies.....	75
2.5 Hygrothermal Monitoring.....	76
2.5.1 Monitoring Locations.....	77
2.5.2 Sensors.....	80
2.5.2.1 Relative Humidity.....	80
2.5.2.2 Moisture Content.....	81
2.6 Uncertainty in Hygrothermal Modelling.....	88
2.6.1 Material Properties.....	89
2.6.2 Boundary Conditions.....	92
2.6.2.1 Precipitation.....	93
2.6.2.2 Temperature, RH, Wind velocity.....	96
2.6.2.3 Radiation.....	100

2.6.3 Geometry, Construction and Imperfections.....	101
2.6.4 Model Calibration and Validation.....	105
3. Hygrothermal monitoring and model calibration of an historic masonry tower...	108
3.1 Preface.....	108
3.1.1 Calibrated Hygrothermal Modelling.....	109
3.1.2 Experimental set-up.....	111
3.1.3 Hygrothermal monitoring results.....	112
3.1.4 Calibration.....	113
3.2 Abstract.....	117
3.3 Introduction.....	118
3.4 Case Study Building – Southwest Tower.....	119
3.5 Literature Review.....	122
3.6 Methodology.....	126
3.6.1 Sensor Installation and Data Collection.....	126
3.6.2 Calibrated Energy Model.....	129
3.6.2.1 EnergyPlus Model.....	130
3.6.2.2 Sensitivity Analysis.....	133
3.6.2.3 Sensitivity Analysis Results.....	137

3.6.2.4 Model Calibration.....	138
3.6.2.5 Calibration Results.....	139
3.6.2.6 Second Calibration Model.....	141
3.6.3 Hygrothermal Analysis of Possible Retrofits.....	145
3.6.3.1 Modelling retrofits in EnergyPlus.....	147
3.6.3.2 Hygrothermal Models.....	148
3.6.3.3 Discussion.....	155
3.7 Conclusion.....	157
4. Calibrated Envelope Modelling.....	160
4.1 Wall Calibration.....	160
4.1.1 Calibration against measured temperatures.....	163
4.1.2 Calibration against measured heat flux.....	166
4.1.3 Conclusions.....	169
5. Masonry Interface Modelling.....	171
5.1 Abstract.....	171
5.2 Introduction.....	173
5.3 Literature Review.....	176
5.3.1 Mortar – Unit Interface Resistance.....	177

5.3.2 Fracture Modelling.....	180
5.3.3 Hygrothermal Simulation Tools.....	185
5.3.4 Synthesis.....	185
5.4 Methodology.....	186
5.4.1 Delphin Model.....	187
5.4.2 Material Properties.....	190
5.4.2.1 Bulk Materials.....	190
5.4.2.2 Fractures.....	193
5.5 Results and Discussion.....	195
5.5.1 Model 1 – Absorption: Fracture without interface resistance.....	196
5.5.2 Model 2 – Absorption: Interface resistance only.....	200
5.5.3 Model 3 – Absorption: Fracture with interface resistance.....	201
5.5.4 Model 4 – Drying: Fracture with interface resistance.....	204
5.5.5 Model 5 – Cyclical: Fracture with interface resistance.....	207
5.5.6 Additional Notes.....	210
5.6 Conclusion.....	212
6. Spatially-stochastic geometry in masonry-walls.....	214
6.1 Abstract.....	214

6.2 Introduction.....	215
6.3 Literature Review.....	220
6.3.1 Heat Transfer and U-values.....	220
6.3.2 Hygrothermal simulations including moisture transfer.....	222
6.3.3 Spatially stochastic masonry models.....	223
6.4 Methodology.....	225
6.4.1 Case Study.....	225
6.4.2 Building Geometry.....	227
6.4.3 3.3. Model Geometry.....	229
6.4.4 Simplified Models.....	233
6.4.5 Material Properties.....	235
6.4.5.1 Sandstone and Mortar.....	235
6.4.5.2 Air Properties and Longwave Radiation.....	237
6.4.5.3 Blended Materials.....	239
6.4.6 Boundary Conditions.....	240
6.5 Results.....	242
6.5.1 Steady State Heat Transfer.....	242
6.5.2 Drying.....	247

6.5.3 Wetting.....	251
6.5.4 Actual Weather Years.....	254
6.6 Discussion.....	260
6.7 Conclusion.....	263
7. Conclusion.....	265
7.1 Contributions.....	268
7.2 Future Work.....	270
8. References.....	273

## List of Tables

Table 2-1: Classification of HAM models according to hygrothermal material characterization. (Grunewald et al., 2003).....	33
Table 3-1: Summary of calibration model input parameters and final results.....	135
Table 3-2: Summary of calibration results.....	140
Table 3-3: Material properties for Delphin simulation.....	149
Table 4-1: Parameters for wall calibration.....	163
Table 4-2: Wall calibration results.....	166
Table 5-1: Bulk material properties used in Delphin simulations.....	191
Table 6-1: Dimensions [mm] used to create geometry in hygrothermal models.....	228
Table 6-2: Hygrothermal properties of sandstone and mortar used in Delphin simulations.....	236
Table 6-3: Blended material properties used in Delphin simulations.....	240

## List of Figures

Figure 1-1: Gaussian double curve demonstrating a general limit-states application. .....	8
Figure 2-1: <i>Moisture retention curves</i> for various different sandstones (both dashed and solid lines) in the Delphin material database.....	45
Figure 2-2: Liquid conductivity curves for various different sandstones (both dashed and solid lines) in the Delphin material database.....	49
Figure 2-3: Moisture storage regimes of a porous material (Carmeliet & Roels, 2002).....	53
Figure 2-4: Approximate rain admittance factors for simple buildings (Straube & Burnett, 2000).....	61
Figure 2-5: Annual precipitation for Ottawa. (Weather Station 49568 is from the Ottawa International Airport).....	95
Figure 2-6: Monthly temperature data from five Ottawa weather sources.....	97
Figure 2-7: Monthly relative humidity data from five Ottawa weather sources.....	98
Figure 2-8: Monthly wind speed data from five Ottawa weather sources.....	99
Figure 3-1: Hygrothermal calibration results of the sixth floor wall.....	114
Figure 3-2: Typical Cross-section of an East Block wall (modified from Ashurst (1977)).....	121

Figure 3-3: Measured dry-bulb temperatures inside the Southwest Tower from September 2017 to August 2018.....	127
Figure 3-4: Measured dry-bulb temperatures inside the Southwest Tower from January 2012 to April 2013 as measured by National Research Council (Glazer, 2013).....	128
Figure 3-5: Measured relative humidity inside the Southwest Tower from September 2017 to August 2018.....	128
Figure 3-6: Wireframe geometry of EnergyPlus model.....	130
Figure 3-7: Sensitivity analysis results. Black Bars are the overall RMSE for all 4 zones and gray bars are the maximum RMSE recorded for an individual zone.....	137
Figure 3-8: Calibrated v. Measured data for the first calibrated model.....	141
Figure 3-9: Calibrated versus Measured data for the second calibration model....	143
Figure 3-10: Freeze-thaw performance for fourth floor wall - South façade.....	151
Figure 3-11: Freeze-thaw performance for sixth floor wall - South façade.....	151
Figure 3-12: Moisture Content versus Time for the sixth floor wall under low moisture conditions.....	153
Figure 3-13: moisture content versus time for the sixth floor wall under high moisture conditions.....	154
Figure 4-1: Delphin 6.0 model used for calibration of wall thermal properties. Red = sandstone, grey = mortar.....	162

Figure 4-2: Calibrated v. Measured data for the wall temperature calibration along the interior surface, 300mm and 600mm depths.....	164
Figure 4-3: Measured v. Calibrated surface heat flux for the fourth-floor South facade.....	167
Figure 5-1: Sandstone masonry wall with open joint (Orange) and hairline crack (dark blue) between stone and mortar.....	175
Figure 5-2: Illustration of various contact conditions and how it affects moisture transfer in the interface.....	180
Figure 5-3: Geometries used in the Delphin simulations.....	188
Figure 5-4: Material property curves used in simulation.....	191
Figure 5-5: Moisture content comparison for Model 1 (250 Pa).....	197
Figure 5-6: Moisture content at Centre Brick – 50mm for three different boundary conditions. The bottom graphs illustrate the moisture contents from t=0 (light gray) to t=24 h (black). Note that there are different y-axis scales.....	198
Figure 5-7: Moisture content comparison for Model 2 (250 Pa).....	201
Figure 5-8: Moisture content comparison for Model 3 (250 Pa).....	203
Figure 5-9: Moisture content at Centre Brick – 50mm for three different boundary conditions. The bottom graphs illustrate the moisture contents from t=0 (light gray) to t=24 h (Black). Note that there are different y-axis scales.....	204
Figure 5-10: Moisture Content comparison for Model 4.....	205

Figure 5-11: Annual MC for the baseline model and select apertures.....	207
Figure 5-12: Moisture content for the baseline model and select apertures during the summer months.....	208
Figure 6-1: Example drawing of rubble core wall and voids (blue).....	218
Figure 6-2: A sample of stochastically generated grids with V=0% on the left and V=15% on the right.....	232
Figure 6-3: Simplified geometric representations of rubble core walls.....	234
Figure 6-4: Hygroscopic material properties of materials used in the simulations including some blended material properties.....	237
Figure 6-5: Results of the steady-state heat transfer simulations. The reported values are taken at the exterior surface. The violin plots are created from the mean values from each simulation with 95% confidence intervals. [Note the heat flux is not equivalent to the U-value because surface resistance was not considered].....	243
Figure 6-6: Scatter plot of grid variables and their effect on heat transfer. Red = zero voids, Green = 5% Voids.....	244
Figure 6-7: Violin plot of standard deviation in temperature at the centre line of the wall. The y-axis scale is normalized to a 1.0 °C temperature gradient.....	246
Figure 6-8: Results of the drying moisture transfer simulations in terms of the amount of moisture lost per wall area.....	248

Figure 6-9: Correlation between mortar ratio and moisture lost during drying simulation.....	250
Figure 6-10: Results of the wetting moisture transfer simulations in terms of the amount of moisture gained per wall area.....	252
Figure 6-11: Results of the actual weather year simulations in terms of the amount of moisture gained per wall area.....	255
Figure 6-12: RH and Moisture Flux behind the outer wythe of stone. Positive moisture flux are inward and negative fluxes are outward.....	257
Figure 6-13: RHT Index for the actual weather year simulations. Results are taken at the middle of the rubble core wall.....	258
Figure 6-14: Critical Freeze Thaw Cycles as a function of depth and their maximum and minimum extents. ( $T = 0^{\circ}\text{C}$ , $S_{\text{Crit}} = 50\%$ ).....	260

## 1. Introduction

Hygrothermal models are important tools for assessing building envelopes in terms of heat and moisture transfer and pathological risks, such as biological growth (mould and wood rot fungi), corrosion and freeze-thaw action. These pathological conditions can compromise structural integrity, affect the health and wellness of occupants and lead to irreversible loss of architectural material and features; some of which may have historical significance.

Hygrothermal modelling is known to have numerous weaknesses and gaps in our understanding. First, there are significant uncertainties relating to model inputs including material properties (porosity, absorption coefficients, moisture retention curve, etc.), boundary conditions (wind-driven rain, temperature, heat and vapour convection coefficients etc.), construction (eg. leaks, deteriorated mortar joints, irregular geometry etc.) and two or three-dimensional interactions between adjacent materials.

Second, it is difficult to calibrate predicted model performance to that which is measured in the field and not under controlled laboratory conditions. This is partly caused by the previously mentioned uncertainties with material properties, boundary conditions and construction; but also with obtaining long-term in-situ measurements with which to compare the models against.

Third, two and three-dimensional interactions are poorly understood and are difficult to model in practice. This becomes important when modelling assemblies with composite layers that have materials with contrasting material properties. An example of this would be historic masonry walls where there may be preferential moisture transfer paths through the mortar compared to the masonry unit or vice versa. This is important because most practitioners only consider simplified one-dimensional models, whereas two-dimensional modelling would be more prudent.

A fourth issue is that imperfections, geometric irregularities and material decay are rarely, if ever, considered in the modelling methodology. This becomes increasingly important with the age of the building, decay sets in and maintenance activities struggle to keep up.

The presence of these four gaps can lead to the following generalizations made about hygrothermal modelling:

- The uncertainty in material properties and boundary conditions reduces our confidence in the model's ability to accurately capture or predict the true extent of moisture issues in an assembly.
- The wide range of uncertainty in material properties and boundary conditions compounds and that implies that the results have a wide range of uncertainty.

- The lack and difficulty of calibration can imply that there is limited validity to the models
- Hygrothermal models are oversimplifications of reality

Combined these generalizations, can lead to limited confidence in the model's conclusions from architects and decision-makers. This can be amplified when the model is supporting arguments for major alterations to an existing building, such as adding interior insulation to a heritage masonry wall. In instances where the existing walls are already stressed by high moisture loads, or on high-profile/heritage-designated buildings, the requirement for a solid baseline model becomes increasingly imperative.

### **1.1 Motivations**

The motivation for this doctoral thesis originated in my work with heritage masonry buildings in Ottawa. While examining the masonry envelopes, I began to build an understanding of the many nuances in heritage masonry construction and how the cumulative effects of decay, damage and defect have impacted the physical state of the envelope over time. When creating the hygrothermal models for these assemblies, I discovered that it was difficult to incorporate these nuances into the models using conventional hygrothermal models. There was

also a lack of guidance from standards and easily translatable examples from the academic literature.

It became apparent that there were simplifications and assumptions made in practice when performing hygrothermal models which may not be ideal or appropriate. Simplifications may include modelling in one-dimension instead of two, simplified boundary conditions, neglecting interface resistances, decay and other imperfections amongst others. Assumptions may include that material properties and boundary conditions are deterministic in nature is appropriate even though a stochastic approach is more appropriate, using library material properties in lieu of material testing, and judging the degree of exposure of the envelope to wind-driven rain. These simplifications and assumptions may be forced by a lack of data, knowledge, or computational time and set-up.

Combined, these often, necessary simplifications and assumptions imply uncertainty onto the model results. This uncertainty is worthy of further exploration, especially within the context of heritage buildings where construction materials, assemblies and techniques are less standardized and studied.

The importance of this uncertainty should be understood by practitioners and decision-makers. There is a lack of guidance available for practitioners about if, and how they should be considering this in their modelling procedure, and is usually not standard procedure for hygrothermal modelling and reporting.

The contemporary North American standard for hygrothermal analysis is *ASHRAE 160 – Criteria for Moisture-Control Design Analysis in Buildings* (ASHRAE, 2016). The foreword of ASHRAE 160 reflects this concern over uncertainty and the need for a more stochastic approach:

*“Ideally, a design analysis involves the determination of the probability of failure and treats all design parameters and loads as stochastic variables. However sufficient data are often not available to make a full statistical treatment practical. Instead, where only limited data exist, a moisture design protocol must be based on a combination of statistical data and professional judgment. Another judgment involves the choice of an acceptable probability of the occurrence of damage. Although it is common to impose very stringent criteria for structural design because of safety concerns, moisture damage usually occurs over a long period of time and usually has less catastrophic, although sometimes costly, consequences. An international consensus has emerged that the analysis should be predicated on loads that will not be exceeded 90% of the time. This standard adopts this approach.*

It is felt that some of this uncertainty can be addressed by taking a more stochastic approach over a deterministic approach in expressing modelling results, and by adopting more of a limit-states approach. Adopting these approaches can benefit the practice of hygrothermal modelling by illustrating the

relativity of optimal and worst-case scenarios, improving baseline understanding of the envelope's present condition, and minimizing the chances of detrimental retrofits and repair actions being taken. This could be beneficial when working with heritage professionals who may be inherently conservative in their attitudes to retrofits and risk.

### **1.1.1 Limit States Approach**

A concept which is formally lacking in hygrothermal analysis (and arguably building science in general) is a probabilistic approach to load and resistance factors, similar to limits-states design philosophy in structural design. This concept has only been minimally explored in my opinion (De Rose et al., 2014).

Limit-states design was introduced to National Building Code of Canada in 1975 (*Structural Commentaries (User's Guide – NBC 2015: Part 4 of Division B)*, 2017) and is utilized in many other international building codes and standards. It is an alternative approach to allowable stress design. Limit states design utilizes multiple factors of safety compared to only one in allowable stress design and this allows for a more refined, consistent and accurate design calculation (Galambos, 1981). Limit-states design begins with the underlying assumption that the design resistance and applied loads are not deterministic in nature and have a natural variance. For example, the actual load resistance of reinforced concrete

may be less than expected because of poor workmanship, imperfect concrete mixing procedure, or decay from exposure to the elements. A limit state refers to a predetermined and measurable point or threshold that should be avoided within a reasonable probability.

The general form of a limit-states design formula is as follows in Equation 1-1 and demonstrated visually in Figure 1-1.

$$\phi R > \alpha D \quad (1-1)$$

- $\phi$  = Material Resistance Factor (< 1.0)
- R = Nominal Material Resistance
- $\alpha$  = Load Combination Factor (> 1.0)
- D = Nominal Design Loads

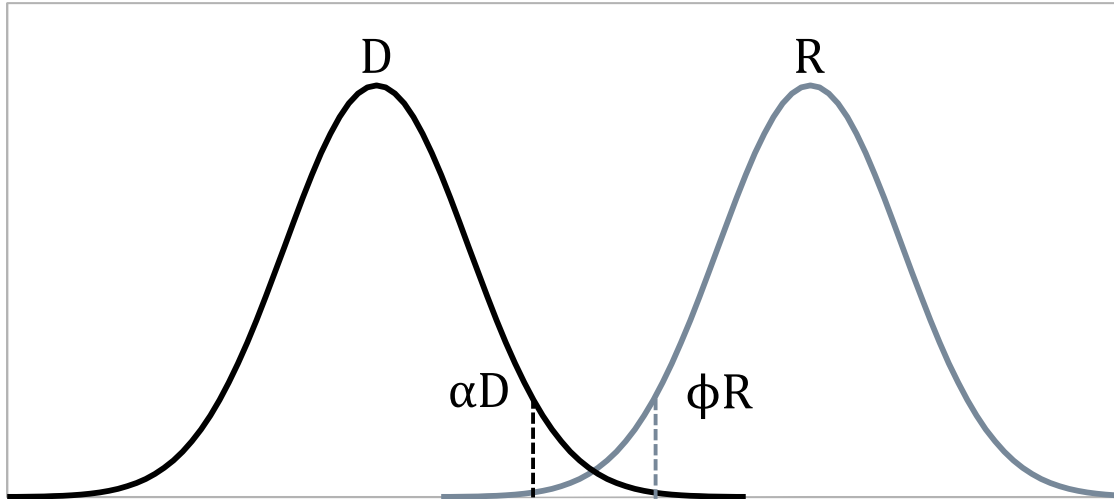


**Figure 1-1: Gaussian double curve demonstrating a general limit-states application.**

Using the structural design analogy as an example, Equation 1-1 tells us that the structural capacity (shear, compression, tension or bending) of the assembly must be greater than the applied loads (gravity, live, wind, snow etc.). The left-hand side of the equation is the product of the nominal material resistance ( $R$ ) and the material resistance factor ( $\phi$ ). The nominal material resistance is a combination of the material's mechanical properties (e.g. compressive strength) and geometry (e.g. cross-sectional area, section-modulus). The material resistance factor accounts for cumulative construction and manufacturing defects, and decay over time, which will cause a reduction in the expected capacity of the structure. These have calculated through statistical processes for many common structural systems such as wood, concrete, masonry etc. The Material Resistance Factor is usually less than 1.0.

The right-hand side of the equation is the product of the nominal design loads ( $D$ ) and the load combination factor ( $\alpha$ ). The nominal design loads are determined based on occupancy loads (live, dead, self-weight) or environmental loads (wind, snow, earthquake etc.) and are provided via codes or standards. The load combination factor is a multiplier which accounts for rare, unexpected or unpredictable loads being applied. In most instances this value is greater than 1.0, with the exception of when combination loads are used.

The limit states criteria for structural design are ultimate limit state (ULS) and serviceability limit state (SLS). ULS refers to point of structural failures such as buckling, inelastic behaviour, cracking etc. This limit state concerns safety. SLS refers to the point of excessive deflection or vibration which may malfunction to the building and discomfort to the occupants.

An analogous limit-states design approach can be applied to hygrothermal modelling. The limit states can be defined as one of the many published damage functions for many materials (De Rose et al., 2014). Examples being the Mould Index for biological growth, RHT Index for corrosion or critical degree of saturation for freeze-thaw (See Section 2.4).

Nominal material resistances for materials and design loads for climate are generally available in literature. In the hygrothermal context, the material resistance (or as often used their inverses – conductivity and permeability) are

with respect to heat, air, vapour and liquid transport of the materials, or perhaps more appropriately, a material layer or whole assembly. The design loads are the interior and exterior boundary conditions; temperature, RH, wind-driven rain, solar radiation, and heat and vapour convection coefficients.

What are less appreciated and understood in the hygrothermal context are the analogous material resistance factor ( $\varphi$ ) and load combination factor ( $\alpha$ ). The material resistance factor is intended to account for many things, included natural variance in the material properties and construction, manufacturing defects, and decay over time. There has been acknowledgement of the natural variance of materials in modelling procedure through the use of stochastic process and modelling of worst-case scenarios (See Section 2.6.1). What has not been adequately explored are the effects of construction and manufacturing defects, decay and two-dimensional interactions. Some examples of this include:

- A masonry wall with decayed mortar joints or hairline cracks would theoretically allow more liquid water penetration.
- A contemporary wall has its air/vapour barrier penetrated or was not properly installed in a continuous fashion.
- Tension cracks form in concrete allowing more liquid water penetration.
- The decay in the thermal resistance of foam insulation products over time.

- The interface between mortar and masonry unit are imperfect and impeded liquid water penetration.
- The geometry and physical composition of historic walls can vary from wall section to wall section. This isn't always obvious through visual inspection.

Load combination factors have been used in practice with regard to boundary conditions. There is variability in climate year-on-year and variability in exposure to wind-driven rain that vary from facade-to-facade or level-to-level on a building. Research has been published on procedures for determining climatic loads and these are summarized in Section 2.3.4 and 2.6.2.

### **1.1.2 Validation**

Another issue with hygrothermal modelling which became apparent while analyzing heritage masonry walls was model validation. Lack of validation is a common criticism that I have heard about hygrothermal models by heritage professionals in the past, and their point is justifiable.

Validation of models to in-situ measurements of masonry can be difficult because of challenges regarding sensors (See Section 2.5.2) and the aforementioned uncertainties regarding material properties, boundary conditions, and decay. Without proper model validation, we have less confidence in the model's

prediction. This is important when trying to establish a solid baseline model when assessing retrofits or reporting the current moisture risk of the building.

Extensive monitoring of moisture in masonry envelopes is currently rare in practice, but is becoming increasingly common. Without data that monitoring can provide, professionals are often left to their own personal judgment to determine the severity (good or bad) or root causes of the moisture problems within the envelope. Prior field experience (not published or presented in this thesis) has shown that conditions can be non-uniform and seemingly random when sampling around the building. On the same orientation, one facade can be critically wet, while a nearby monitoring point the wall appears to be healthy and at a low moisture-risk. This attributed to variations in the level of decay and the exposure to wind-driven rain, run-off and leaks. This shows how a wide range of load factors need to be assessed to obtain a more complete picture of the building. To obtain a complete cross-sectional picture of the building's condition, a thorough sampling may be required.

The absence of monitoring data means you are unable to validate the models. Instead you would need to rely on engineering judgment, past experience or visual/anecdotal evidence to determine how accurate the model is. This is obviously not ideal. Validation can be achieved through a model calibration procedure. There are not any formal standards or guidelines for calibrating

hygrothermal models to measured data, similar to that of ASHRAE Guideline 14 for energy models (ASHRAE, 2014). Data to calibrate against is more readily available for energy modelling (monthly energy bills, sub-metering). This creates a gap in our understanding which may impair our ability to surgically address building pathologies and propose appropriate retrofit or repair measures that are neither overconservative nor reactionary.

## **1.2 Research Objectives and Questions**

The focus of this thesis is on hygrothermal modelling of historic masonry walls, with greater emphasis on rubble core masonry walls and in cold climates. The research was motivated by knowledge gaps and inadequacies in the contemporary modelling procedure which I found while working on heritage buildings in Ottawa and Parliament Hill area. From this background I established three research objectives:

1. Understanding the correlation between hygrothermal models and in-situ field measurements inside the masonry.
2. Understand how the inclusion of two-dimensional interactions and imperfections in hygrothermal models of masonry may effect results compared to when these details are omitted

3. Understand how the inherent uncertainty in hygrothermal material properties, boundary conditions and quality of construction effects hygrothermal outcomes and how this can be incorporated into practice.

Each of these three research objectives contributes to the goal of improving the process of hygrothermal modelling by examining sources of uncertainty in greater detail. There is a strong focus on forming an understanding the physical behaviour and how established simplifying assumptions may or may not be appropriate. Each of the three research objectives are addressed in at least one of the published papers/chapters of this thesis, and in some instances multiple objectives are examined in the same chapter.

The research conducted is largely simulation-based and supported by field measurements and observations. Each chapter was inspired by real world modelling questions during my internships and work with a private sector engineering firm. Issues with the masonry on the Parliament Buildings, and the East Block building in particular were the inspiration or case studies for each of the published manuscripts.

## **2. Background**

### **2.1 Heritage Conservation Principles**

In North America, there are many mass masonry buildings that have been constructed over the centuries and are increasingly in need of conservation work and/or rehabilitation. Both lower profile “utilitarian” buildings (such as housing, workshops, main street shops) and higher profile institutional buildings (churches, governmental buildings, monuments) require such work. With this demand, there is a growing need for specialists with the required knowledge of heritage materials, systems, or maintenance to correctly inspect, analyze and prescribe treatments for heritage masonry whether the need is in structural engineering, building physics, materials conservation or other disciplines. This work should be guided by ethical conservation philosophy so as to preserve the character the building as much as possible.

Modern heritage conservation philosophy has its roots in 19<sup>th</sup> century led by people like Ruskin, Morris and Viollet-le-Duc. Over time it became more formalized with a series of charters to guide the practice. These include a series of international charters including the 1931 Athens Charter, 1964 Venice Charter and the 1992 Nara Document. This subsequently led to the development of local policies guided by the international charters. In Canada, the *Standards and*

*Guidelines for the Conservation of Historic Places in Canada* is used to direct the approach when working on heritage buildings (*Standards and Guidelines*, 2010). This document outlines many best practices for conserving buildings in Canada, outlining recommended steps that can be taken at all stages: understanding, planning and intervention. The *Standards and Guidelines* presents 14 general standards to follow which emphasize minimal intervention, maintaining character-defining elements, reversibility of repairs and additions amongst other things.

The charters and the *Standards and Guidelines* are intended to prevent wanton, insensitive or perhaps, unsafe, or materially detrimental interventions. Many buildings are designated as historically or culturally significant in Canada either by the federal government (FHBRO), provincial government (Ontario Heritage Act), or municipal governments (Heritage Services Unit). Designation is intended to offer protection against demolition, alterations or additions which may be incompatible or compromise a building's character-defining elements, integrity, authenticity, or safety. Heritage advocacy groups (Heritage Trust for Canada, Heritage Ottawa, International Council on Monuments and Sites, Society for the Protection of Ancient Buildings etc.) also contribute to the cause through promotion, awareness, resources and other forms of support. The goal of conservation is that buildings are preserved, properly maintained, maximize their useful life expectancy, and avoid unnecessary demolition and waste.

### **2.1.1 Preservation, Restoration and Rehabilitation**

The Standards and Guidelines defines three common approaches to heritage conservation interventions: preservation, rehabilitation and restoration.

Preservation focuses on maintaining the present form, materials and integrity of an historic building. It is an approach commonly attributed to John Ruskin and William Morris in 19<sup>th</sup> century England as a response to excesses of the restoration mindset (sometimes referred to as the anti-restoration movement).

The preservation approach encourages a hands-off approach, minimal intervention as to maintain the historical-cultural context from its time of construction (Jokilehto, 1986). It highly prioritizes authenticity. Routine maintenance and interim stabilizing measures are strongly preferred over intrusive interventions, additions, and replacement of historical material. The preservation mindset can often be at odds with modern demands, for example reducing energy emissions or adaptive reuse to facilitate continuing use of the building. Rigid adherence to this mindset can be detrimental to the building's longevity. For example, interventions which improve a building's water-shedding, structural resilience or economic viability may be frowned upon.

Restoration involves returning the state of a building, or component of a building to its original state, often to the time of its construction. This philosophy is commonly attributed to Eugène Emmanuel Viollet-le-Duc, George Gilbert Scott

and architects in the Italian Renaissance. Restoration does not associate a building's historical significance with authenticity or continuity, but rather a particular moment in the building's history or history in general, even if that moment may be exaggerated or idealized (Jokilehto, 1986). Restoration can involve removal of unoriginal non-character defining elements and the recreation of lost or damaged features. Restoration has fallen out of favour for whole buildings, but still remains popular for specific character-defining elements (*Standards and Guidelines*, 2010). Restoration philosophy can be at odds with modern demands such as energy efficiency and durability. Additions which improve thermal resistance or water-shedding may be frowned upon if it was not part of the original design. There may be a reluctance to address inherent vices in the building if they are not true to the form of the building being aspired to.

Rehabilitation is the sensitive and compatible adaptation of a building to allow for continuing usage and health, while protecting its heritage value. Compared to preservation and restoration philosophies, rehabilitation can be considered the more pragmatic or neutral approach to heritage conservation. The concept of rehabilitation was not prominently discussed in discourse about heritage conservation until relatively recently. This may have been because of the preoccupation of the discussion towards monuments and high-profile buildings. However rehabilitation's philosophy can be traced deep into the past.

*“The traditional approach that has probably existed as long as society, in which historic structures are preserved so long as they continue to have use values, or because there is no specific reason for their destruction; changes and new constructions in large buildings are slow and can take generations, showing in many cases a desire to continue the efforts of previous generations in a harmonious way, as was the case in mediaeval cathedrals” (Jokilehto, 1986)*

This quotation demonstrates the practical desire to keep our buildings relevant and the evolutionary nature of buildings during its lifespan. This allows rehabilitation philosophy to be more compatible with modern sustainability, social and economic needs. Envelope upgrades, repair and replacement and additions are in accord with rehabilitation philosophy provided changes are executed in a sensitive and compatible fashion.

The application of the term ‘heritage’ implies an importance or significance to the building, often codified by a formal designation. Conservation theory and the points discussed in this thesis could be equally applied to non-designated buildings, or buildings which are not yet seen as heritage by the general public. This includes buildings of a relative recent vintage which have contemporary masonry construction (eg. rainscreen cladding). In Canada, our definition of what classifies as a heritage building is continuously expanding outside of the classical archetypes to include modern heritage constructed post-war in a variety of

architectural styles, materials and technologies. An increasing swathe of modern buildings are being assessed for heritage designation in Canada as the Federal Heritage Buildings Review automatically reviews federal buildings which are 40 years old or greater (post 1982).

## **2.2 Heritage Masonry**

Heritage masonry is constructed using several techniques, materials, shapes and sizes, and is exposed to a variety of climatic conditions. There are a near-infinite number of ways to construct masonry which makes it difficult to generalize about their performance. A few of the many styles of walls included multi-wythe brick, rubble core stone walls (East Block) and stone veneer with brick back-up (Centre Block). Common materials for walls in the Ottawa region are clay brick, sandstone, and limestone which vary in age and quality. The mortars used vary greatly depending on time and region. Traditional mortars typically used lime as the binder. At the turn of the 20<sup>th</sup> century Portland Cement based mortars became more prevalent and are the de facto binder of modern masonry construction. The different materials and mortars have distinct mechanical and hygrothermal properties from one another which can affect structural performance, moisture transfer, and consequently the durability of the envelope.

Heritage masonry buildings in North America are in increasing need of maintenance, repair, rehabilitation, and intervention. This could be for structural issues to ensure the safety of the building, or for non-structural concerns related to durability, energy or occupant comfort. With this increasing demand, there is a growing need for qualified specialists with the required knowledge in masonry conservation to correctly inspect, analyze and prescribe treatments whether the need is in structural engineering, building physics, materials conservation or other disciplines. The need for qualified specialists is hindered because the study of heritage masonry and heritage conservation are generally under-taught in Canadian colleges and universities.

There are numerous nuances with heritage masonry construction that need to be understood and are in contrast to contemporary construction. These are not often taught in the engineering and architectural curricula or always mentioned in Canadian codes and standards. These nuances may be related to construction techniques, materials, effects of decay and appropriate analysis procedures.

Simple examples include:

- the different moisture mechanics of a rainscreen wall versus an absorbent mass masonry wall,
- the need for softer and more vapour-permeable mortars that are often necessary in tandem with heritage units.

- the variability in material properties of historic materials.

### **2.2.1 Heritage Masonry in Standards**

Canadian masonry standards are intended for modern construction and materials, and are not written from heritage construction and materials. *CSA304-14 – Design of masonry structures* is primarily for engineered masonry design (CSA, 2014b). There is an annex for empirical design for unreinforced masonry which may be appropriate for heritage masonry. This appendix has been written so that analysis using this method are more conservative than the engineered design methods (Drysdale, 2012). The Canadian standard for mortar *CSA A179-14 – mortar and grout for unit masonry* is also dedicated to contemporary construction, focusing on higher-strength and Portland-rich Type N and Type S mortars (CSA, 2014a). This standard includes Annexes which are applicable to heritage mortars. Annex A refers to the selection of mortar types including softer and lime-rich Type O and Type K mortars. Annex D describes the process of selecting repair mortars for older, traditional masonry. *ASTM C1713-17 Standard Specification for Mortars for the Repair of Historic Masonry* has recently been introduced to guide specification of Type K mortars (ASTM, 2017).

The lack of coverage in the main section of the standards indicates that heritage masonry requires specialized knowledge and analysis (eg. structural finite-

element analysis). The heritage-focused annexes tend to be generalized, qualitative, and avoids giving detailed design procedures or recommended design values for materials and other parameters. This can partly be attributed to the uncertainty and non-standardized nature of heritage structures and their materials.

This conflict between heritage masonry design and contemporary masonry design in the structural design standards is also reflected in hygrothermal design. Hygrothermal design standards (ASHRAE, 2016; *EN 15026*, 2007) do not provide detailed guidance for dealing with historic buildings and materials. *ASHRAE Guideline 34 – Energy Guideline for Historic Buildings* is also generalized, qualitative and has an absence of detailed design recommendations (ASHRAE, 2019).

The lack of guidance for heritage masonry means practitioners overly rely on the contemporary standards for design, even if they may not be applicable. This can lead to inappropriate analyses and originating from this, of which there is anecdotal evidence. General examples include incompatible mortars, installation of vapour-tight insulation products, and structural reinforcement when none was required. Sometimes structural concerns and non-structural concerns can be interlinked (e.g. corrosion of lintels, erosion of mortar).

Heritage masonry buildings in Northern cold climates have one commonly cited weakness, and that is high energy consumption and poor occupant comfort due to their poorer R-value. As a result, there is an increasing pressure to make historic buildings more energy-efficient, often through interior insulation. However, there are legitimate concerns from conservation professionals against doing this because of the increased risk of deterioration. Interior insulation and sustainability in general can be a controversial topic amongst the conservation community due to the perceived risks and intrusiveness of some interventions. As climate change becomes an ever increasing concern among citizens and policymakers, the heritage conservation community needs to consider energy efficiency as an integral part of their work. A balance needs to be sought that considers preservation of character-defining elements, minimizing deterioration risk versus the consequences of increased energy consumption (environmental and financial) and reduced occupant comfort. There are several organizations which are promoting and researching energy efficiency and as far as net-zero in heritage buildings, including International Energy Agency Task 59 (Herrera-Avellanosa et al., 2019), RiBuild (2020) and technical standards *ASHRAE Guideline 34* and *EN 16883 - Conservation of cultural heritage - Guidelines for improving the energy performance of historic buildings* (ASHRAE, 2019; CEN, 2017).

### **2.2.2 Energy Retrofits of Masonry Walls**

An integral part of worldwide climate-change mitigation is to reduce the energy and fossil fuel consumption of buildings. Historic buildings are not and should not automatically be exempt from this need and there is an increasing pressure to retrofit historic buildings to be more energy-efficient. Energy-efficiency measures can include “low-hanging fruit” like upgrading lighting systems, weatherstripping around windows and doors, to more intensive intervention to upgrading HVAC systems, installing on-site generation, or adding thermal insulation to the building envelope. The addition of thermal insulation is a common intervention discussed in the rehabilitation of masonry, and is an intervention which hygrothermal analysis is well positioned to help answer.

The topic of adding thermal insulation can be controversial among conservation professionals because there are legitimate concerns about an increased risk of deterioration and irreversible changes to character-defining elements. In most instances, insulation needs to be placed on the interior face of the building envelope because of heritage protections against altering the façade, and logistical issues with building outwards a new cladding system. This is not ideal from a hygrothermal perspective, compared to rainscreen technology where the environmental barriers protect the structure. Interior insulation also has other

negative consequences in the loss of usable floor area, and intrusiveness and/or loss of character-defining finishes on the interior.

The addition of insulation will alter the temperature profile across the cross-sectional plane of the wall. In a cold climate, this will mean that components on the external side of the insulation will experience colder temperatures than it had previously. This can lead to an increase in freeze-thaw issues, condensation on surfaces and increased relative humidity.

Insulation retrofits can also inhibit vapour transport for positive and negative effect depending on circumstances such as climate and rain exposure. In historic masonry, it is recommended to have the wall be able to dry to both sides. The placement of vapour-closed insulation will inhibit drying to the inside. If a wall is wetted primarily from rain-absorption from the exterior, this can increase the chance of decay. In this case a vapour-open insulation or a capillary-active insulation such as calcium silicate may be the preferred option. If wind-driven rain exposure is low and/or the wall is primarily wetted through vapour drive from interior to exterior, then vapour-closed insulation may be the preferred option with their increased R-values and airtightness advantages. The choice of interior finishes, stud wall structure and vapour retarders should also be considered for their impact on hygrothermal performance.

As climate change becomes an ever increasing concern among citizens and policymakers, the heritage conservation community needs to consider energy efficiency as an integral part of their work. A balance needs to be sought that considers preservation of character-defining elements, minimizing deterioration risk versus the consequences of increased energy consumption (environmental and financial) and reduced occupant comfort. There are several organizations which are promoting and researching energy efficiency of historic buildings up to the goal of net-zero. This is a research pursued by organizations such as International Energy Agency Task 59, RiBuild, Building America and Historic Scotland and several others (Herrera-Avellanosa et al., 2019; Little et al., 2015; *RiBuild*, 2020; Straube et al., 2011). Slowly the discussion of retrofitting historic building has been adopted into standards such as *ASHRAE Guideline 34-2019 - Energy Guideline for Historic Buildings* and *EN 16883 - Conservation of cultural heritage - Guidelines for improving the energy performance of historic buildings* (ASHRAE, 2019; CEN, 2017). These organizations and standards aim to provide guidance to professionals about best practices when performing a rehabilitation to avoid the performance risks and loss of character-defining elements while avoiding being too inherently conservative and potentially not performing upgrades at all.

### **2.3 Hygrothermal Modelling**

Hygrothermal models (also called HAM models for heat, air and moisture) assesses the coupled heat and moisture flow (vapour and liquid) through building envelopes. They are used to calculate the heat and moisture flux across wall assemblies and project the moisture risk from pathologies such as biological growth, freeze-thaw, corrosion etc.

Hygrothermal analysis is required under three scenarios: design, assessment and study (Straube & Burnett, 2001). Design analysis encompasses new building design, retrofits of existing buildings, and ensuring compliance with codes and moisture-safe building practices. Hygrothermal assessment includes forensic investigation of past envelope failures and evaluating the condition of existing envelopes (baselining). Study includes the research, development, and evaluation of new products, validation of laboratory experiments, and also teaching of fundamental concepts. The topics discussed in the four publications focus on using hygrothermal models as an assessment and study tool.

Hygrothermal analysis is not required in all situations. When analysis is required, differing levels of complexity and detail may be applicable. The depth of analysis that is required is dependant on climate (those with high moisture indices), building archetype (eg. low-rise residential), sensitivity of material used, condition of the existing envelope, importance factor (subjective heritage and non-heritage

criteria), amongst other factors. Hygrothermal modelling procedures also vary in complexity ranging from the most basic steady-state 1D Glaser Method or ASHRAE Dewpoint Method (ASHRAE, 2013a) to modern hygrothermal modelling software such as Delphin or WUFI capable of transient multi-dimensional calculations (Bauklimatik Dresden, 2020; Fraunhofer Institute for Building Physics, 2019).

Heritage masonry is a prime candidate for hygrothermal analysis. As mentioned in the previous chapter, many masonry walls are being evaluated for retrofits which will improve their thermal performance and this can alter their temperature profiles, and drying and wetting characteristics. Models can aide the designer in developing an understanding of both the positive and negative effects of the retrofit. This allows stakeholders to make a more informed decision whether to proceed with a retrofit which neither compromises the envelope's durability or is too conservative from a thermal performance viewpoint.

Analysis can also be used on heritage masonry to evaluate its present condition or to perform a forensic investigation into an existing failure. Here the modeller would seek to understand why the failure occurred and examine retrofits which could rectify the observed conditions. This process would be backed with observations and data collected from the site.

### 2.3.1 Theory

The theoretical equations for coupled heat, moisture and air transport are given below. Heat transport is given in Equation (2-1) and Equation (2-2). Moisture transport in Equation (2-3) and Equation (2-4) and air transport in Equation (2-5).

$$\frac{\partial H}{\partial t} = -\nabla(q_c + q_v) \quad (2-1)$$

- $H$  = Internal enthalpy or energy [ $\text{J}/\text{m}^3$ ]
- $q_c$  = Conductive Heat Flux [ $\text{W}/\text{m}^2$ ]
- $q_v$  = Latent Heat Flux [ $\text{W}/\text{m}^2$ ]

$$\frac{\partial H}{\partial t} = -\nabla[\lambda \nabla T + h_v(k_v \nabla P_v) + h_l(k_l \nabla P_c)] + S \quad (2-2)$$

- $\lambda$  = Thermal Conductivity [ $\text{W}/\text{m}\cdot\text{K}$ ]
- $T$  = Temperature [ $\text{K}$ ]
- $h_v$  = Enthalpy of vaporization [ $\text{J}/\text{kg}$ ]
- $k_v$  = Vapour Permeability [ $\text{s}$ ]
- $P_v$  = Vapour Pressure [ $\text{Pa}$ ]

- $h_l$  = Enthalpy of Fusion [J/kg]
- $k_l$  = Liquid Conductivity [s]
- $P_c$  = Capillary Pressure [Pa]
- $S$  = Energy Sources or Sinks [ $W/m^3$ ]

$$\rho_w \frac{\partial \theta_l}{\partial t} = -\nabla \cdot (g_v + g_l) \quad (2-3)$$

- $\rho_w$  = Density of water [ $kg/m^3$ ]
- $\theta_l$  = Material Water Content [ $m^3/m^3$ ]
- $g_v$  = Vapour Mass Flow Rate [ $kg/m^3 \cdot s$ ]
- $g_l$  = Liquid Mass Flow Rate [ $kg/m^3 \cdot s$ ]

$$\rho_w \frac{\partial \theta_l}{\partial t} = -\nabla \cdot (k_v \nabla p_v + k_l \nabla P_c + c_g k_g \nabla P_g) + S_l \quad (2-4)$$

- $c_g$  = Concentration of Vapour in Gas Phase [kg/kg]
- $k_g$  = Gas Permeability [s]
- $P_g$  = Gas Pressure [Pa]
- $S_l$  = Liquid Water Sources or Sinks [ $kg/m^3 \cdot s$ ]

$$\rho_g \frac{\partial \theta_g}{\partial t} = -\nabla \cdot (k_g \nabla P_g) + S_g \quad (2-5)$$

- $\rho_g$  = Density of gas [kg/m<sup>3</sup>]
- $\theta_g$  = Material Gas Content [m<sup>3</sup>/m<sup>3</sup>]
- $S_a$  = Air Sources or Sinks [kg/m<sup>3</sup>-s]

The dependant variables in the coupled equations are temperature and vapour pressure (Capillary pressure is theoretically linked to vapour pressure using the Kelvin Equation and Young-Laplace Equation). Air transport is not often modelled in practice (though can be quite important in reality) and is not included in most hygrothermal modelling software. To solve these equations both material properties and boundary conditions are required as discussed in the subsequent sections. As with most simulation software, the input of accurate material properties and boundary conditions is crucial to getting accurate results.

### 2.3.2 Tools

There are several methods and tools available for hygrothermal modelling. These vary in complexity and appropriateness depending on the context. The tools can be classified into simplified, engineering and research models as per Grunewald in Table 2-1 below:

**Table 2-1: Classification of HAM models according to hygrothermal material characterization. (Grunewald et al., 2003)**

<b>Model</b>	<b>Material Characterisation</b>	<b>Used Transport Potentials</b>	<b>Material Properties</b>
Simplified	one fixed set of functions	empirical (for example: water content gradient)	secondary (diffusivity)
Engineering	one fixed set of functions	based on thermodynamics (for example: capillary pressure gradient)	primary (conductivity)
Research	individual description by selection of best function type	based on thermodynamics (for example: water pressure gradient that includes capillary pressure gradient and further driving forces)	primary (conductivity)

The methods and tools have evolved from simplified methods such as the Glaser Method to advanced engineering and research tools such as WUFI and Delphin. The evolution towards more advanced tools has been sparked by an increase in computer processing power, improved understanding of material properties and laboratory measurement techniques for validation purposes. Further information on the development of these tools can be found in the publication, *Moisture Analysis and Condensation Control in Building Envelopes (Trechsel, 2001)*. A critical review of available hygrothermal software tools can be found in Delgado et al. (2010).

### 2.3.2.1 Glaser Method

The most basic is the Glaser Method or ASHRAE Dewpoint Method (ASHRAE, 2013c). This method is familiar to many and is simple to calculate using graphical methods or spreadsheets. The goal of the Glaser method is to find points in a 1-D wall assembly where partial vapour pressure ( $p_v$ ) exceeds the saturation vapour pressure ( $p_{v,sat}$ ) and interstitial condensation will form. This analysis is performed by calculating the steady-state conductive heat flow, steady-state vapour flows, and saturation vapour pressures at interstices in the assembly. Exterior boundary conditions are typically assumed to be design day extreme temperatures (99% or 99.6%) and interior conditions are assumed to be typical room temperatures and humidities.

This method has limitations because it only considers heat and vapour transport and is steady state only. Capillary transport and air advection are neglected. As a result, this method is only applicable for wall constructions that are airtight, where liquid water absorption from wind-driven rain is minimal. The calculation typically considers only worst-case conditions. The ability for a wall to safely hold moisture or its ability to dry under more favourable conditions is not considered. If condensation is calculated to occur under the design day extreme conditions, then the wall is deemed to have failed. This is an overconservative approach

because many building materials can safely be subjected to these conditions periodically.

Due to the steady-state and wind-driven rain absorption of the Glaser Method, it should not be relied upon to simulate heritage masonry construction. The ASHRAE Fundamentals does not recommended this analysis other than for historical continuity or for illustration of the principles of heat and vapour flow in building envelopes.

Some improvements to the Glaser methods have been made to address these shortcomings. TenWolde (1985) and Handegord (1990) developed models using monthly average temperatures and relative humidity. This helped to address the issue of using extreme temperatures and to help quantify storage and evaporation. These models also accounted for air advection.

### **2.3.2.2 Numerical Methods**

The advent of numerical methods of analysis and increasing computer processing power, allowed for more complex analysis of hygrothermal behaviour than the simple Glaser Method could allow. These advanced hygrothermal software allow for the coupled partial differential equations (Equations 2-1 to 2-5) to be solved. These hygrothermal software allow for transient solutions, inclusion

of both liquid, vapour, and air transport as well as storage of both heat and moisture, which the Glaser Method could not provide.

The most common numerical analysis method in hygrothermal models is the finite-volume method (as used by WUFI and Delphin). This method is suited to hygrothermal modelling because it maintains conservation of mass and heat flows, both of which are critical from a hygrothermal perspective. The finite-element method (COMSOL) can be used but is regarded as less inaccurate because it struggles to model the non-linear overhygroscopic range of moisture retention and liquid conductivity curve (J. I. Knarud & Geving, 2017) and has not been validated to the same extent as the finite-volume software.

The two most popular finite-volume software on the market are WUFI and Delphin (Bauklimatik Dresden, 2020; Fraunhofer Institute for Building Physics, 2019a). Delphin allows up to 3-dimensional simulation while WUFI currently allows for two. Both software come with a material library and with climate data available for some locations.

### **2.3.2.3 Coupled Hygrothermal – Building Energy Models**

A trend in hygrothermal modelling is to couple it with building energy simulation. The hygrothermal behaviour of the envelope can influence the interior ambient

conditions, building energy performance and occupant comfort and vice versa.

There are several ways in which this happens:

1. Increased thermal conduction and heat capacitance if envelope materials are wet (Example in Section 4.- Calibrated Envelope Modelling). Water with high a higher heat capacity and thermal conductivity displaces air in the system, resulting in greater thermal mass effect and heat transfer. This is especially important in building envelopes with hygroscopic materials that make up a significant proportion of the total thermal resistance. Examples include mass masonry and certain types of absorbent insulation materials.
2. Moisture transfer between the ambient air and inner wall surfaces continuously occurs. As a result a moisture buffer between the two can develop which modulates the relative humidity of the space. This is important in mass masonry walls which stores moisture throughout the year. This moisture can be transferred to the indoor air, raising relative humidity, and perhaps changing occupant comfort.
3. More accurate definition of interior boundary conditions in the hygrothermal models. This is important in buildings which are not always actively conditioned or controlled, (naturally ventilated buildings, buildings without air conditioning), buildings with high internal moisture loads, or wall

assemblies which are sensitive to interior humidity. This would be an improvement over simplified methods of defining the interior conditions such as annual sine curves, ASHRAE 160 or EN 15026 methods.

Usage of these programs would be limited to situations where the previous three points are significant. Coupled programs have been integrated into the software WUFI Plus (Antretter et al., 2011; Fraunhofer Institute for Building Physics, 2019c), EnergyPlus through its HAMT and EMPD models (*EnergyPlus*, 2018), and in ESP-r (J. Clarke, 2013). The downside to using these models are increased simulation time (especially for very absorbent envelopes) and that they are 1-dimensional.

#### **2.3.2.4 Software Validation**

There isn't a formal standard for validation of hygrothermal software equivalent to ASHRAE 140 for energy modelling (ASHRAE, 2017). Validation is done by benchmarking against examples given in EN 15026 (*EN 15026*, 2007) or HAMSTAD (*HAMSTAD*, 2002). Both Delphin and WUFI have published their validation findings (*Fraunhofer*, 2020; Sontag et al., 2013). COMSOL has been able to pass the HAMSTAD benchmark examples (J. Knarud & Geving, 2015; van Schijndel et al., 2016). The benchmark examples used are simple 1-D

constructions which the software must simulate within the temperature or RH range given.

Different simulation software can also give different results for the same simulation problem, controlling for climate, material properties etc. (Defo et al., 2021). The discrepancy between tools could be caused by internal algorithms for wind-driven rain absorption at the surface, radiative heat transfer or advection in air cavities.

Hygrothermal software has also been validated against lab experiments but validation against in-situ measurement is more difficult (Busser et al., 2018). This is because control of boundary conditions, understanding of construction quality and material properties, and the timescale needed to measure the natural moisture response is more difficult to achieve.

### **2.3.3 Material Properties**

#### **2.3.3.1 Porosity**

The most fundamental hygrothermal material property is porosity and subsequently pore size distribution. Porosity is often (not always) a good indicator of many other important hygrothermal properties. For example, a low porosity stone is likely to have a higher thermal conductivity than a higher porosity stone, because there is a lower ratio of still, insulating air molecules to the more

conductive matrix material or if wet, water. A lower porosity stone is also more likely to have lower vapour permeability and liquid conductivities because there are fewer and more restricted paths for vapour and liquid to travel through.

Porosity can be expressed in a number of ways. The first is total porosity or vacuum saturation ( $\theta_{Por}$ ). This is the ratio of open-pore volume in a fixed volume of material. This is tested in the laboratory using either a vacuum (*ASTM*, 2016a) or boiling-water method (*ASTM*, 2015). In many hygroscopic building materials, a significant fraction of these air spaces are not available to be filled with liquid water under typical conditions. This because not all pores in the matrix may be inter-connected through pore channels large enough for water to flow, or are disconnected to the main pore network. This is known as the effective porosity ( $\theta_{eff}$ ). Capillary saturation ( $\theta_{cap}$ ) is also sometimes used. This is the saturation resulting from a short-term water uptake experiment.

Pore size distribution is important because it dictates to a large extent the moisture retention curve and liquid and vapour conductivity. In the context of heritage masonry, a material with a greater percentage of smaller pores such as Portland mortars tend to have lower vapour transmission and liquid conductivity which can limit moisture entering the wall, but also inhibit it exiting the wall under favourable drying conditions. Conversely materials which have a greater percentage of larger pores (example lime mortar) tend to absorb water quickly

and also release water quickly, behaving more like a sponge. Porosity is relatively easy to test in the lab by gravimetric methods (ASTM, 2015). Testing for pore size distributions is less common in practice due to the relative complexity and availability of lab testing (e.g. mercury porosimetry).

### 2.3.3.2 Moisture Retention Curve

The moisture retention curve (also called moisture storage function or alternatively expressed as a sorption isotherm) describes the equilibrium relationship between saturation and capillary suction pressure in a porous media as it wets or dries. The moisture retention curves are unique for each material and are reflective of the pore size distribution of the material. Capillary pressure can be converted into an equivalent pore radius using the Kelvin Equation (2-6), which can subsequently converted into a relative humidity using the Young-Laplace Equation (2-7).

$$\ln\left(\frac{p}{p_{sat}}\right) = \frac{2\gamma V_m}{rRT} \quad (2-6)$$

- $p$  = Vapour pressure [Pa]
- $p_{sat}$  = Saturation vapour pressure [Pa]
- $\gamma$  = Surface tension of water [N/m]

- $V_m$  = Molar volume of water [ $m^3/mol$ ]
- $r$  = Pore radius [m]
- $R$  = Ideal gas constant [8.314 J/mol-K]
- $T$  = Temperature [K]

$$\Delta P = \frac{2\gamma \cos(\theta)}{r} \quad (2-7)$$

- $\Delta P$  = capillary rise [Pa]
- $\theta$  = wetting angle [Assumed to be zero]

In general, the moisture retention curve tells us that narrower pores are the first to completely fill and retain moisture more strongly than larger pores. Larger pores are the last to completely fill and are the first to release its water under drying conditions. This has implications on material wetting and drying and some pathologies such as freeze-thaw action.

Capillary pressure as a function of saturation can be measured using a pressure plate apparatus (Plagge et al., 2007), porosimetry or approximated using appropriate correlations for unsaturated flow (also called two-phase flow) in porous media.

In practice, there are few laboratories that can generate detailed moisture retention curves for building materials using pressure-plate apparatus. It is common for the moisture retention curve to be approximated based off of two common laboratory measurements:  $w_{80}$  and  $w_{sat}$  as in Equation (2-8) (ASTM, 2016b; DIN, 2013). These are the moisture contents at RH = 80% and at free water saturation (capillary saturation) (Krus, 1996).

$$w(\phi) = \frac{w_{sat}(b-1)\phi}{b-\phi} \quad (2-8)$$

- $w(\phi)$  = Water content at relative humidity  $\phi$  [kg/m<sup>3</sup>]
- $w_{sat}$  = Free water saturation [kg/m<sup>3</sup>]
- $\phi$  = Relative humidity [--]
- $b$  = Approximation factor determined when  $\phi = 0.80$

There are some drawbacks to this simplification. The method is good for the hygroscopic range where the line is relatively linear, but in the overhygroscopic region there is not enough information to adequately represent this part of the curve. Depending on the material the apex of the line may be relatively gradual or quite sharp.

Another commonly used approximation is Van Genuchten's equation (van Genuchten, 1980) which comes from the field geohydrology.

$$P_c = \frac{1}{\alpha} \left[ S_{eff}^{-\left(\frac{n}{n-1}\right)} - 1 \right]^{\left(\frac{1}{n}\right)} \quad (2-9)$$

- $P_c$  = Capillary Pressure [m];
- $S_{eff}$  = Effective Saturation [-];
- $\alpha, n$  = material-specific dimensionless parameters [-]

The van Genuchten equation assumes a log-normal pore distribution. Many masonry materials exhibit multimodal distributions. In this case, the moisture retention curve can be approximated by a sum of van Genuchten functions with different weighting (Carmeliet et al., 1999; Durner, 1994). An example of moisture retention curves for sandstones is given in Figure 2-1.

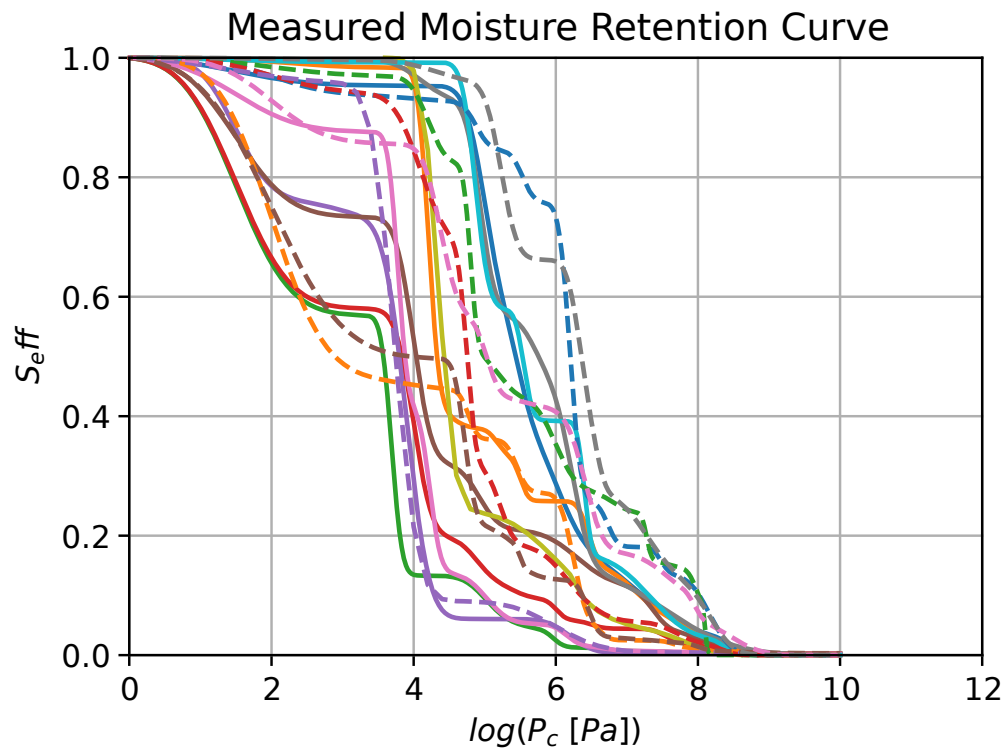


**Figure 2-1: Moisture retention curves for various different sandstones (both dashed and solid lines) in the Delphin material database.**

Many building materials exhibit hysteresis in the absorption and desorption phases of the moisture retention curves. This means that two different paths are followed on the moisture retention curve. Materials typically require more energy to release water than to absorb it (air-expulsion and air-entry pressures).

Hysteresis based on Van Genuchten curves can be estimated (Likos et al., 2014) based on type of material. Hysteresis curves have been measured in the lab for some building materials (Derluyn et al., 2012; Karoglou et al., 2005; Patera et al.,

2013). Some materials show minimal hysteresis while some show significant hysteresis (Karoglou et al., 2005). Hysteresis is another complicating factor when characterizing material properties.

### **2.3.3.3 Liquid Conductivity**

Moisture transport occurs in two distinct phases: liquid and vapour. Liquid transport occurs through capillary action and is prominent at elevated moisture contents. Vapour transport is a diffusive process acting on vapour pressure differentials. Both modes of transport can occur simultaneously. Though it is advantageous to separate the two distinct modes of transport in our minds and in physical models, we sometimes combine the two into a measure called moisture diffusivity. This measure can be more convenient to determine in labs than separate liquid and vapour transport curves and is used in some finite-element software.

Liquid conductivity is important in the absorption phase for walls that are exposed to wind-driven rain or saturated soils. The liquid conductivity curve is theoretically linked to pore size distribution and the moisture retention curve by the Hagen-Poiseuille Equation:

$$k_l = \frac{\rho r^2}{8 \eta_l} \quad (2-10)$$

- $k_l$  = Liquid Water Permeability [s]
- $\rho$  = Density of water [kg/m<sup>3</sup>]
- $r$  = Capillary radius [m]
- $\eta_l$  = Dynamic viscosity [kg/m-s]

The Hagen-Poiseuille Equation shows that liquid transport increases with the square of capillary radius, meaning that a material with many narrow pores will have a significantly reduced liquid conductivity. Liquid transport only occurs when capillaries are filled. From the moisture retention curve, at low degrees of saturation, only the small capillaries are filled and available for liquid transport. As a result liquid conductivity is minimal when the material is dry. As the porous media becomes more saturated the liquid conductivity increases as the more open and freer flowing pores become active. Consequently liquid conductivity is non-linear and increasing with degree of saturation. There are several ways that the liquid conductivity curve ( $k_l(\theta_l)$ ) can be estimated. A fundamental approach can be used based on the Hagen-Poiseuille equation and integrating over the range of active capillaries at that degree of saturation.

$$k_l(\theta_l) = \frac{\rho}{\tau} \int_{R_{min}}^R \frac{\pi r^4}{8 \mu_l} \frac{dn}{dr} dr \quad (2-11)$$

- $k_l(\theta)$  = Moisture-dependent liquid conductivity [S]
- $\rho$  = Density [kg/m<sup>3</sup>]
- $\tau$  = Tortuosity [--]
- $r$  = Capillary radius [m]
- $\mu$  = Dynamic viscosity [kg/m-s]
- $n$  = number of capillaries of that size [--]

In most scenarios the theoretical curve will not match measured liquid conductivity because of the effects of tortuosity, pore shape and interconnectivity of pores (Scheffler et al., 2004). The liquid conductivity curve can be modified by a tortuosity factor ( $\tau$ ), similar in concept to a vapour-diffusion resistance factor ( $\mu$ ). Tortuosity is difficult to measure and can also be moisture dependent. Therefore, it is practical to scale the theoretical liquid conductivity curve, to measured data points at different degrees of saturation (Grunewald et al., 2003).

Liquid conductivity curves for sandstones from the Delphin library are shown in Figure 2-2. Observable is a significant order of magnitude difference in the liquid conductivity between when a material is dry or when it is saturated, and between materials of the same classification (ie. sandstone).

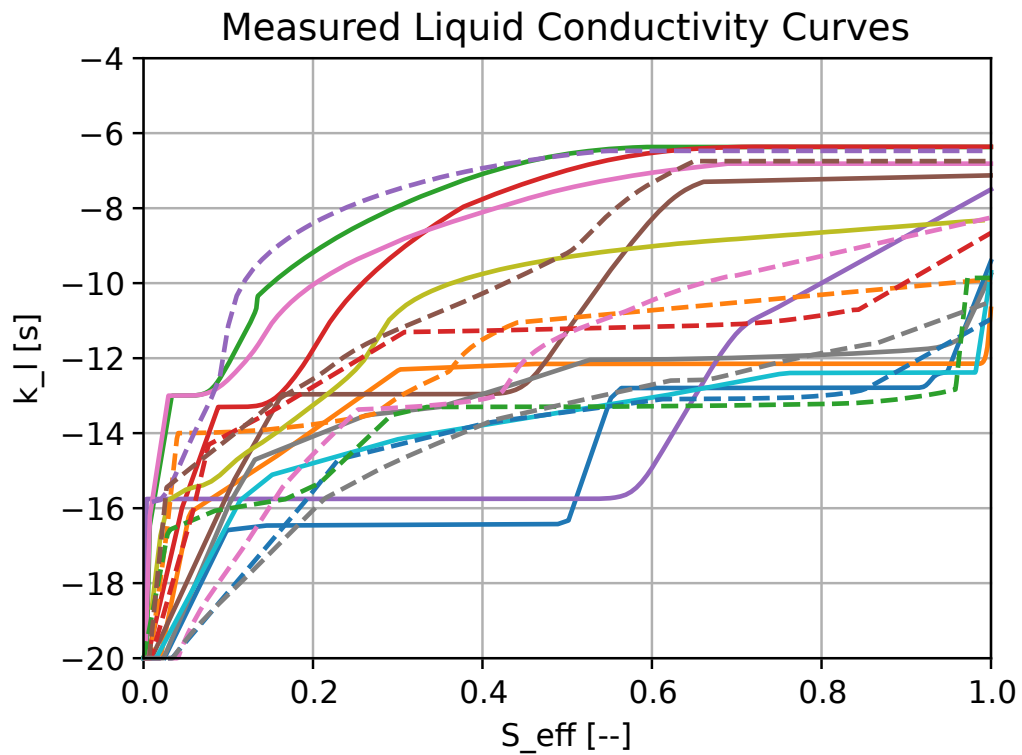


**Figure 2-2: Liquid conductivity curves for various different sandstones (both dashed and solid lines) in the Delphin material database.**

In practice, few laboratories measure a moisture-dependant liquid conductivity curve. It is more common for simpler water absorption tests to be performed and the liquid conductivity curve estimated from what is known as the water absorption coefficient or A-value measured in units of  $\text{kg}/\text{m}^2\cdot\text{s}^{1/2}$  (ASTM, 2019).

In the liquid conductivity curve, the capillary pressure gradient is the driving force Equation 2-4. An alternative method of expressing liquid conductivity is the

capillary transport coefficient ( $D_w$ ) as used by WUFI (Künzel, 1994). In this expression the driving force is the gradient in water content ( $w$ ).

$$g_w = D_w(w) \nabla w \quad (2-12)$$

This can be transformed into a liquid conductivity curve using the derivative of the moisture storage function.

$$k_l = D_w \frac{dw}{d\phi} \quad (2-13)$$

$D_w$  can be estimated using the measured A-value and saturation data using the following empirical equation (Künzel, 1994)

$$D_w(w) = 3.8 \left( \frac{A_w}{w_f} \right)^2 * 1000^{\frac{w}{w_f} - 1} \quad (2-14)$$

- $D_w(w)$  = Moisture-dependant capillary transport coefficient [ $m^2/s$ ]
- $A_w$  = Absorption coefficient [ $kg/m^2s^{0.5}$ ]
- $w$  = moisture content [ $kg/m^3$ ]
- $w_f$  = free water saturation [ $kg/m^3$ ]

### 2.3.3.4 Vapour Permeability

Vapour permeability is important in the drying phase of masonry wall assemblies and minimizing interstitial condensation. A material's vapour characteristics are described as a permeability (mass transfer rate) or as a vapour resistance factor relative to the vapour transport of still air. Like liquid conductivity, vapour permeability is a function of saturation and is calculated by Equation 2-15.

$$k_v(\theta_l) = \frac{\delta_a}{\mu} (1 - S_{eff}) \quad (2-15)$$

- $k_v(\theta_l)$  = Moisture-dependant vapour permeability [s]
- $\delta_a$  = Vapour diffusion coefficient for still air [ $1.8-2.0 * 10^{-10}$  s depending on model and reference temperatures used]
- $S_{eff}$  = Degree of Saturation [--]

The moisture-dependence arises because as the pores become increasingly saturated, the paths which the vapour diffuse through become increasingly restricted by liquid water. If the media is completely saturated than vapour diffusion theoretically stops.

Vapour diffusion is a relatively simple and common test to perform (*ASTM*, 2016c). There are two types of vapour permeance testing: dry-cup and wet cup.

Both tests are performed with an ambient temperature of 25°C and relative humidity of 50% and the sample sealed against the cup. The dry-cup test has anhydrous salts which give a relative humidity of 0% (vapour flows into the cup). The wet-cup is filled with distilled water filled just below the sample and gives a relative humidity ~ 100% (vapour flows out of the cup). The wet-cup will give a higher permeance than the dry-cup. This is because at elevated RH, water is able to travel efficiently in the liquid phase in addition to the vapour phase. At the very low RH of the dry-cup test, liquid transport is minimal. Because the wet-cup test indirectly measures both vapour and liquid transport, care must be taken when using wet-cup measurements in hygrothermal models because liquid and vapour transport are modelled separately. A method for decoupling the two transport methods is given by Scheffler (2004). Ideally dry-cup measurements are used in hygrothermal models.

Depending on the degree of saturation, either vapour diffusion or capillary transport dominates moisture transport. At low moisture contents, vapour diffusion is the dominant transport mechanism and at higher moisture contents, capillary transport becomes dominant. Distinct regions of the liquid conductivity and vapour permeability curves can be identified (Carmeliet & Roels, 2002).

1. Hygroscopic range where vapour dominates liquid transport
2. Overhygroscopic range where liquid water dominates the vapour transport

### 3. Capillary range where a continuous liquid phase exists

The transition points between regions are dependant on the material.

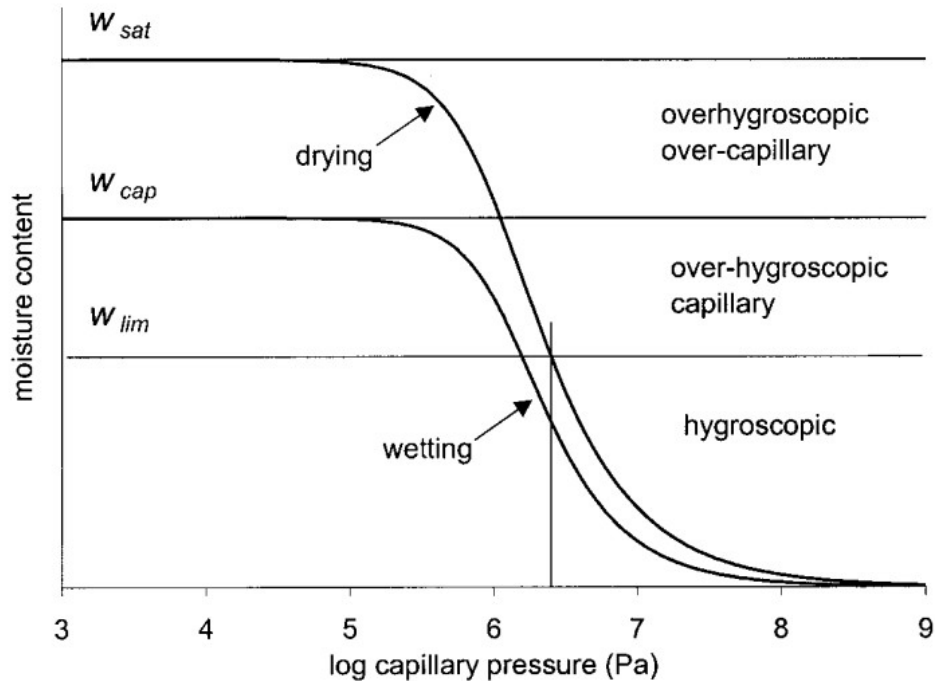


**Figure 2-3: Moisture storage regimes of a porous material (Carmeliet & Roels, 2002)**

#### 2.3.3.5 Thermal Conductivity and Heat Capacity

The thermal conductivity and heat capacity of materials is important when calculating heat flux through an envelope. The thermal conductivity of building materials can have significant moisture-dependency (masonry, wood) or temperature-dependency (insulation products). Of particular interest is moisture-dependency in masonry walls which has been measured to significantly increase

the U-value of the wall (Baker, 2011; Litti et al., 2015; Lucchi, 2017; Rye & Scott, 2012). In wet porous media, the low thermal conductivity and low thermal mass of still air is displaced by the higher thermal conductivity and thermal mass of water. This is important for energy modelling purposes and for identifying high moisture areas with infrared imaging. A simple linear relationship is used to describe the moisture-dependency:

$$\lambda(\theta_l) = \lambda_{dry} + 0.56 \theta_l \quad (2-16)$$

While the U-value increases in wet masonry, there likely won't be a significant change in the temperature profile across the cross-section of the assembly. In uninsulated masonry there is not a definitive controlling layer in the assembly. This means there shouldn't be a large deviation in the freezing plane or temperature profile depending on which value is used. If an insulating layer is introduced, then the contribution of the higher conductivity masonry layers is diminished and the temperature and moisture profiles of the masonry will change too. Another case where thermal conductivity becomes important is when thermal bridges are present in 2D models such as embedded beam ends (Harrestrup & Svendsen, 2016; Morelli & Svendsen, 2013; Vereecken & Roels, 2021).

### **2.3.4 Boundary Conditions**

Hygrothermal modelling requires the input of detailed boundary conditions on the both the interior and exterior sides of the assembly. Typical boundary conditions include temperature, RH (or vapour pressure), wind-driven rain, longwave radiation, and shortwave radiation and their corresponding transfer or adsorption coefficients.

#### **2.3.4.1 Exterior Climate**

The exterior climate of a hygrothermal model is more complex than the interior climate is. Necessary climate data includes temperature, relative humidity, wind speed and direction, precipitation, and short-wave radiation, long-wave radiation (atmospheric pressure may also be necessary). This data should be collected on an hourly basis.

The weather files used can be continuous actual meteorological data or synthesized into a typical weather file (aka. Typical Meteorological Year or Moisture Reference Year). There are several methods for determining the typical weather files. ASHRAE RP-1325 (Salonvaara, 2010) developed a process for determining what the 10%, 50% and 90% worst hygrothermal year from a 30 year period of measured weather data. ISO 15927-4 provides an algorithm for determining typical weather years using the Finkelstein-Schaefer statistic method

(ISO, 2005). ISO 15297-4 was developed for energy modelling and its applicability for hygrothermal modelling is debatable. Modified procedures from ISO 15297-4 have been developed to improve their applicability to hygrothermal modelling (Libralato et al., 2018).

A disadvantage of using typical weather years as defined by ASHRAE and ISO procedures is that different wall assemblies and building materials respond to different climactic factors. For example a mass masonry wall will be more sensitive to wind-driven rain than a modern rainscreen assembly. Another method for determining hygrothermal weather years is the RHT method (Zhou et al., 2016). This method differs from the ASHRAE RP-1325 in that it can be applied to specific wall assemblies, whereas ASHRAE RP-1325 and ISO 15927-4 is a general formula applied that can be applied to all assemblies.

Another disadvantage of using a typical weather year for design is that extreme weather events will likely not be captured. For example, in Ottawa average annual rainfall can fluctuate  $\pm 50\%$  from the average year. Stressor events such as extremely high annual precipitation and storms and contrary drying response of drought years will unlikely be captured using the typical weather file. ASHRAE RP-1325 and RHT method are capable of incorporating this to some extent by choosing other than the median worst year. Other approaches for evaluating extreme weather years are adding or subtracting 2 K from the outdoor air-

temperature or scaling the amount of precipitation. Another procedure to find extreme weather years has been developed by searching for extreme dry-bulb air temperatures and/or relative humidity (Libralato et al., 2020).

Usage of multiple years (~10 years) of actual meteorological data is becoming increasingly recommended for heritage buildings (Libralato et al., 2021). This comes at the expense of computational time for the longer simulation time and time needed to compile the data because some locations may not have hourly climate data easily available.

Weather files which consider the effects of climate change are being developed to be used in hygrothermal modelling. The National Research Council of Canada is in the process of developing and publishing a set of files for multiple locations in Canada which can be used by practitioners (Gaur et al., 2019). A summary of how climate change will impact hygrothermal performance of structures is given in Lacasse et al (2020). Studies which examined the effects of future climates on historic masonry have been performed and shown increasing risk of freeze-thaw damage in some climates (Orr et al., 2018; Sahyoun et al., 2020; Vandemeulebroucke et al., 2020).

### 2.3.4.2 Wind-Driven Rain

Absorption of liquid water from a façade is the combination of two different factors: wind-driven rain and rainwater run-off. Wind-driven rain is a key variable in hygrothermal simulation of masonry because it is the prime way that moisture enters the wall through absorption from the outside boundary condition.

Wind-driven rain is calculated by the following semi-empirical formulae from ASHRAE 160 (Equation 2-17) and ISO 15927-3 (2009) (Equation 2-18 and 2-19).

$$r_{bv} = F_E \cdot F_D \cdot F_L \cdot U \cdot \cos \theta \cdot r_h \quad (2-17)$$

- $r_{bv}$  = Rain deposition on a vertical wall [kg/m<sup>2</sup>-h]
- $F_E$  = Rain Exposure Factor [--]
- $F_D$  = Rain Deposition Factor [--]
- $F_L$  = Empirical Constant [0.2 kg-s/m<sup>3</sup>-mm]
- $U$  = Wind Speed at 10m elevation [m/s]
- $\theta$  = Angle between wind direction and normal to the wall [°]
- $r_h$  = Rainfall Intensity [mm/hr]

The two factors  $F_D$  and  $F_E$  account for the exposure and sheltering of a façade respectively. These can be estimated with the guidance of a table based on building height, exposure and the level of run-off from a roof.

The ISO model is very similar to the ASHRAE 160 model but with a non-linear rainfall coefficient and more descriptive factors to account for exposure ( $C_R$ ,  $C_T$ ,  $O$ ,  $W$ ).

$$I_w = I_A \cdot C_R \cdot C_T \cdot O \cdot W \quad (2-18)$$

$$I_A = 2/9 \sum v \cdot r^{8/9} \cdot \cos(D - \theta) \quad (2-19)$$

- $I_w$  = Rain deposition on a vertical wall [L/m<sup>2</sup>]
- $I_A$  = Air-field driving rain indices
- $C_R$  = Factor for terrain variations [--]
- $C_T$  = Factor for topography [--]
- $O$  = Obstacle factor [--]
- $W$  = Wall factor [--]
- $v$  = Hourly mean value for wind speed [m/s]

- $r$  = Hourly rainfall [ $L/m^2$ ]
- $D$  = Hourly mean wind direction from North [ $^\circ$ ]
- $\theta$  = Wall orientation relative to North [ $^\circ$ ]

Another model which is not formally included in the standards is the Straube and Burnett (2000) model. This model builds off of the work of Lacy (1965) and has contributed to the development of the ASHRAE and ISO wind-driven rain model.

$$r_{wdr} = DRF \cdot RAF \cdot U \cdot r_h \cdot \cos \theta \quad (2-20)$$

- $R_{wdr}$  = Rain deposition on a vertical wall [ $L/m^2/h$ ]
- DRF = Driving Rain Factor [-]
- RAF = Rain Admittance Factor [-]

This model includes the effect of terminal velocity and diameter of the raindrops in the driving rain factor (DRF). The larger the raindrop, the less likely its trajectory will be impacted by wind. The heavier the rain intensity, the more likely there will be larger raindrops. Therefore, there is a non-linear relationship between rainfall intensity and wind-driven rain striking a vertical surface. This is reflected in the 8/9 exponent on the rainfall intensity in the ISO model. In this

model DRF is the inverse of the raindrops' terminal velocity  $v_t$ , which is an empirical function of the raindrop's spherical diameter ( $\phi$ ):

$$v_t(\phi) = -0.166033 + 4.91844\phi - 0.888016\phi^2 + 0.054888\phi^3 \leq 9.20 \quad (2-21)$$

The rain admittance factor (RAF) is dependant on the height of the vertical wall and its degree of sheltering from overhangs. Because wind speed increase with height following a power law distribution, taller portions of buildings will have a greater RAF (close to 1.0) than shorter buildings. Recommended RAFs for simple buildings are shown below.

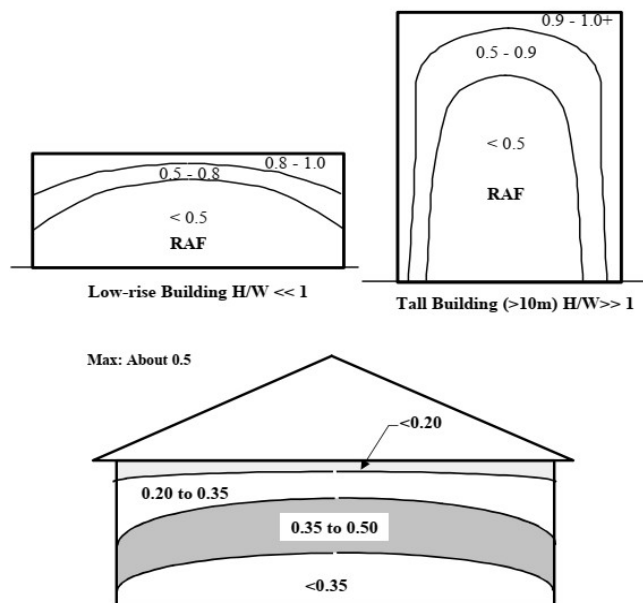


**Figure 2-4: Approximate rain admittance factors for simple buildings (Straube & Burnett, 2000)**

Wind-driven rain is a complex science and it is difficult to ascertain and generalize the amount of wind-driven rain hitting all surfaces of a building using Equations 2-17 to 2-20 (Blocken & Carmeliet, 2006). There are several extenuating factors which make it difficult in practical terms to estimate just how much water is being presented to a vertical wall surface. These include aerodynamic effects from the building's shape and/or surrounding buildings, run-off streams from roofs and other factors related to the site and which the factors from the semi-empirical models may be limited in addressing. This was discussed in a literature review by (Blocken et al., 2013). Advanced numerical models and methodologies have been proposed to better predict wind-driven rain and runoff from roofs (Blocken & Carmeliet, 2012; Hall & Kalimeris, 1982). CFD studies to determine wind-driven rain on facades are increasingly common (Blocken & Carmeliet, 2007; Khalilzadeh et al., 2016; Kubilay et al., 2017, 2018). These physics-based simulations may be too impractical to do for routine hygrothermal assessments.

#### **2.3.4.3 Exterior Transfer Coefficients**

Exterior heat and vapour convection coefficients are included in hygrothermal models. These can be set to dynamic values to account for changes in the hourly mean wind velocity. These can affect heat transfer and the rate of drying. Short and long-wave radiation should be included in the weather data, but may be

difficult to obtain from public sources on an hourly basis (Section 2.6.2.3). These are applied as Neumann type boundary conditions to the finite-volume grid. The magnitude of solar radiation incident can be calculated using standard solar geometry calculations if two of Global Horizontal Irradiation (GHI), Direct Normal Irradiation (DNI) and Diffuse Horizontal Irradiation (DHI) are known.

Long-wave radiation exchange can also be incorporated into the model and is important during clear nights as this can increase heat transport, reduce temperatures on the exterior surface and increase RH in the outer portion of the masonry. Water-repellent coatings can also be simulated in hygrothermal models. This can be accomplished by either reducing the absorption coefficient of the treated layer of masonry or adjusting the adhering fraction of rain in models (Soulis et al., 2021; Vereecken & Roels, 2021). These coatings have been demonstrated to reduce moisture problems over the short-term but their long-term efficacy is uncertain in many situations (Charola, 1995).

#### **2.3.4.4 Interior Climate**

The interior climate of a hygrothermal model usually consists of just temperature and relative humidity. These are relatively consistent throughout the duration of a simulation compared to the exterior surfaces. There are several methods for defining the interior climate including measured data, annual sine curves and

methods outlined in EN 15026 or ASHRAE 160 (ASHRAE, 2016; *EN 15026*, 2007). Coupled building energy models can also be used to define hourly inputs.

#### **2.3.4.5 Interior Transfer Coefficients**

Heat and vapour convection coefficients are included in hygrothermal models. Often constant values are obtained from standards, but Nusselt, Sherwood and Lewis relations can be used to estimate these coefficients as well based on fluid stream properties. Additional vapour resistances can be applied to the interior boundary condition to account for different paints, coatings or foils which may inhibit vapour transport. These are often given as  $S_D$ -values (equivalent length of still air). The addition of these vapour-resistant coatings can act like a vapour retarder and prevent moisture from drying out toward the interior.

### **2.4 Masonry Pathologies**

There are many building pathologies which are directly caused or exacerbated by moisture which hygrothermal modelling can predict. These pathologies can compromise the structural integrity, health and wellness issues of occupants, and contribute to the loss architectural features and material; some which may have historical significance. Building pathologies may be caused by excessive exposure to the elements (erosion, wind-driven rain, atmospheric pollutants), inherent vice (improper design or repairs) or damage (natural disaster, impacts,

graffiti). Alternatively, pathologies can be classified as being caused by decay, defect, or damage.

There are four primary pathologies in masonry which can be quantified through hygrothermal modelling: Freeze-thaw action, biological growth, corrosion, and efflorescence. There are other pathologies which are caused by excessive moisture such as soiling/staining or deconsolidation of mortar, but these are not quantifiable through hygrothermal modelling. Pathologies related to construction quality such as open joints, cracks, failed seals are difficult to explicitly include in hygrothermal models without using simple empirical adjustments to parameters.

#### **2.4.1 Freeze-Thaw**

Freeze-thaw action is a pathology which occurs in several types of porous building materials including masonry and concrete. The physical mechanism of freeze-thaw damage is the expansion of water when it freezes inside the pores of a material. The expansion exerts an outward force which if great enough, can fracture the material matrix and lead to a permanent strain on the material matrix. The greater number of pores which are filled (saturation) upon freezing, the greater the force exerted. Over time and repeated cycles, accumulated strain on the material can lead to failures in the form of thin sections of material delaminating or spalling away causing irrecoverable damage to the material. For

damaging freeze-thaw cycles which lead to permanent strain to occur we need both sufficient water inside the material's pores and repeated freeze-thaw cycles. If the material is sufficiently dry the material can undergo an infinite number of cycles without incurring damage. This makes freeze-thaw primarily a moisture issue.

For the analysis of freeze-thaw risk, it is important to know the level of saturation at which freeze-thaw damage begins to incur. This is known as the critical degree of saturation ( $S_{crit}$ ) and can be tested for in the laboratory (Fagerlund, 1977; Mensinga, 2009). This test is known as frost dilatometry. If the material has a higher water content than  $S_{crit}$  during the freeze stage of a freeze cycle, then a permanent strain is assumed to occur and this can be measured with a high-resolution caliper. The accumulation of these critical freeze cycles and permanent strain will eventually lead to delamination and spalling of material.

It is difficult to determine whether freeze-thaw conditions are occurring in-situ. Visual evidence of freeze-thaw damage can be difficult to find on a building, and suspected evidence may have been caused by another mechanism such as efflorescence/subfluorescence. *ASHRAE Guideline 34 – Energy Guideline for Historic Buildings* states “Freeze-thaw damage appears to be rare, even in insulated masonry buildings” (ASHRAE, 2019).

The moisture conditions inside the most critical parts of the wall are heavily influenced by the exterior climate and highly dynamic. Measurement techniques for freeze-thaw are also limited using commonly available sensors, especially at the elevated moisture contents needed for critical freeze-thaw action to occur and at the extreme outer fibres of the material where it is likely to occur (Ridout & McCaig, 2016).

The pore structure of the masonry also affects freeze-thaw action. Shear stress inside the pores resists ice from forming into its crystal state. The freezing point of liquid inside a pore can be calculated by a variant of the Gibbs-Thomson:

$$T_f(r) = T_0 - \frac{2\gamma_{IL}T_0}{\rho_l h_f r} \quad (2-22)$$

- $T_f$  = Freezing Temperature [K]
- $T_0$  = Reference freezing temperature [273.15 K at standard conditions]
- $\gamma_{IL}$  = Ice-liquid interface energy [ $\sim 0.025$  J/m<sup>2</sup>]
- $\rho_l$  = Density of water [kg/m<sup>3</sup>]
- $h_f$  = Latent heat of freezing [334 kJ/kg]
- $r$  = Pore radius [m]

This equation tells us that liquid in larger pores will freeze first before liquid in smaller pores. Using the moisture retention curve, we can calculate the threshold temperature which a critical freeze thaw cycle will occur  $T_f(S_{crit})$  given a specific degree of saturation. At higher freezing temperatures (eg.  $-2^{\circ}\text{C}$ ) only a few of the largest pores containing liquid will be able to freeze assuming that they are filled (from the moisture retention curve, they are the last to fill with water). The ice in these pores likely cannot exert enough force to cause a permanent strain. As the temperature decreases further, more pores will freeze, and they are more likely to be filled. This increases the chance that enough force will force will be exerted to crack the masonry matrix. Therefore the temperature which a critical-freeze-thaw cycles occur is less than  $T_f(S_{crit})$ . Equation 2-22 can then be used to calculate ice formation within the material when analyzing results to calculate the number of critical freeze-thaw cycles (Zhou et al., 2017). Salt concentration can also change freeze-thaw risk because the presence of salts will suppress the freezing point of water.

There are a few ways to calculate the number of freeze-thaw cycles. The simplest is a line-crossing method where a freeze-cycle is counted every time the temperature crosses either below or above  $T_f$ . The method used in the journal papers, is similar but assumes that the temperature must remain either above or below  $T_f$  for a minimum of  $n$  hours for a phase-change to occur. In these two

methods, if the saturation exceeds  $S_{crit}$ , a critical freeze-thaw cycle is counted. Another method is the FTDR Index introduced by Zhou (2017) which sums the difference between minimum and maximum ice contents during a freeze-thaw cycle.

$$FTDR\ Index = \sum_{cycle} (S_{Ice,max} - S_{Ice,min}) > 0.05 \quad (2-23)$$

This method considers that ice-formation is temperature and saturation-dependent and is more accurate than the line-crossing methods. The issue with this method in its current state is that it does not consider  $S_{crit}$  and that some building materials are more resistant to freeze-thaw than others. Repeated small formations of ice can inflate the FTDR Index even though they may be of inconsequential risk.

#### **2.4.2 Biological Growth**

It is unusual for biological growth to directly impact masonry, but it does affect adjacent materials such as wooden beam ends, interior finishes, and insulating materials. Biological growth is both a structural hazard for load-bearing wood assemblies and a health and wellness hazard. There are two types of biological growth of concern in buildings: rot fungi and mould fungi. Both require elevated moisture contents and warm temperatures to fuel their growth.

Wood rot fungi grows on wood and breaks down the molecular structure of wood (primarily lignin), which can lead to structural failures. Wood rot fungi require the presence of liquid water to grow. A safe limit for which fungi will not germinate or grow is at a moisture content of 20%. The minimum moisture content for the onset of growth is between 22-24% with optimum growth rate between 40-80% (Morris, 1998).

Mould fungi grow on the surfaces of materials. Their growth is governed by humidity and not liquid water. There are three primary methods for determining mould growth risk. The first is a simple threshold method of which there are several. The first is for RH to not exceed 80% and temperature not exceed 5°C on a monthly mean basis (Hens, 1990). Another is for the surface RH to never exceed 65% (CMHC, 1999). These simple thresholds have evolved to state that if conditions exceed RH = 80% and 5 °C for 30 days, or conditions exceed RH=98% and T = 5 °C for 7 days, mould growth will occur.

The second method is the isopleth model developed by (Sedlbauer, 2001). Using this method two isopleths are drawn as a function of relative humidity and temperature. The two isopleths LIM<sub>B</sub>I and LIM<sub>B</sub>II (Lowest Isopleth for Mould) denote the minimum thresholds for mould fungi to spore and germinate.

Substrate category I denotes bio-utilizable substrates (easily degradable materials) and substrate category II denotes substrates with porous structures

(plasters, mineral building materials, wood). Every hour where the temperature and relative humidity are above the isopleth increases the risk for mould growth. Similar concepts were previously developed by Clarke (1999) and Hens (1999), but Sedlbauer's model more thoroughly analyzed a wider range of mould species and is more conservative.

The third method is the Mould Index method developed by Ojanen et al (2010) and is recommended by the ASHRAE 160 standard. This model is unique from the others in that it considers both the intensity of growth during unfavourable conditions, but also the decrease in mould risk during favourable conditions. The Mould Index is presented as a time-series over the duration of the simulation period. The threshold for mould growth to initiate is if the Mould Index exceeds a value of 3.0. This model considers 4 categories of substrate (very sensitive, sensitive, medium resistant and resistant) with different parameters used in the calculations depending on the substrate.

### **2.4.3 Corrosion**

Metal elements embedded within a wall whether structural or non-structural are susceptible to corrosion. Corrosion is bad for the longevity of the metal, but also for the surrounding masonry or concrete. Corrosion causes the metal to expand

which exerts a force which can lead to cracking of the masonry or concrete.

Common examples of concern are lintels and re-bar.

For corrosion to occur, water molecules, oxygen and a free electron are required.

An anodic and cathodic reaction occur simultaneously to produce iron ions ( $Fe^{2+}$ ) which then combine with other ions to form one of many corrosion products ( $FeO$ ,  $FeO(OH)$ ,  $Fe_2O_3$ ,  $FeS$ , etc.):



The corrosion rate is dependant on the availability of water and oxygen, PH, properties of the steel, properties of the surrounding material, and availability of chlorides. If the wall is near saturation, air (oxygen) is displaced and is not as available, and corrosion will be less likely to occur.

A commonly used threshold for corrosion risk in hygrothermal modelling is time of wetness (TOW) from ISO 9223 (2012a). This is defined as the summation of time where relative humidity exceeds 80% and temperature exceeds 0 °C. A more

advanced method proposed by Marra et al (2015) which considers that the corrosion rate is dependant on both temperature and RH. The authors developed a corrosion curve for metal in a lime-gypsum mortar. Its applicability to other porous materials is uncertain. Corrosion rate is also dependant on the alkalinity and composition of the surrounding material (Carsana et al., 2015). This material-dependency cannot easily be included in hygrothermal analysis without laboratory analysis. There is debate about whether the corrosion rate peaks below saturation levels. The previous authors indicate that corrosion rate continues to increase or levels off above RH=95%. This is contradicted by other studies on concrete where corrosion rate peaked between RH=91-97% (Ahlström, 2014).

#### **2.4.4 Efflorescence**

Efflorescence is the formation of crystallized salts on the outer surface of masonry and other materials in the form of white crusts. Efflorescence is usually considered an aesthetic problem which only harms the visual integrity of the masonry. It generally does not physically damage the masonry because it is a deposition which can be cleaned off. However, the appearance of surface efflorescence can signal the presence of moisture issues and the potential of more serious salt crystal formation below the surface known as subfluorescence.

Subfluorescence is known to lead to material loss in the form of flaking, spalling, sugaring, and pitting of the masonry units and the mortar.

Efflorescence formation begins when water saturated with dissolved salts evaporates from the surface leaving the precipitated salts behind. The source of the dissolved salts may come from the masonry units themselves, the mortar, de-icing salts, or are absorbed from the atmosphere in marine climates.

Efflorescence usually appears in wintertime when the air is cool and dry and tends to disappear in warm and humid conditions. A proposed damage mechanism for subfluorescence is similar to that of freeze-thaw action with the expansion and contraction of salt crystals causing stresses within the pore network (Charola et al., 2007). The rate of formation and dissolution of salt crystals inside pores is determined by the types of salts in solution, their solubility, the pore size/curvature of the matrix, and external factors such as temperature and humidity (Lehmann, 2018). It is not practical to define critical degree of salinity (analogous to  $S_{crit}$ ) because solubility is influenced by the presence of other salts in the mixture.

It is possible to model salt transport in Delphin, but there are not many examples to be found in literature modelling salt transport in building envelopes (Nicolai, 2008). This model is capable of modelling various salt mixtures using the Pitzer-based model which accounts for the thermodynamic properties of the salt mixture

and their activities and solution density. The module considers diffusion of salts, phase transitions from super-saturated crystals, hydrated and dehydrated forms in solution, and the reduction in vapour pressure inside pores in the presence of salts.

#### **2.4.5 Other Pathologies**

There are other masonry pathologies which are caused or are indicative of moisture problems, but cannot be simulated through hygrothermal modelling.

Surface staining (those unrelated to efflorescence) such as those from atmospheric sources (sulphur dioxide, nitrous oxide, particulates from combustion), ionic sources or biological growth (moss, lichens) on the exterior surface are indicative of elevated moisture levels in the masonry and/or poor moisture shedding details. Accumulation of these stains can not only impact the aesthetics of the masonry, but change the pore structure and damage the masonry.

Atmospheric pollution from sulphur dioxide, nitrous oxide and particulates can to dry or wet acidic deposition on masonry surfaces. This can damage masonry through the formation of gypsum and/or epsomite crystals inside pores near the surface or the dissolution of carbonate. The rate of formation depends on the time of wetness and the chemical and pore structure of the material. The formation of

crystals can crack or exfoliate the surface of masonry causing mechanical damage. The addition of crystals can plug the surface pores changing the absorption and permeability characteristics (Charola, 1998; Hoffman & Niesel, 2008).

Leaching or washout of mortar is a pathology directly related to traditional lime-based mortars. Leaching occurs in mortars with high concentrations of lime binder when exposed to elevated moisture contents. The subsequent loss of the calcium in the mortar can lead to structural concerns and accelerated decay of mortar joints through crumbling and leaching. Uncarbonated calcium hydroxide ( $\text{Ca}(\text{OH})_2$ ) is more susceptible to leaching than calcium carbonate ( $\text{CaCO}_3$ ) and mortars with pozzolanic components. High moisture contents encourage leaching by mobilizing the  $\text{Ca}^{2+}$  ions and blocking the ingress of  $\text{CO}_2$  to form the less soluble calcite (Forster, 2007). I am not aware of mortar leaching risk being incorporated into hygrothermal models.

## **2.5 Hygrothermal Monitoring**

Hygrothermal modelling provides a record of the walls past or present state and point to the severity of an issues which have occurred. It will not inform you has to why those issues have occurred or what may happen in the future. This is where future analyses and modelling enter the equation – understanding of the

past and prediction of the future. Hygrothermal monitoring and modelling are not complete substitutes for one another, but should be viewed as complimentary to one another.

Collection of long-term monitoring is important because it indicates the current health of the wall, changing moisture conditions over time, and can be used to calibrate models. Monitoring data can also guide maintenance strategies and the risk/benefit of retrofit strategies such as adding insulation. Before beginning a monitoring program, it is important to decide where to monitor, what variables to monitor for, and for what duration the monitoring program should be.

### **2.5.1 Monitoring Locations**

Monitoring programs consist of measurement of the interior/exterior ambient conditions in tandem with surface and interstitial measurements. The interior ambient conditions of primary interest are temperature and RH. There are an array of sensors capable of doing these measurements and some data loggers are equipped with built-in internal temperature and RH sensors. The interior ambient conditions are informative of many issues. These include spotting conditions which are conducive to moisture issues (high RH in winter) or abnormal or out-of spec HVAC operation and control (excessively dry, overcooled in summer etc). Ambient sensors must be placed thoughtfully to avoid direct

sunlight, exterior wall surfaces which may be hotter or cooler than the ambient, and heat and moisture sources such as cooking, electronics, ducts etc..

Exterior ambient conditions can be measured on-site via a nearby weather station installation, or by relying on publicly available weather data. Other data to be obtained from the exterior include a wind-driven rain gauge mounted to the wall surface and surface temperature measurements to help estimate solar absorption and solar vapour drive.

In my experience, there can be large variability in the moisture conditions across different facades of a building. A section of façade may be bone dry and a façade a few metres away may be critically wet. Not all façades experience the same level of exposure, rain-shedding features or contact with patches of damp ground. Choosing which facades and how many facades to monitor is an important decision to make at the beginning of a monitoring project.

Consideration must be given to selecting an unbiased selection of walls. This means installing sensors on some walls which are dry, some which are wet, different floors, different orientations etc. If only the most critical areas are chosen, this can bias our opinion of the building's current health toward the negative and alter the approach to maintenance and intervention plans. Instead of targeted and localized maintenance, a more intrusive and widespread

intervention may get planned instead. Some retrofits such as interior insulation may be seen as too risky.

Interstitial measurements are required to understand the condition of the masonry. Placing interstitial sensors imparts a degree of intrusiveness to the finishes and/or composition of the wall assembly itself. Careful consideration should be given before installation of sensors to protect character-defining elements and how to route, conceal and protect wires and data loggers for aesthetics and security if the situation warrants it. Often it will be dictated that sensors be installed from the interior because of logistical or heritage concerns.

Sensors can be placed in internal cavities or be inserted into the masonry itself. Insertion into the masonry is intrusive and involves drilling out the mortar or unit (as in Section 3.1.2) or removal of units and mortar to place the sensors.

Intrusions should be minimized and any openings made for insertion of sensors should be repaired in like. The “observer effect” applies to monitoring because the act of measurement can disturb the transport physics in the wall. This can include construction moisture from repair materials, air leakage through imperfectly sealed holes, or different properties of repair material.

## **2.5.2 Sensors**

The three variables commonly measured are temperature, relative humidity, and moisture content (heat flux sensors and pressure differential sensors may also be used). Common types of temperature sensors include thermocouples and thermistors. Different types are available for the temperature range being measured and accuracy required. Temperature sensors are also incorporated into RH and MC sensors because the methods used to obtain the readings are affected by temperature.

### **2.5.2.1 Relative Humidity**

Relative humidity sensors are of resistance and capacitance types. There are numerous challenges to obtaining accurate RH readings in interstitial spaces. The ideal RH sensor for this application is compact, responsive, accurate throughout the wide range of temperatures (-20°C to 30°C) and relative humidities (30-100%) experienced in wall assemblies, can connect to a data logger, and not be susceptible to sensor drift (Cammalleri & Lagus, 2009). There isn't a cost-effective sensor on the market which perfectly meets all these criteria for hygrothermal modelling. The main issues for use inside walls are sensor drift and accuracy in high humidity. Sensor drift is caused by condensation, corrosion, salts or pollutants accumulating on the sensing elements and changing its

electrical properties. Hysteresis between wetting and drying can also impact recordings. RH sensors lose their accuracy at elevated RH. Cammalleri and Lagus list the accuracy of capacitance based sensors as  $\pm 2\%$  and  $\pm 3\%$  below and above 80% RH respectively. The Vaisala sensors used in the East Block monitoring project have an accuracy of  $\pm 5\%$  above 90% RH (Vaisala, 2011).

In masonry walls, it is common for the RH to very high ( $> 95\%$ ) as small quantities of absorbed moisture can translate into high RH. An uncertainty of 3% RH can result in a large uncertainty in the amount of moisture in the material being measured. Hence these two issues are of importance when monitoring RH in masonry and need to be considered when analyzing results.

#### **2.5.2.2 Moisture Content**

Measuring moisture content in masonry presents a unique problem, because there isn't a reliable method on the market which can continuously record moisture content in-situ. There is a combination of destructive, invasive, and non-destructive methods available. Some of these are set and forget devices connected to a data logger and provide continuous readings, while others are spot measurement techniques. Each method has its advantages and disadvantages and its appropriate applications. A comprehensive summary of

moisture measurement in masonry is provided by Agliata et al (2018) and Phillipson (2007).

#### **2.5.2.2.1 Destructive Techniques**

A destructive technique is one where a sample from the building is removed for measurement of water content. Destructive techniques use gravimetric weighing or the calcium carbide technique to determine the moisture content of a sample removed from the wall. This method has obvious limitations that mean it is not recommended for long-term measurement in heritage buildings. First, it is a spot measurement technique, with limited repeatability as the water content can only be measured once. Second, the process of removing and repairing samples may damage or destroy heritage material. And third, it is prone to the observer effect, because it heavily disturbs the system being measured.

#### **2.5.2.2.2 Invasive Techniques**

Non-destructive techniques can be classified as invasive and non-invasive. An invasive techniques require localized disturbances to insert a probe and may cause minor damages and loss of some heritage material. It differs from a destructive technique in the amount of material affected is minimized and large sections are not removed which then need to be repaired. With invasive and fully

non-destructive and non-invasive techniques, indirect methods are required to determine the moisture content (compared to gravimetric methods).

One such method is to use wood or gypsum plug sensors also known as duff gauges which can be inserted into a drilled cavity in the masonry (SMT Research, n.d.). These were used in the Southwest Tower project. These are electrical resistance-based sensors and work on the same principle as hand-held moisture meters for wood. As moisture content increases, the electrical resistance between two wires in the sensor decreases. The sensors measure the moisture content of the wood which can theoretically be translated into the moisture content of the masonry material if both moisture retention curves of the wood and masonry are known. One known issue with this process is that if there is uncertainty in both material's curves (hysteresis, natural variation), and therefore the uncertainty in the masonry's moisture content is magnified.

These sensors work well in damp walls but begin to lose accuracy at elevated moisture contents. Wood based sensors have been reported to lose accuracy above 22% MC (Ridout & McCaig, 2016) and have only been demonstrated to work accurately below 15% MC, which is representative of a relatively dry wall (Walker et al., 2016). The presence of salts in the wall may also affect the readings because the ions may change the electric resistance of the water.

Typical hand-held moisture meters have been studied for their effectiveness on

stone (Eklund et al., 2013). The authors noted that the readings should be treated as relative, instead of actual moisture contents.

Other probe-like invasive sensors for measuring moisture content are based on electrical capacitance, electrical impedance, thermocouples and heat capacity, or propagation of electromagnetic signals. A capacitance sensor was developed at the University of Manitoba and trialled at Parliament Hill (Thomson et al., 2013), but from conversation with a Public Works technologist the sensor did not perform reliably in the field.

Impedance based sensors are similar in structure and work on similar principle to resistance sensors but use alternating current instead of direct current. These sensors have been tested in the laboratory and in-situ in German heritage buildings (Lehmann, 2018).

Thermocouple based sensors inject a finite amount of heat energy through an electrical pulse which heats the surrounding material (Kubičár et al., 2010; Phillipson et al., 2007). The moisture content can be calculated based on the temperature increase, heat capacity of the dry material, and the greater heat capacity of water. A wetter sample will have a smaller temperature increase.

Time Domain Reflectometry (TDR) are sensors based on the principal of the propagation of electromagnetic signals and dielectric constants of water and the media (Černý, 2009).

A common disadvantage with these sensors are their reading's temperature-dependence and the susceptibility to the presence of salt-ions. They also need to be calibrated to each material, which hurts their deployability to a variety of building typologies (Lehmann, 2018; Thomson et al., 2013).

#### **2.5.2.2.3 Non-invasive Techniques**

Non-invasive techniques are strictly non-destructive. They are capable of measuring moisture with touching or altering the heritage fabric in any fashion.

This is especially beneficial if analyzing walls that have historic finishes, artwork, frescoes etc. which must be left untouched. Non-invasive techniques have been developed using an assortment of imaging techniques. Some are more accurate in measuring moisture content than the previously mentioned invasive sensors. Some of these techniques have their advantages and disadvantages relative to one another, and compared to the invasive sensors.

Infrared thermography is the most common imaging method and the least accurate because the results are qualitative and not translatable into a moisture content. This method is good for detecting the relative difference in moisture

contents in the cameras field of view. Damp areas from leaks, run-off etc. can be detected because wet materials have a greater heat capacity and take longer to heat and cool down.

Non-invasive Imaging techniques can also be used to detect salt contents. Weritz et al. (2009) used Spectral-Induced Polarization (SIP) to determine salt content profiles in an historic German church. The moisture contents were validated with microwave transmission measurements. The salt analysis was found to be inconclusive when validated with Laser-induced Breakdown Spectroscopy (LIBS).

Nuclear magnetic resonance (NMR) measures the increases molecular mobility of water when exposed to a magnetic field. Their usage has been restricted to laboratory experiments but portable devices have been developed but can only sense depths of approximately 25 mm limiting their usefulness in thick assemblies (Blümich et al., 2010; Di Tullio et al., 2012; Oligschläger et al., 2015; Proietti et al., 2021).

Microwave and radar techniques such as ground-penetrating radar use an electromagnetic field to find the moisture content. The electromagnetic field loses energy as it interacts with water and the material matrix at different rates. The moisture content can then be back-calculated. These techniques have the disadvantage of being most heavily influenced by shallow layers compared to deeper layers in the assembly and is prone to inaccuracy if there is a moisture

gradient or voids within the wall (Agliata et al., 2018). As a result its usefulness is limited to near-surface measurements, instead of the full cross-section of the wall assembly.

Radiation attenuation techniques using X-rays, gamma rays or neutrons have been used to measure moisture content in masonry in laboratory conditions with small samples (De Freitas et al., 1996; Derluyn et al., 2011; Kumaran & Bomberg, 1985; Roels & Carmeliet, 2006; Rouchier, 2012; Zhou et al., 2020). Radiation attenuation is regarded to have the highest resolution and accuracy of the non-invasive imaging techniques, however it suffers from limited investigation depth, health and safety concerns because of radiation, and the equipment is too complex (Agliata et al., 2018; Phillipson et al., 2007). This limits radiation attenuation's usefulness to in-situ monitoring. As a result this technique is limited to laboratory settings where the physics of moisture transport can be explored.

Some of these non-invasive methods are capable of probing into the depth of a wall to obtain a cross-sectional moisture profile, however this is somewhat limited in accuracy and depth. As a result they tend to give a clear picture of moisture conditions near the surface.

One of the disadvantages of these techniques is that they are snapshots in time. It is not practical to obtain a time-series of data over the long-term to observe changes in moisture. Another disadvantage regards their logistics. The devices

are not as portable, cost effective (operational and capital), able to be deployed in numbers to capture multiple surfaces, or able to be installed over the long-term, especially if longer-term moisture responses of the masonry are being sought.

The difficulty in measuring elevated moisture contents is an issue when trying to verify the risk for freeze-thaw especially, and to a lesser extent corrosion and biological growth. It is a challenge to calibrate models of high-moisture walls with confidence because of this challenge. Despite these drawbacks, these sensors are still useful for observing seasonal patterns, trends over an extended period, gathering a snapshot of moisture distribution of a wall surface, and judging the overall health of a wall.

## **2.6 Uncertainty in Hygrothermal Modelling**

All engineering models carry a degree of uncertainty. This is because of many reasons from the uncertainty range in model inputs, to assumptions made to simplify complex physics at the microscopic scale. Modelling of heritage masonry buildings is no different in this regard. Part of this can be explained by a lack of guidelines for model inputs that are appropriate for historic buildings (Webb, 2017) or the limited use of limit-states design concepts in building physics (De Rose et al., 2014). Uncertainty in hygrothermal models can lead to the following assertions being made:

- The uncertainty in material properties and boundary conditions reduce our confidence in the model's ability to accurately capture or predict the true extent of moisture issues in an assembly.
- The wide range of uncertainty in material properties and boundary conditions compounds implies that the results have a wide range of uncertainty
- The lack and difficulty of calibration can imply that there is limited validity to the models
- Hygrothermal models are oversimplifications of reality

The manner in which uncertainty can alter a hygrothermal model are demonstrated using three general examples: material properties, boundary conditions and geometry, construction and imperfections.

### **2.6.1 Material Properties**

Correctly defining material properties is an important step in any engineering simulation to get representative results. In hygrothermal models of heritage buildings, this is especially crucial. One of the issues is that material properties can have a large range of values for materials which are in the same general

class (ie. sandstone, clay brick, lime mortar). Published material properties for sandstone will be used as an example.

Figure 2-1 and Figure 2-2 shows the moisture retention curve and liquid conductivity curves for all materials in the Delphin library for the material class sandstone. As is evident, there is a wide variety of shapes to the moisture retention curve and the difference between the max and min liquid conductivity is six orders of magnitude at some points on the curve. For thermal conductivity, the ASHRAE Handbook gives a range for sandstone from 1.88 to 6.2 W/m-K (ASHRAE, 2013b), the Delphin library gives values from 0.96 to 3.28 W/m-K, while a study by Pechnig et al (2007) gives values ranging from 1.5 to 4.0 W/m-K. Sandstones exhibit this wide range of values partially because of their chemical composition and the conditions they were formed in underseas.

Depending on which end of the range of material properties you choose for your model, a different story on the health and performance of the wall can be told. Consider, in the absence of material testing data for a sandstone wall that is being simulated. Which liquid conductivity will you use? Do you choose one of the minimum, maximum or median curves? Selecting the maximum value will most likely give the worst-case scenario and give the impression that the wall is at high risk. Selecting the lowest value will give the impression it is low risk, and a median curve will strike a balance between the extremes but may still be too

optimistic. In a published guide, the Society for Protection Buildings (SPAB) suggests doing simulations with all materials in the library of the general class 'brick' and decided that the worst-case scenario should be used as a basis for retrofit modelling (Browne, 2012). The problem with this approach is that it is inherently too conservative and may give an alarmist impression about the health of the wall.

The naturally wide range of properties in sandstone highlights the value of doing material property testing on samples from the building. However, this too may come with a wide range of uncertainty. For a project that I worked on, material testing of several stone, brick and mortar samples taken from the building was undertaken. These were purportedly from the same quarry/manufacturer and of similar age. The testing results gave as large as an order of magnitude difference in the absorption coefficient between samples which means water absorbs ~ 100 times faster in one sample than another. Other tested properties such as  $RH_{80}$ , and  $\mu$  had similarly large ranges. Again, the question becomes which set of material properties do you choose to form a representative baseline for decision-making? Should the min, max, mean or median be used?

The aging of materials from decay or damage can also change material properties over time. This has been illustrated by several authors regarding micro-scale cracks, freeze-thaw effects and mortar damage impacting absorption

(Kočí et al., 2018; Li et al., 2018; Roels et al., 2003; Rouchier, 2012; Smyl et al., 2016).

The above examples illustrate the issue with a deterministic approach to hygrothermal modelling. A stochastic approach may be more appropriate as first outlined by Salonvaara (2001). Further examples of stochastic hygrothermal models have been performed often with a view toward calibration (Akkurt et al., 2020; Freudenberg et al., 2017; Goffart et al., 2017; Gutland, Bucking, et al., 2019; Sahyoun et al., 2020; Zhao et al., 2011). Some blocks to stochastic hygrothermal modelling in practice, include the increased set-up and simulation time and lack of easy-to-use software that can handle this problem.

### **2.6.2 Boundary Conditions**

As mentioned in Section 2.3.4, the exterior boundary conditions have a significant influence in hygrothermal modelling of heritage masonry, especially wind-driven rain. The exterior boundary conditions are defined by the weather file used.

Hygrothermal weather files are available for many large cities worldwide.

However, they may not be available for rural areas, and actual meteorological weather data complete with hourly rainfall and solar data can be difficult to obtain.

If the standard weather files are not suitable, then the user needs to create their own weather file.

There are some challenges in developing accurate weather files for use in hygrothermal models. Weather files can be constructed using publicly available data or through a private weather station (which can be site-specific).

Publicly available weather data can have varying degrees of completeness.

Environment Canada has published data for 8760 weather stations, many which have been decommissioned (*Environment and Climate Change Canada, 2020*).

Most stations measure temperature, relative humidity, wind speed and direction.

Only a small percentage of Environment Canada's stations measure variables important to hygrothermal modelling such as precipitation, solar radiation, long-wave radiation, or observational weather codes. Other methods and sources are required to fill-in the missing data including satellite-derived weather information

#### **2.6.2.1 Precipitation**

For the Environment Canada weather stations that do publish precipitation data, it is most often in daily format, and not in an hourly format required for good hygrothermal simulation. Hourly resolution is important because a short intense storm can induce a different hygrothermal response to that of a persistent drizzle. A method is needed to convert daily precipitation to hourly or another data source is required. There are a few methods which I have used to obtain hourly weather precipitation data in the absence of measured hourly data:

1. Apportion daily precipitation equally for the whole 24 hours. This is not ideal because persistent rain can skew the results and does not allow for the proper amount of drying periods.
2. Use the observational weather codes to apportion daily precipitation. This method is better, but these codes are often incomplete and are generally descriptive (drizzle v. storm) and do not reliably indicate quantity of precipitation for that hour.
3. Determine “characteristic hourly rainfall patterns” and apply them to the daily or monthly precipitation data (Schroeter, 2007). This method uses realistic daily weather patterns, but there is no guarantee that the characteristic patterns match the actual weather patterns.
4. Use satellite-derived precipitation data from the National Center for Atmospheric Research (NCAR) or the Consortium of Universities for the Advancement of Hydrologic Science, Inc. (CUAHSI) project (CUAHSI, 2020; Saha et al., 2011). This gives hourly precipitation values as derived from satellite-based imagery but is only loosely calibrated to local ground measurements.

Method 4 solves the question of which hours of the day precipitation and how much fell. The sum of the hourly precipitation data from NCAR and CUAHSI does not reliably match Environment Canada ground readings (Figure 2-5).

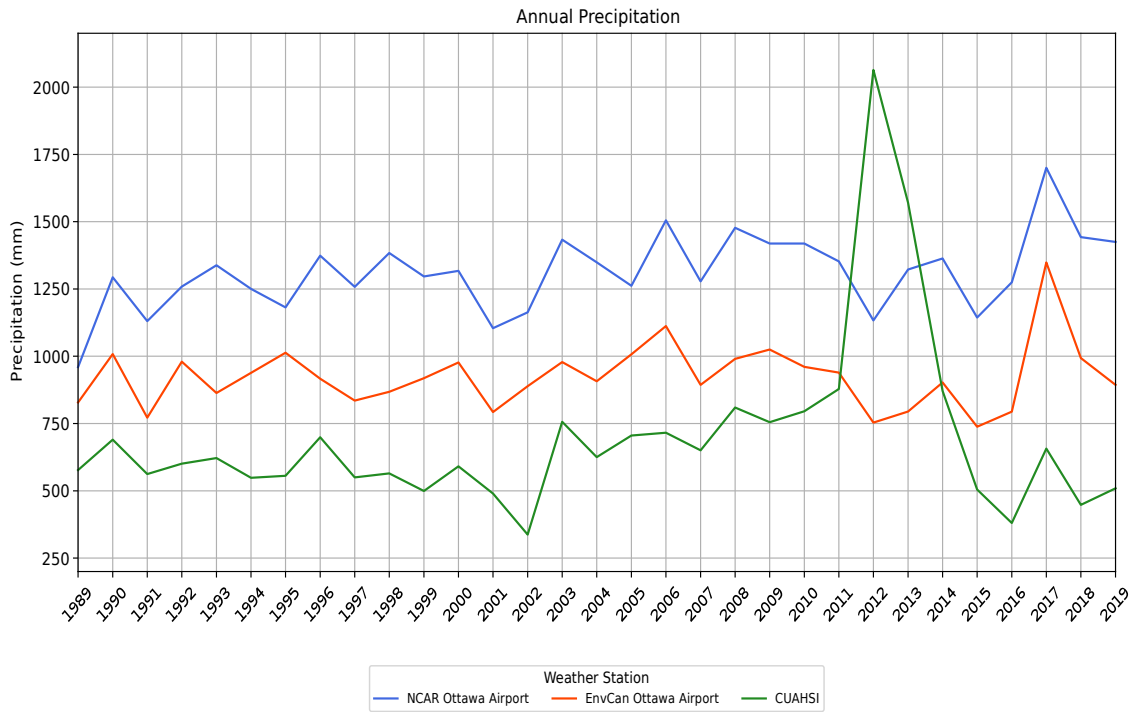


**Figure 2-5: Annual precipitation for Ottawa. (Weather Station 49568 is from the Ottawa International Airport)**

CUAHSI tends to underpredict precipitation, while NCAR tends to overpredict compared to ground measurements from the Ottawa International Airport. Trends were similar when broken down at a monthly basis. Intuitively, it is logical to think the ground measurements are most accurate. Commonly used tipping-bucket rain gauges have an error ranging from -9.3 to -23% meaning that the ground

measurements are underestimating precipitation (Pollock et al., 2018). The implication of this is that the rainfall intensities used in Equations 2-17 to 2-20 are underestimated and consequentially wind-driven rain absorption is underestimated. Assuming this correction, the actual precipitation may be closer to the NCAR data.

#### **2.6.2.2 Temperature, RH, Wind velocity**

Precipitation is not the only variable which shows different values depending on the source of the data. Figure 2-6 - Figure 2-8 show monthly data from five Ottawa area weather stations: Environment Canada Weather Station 49568 (Ottawa International Airport), Environment Canada Weather Station 30578 (Central Experimental Farm), NCAR (Ottawa International Airport), CHEeR House (Carleton University Campus) and CBR Weather Station (Centre Block).

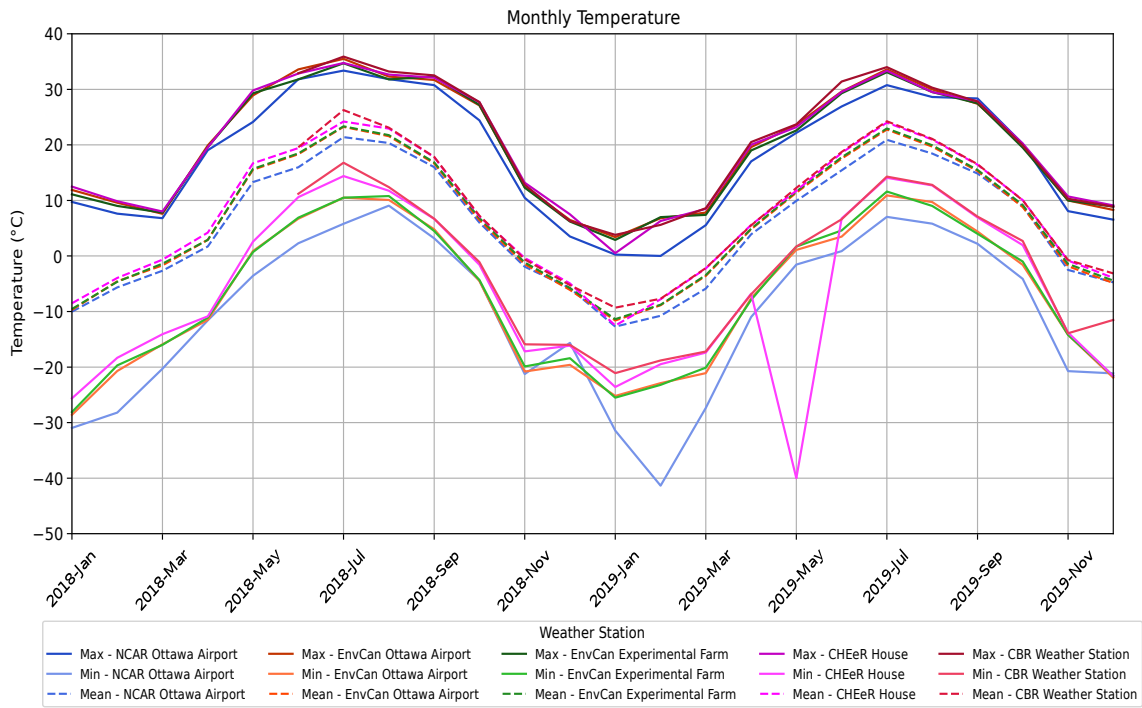


**Figure 2-6: Monthly temperature data from five Ottawa weather sources**

There is a noticeable difference in temperature between the various weather stations, with average temperature differing by as much as 3 °C on some months. There also seems to be a bias with some weather stations consistently measuring higher (CBR) or lower (NCAR) temperatures than other stations. This can be caused by several factors such as urban heat island (CBR is roof mounted), different exposure to wind or solar, or sensor bias. The difference in temperatures has implications for hygrothermal modelling, but also for energy modelling, with the number of cooling degree-days and heating degree days changing. Choice of weather data source could have implications on calibration.

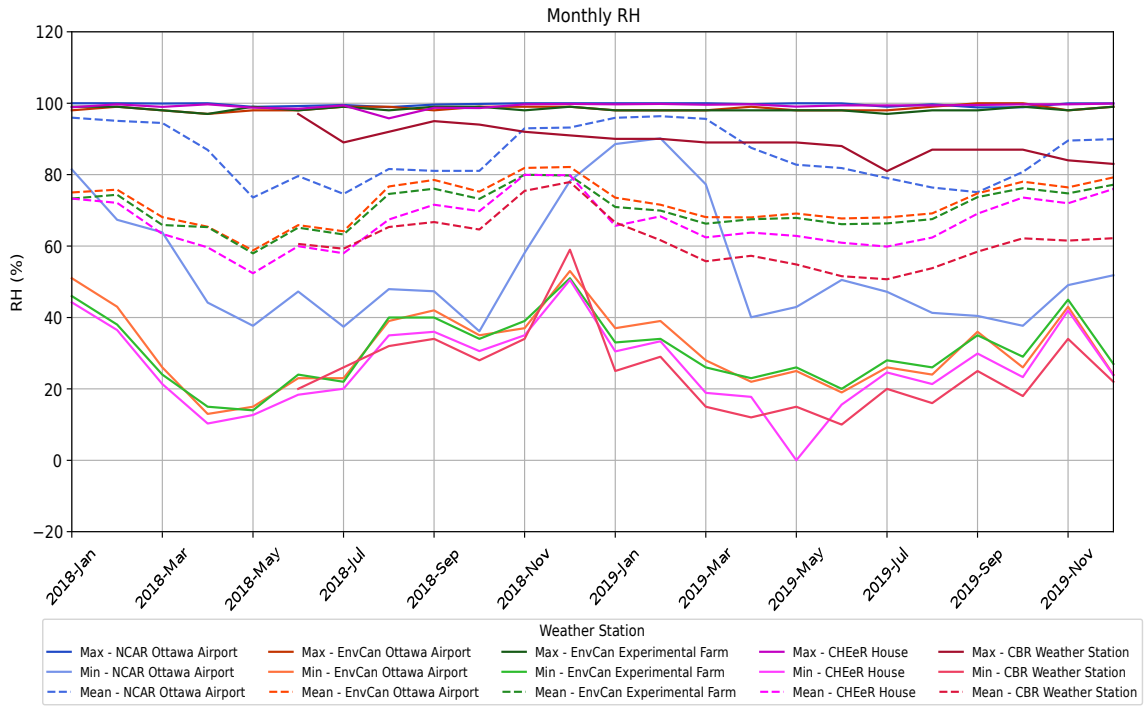


**Figure 2-7: Monthly relative humidity data from five Ottawa weather sources**

There is a large discrepancy in average RH between the five weather stations. The NCAR has extremely high and unrealistic RH, especially in Winter. The elevated RH in the data, may help to explain the overestimation of precipitation and the excessive number of hours with precipitation in the NCAR data. The NCAR data should not be utilized for RH because of the discrepancy compared to the ground stations.

Both Environment Canada stations are consistent with each other while the CHEER House and CBR Weather Station have considerably lower RH. This has implications for hygrothermal modelling because the exterior RH/vapour pressure

controls the rate of evaporation. Models using the CBR data will dry quicker than models using the NCAR and Environment Canada models will.

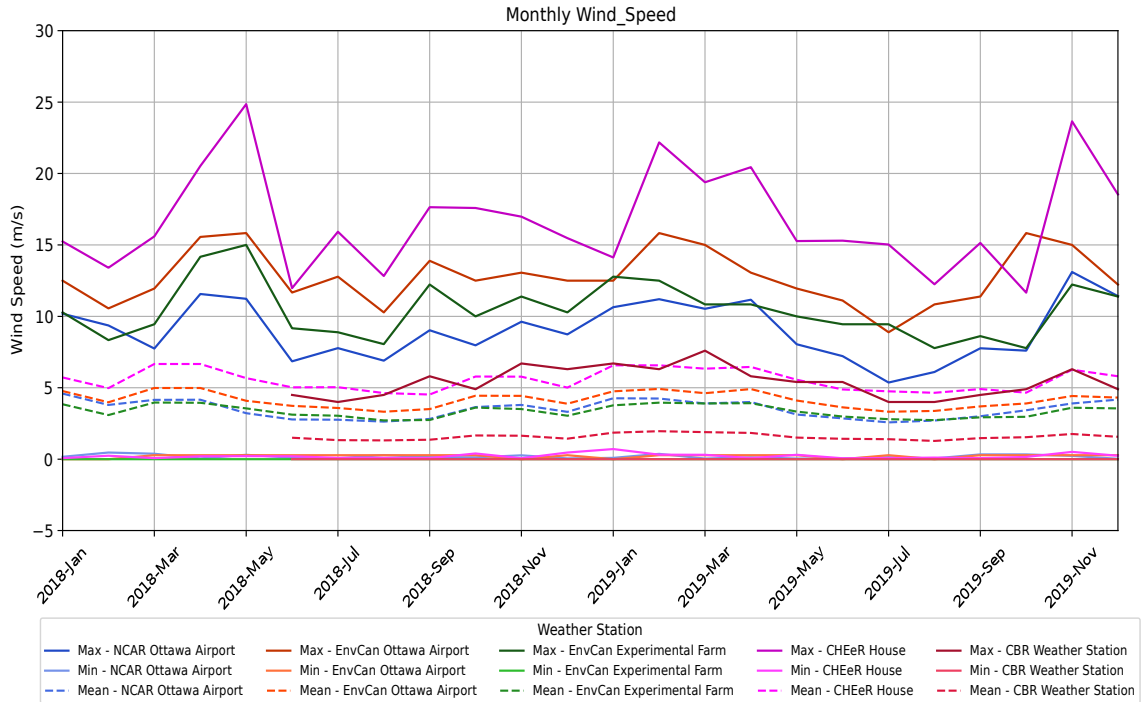


**Figure 2-8: Monthly wind speed data from five Ottawa weather sources**

There is a significant difference in wind speed across the five weather stations.

The data from the CHEeR house has the highest wind speeds and the CBR has the lowest average wind speed amongst the five weather stations. The most likely explanation for this is exposure. The CBR weather station is rooftop mounted and may be shielded from the towers on that building, and/or turbulence reduce the measured speed. The CHEeR does not have many neighbouring buildings and obstructions and is towards the top of a hill. The difference in wind speed matters

because wind-driven rain is proportional to wind speed. If the CBR data is used instead of the Environment Canada, the amount of wind-driven rain can be reduced by as low as 25%. The wind-driven rain equations account for this to some degree with their exposure factors. Another reason this affects a hygrothermal model is that the convection coefficients are a function of wind velocity.

### **2.6.2.3 Radiation**

Solar radiation (both short-wave and long-wave) is another important climate parameter in which hourly data is required and is difficult to find in Canada. Environment Canada does not publish this data for any major cities. To obtain this it is necessary to rely on private weather stations, satellite-derived data, or use approximate methods (based on cloud index, solar geometry etc.).

For the calibrated models of the Southeast Tower (Sections 3. and 4.), radiation data from the CHEeR House was used which contained sub-hourly ground horizontal and direct normal radiation. For the actual meteorological years used in Section 5. and 6., hourly satellite-derived data from the NCAR was used. An issue with using satellite-derived data (and other approximated methods) is that it only provides the Ground Horizontal Irradiation (GHI) and one of the other two necessary components Direct Normal (DNI) or Diffuse Horizontal (DHI) must be

estimated from GHI. One such method is the DISC/Maxwell or Perez models (Maxwell, 1987; Perez et al., 1992). Hourly long-wave radiation was also sourced from NCAR data.

### **2.6.3 Geometry, Construction and Imperfections**

It is common procedure to make the following assumptions for hygrothermal modelling:

1. Materials are homogeneous. There are no localized variations in pore structure, physical properties or chemical composition.
2. Adjacent materials are in perfect contact with each other.
3. There are no imperfections in the materials or assembly.

For masonry walls, these assumptions are not always valid. Building of what was discussed with uncertainty in material properties in a class of materials and samples of the same material taken from a building, the unit or mortar joint may have inhomogeneous material properties. Examples of inhomogeneous materials include sedimentary stone bedding with clayey deposits (stylolites), bricks with a fire-hardened surface and relatively softer core, and concretes with decorative aggregate finishes.

Assumption 2 assumes perfect contact between materials (e.g. brick/mortar interface) meaning that there are no small gaps in between. This is rarely a good assumption because it has been demonstrated that there is imperfect contact between unit and mortar (Figure 5-2). This exhibits itself as interface resistances affecting transport perpendicular to the interface only and transport parallel to the interface similar to fluid flow in a fracture. This concept was explored in Section 5.

- Masonry Interface Modelling.

There are other examples of imperfections in construction which influence results if not properly considered. Direct leaks into the middle of the assembly are one example. In practice, this is often done as a resilience exercise. Imperfect membranes such as vapour retarders and air barriers are rarely considered and can contribute to serious problems if breached.

A specific example of imperfect construction are the walls of the 1867 Wing of the East Block. Ground-penetrating radar and dismantling of select walls have shown many walls have a large percentage of voids in the rubble core. The presence of voids can alter heat, vapour, and liquid transfer in the wall. The relatively still air in the voids will have a lower thermal conductivity than the sandstone, and the voids can behave like mini-rainscreens causing capillary breaks and reducing vapour resistance. This can form thermal bridges and preferential moisture transfer paths. The wythes of the rubble core walls do not have consistent repeated

geometry. Different sized stones are used on the exterior and inner wythe, while the core is a seemingly random mixture of different size stone shards, mortar grout and air voids. This geometry is tough to characterize. The presence of voids and how they are orientated could theoretically influence heat and moisture transfer. If the voids are laid out in series vs. in parallel will change heat and moisture migrate through the wall. The example of the 1987 Wing of the East Block was explored in Section 6. - Spatially-stochastic geometry in masonry-walls.

In general, two and three-dimensional interactions in hygrothermal modelling are poorly understood and are rarely modelled in practice. One-dimensional modelling of masonry is still prevalent even though masonry is a two-dimensional matrix of sometimes vastly differing materials. This is a similar error to that of energy modellers not accounting for thermal bridges in their energy models until recently. Many masonry conservation specialists will say drying occurs through the mortar joint, yet it does not always get modelled.

Two-dimensional hygrothermal models have the drawback of increased complexity, set-up time, and greatly increased computational time. One-dimensional models may be appealing if many iterations are being modelled. Downscaling two- or three-dimensional geometry requires some assumptions and modifications to recreate the problem as faithfully as possible. Some

techniques used include, modifying material properties on weighted basis between brick and mortar, alternating layers of masonry and mortar and running separate models for lines through the brick and mortar joint. These methods have been shown to deviate significantly from the 2D results as shown in (Bottino-Leone et al., 2021; Little et al., 2015; Nagy, 2019) and was also demonstrated in Section 6. where simplified one and two-dimensional models were often well outside the range predicted by the complex models.

It is tempting to think that simpler models are inferior and adding more complexity (geometric complexity in this discussion) and fidelity into the models will always produce better and more accurate results. This is not always the case, as simple inverse models based on multivariate regression have proven satisfactory under many circumstances (eg. energy model calibration). There are instances where the added complexity or parameters may not have the expected magnitude of effect. In some instances it is perfectly acceptable for complex physics or geometries to be downscaled into a single parameter. This is accepted practice when modelling convection on surfaces which is a function of many variables (air velocity, surface roughness, etc.). Sensitivity analyses can assist in determining which model parameters can be set as fixed, minimized, or even neglected. Modelling effort and resources can be directed towards understanding and tuning the parameters which do have a significant role. Ultimately, it is not accurate to

say that a complex model is more accurate than a simpler model until you compare it to the experimental data for validation.

#### **2.6.4 Model Calibration and Validation**

Calibration and validation of hygrothermal models poses a significant challenge. Validation and calibration of models to in-situ measurements of masonry can be difficult because of challenges regarding sensors, material properties, boundary conditions, and the effects of decay and/or damage. Calibration and validation are essential for establishing a baseline model for forensic investigation, assessing the current condition of an envelope, and examining retrofits.

Both the calibration and validation processes require measure data for which to compare against. This data can come from in-situ monitoring (as in Chapters 3. and 4.) or from laboratory data. In-situ monitoring of masonry is rare in practice, but is becoming increasingly common.

Model calibration is the process of tuning a unique set of model parameters, so that they confirm a set of measured data within an acceptable limit. There aren't any formal standards or guidelines for calibrating hygrothermal models to measured data, similar to that of ASHRAE Guideline 14 or inverse methods for energy models (ASHRAE, 2014). With energy models, data such as monthly energy bills and sub-metering of electrical loads are used and are more readily

available compared to data with which to calibrate a hygrothermal model. For hygrothermal models of envelopes, we seek to calibrate using interstitial monitoring points within the building envelope. The more points distributed across the envelope the better for accurately capturing the transport characteristics of the envelope.

Using ASHRAE Guideline 14 as an example, calibration is considered complete once a statistical criteria is met. Here, it is either an hourly normalized mean bias error (NMBE) of  $\pm 10\%$  or a coefficient of variation of the root mean square error (CVRMSE) of  $\pm 30\%$ . With hygrothermal modelling, acceptable values for these statistical measures have yet to be defined.  $10\%$  would be an unacceptable inaccuracy when calibrating to a state variable such as temperature, humidity, or moisture content. In the absence of an established acceptable calibration target, an optimization process can be used for calibration. This was done in Chapters 3. and 4. where the model was optimized by using a training data set and searching for the minimized RMSE between the measured temperatures and modelled temperatures. The calibrated models can be validated using a testing or validation data set to ensure the calibrated model performs acceptably when subjected to different circumstances.

Hygrothermal models can also be validated to laboratory measurements which may or may not be representative of real-world conditions. As a final resort models can be validated against theoretical models or equations.

### **3. Hygrothermal monitoring and model calibration of an historic masonry tower**

This section contains content published in:

Gutland, M., Bucking, S., & Santana Quintero, M. (2019). Assessing Durability of Historic Masonry Walls with Calibrated Energy Models and Hygrothermal Modeling. *International Journal of Architectural Heritage*, 1–17.

<https://doi.org/10.1080/15583058.2019.1618976>

#### **3.1 Preface**

This project was originally conceived as a hygrothermal monitoring project of the Southwest Tower of the East Block Building in Ottawa, Ontario. The initial goal of the project was to create a calibrated hygrothermal model based on the monitoring data obtained. After the sensors were installed throughout the Tower and data was collected for over one year, the hygrothermal model calibration was attempted. For reasons that will be discussed, the hygrothermal model calibration process was not successful, and the results would not have been acceptable to an academic journal. The findings from this process are applicable to the discussion of this thesis and are presented in this preface sub-section.

While analyzing the data to be used in the hygrothermal calibration, it was noticed that there was some interesting energy modelling calibration and hygrothermal model applications that could be done on the tower as a whole because of the unique interior climate observed in the data. This became the basis for the paper published in the *International Journal of Architectural Heritage*.

The data collected as part of the in-situ monitoring project was used to support the published journal paper in this section and the conference paper in the following section (4. - Calibrated Envelope Modelling).

### **3.1.1 Calibrated Hygrothermal Modelling**

Obtaining accurate in-situ data is important for calibrating models with confidence. As discussed in Section 2.5 - Hygrothermal Monitoring obtaining accurate long-term in-situ moisture readings can be challenging to obtain and a significant measurement error needs to be accepted in many instances. Partly this is due to the performance of the sensors at elevated moisture, the destructive nature of most viable long-term monitoring instruments and the potential for salts in the masonry affecting the reading.

As discussed in Section 2.6 - Uncertainty in Hygrothermal Modelling, there are significant uncertainties in material properties and boundary conditions in

hygrothermal modelling. In the context of the Southwest Tower project, this was evident by a lack of complete material property testing data (especially for the mortar) and some uncertainty over the boundary conditions, specifically the amount of water being presented to the outer surface via wind-driven rain or through run-off. The tower (and the building in general) has poor water shedding features and you can envision a cascading waterfall effect of water falling off a roof edge falling onto a projecting stone surface below. The poor water-shedding plus the Southwest Tower being tall and exposed to wind mean it is challenging to determine the wind-driven rain exposure factors in Equation (2-17) or (2-19). The diagrams in 2-4 likely have limited applicability to this case.

With these uncertainties in mind, the concept of using a calibrated model to estimate unknown material properties and exposure factors seemed like a plausible method. This would be done in lieu of doing more lab testing or relying on engineering judgment and/or worst-case scenarios to model the building. The model would be calibrated off of moisture content and RH which were inserted into the wall. Parameters which could be changed included porosity, thermal conductivity, absorption coefficients, rain exposure factors, internal water sources, air exchange amongst others. While the ratio of mortar to stone may have been difficult to conclude, it was thought that “effective absorption coefficients or vapour resistance factors” could be inferred through the process. It

was also anticipated that responses to rain events or seasonal patterns could be observed and replicated through the calibrated models.

### **3.1.2 Experimental set-up**

A network of sensors additional to those referred to in section 3.6.1 were installed for the purpose of monitoring moisture conditions inside the masonry. Three monitoring stations were selected on three unique wall sections of the tower.

They were:

1. **Fourth-floor South façade** – near the water-shedding course. Highly exposed and high likelihood of moisture problems. Exposed to more freeze-thaw cycles and solar vapour drive.
2. **Fifth floor East façade** – area under windows which had recently been re-pointed and known to have moisture problems.
3. **Sixth floor South façade** – relatively sheltered area compared to the other two stations. Exposed to more freeze-thaw cycles and solar vapour drive.

At each monitoring station moisture content and RH sensors were inserted into the wall at approximately 1/3 and 2/3 depths into the wall. To install the sensors, holes needed to be drilled from the interior side. During the drilling, the drill would

often be met with little or no resistance indicating soft and sandy mortar or the presence of a void. These changes were noted at their corresponding depth. Duff gauges were inserted to measure moisture content. First, gypsum sensors were installed and then afterwards wood sensors were installed. RH sensors were also placed in holes next to the moisture content sensors. Both the MC and RH sensors recorded the interstitial temperature. The holes were then filled-in.

More stations and more interstitial sensors would have been beneficial, but we were limited by funds and the number of dataloggers available. We were not able to install equipment from the exterior because of logistical and heritage considerations. Being able to place sensors nearing the exterior face could have allowed for better measurement of the rain absorption response of the wall.

### **3.1.3 Hygrothermal monitoring results**

The results from the fourth and fifth floor stations were not usable in the end. The gypsum moisture content sensors were outputting a constant 1000Pa (RH >> 99%), which was the limit of their sensing range. This indicated an extremely wet and saturated wall and prompted a switch to the wood sensors on these two walls to see if more resolution could be found in the data. The wood sensors were not much more informative with readings constantly >> 30%MC<sub>wood</sub> which was outside the sensor's practical range. Essentially these two walls were saturated in

the core and the hygrothermal responses to the stimuli of changing boundary conditions could not be observed. It is a moot exercise to calibrate a constantly saturated wall assembly.

The sixth floor station showed more promise than the other two stations for calibration. The wall was relatively dry and there were fluctuations in the data that indicated some dynamism in the wall. This data was used for hygrothermal calibration.

#### **3.1.4 Calibration**

The hygrothermal modelling calibration used a similar calibration technique as done in the calibrated energy model (refer to section 3.6.2.4). GenOpt's Particle Swarm Algorithm was used to find the minimized RMSE based on the difference between the measured and modelled RH at 1/3 and 2/3 distance into the wall. A 2-D model similar to that shown in Figure 4-1 was used. Parameters which were changed in each iteration included:

- Thermal conductivity and heat capacity of the stone and mortar
- Absorption coefficient of the stone and mortar
- Vapour resistance factor of the stone and mortar
- Porosity of the stone and mortar

- Rain exposure coefficient
- Magnitude of water sources and air sources in the rubble core
- Air sources in core

The calibration of the model was not deemed a success in terms of achieving an acceptable minimized RMSE, or the quality of the fit. Figure 3-1 shows the fit of the calibrated model (dashed) to the measured data (solid). The model results do not share the dynamism of the measured data and there are unacceptable differences of up to 15% between the two lines.

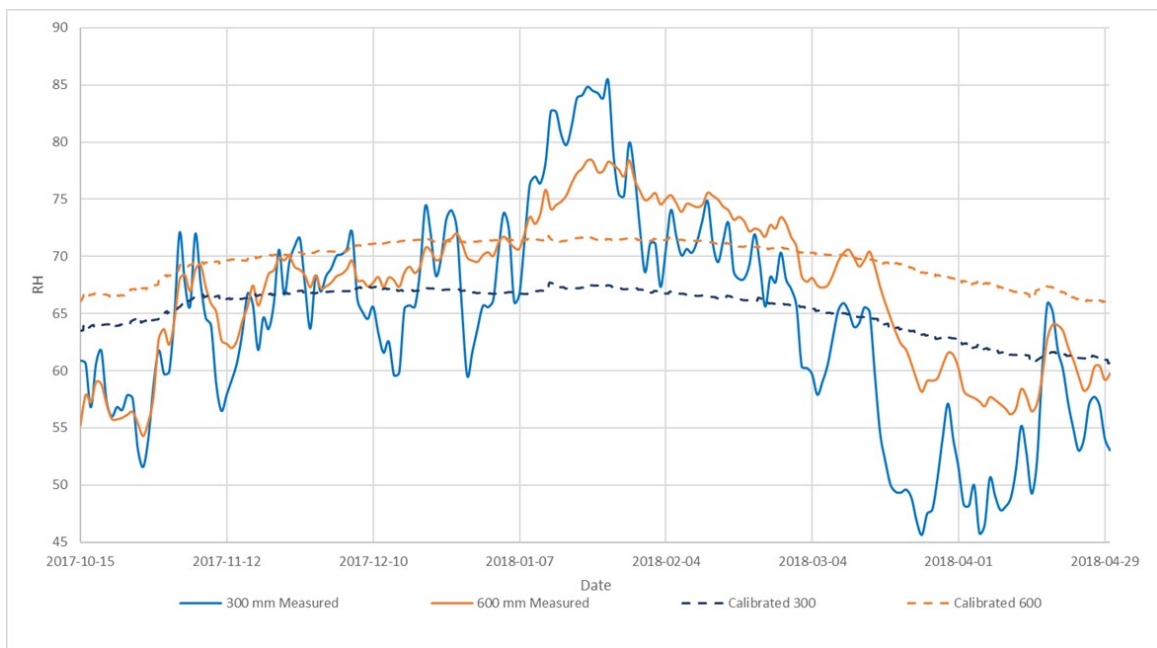


**Figure 3-1: Hygrothermal calibration results of the sixth floor wall.**

As can be seen the wall is generally very dry with RH always below 85%. From the one year of data there appeared to be a sinusoidal seasonal trend with the wall being damper in winter than summer. The dryness was attributed to the sheltered nature of this wall and the possibility of air flowing through the rubble core. Some significant voiding was observed when installing the sensors and it was assumed there is an airflow network connected to both the interior and exterior that helps dry the core of the wall. It was hypothesized that this could partially explain the RH fluctuations picked up by the sensors.

The calibrated models tended to exhibit inertial behaviour in terms of RH compared to the measured data, which is what would be anticipated for a masonry wall of this size. The models were more heavily influenced by air exchange in the core compared to changes in material properties. The seeming dominance of air flow in the assembly hindered calibration in many ways:

1. The magnitude of the air exchange can fluctuate on a regular basis depending on wind, stack effect pressure and other factors.
2. The direction in which the air is flowing is uncertain. Is it coming from the inside out or vice versa? The temperature and humidity of the air will be different depending on the source of that air.

3. To improve the quality of the line fit and further minimize the RMSE, we would require a degree of overfitting of the air exchange parameter that would not be acceptable. An example being the calibrated model lines in Figure 3-1 which show a model iteration with a sinusoidal annual air exchange rate in an attempt match the observed seasonal trend.
4. Implies an uncertainty with the physical composition of the wall assembly. What percentage of the wall is void? And how does this impact heat, air and moisture transport?

The problem of voids and the physical composition of the wall was explored in Section 6., and how this may explain the difficult faced in calibrating a wall similar to this.

While collecting the data from the tower it was noticed that a unique interior climate was present. The tower can be described as semi-conditioned with residual heat from the building warming the tower to varying degrees. This posed some durability concerns. During one visit, frost was observed to have formed on the interior wall surfaces of the sixth floor and the ambient RH was greater than 90%. The ambient conditions up until recently had been much warmer and drier before heat-generating equipment had been removed from the fourth floor. In-fact it the measured interior conditions were more representative of the conditions during the majority of the tower's life. With these concerns in mind, a new

research question of how the interior climate impacted the durability risk was asked. In order to solve that question the interior climate needed to be characterized beginning with a calibrated baseline model.

### **3.2 Abstract**

This article presents a methodology for calibrating an energy model to hourly measured temperature data with the goal assessing durability of a mass masonry tower in its present state and projecting the impact, that plausible retrofit scenarios may have on durability. The case study for this project is a load-bearing masonry structure constructed in 1867 which has been suffering from chronic moisture-related deterioration for much of its existence. The tower was instrumented to record relative humidity and temperature beginning in September 2017. Energy modeling software in combination with an optimization program was used to develop a calibrated model that could predict interior temperatures and relative humidity. Using the calibrated energy model, hygrothermal simulations were performed to see how changes to the interior ambient conditions affected the wall. The number of freeze cycles and moisture content were projected throughout the cross-section of the masonry compared to baseline conditions.

### 3.3 Introduction

Interior environmental conditions can influence the hygrothermal performance of masonry walls. Elevated relative humidity from seasonal changes, can lead to either increased sorption into, or inhibit desorption from the masonry. This is controlled by the moisture storage function or sorption curve of the material.

Lower interior ambient temperatures will negatively impact moisture in the wall in two ways; first it will cause an increase in relative humidity (RH) which will cause a corresponding increase in sorption. Secondly it will decrease the heat flux through the wall and will inhibit the ability to dry the walls through evaporation.

To obtain an understanding of the ambient interior conditions for modelling and calibration purposes in these structures, the best option is to install a monitoring system which logs at minimum, the interior RH and temperature (Künzel & Holm, 2009). This is perfect for understanding the baseline condition. But suppose, there are retrofits that may fundamentally alter the ambient conditions inside the building; such as the addition or removal of heat or humidification; or changes to the building envelope to reduce heat loss or improve thermal comfort. How will this affect the hygrothermal performance of the masonry envelope?

This paper demonstrates a procedure which uses calibrated energy models and hygrothermal modelling to assess the durability of a case-study masonry building in Ottawa, Canada which has undergone a fundamental shift in its interior

climate. Calibrated energy models were created using measured data to establish a baseline condition. From the baseline, an options analysis of retrofits that will alter the ambient conditions was performed and a durability assessment using hygrothermal models was done to project what, if any, impact each of the retrofits would have on the long-term health of the masonry walls.

### **3.4 Case Study Building – Southwest Tower**

The Parliamentary Buildings of Canada are federally designated buildings, distinguishable for the role they have played in Canadian democracy; and as a unique and beautiful piece of Gothic Revival architecture (*FHBRO*, 1987). Three buildings were constructed between 1859-1867 (known as the West, Centre and East Blocks). These buildings are load-bearing masonry and have been known to suffer from chronic moisture damage for most of their existence resulting in pathologies such as freeze-thaw damage, efflorescence, erosion and deconsolidation of mortar. The root causes of these issues are numerous, including high exposure to water, poor maintenance of mortar joints and the cascading effect of water falling from insufficient eaves onto the water tables and plinths below.

The Southwest Tower of the East Block is the focal point of this study. The Southwest Tower rises approximately 47m tall and is the architectural focus of the building.

The two-storey lobby of the tower serves as the ground floor of the tower and is capped by a groin vault ceiling. An intricate stained-glass window provides light into the space. The fourth level (immediately above the lobby) serves as the base of the upper part of the tower. There are three stories above the fourth level including the attic space. The tower's zones are characterized by large floor-to-ceiling heights (~12.0m, 7.9m and 7.9m for the lobby, fifth and sixth floor respectively).

The cross-section (Figure 3-2) of the mass masonry walls consisting of inner and outer sandstone wythes (typically 200 – 225 mm) sandwiching a grouted rubble core (Province of Canada, 1861). The thickness of the walls varies – tapering from 2100mm at the plinth level to 860mm at the top. The load-bearing walls have been known to experience chronic moisture-related decay for many years. Intricate single-pane leaded windows, including a stained-glass window in the lobby allow light into the spaces.

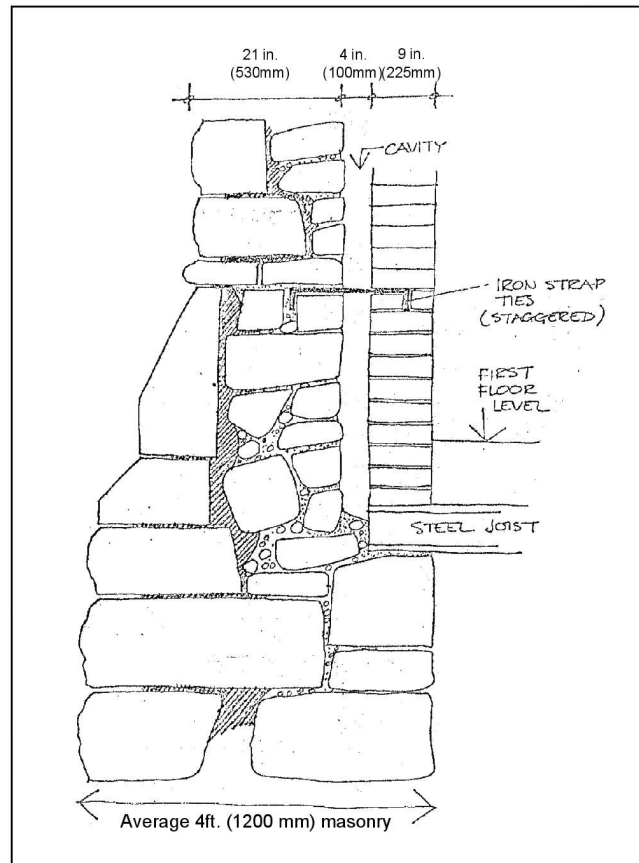


**Figure 3-2: Typical Cross-section of an East Block wall (modified from Ashurst (1977))**

The upper parts of the tower do not have a dedicated HVAC system. The fourth level used to house electrical/electronic equipment which generated significant amount of heat, but this equipment has recently been removed in anticipation of rehabilitation works. The heat generated was exhausted via a constant volume fan up the tower to the fifth, sixth and seventh floor (attic). After the removal of the equipment, the tower receives its heat from adjoining pavilions through a combination of conduction, convection and air infiltration which is difficult to

ascertain. Because of the semi-conditioned nature of the upper stories of the tower the interior conditions fluctuate greatly over the seasons and as a rule, the interior ambient conditions approach the exterior ambient conditions as you increase in altitude inside the tower. This temperature curve cannot accurately be represented in hygrothermal simulations by fixed values or sine curves that would be appropriate for typical inhabited spaces. To improve the accuracy of the hygrothermal simulations we must integrate building energy modelling.

### **3.5 Literature Review**

Calibrated energy models are typically done on periodic (hourly, daily, monthly) energy consumption data. A model is considered calibrated when the statistical difference between measured and modelled falls under a given threshold. The thresholds are determined by statistical measures such as Mean Average Error (MAE), Root Mean Square Error (RMSE) or variations of these. ASHRAE Guideline 14 is commonly used and gives thresholds of  $\pm 10\%$  Mean Bias Error (MBE) and  $CVR_{RMSE}(\text{hourly}) \leq 30\%$  (ASHRAE, 2014) to measured monthly energy consumption. Calibration can be done in iterative and more manual process such as described by Raftery, Keane and Costa (2011). Another method is to use raw computer power coupled with an optimization software to run multiple simulations to find the optimum solution.

In the literature, there is a limited number of calibrated energy modelling studies performed on heritage buildings compared to the number on contemporary construction (Roberti et al., 2015).

Calibration of energy models is not always performed against measured energy consumption. In some scenarios, like this project, other metrics are required to calibrate such as temperature, daylighting or RH. Reasons for calibrating for temperature may include determining effectiveness of passive systems such as natural ventilation or thermal response of a zone. There aren't any standards available for calibrating a building in this fashion. Work done by Pernetti et al, Roberti et al and Giuliani et al are examples where calibration was performed against interior temperatures in historic buildings (Giuliani et al., 2016; Pernetti et al., 2013; Roberti et al., 2015). In these case studies, Pernetti et al achieved an RMSE between 1.0°C – 1.7°C with real data sets doing only 24 simulations. Roberti et al achieved an RMSE of 0.66°C. Giuliani achieved an RMSE of 0.49°C. Berger et al also calibrated their models to measured temperatures using Bayesian techniques in an attempt to determine convection coefficients and thermal conductivities (Berger et al., 2016).

Understanding and being able to predict interior ambient conditions is important because the interior ambient conditions can lead to moisture-related damage in an exterior wall in many ways. Elevated RH in a room can lead to issues with

mould growth, increased moisture accumulation through vapour diffusion or advection, and sorption into porous media. The calibrated energy model can help to characterize the interior, especially for buildings which are unconditioned.

There are examples where changes in interior conditions effected hygrothermal behaviour in masonry walls. On the nearby Library of Parliament, Lawton and Hoffman monitored interior RH and temperature and concluded that interior environmental conditions were linked to high stone moisture contents and surface condensation in localized areas (Lawton & Hoffman, 1998). Klůšeiko et al (2015) noted that changes in humidification lead to a measured hygrothermal response in a 75cm brick wall with interior insulation retrofits applied. Napp and Kalamees (2016; 2015) developed calibrated models that studied the temperature and humidity effects in medieval Nordic churches.

Interior conditions are a boundary condition in hygrothermal models. When performing hygrothermal modelling on typical masonry sections and with typical occupancies (office, home), it is common practice to utilize either fixed values or annual sine curves for RH and T as inputs into the model. ISO 13788, EN 15026 and ASHRAE 160 provide guidance on values to use as simulation inputs (ASHRAE, 2009; *EN 15026*, 2007; ISO, 2012b). These approaches are suitable for typical occupancies, but what do you do for those unusual buildings which may not be conditioned have seasonal or temporary or no occupancy at all? They

may experience large fluctuations in both RH and dry-bulb temperature over the course of the year which are difficult to encapsulate via simple functions.

Examples of such structures may be churches, castles, tall atriums and towers.

ISO 13788 Annex A states that “wherever possible measured data should be used for the analysis of buildings in class 5, with high internal humidity” (ISO, 2012b).

Pathologies caused by moisture-related damage in masonry include freeze-thaw cycling, efflorescence or subfluorescence due to salt, leaching of lime from mortar due to high moisture contents, and deterioration of embedded joists or trusses. In this building we are primarily concerned with freeze-thaw cycling and deconsolidation of mortar. The science of freeze-thaw damage mechanisms and moisture transport within brick masonry is documented by Mensinga (2009). A material needs to be sufficiently wet for expansive forces to causes permanent strain on the material. All materials have unique threshold called the critical degree of saturation ( $S_{CRIT}$ ) which damaging freeze-thaw cycling occurs (Fagerlund, 1977). Frost dilatometry is a process for measuring  $S_{CRIT}$ .

When dealing with a unique building such as the tower, it is important to establish a baseline condition to build from. Calibrated models are an important step toward this goal, however there aren't any rigid guidelines or procedures to follow when calibrating to temperatures. We can also expand the concept of model

calibration to include assessment of hygrothermal performance to estimate how changes to the interior environment are projected to impact long-term moisture accumulation. This project has three main stages to address this question:

1. Sensor Installation and Data Collection
2. Calibrated Energy Modelling
3. Hygrothermal Analysis of Possible Retrofits

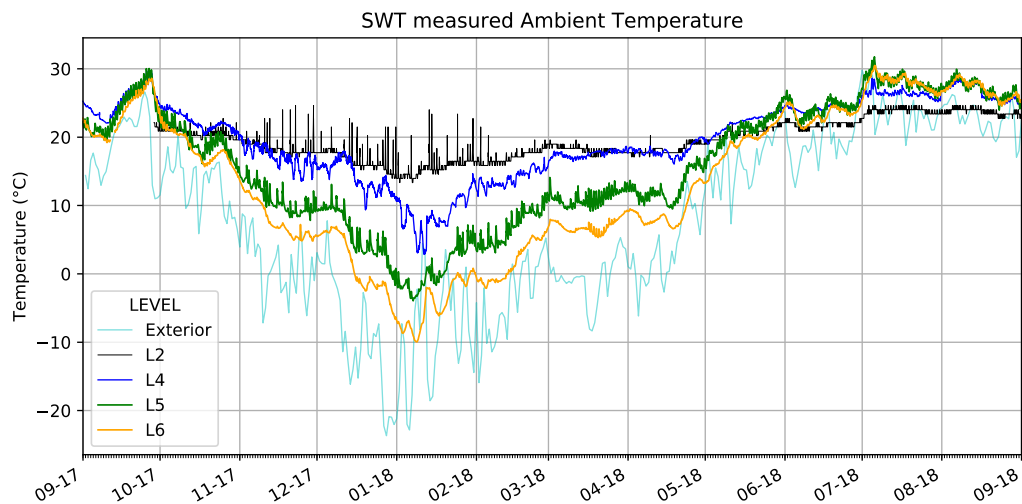
### **3.6 Methodology**

#### **3.6.1 Sensor Installation and Data Collection**

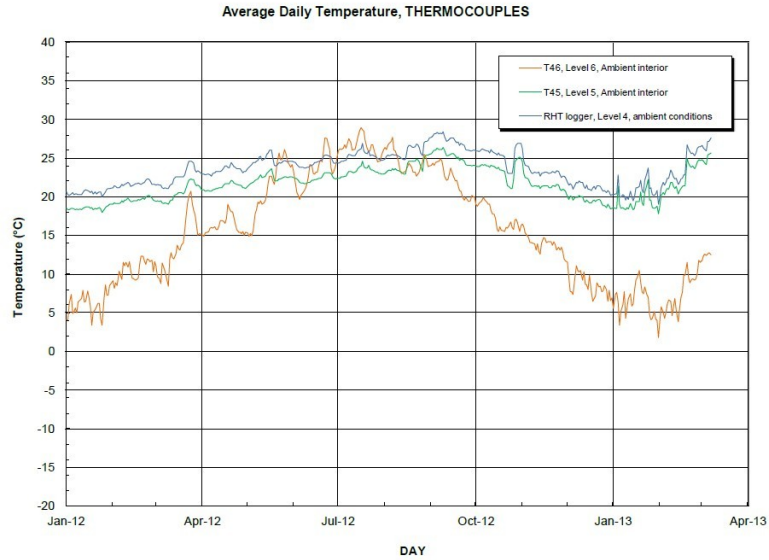
A network of sensors was installed in the tower to record ambient temperature and relative humidity and recorded at 15-minute intervals onto Campbell Scientific data loggers. The ambient temperatures were recorded in the main lobby, fourth floor, fifth floor and sixth floor.

Figure 3-3 shows the measured and ambient temperatures from the period between September 2017 to August 2018. It is seen that as we go higher in elevation within the tower, that the ambient temperatures begin to approach the outdoor temperatures. The temperatures in the fifth and sixth levels dip below freezing in December, meaning the entire cross-section of the walls is subjugated to freeze-thaw cycling. Compare the 2017/18 data to the temperature data

measured from 2012-13 in Figure 3-4 when the heat generating equipment in the fourth floor was still active (Glazer, 2013). Never was there an average daily temperature below freezing, and the temperatures in Zone-4 and Zone-5 were within a reasonably comfortable range throughout the year, never falling below 18°C. The removal of the equipment has had a negative impact on the hygrothermal performance of the tower. It should be noted that with the removal, the tower has reverted to the state it has been in for more than 90% of its existence. The measured RH inside the tower fluctuated between a minimum of 20% in winter to 60% in summer for the fifth and sixth floor during 2017-2018. The RH on the sixth floor was extremely high (>90%) in January leading to frost formation.



**Figure 3-3: Measured dry-bulb temperatures inside the Southwest Tower from September 2017 to August 2018**



**Figure 3-4: Measured dry-bulb temperatures inside the Southwest Tower from January 2012 to April 2013 as measured by National Research Council (Glazer, 2013)**

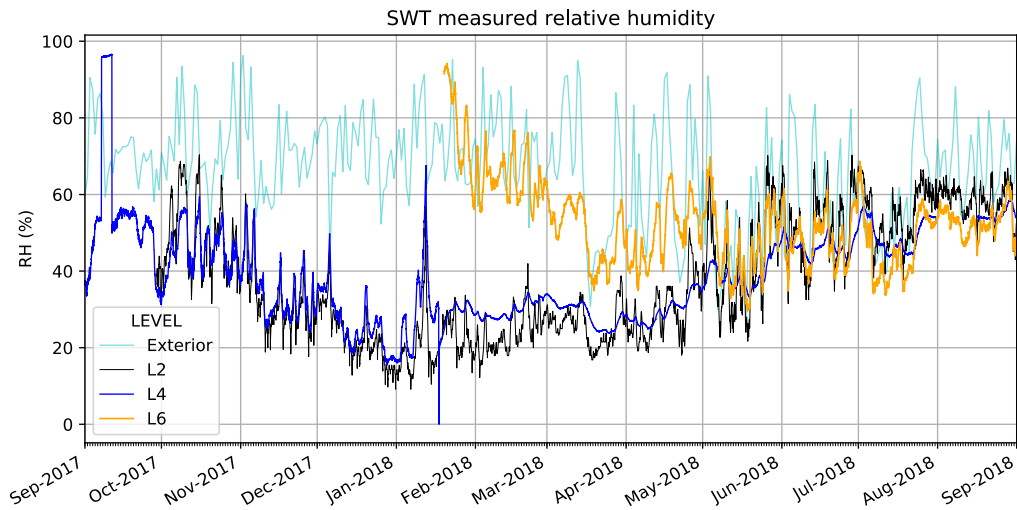


**Figure 3-5: Measured relative humidity inside the Southwest Tower from September 2017 to August 2018**

Other sensors, including thermocouples, heat flux sensors along with RH and MC sensors inserted into the masonry core were installed. The information gained from these sensors are not core to this chapter and are not thoroughly presented. Concisely, what was found from the RH and MC sensors was the measured wall sections on the fourth and fifth floor were experiencing severe moisture problems. RH inside the core was at or near 100% with MC approaching saturation for the entirety of the monitoring period. This furthers the claim of chronic moisture issues which need to be resolved. On the sixth floor, the wall was much drier with a defined wetting period in Winter and drying in Summer.

### **3.6.2 Calibrated Energy Model**

The calibration process was based on a procedure developed by Roberti, Oberegger, and Gasparella (2015) adapted for use in this project. The first step (1) was to develop a baseline model with assumed material properties and modelling parameters retrieved from the ASHRAE Handbooks, Delphin, WUFI and professional judgment in the absence of information (ASHRAE, 2013b; Bauklimatik Dresden, 2018; Fraunhofer Institute for Building Physics, 2019a); (2) perform a sensitivity analysis to determine which parameters had the greatest influence on results compared to the baseline; (3) calibration of the model against measured zone air temperatures over the specified time range by adjusting values for key parameters identified in the previous step.

### 3.6.2.1 EnergyPlus Model

EnergyPlus 8.8 was used to develop the energy model of the Southwest Tower (EnergyPlus, 2017b). To simplify the model, reduce computation time, adiabatic boundary conditions were modelled between the tower and neighbouring pavilions. Geometry was based on available photogrammetric drawings and point clouds. Thermal zoning in the tower was done on a per floor basis resulting in six thermal zones (B, 1, 4, 5, 6,7).

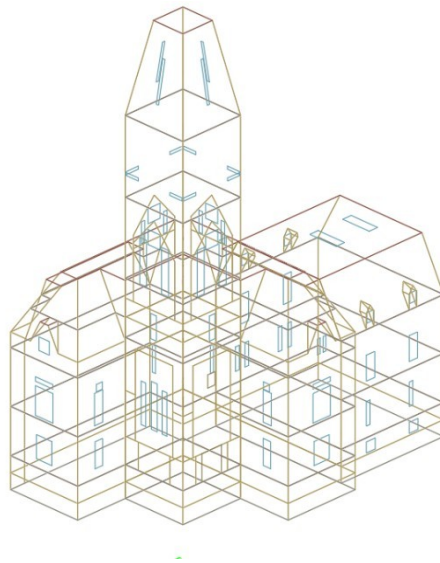


**Figure 3-6: Wireframe geometry of EnergyPlus model**

A clear-field assembly is difficult to assume because of many changes in thickness and decorative elements. For simplicity, all masonry walls were divided into an outer wythe (225 mm), rubble core (variable thickness) and inner wythe layers (225 mm). The thermal properties of the core were assumed to be the

same throughout the building, ignoring the effects of voids and the inconsistent nature of its construction, from one wall to the next. An implicit finite difference algorithm based on the Crank-Nicholson scheme was chosen for all exterior surfaces. The windows are all single-pane glass of equivalent area and perimeter.

For model simplicity, an ideal loads system was entered instead of explicitly modelling an HVAC system. The first floor receives ventilation air from an air handling unit running from the basement. There is also air circulation from large open corridor doors from the adjacent wings of the building. Airflow between the corridors and the tower was modelled as a constant flow rate at room temperature.

The fourth floor of the tower and up has no dedicated HVAC system. A constant volume fan exhausts air up to the fifth floor and is always operating. The volumetric flow rate expelled by the fan was modelled as a constant flow rate. A constant volumetric flow rate was also used to model air transfer for the model zones for the stories above the fourth floor. These volumetric flow rates encapsulate air movement driven by both the fan and from the stack effect.

These are two separate phenomena, and both carry a degree of simplification in this model. Diffusion into the zone, loss of fan pressure in altitude, re-circulation between zones and ambiguity where to define the neutral zone for stack effect were difficult to consider in the model with any degree of confidence. Further

detailed study, such as computational fluid dynamic analysis would be needed to completely understand the airflow patterns in the tower.

Replacement air for the fourth level comes from infiltration from the neighbouring conditioned zones and attics of the South and West Pavilions. The source of the incoming air is uncertain without doing leak detection or tracer tests. The fourth floor is adjacent to a corridor, and both the occupied portion and attic spaces of the neighbouring pavilions. The ratio of air incoming from these spaces is uncertain and the average temperature at which that air enters is uncertain considering the insulated attic will heat up drastically in the summer sun and approach exterior conditions in winter. To model this a constant flow rate at a temperature which fluctuated throughout the year was modelled.

Zone exfiltration for each floor was modelled using a unique constant ACH, with temperature and velocity coefficients based off the BLAST default model in EnergyPlus (2017b).

The first floor (a two-storey circulation lobby), fifth floor and sixth floor have especially tall floor-to ceiling heights (~12.0m, 7.9m and 7.9m respectively) where temperature stratification means the assumption of well-mixed air in a zone may be invalid, especially during winter. Thermocouples were installed at intermediate heights of the fifth and sixth floor beginning in January 2018 (as another datalogger became available). The vertical temperature profiles have been found

to not be linear with altitude at mid-storey height consistently warmer than floor or ceiling level. The exhaust air blowing up through the stairwell, and then diffusing laterally caused enough mixing in each thermal zone that the well-mixed assumption was appropriate.

Lighting and occupancy related loads are minimal. The tower is sparsely occupied compared to a typical office building. The upper stories of the tower are only occupied for rare maintenance and downloading data.

Weather data was compiled into EnergyPlus Weather file format (epw) (*EnergyPlus*, 2017a) from data from the Urbandale Centre for Home Energy Research (*Urbandale*, 2017) project on the Carleton University Campus and supplemented with data from Environment and Climate Change Canada (*Environment and Climate Change Canada*, 2017) and CUAHSI HIS Hydroclient for precipitation data (*CUAHSI*, 2020).

### **3.6.2.2 Sensitivity Analysis**

Prior to calibrating the model, a one-factor-at-a-time sensitivity analysis was performed to determine which model parameters have the largest influence on results. This is also done to reduce the number of simulations required. The sensitivity analysis was done by changing only one variable at a time over a predetermined range. Parameters which do not significantly affect the results

were not included in the final calibration model. The Root Mean Square Error (RMSE) was between each varied model's zone temperatures and the baseline model's zone temperatures were the statistical basis for the sensitivity analysis.

A list of 28 energy model inputs were analysed in the sensitivity analysis, and include EnergyPlus objects related to HVAC, zone mixing, infiltration, conductivity, heat capacity and optical properties. Table 3-1 shows the parameters which were analysed. Minimum and maximum values were judged from plausible values in documentation and from pre-calibration trials. The sensitivity analysis was performed over time range of 1 September 2017 to 17 December 2017, encompassing a wide variety of weather conditions in Ottawa including an unseasonably warm week in September ( $T > 30^{\circ}\text{C}$ ) and typically cold Ottawa winters ( $T \leftarrow 20^{\circ}\text{C}$ ).

**Table 3-1: Summary of calibration model input parameters and final results**

Parameter	Min Range		Max Range		Interval		Calibration Results	
	First	Second	First	Second	First	Second	First	Second
Calibration								
Tower1 Inflow Air Temperature (°C)	18	20.375	24	20.875	0.25	0.125	20.75	20.75
Tower 4 Temperature Amplitude (°C)	--	2	0	5	0	0.5	0	3
Tower4 Inflow Air Temperature Maximum (°C)	--	28	0	31	0	0.5	0	29
Tower4 Inflow Air Temperature Minimum (°C)	--	20	0	22	0	0.5	0	21
Tower1 Inflow Air Flow Rate (m <sup>3</sup> /s)	0	0.375	1.5	0.5	0.125	0.03125	0.5	0.4375
Tower4 Inflow Air Flow Rate (m <sup>3</sup> /s)	0	0.025	1.5	0.1	0.125	0.025	0.1	0.05
Tower 4 to 5 Mixing (m <sup>3</sup> /s)	0	0.1875	2.5	0.3125	0.25	0.03125	0.25	0.25
Tower 5 to 6 Mixing (m <sup>3</sup> /s)	0	0.125	2.5	0.25	0.25	0.03125	0.25	0.1875
Tower1 Exfiltration (1/h)	0.1	0.25	0.9	0.5	0.1	0.05	0.4	0.3
Tower4 Exfiltration (1/h)	0.1	0.025	0.9	0.1	0.1	0.025	0.1	0.05
Tower5 Exfiltration (1/h)	0.1	0.025	0.9	0.15	0.1	0.025	0.15	0.05
Tower6 Exfiltration (1/h)	0.1	0.025	0.9	0.1	0.1	0.05	0.15	0.05
Design Flow Rate Temperature Coefficient (--)	0	0	0.08	0.01	0.0188	0.005	0	0
Design Flow Rate Velocity Coefficient (--)	0	0	0.25	0.03	0.0625	0.01	0	0
Conductivity Sandstone (W/m-K)	1	1.5	4	2.25	0.25	0.25	1.5	2
Conductivity Core (W/m-K)	1	2	4	2.5	0.25	0.125	2.75	2.25

Some parameters of note relate to zone-to-zone mixing. The exhausts fan's output was estimated to be between 0.5 and 1.0 m<sup>3</sup>/s. Pre-sensitivity analysis trials showed that volumetric flow rate up the tower had a significant on model results. The pre-sensitivity analysis trials also showed that very high flow rates up to 2.5 m<sup>3</sup>/s were plausible solutions to the optimization problem even though they would be considered unrealistically high. This is the reason for the particularly high RMSE in the sensitivity analysis.

A wide range was given for the conductivity of masonry materials was inserted into the sensitivity analysis. This reflects the typical uncertainty involved with the

hygrothermal properties of masonry materials. As an example, the ASHRAE Handbook gives the thermal conductivity of sandstone from 1.88 to 6.2 W/m-K (ASHRAE, 2013b), while a study by Pechinig et al (2007) gives values ranging from 1.5 to 4.0 W/m-K. The Nepean sandstone used in the majority of the exterior walls is a dense, high quartz stone, which would tend to indicate a higher conductivity. Likewise, the thermal conductivity of the core was cast with a wide range. The thermal properties (conductivity, heat capacity) of the masonry as a unit, are influenced by the individual properties of both stone and mortar; and the ratio of each. This can be difficult to characterize through material sampling or theoretical modelling and was noted as an obstacle to achieving calibration of historic buildings by Roberti, Oberegger, and Gasparella (2015).

The 1861 specs of the East Block describe the composition of the core as *“The interstices of the stonework to be filled with stone chips or spalls, and grouted with lime and sand in a liquid state every foot”* (Province of Canada, 1861).

Considering that the core is a higher percentage of mortar with known voids, it is thought that the core would have a conductivity that is substantially less than that of the sandstone. Because the ratio of stone to core changes in the wall cross-section as you go up the tower, it was important to separate the wall into two materials. The ranges for optical properties were estimated from WINDOW 7.3 assuming a 3 mm single-pane clear glass (LBNL, 2015).

### 3.6.2.3 Sensitivity Analysis Results

The sensitivity analysis results can be seen in Figure 3-7. Black bars indicate the overall RMSE for all four measured zone temperatures and grey bars represent the maximum RMSE recorded for an individual zone. Some parameters are more sensitive for a particular zone than on the global scale.

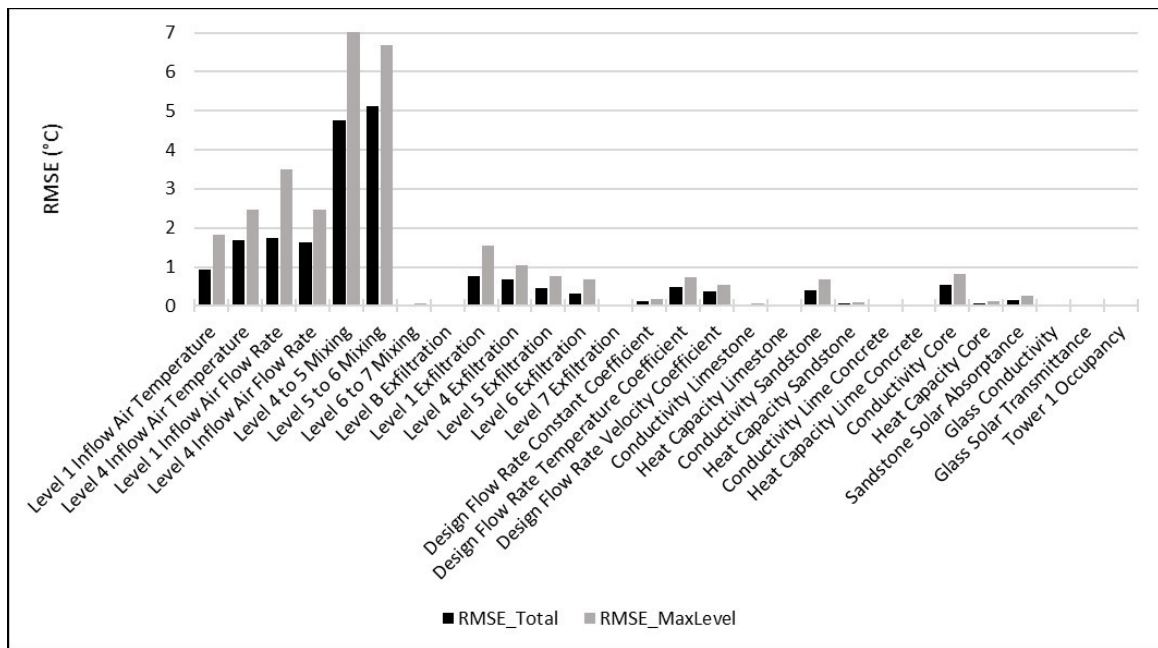


**Figure 3-7: Sensitivity analysis results. Black Bars are the overall RMSE for all 4 zones and gray bars are the maximum RMSE recorded for an individual zone.**

The largest RMSEs were for parameters related to air transfer into a zone and mixing between zones, specifically for the zone to zone mixing parameters. The change in RMSE from the baseline assumption of 1.0 m<sup>3</sup>/s was skewed heavier towards flow rates approaching zero than flow rates that were higher than 1.0

m<sup>3</sup>/s. This non-linearity shows that anything higher than the maximum value in the range has a diminishing effect when compared to the baseline and that an assumption of zero vertical mixing is likely incorrect.

Base exfiltration rate, and the coefficients used to modify it have a moderate effect on results and were included in the final calibration. Building envelope parameters such as thermal conductivity and heat capacity had a surprisingly low influence on the temperatures of the tower. The conductivity of sandstone and the core have a measurable influence and was included in the final calibration model. The heat capacity of the masonry and the floors had little effect on the model and was not included in final calibration. Optical properties did not have a significant impact on results. This was expected because, apart from the fifth level, the window-to-wall ratio is quite low on the building (Maximum 0.12). Parameters relating to the Basement or the seventh storey have little effect, largely because there was no measured data in those zones to compare to.

#### **3.6.2.4 Model Calibration**

The GenOpt optimization software was used to calibrate the EnergyPlus model against measured interior ambient temperatures (Wetter, 2016). The Particle Swarm Algorithm (PSO) was used to minimize the RMSE of the model's results compared to measured data. The cost function that was minimized in GenOpt

was the RMSE for all 4 zones with respect to measured temperatures. The RMSE was also reported for each level to see if specific zones are better calibrated than others. Discrete values were used in the calibration. The most sensitive parameters such as zone mixing, were defined with finer intervals between consecutive values, while the least sensitive were defined with coarser intervals between consecutive values. A summary of the parameters is shown in Table 3-1. The timeframe of the final calibration model was from 1 September, 2017 to 29 January, 2018.

The 14 most significant parameters found in the sensitivity analysis were included in the calibration model. Parameters which were not included typically had an RMSE less than 0.2°C.

#### **3.6.2.5 Calibration Results**

Final values from the calibration are summarized in Table 3-2. Overall, an RMSE = 1.162°C was achieved for all four measured stories. Figure 3-8 shows the measured v. calibrated curves for each of the four storeys. The fourth floor has the weakest correlation (RMSE=1.753°C) between measured and modelled data, particularly in the cold winter months of December and January. The model also lacks the diurnal temperature fluctuations of the measured data. Possible reasons for this could be excessive thermal mass, underestimated air infiltration

and the fact that inflowing air into fourth-floor fluctuates diurnally, whereas the model is at a fixed temperature. The fifth floor (RMSE=1.078°C) and the sixth floor (RMSE=0.957°C) have a much stronger correlation than the fourth floor. The sixth-floor calibrated model shows noticeable diurnal fluctuations whereas the measured data does not. Further dissecting, the calibration results, the RMSE during a cold week was much higher than the rest of the calibration period. The parameter which seems to improve the RMSE during cold periods the most is the volume of inflowing air into the fourth floor.

**Table 3-2: Summary of calibration results**

	First Calibration Model		Second Calibration Model	
	1 September – 29 January)	Full Period (1 September, 2017 – 2 August, 2018)	First Part (1 September, 2017 – 29 January, 2018)	Second Part (30 January, 2018 – 2 August, 2018)
Overall	1.162°C	1.040°C	1.157°C	0.909°C
Tower-1	0.522°C	0.489°C	0.524°C	0.451°C
Tower-4	1.753°C	1.516°C	1.749°C	1.246°C
Tower-5	1.078°C	1.066°C	1.146°C	0.982°C
Tower-6	0.957°C	0.808°C	0.848°C	0.767°C

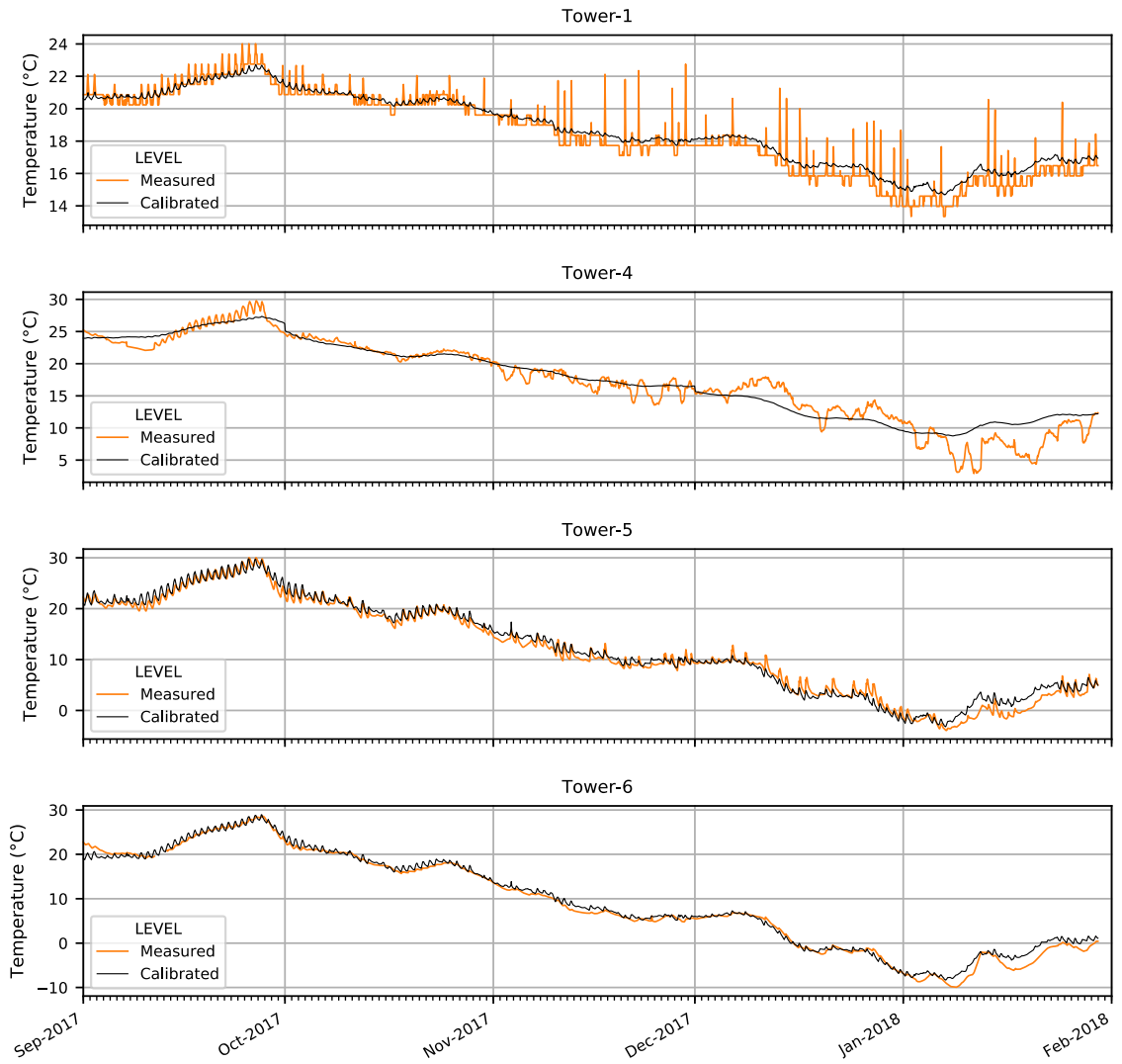


**Figure 3-8: Calibrated v. Measured data for the first calibrated model**

### 3.6.2.6 Second Calibration Model

The calibrated model was good at modelling the past, but its predictive capabilities needs to be verified. As new data arrives, a second calibration

provides the opportunity to verify the existing model, evolve the model, improving its weaknesses, and to further improve the confidence of our inputs.

A second calibration was performed extending the timeframe from 29 January, 2018 to 2 August, 2018(6 months). Some new features and changes were incorporated into the model. Based on the results in Figure 3-8, opportunities to improve and evolve the model were apparent. The first evolution was to change how the temperature of the incoming air was modelled. Previously this was modelled as a step function based on time of year and was not adaptive to week-on-week fluctuations in weather. This was changed to a function dependent on the previous 48 hours of measured exterior ambient temperatures and supplemented with a daily sine curve with an amplitude controlled by a new GenOpt parameter. This was done to better reproduce the diurnal effect of the midday sun warming up the incoming air.

Also, a tighter range of parameters with smaller intervals centred about what was found in the first calibration were used. Table 3-1 shows how the input parameters of the model have changed from the first calibration and the results from the second calibration. Figure 3-9 shows the results of the second calibration overlaid with the previous model extrapolated in green. Table 3-2 shows the improvement in the RMSE between the two calibrated models.

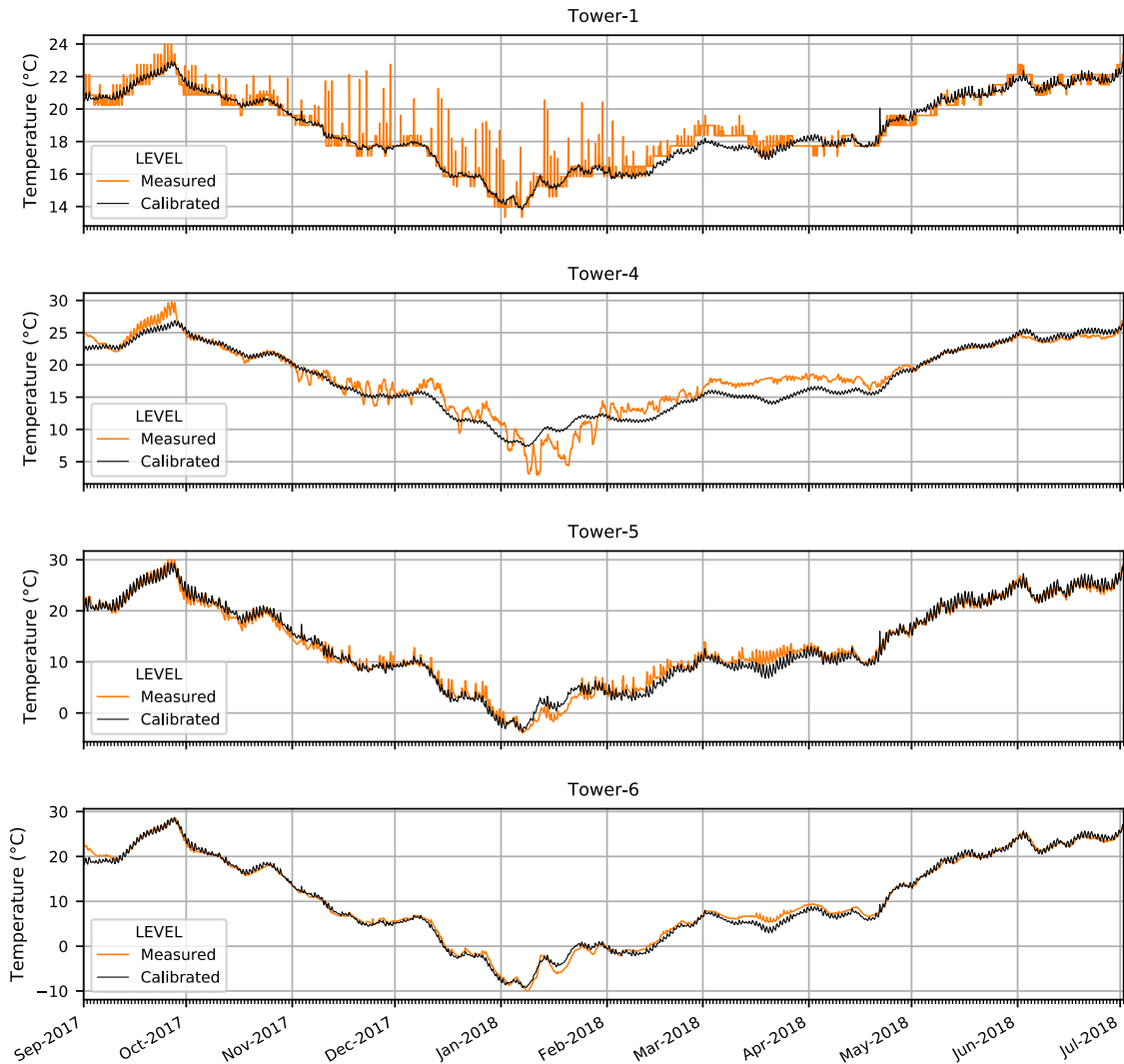


**Figure 3-9: Calibrated versus Measured data for the second calibration model**

The RMSE of the first floor is comparable to what was found in Perneti and Roberti's studies. This zone would be more comparable to the types of rooms where there is not as great of a difference between summer and winter temperatures. The other zones especially the fourth floor have RMSE greater or

within the range that they had found. Temperatures are less stable in these zones.

There are some data that the model can still not explain. Again, focusing on the fourth floor, a noticeable difference is evident in late Winter and early spring of around 3-5°C. This could be caused by a change in building operation around the holiday season, an unidentified seasonal heat source or change in stack effect. In general, there are some sharp fluctuations in winter. Overall, the model does better in warmer conditions than colder conditions.

With regards to the final calibrated model parameters, the values for flow rate were much lower than what was originally assumed. The volumetric flow rate from the fourth floor to fifth floor was between 25-50% less than the estimated output of the fan. This is plausibly explained by the fact that the stairwell which the air is forced up is imperfectly sealed, meaning that air is immediately being short-circuited back into the fourth-floor zone. Also, there are two sizable openings in the fourth-floor ceiling. Air may be re-circulating back in from the fifth floor in a loop.

Air exfiltration was also lower than what had been originally estimated in the upper floors of the tower. Though the windows are only held in place with stone on the exterior face, metal stops on the interior and have no visible sealant or weatherstripping, there are not many of them and they are not operable.

If monitoring of the Southwest Tower is to continue in the future, we can deduce whether these are recurring patterns or anomalies. If they are recurrent, and the model still cannot explain this behaviour, it provides impetus to further evolve the model. As more data comes in, strong seasonal (Winter, summer, shoulder) patterns may emerge; such as the strength of the stack effect. If this is the case, consideration should be given to further break the fixed constant input parameters into step functions or sine curves. Data will continue to come in until the tower will undergo a rehabilitation. Until this happens it will give further opportunities to perform calibrations and fine-tune the model inputs.

### **3.6.3 Hygrothermal Analysis of Possible Retrofits**

One potential retrofit that is likely to be brought up in the upcoming rehabilitation is fully-conditioning the towers to help with the chronic build-up of moisture in the walls. There is precedent for installing an HVAC system in the towers of the Parliament Buildings. The Northwest Tower of the East Block had a heating and cooling system installed after elevated moisture levels were noticed subsequent to a rehabilitation completed in 2013. Conditioning an unoccupied space is not appropriate in terms of sustainability; and the benefit of the system is unclear with the absence of a good baseline.

Using the calibrated EnergyPlus model and the typical weather year for Ottawa (CWEC 2016 format) as a basis, the impact that retrofits will have on the hygrothermal performance were studied. The retrofits are:

- 1) Reinstall electronic equipment
  - a) 2000W capacity
  - b) 4000W capacity
  - c) 2000W with increased zone-to-zone mixing
  - d) 4000W with increased zone-to-zone mixing
- 2) Install full HVAC system in all tower zones
- 3) Install heating only system in all tower zones

The installation of a full HVAC system was designed to maintain a temperature between 18 and 24°C, and a RH between 30 and 60%, providing dehumidification. The installation of a full HVAC system was designed to maintain a minimum 18°C temperature year-round. Heat injection rates can be variable throughout the year and can be turned off in the warmer months.

The interior RH and temperature of each of these scenarios were then input into Delphin 6.0 hygrothermal modelling software as boundary conditions. The subsequent simulations were analysed for the number of freeze-thaw cycles and the progression of moisture content over the course over five years.

### **3.6.3.1 Modelling retrofits in EnergyPlus**

For the electronic equipment, two capacity levels were modelled representing a smaller and larger installation based on the usable space on the fourth floor. The simulated levels would have power consumption of 2000W and 4000W and based on what the tower could theoretically hold. Loads and operating schedules were based off of the National Energy Code of Canada for Buildings 2015 (*NECB*, 2015). Also modelled was a doubling of air flow rate up the tower, which would increase the amount of heat energy transferred up the tower. This would reduce temperatures on the fourth floor to more comfortable levels and is representative of a higher volume fan and sealing between the fourth and fifth floor.

For the installation of a full heating and cooling system and the heating only system, an ideal loads system was modelled which could always provide sufficient energy to maintain the setpoint temperatures.

EnergyPlus doesn't simulate the hygric buffer effect where masonry can capture and release humidity in the zone. The results tend to be extremely peaky in the tower. To get around this, a multiple linear regression based off measured zone temperatures and exterior temperature and relative humidity was performed to predict RH in each zone.

### **3.6.3.2 Hygrothermal Models**

Using the hygrothermal simulation software Delphin 6.0 (Bauklimatik Dresden, 2018), a simple two-dimensional model of the fourth floor and sixth floor walls were modelled (1360 and 1000mm thickness respectively). The models expressed 200 mm thick inner and outer wythes of sandstone sandwiching a rubble core assumed to be lime mortar. In plan, the width of a stone was assumed to be 400mm with a 15mm lime mortar joint. No sources or sinks were included in the model. It also excludes any possible interstitial airflows, microcracks, contact resistances and other imperfections.

Material properties were based off the Delphin library materials Karlshafener Sandstone and Lime Cement Mortar (ID 142 in library). These materials were judged to have the most similar porosity, absorption coefficient and vapour transmission to the sandstone and mortar of the building. The porosity, vapour diffusion and absorption coefficient were modified to values that were representative of previous tests performed on samples from the Parliament Buildings as shown in Table 3-3.

**Table 3-3: Material properties for Delphin simulation**

	Nepean Sandstone	Mortar and Core
Porosity (--)	0.060	0.408
Vapour Diffusion (g/m <sup>2</sup> -h) / $\mu$ -value [--]	2.0 / [9]	6.0 / [24]
Absorption Coefficient (kg/m <sup>2</sup> - $\sqrt{s}$ )	0.0085	0.33
Density (kg-m <sup>3</sup> )	2410	1570

Simulations for each run were performed for the West and South elevations. Two levels of exterior moisture loading (low and high) were simulated, to represent relatively dry wall conditions as measured on the sixth floor, and, saturated wall condition as has been measured on the fourth and fifth floors.

An exposure coefficient (adhering fraction of rain) of 0.7 with initial RH of 90% was used for the low moisture loading wall. For the high moisture loading wall, an exposure coefficient of 1.3 was used with an initial RH of 99.5% and a distributed water source in the core equal to 0.25% of precipitation. This was done to simulate an already saturated wall with heavy rain infiltration or leaks.

Delphin simulations were run for 5-years to achieve a year-on-year steady-state condition. In the fifth year, the number of freeze-thaw cycles and number of hours where  $T < 0^{\circ}\text{C}$  were counted. Also, the change in moisture content was measured over the duration of the simulation.

For the purpose of this study, a freeze-thaw cycle is defined as 3 hours consecutively above freezing followed by at least 3 consecutive hours below freezing. The change in freeze-thaw performance is shown in Figure 3-10 and Figure 3-11 for the South façade of the fourth and sixth floor walls. These results show that changing the interior conditions reduce the number of hours the wall is below the freezing point but has a marginal decrease on the number of freeze-thaw cycles experienced. Only on a few occasions, with high infiltration were damaging freeze-thaw cycles recorded where a freeze-thaw cycle occurred with moisture contents greater than  $S_{crit} = 0.75$  (Note:  $S_{crit}$  was tested for in the lab using typical replacement stone and mortar used on the Parliament Buildings). These results indicate that freeze-thaw action is still possible deep within the core and that the choice of retrofit does not have a large impact on this.

It has been assumed that choice of interior retrofit can affect the water accumulation in the stone masonry over time and this can turn benign freeze-thaw cycling in to damaging cycles if accumulation becomes severe enough, as has been documented in parts of the tower. The simulated moisture content versus time for low moisture loading is plotted in Figure 3-12 for the sixth floor – South façade and in Figure 3-13 for a high moisture loading condition.

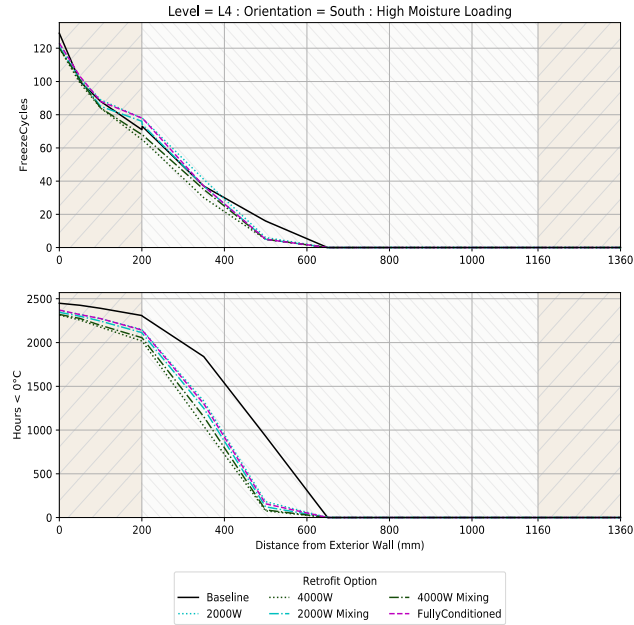


**Figure 3-10: Freeze-thaw performance for fourth floor wall - South façade**

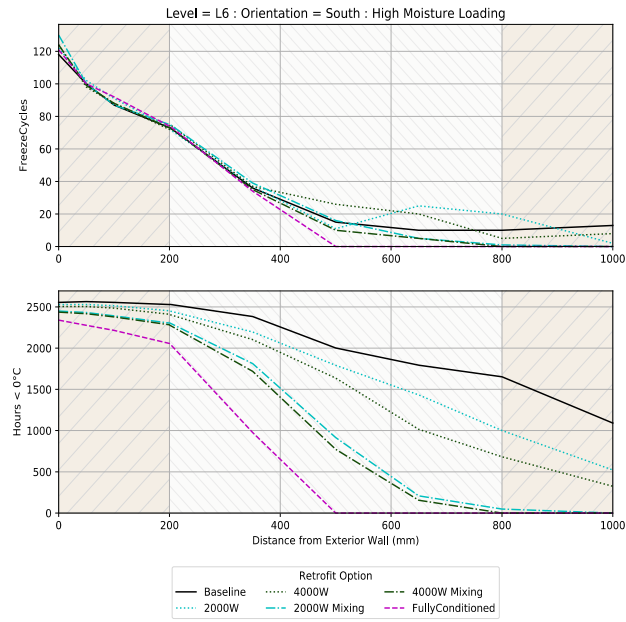


**Figure 3-11: Freeze-thaw performance for sixth floor wall - South façade**

For the low moisture loading wall, from the centre of the wall inward (500mm – 800mm), it is observed that retrofit measures reduced the moisture content in the walls compared to the baseline at the end of the five-year simulation, with the heating only retrofit performing the best. In fact, a year-to-year drying trend can be observed here. In the exterior half of the wall the baseline are predicted to perform the best and the retrofits which were best for the interior half perform worst (Figure 3-12a). As you go outward in the wall, the difference between the retrofits and baseline become more marginal (only a few  $\text{kg/m}^3$  or a few % saturation) and at the exterior stone (200mm not shown), the lines converge.

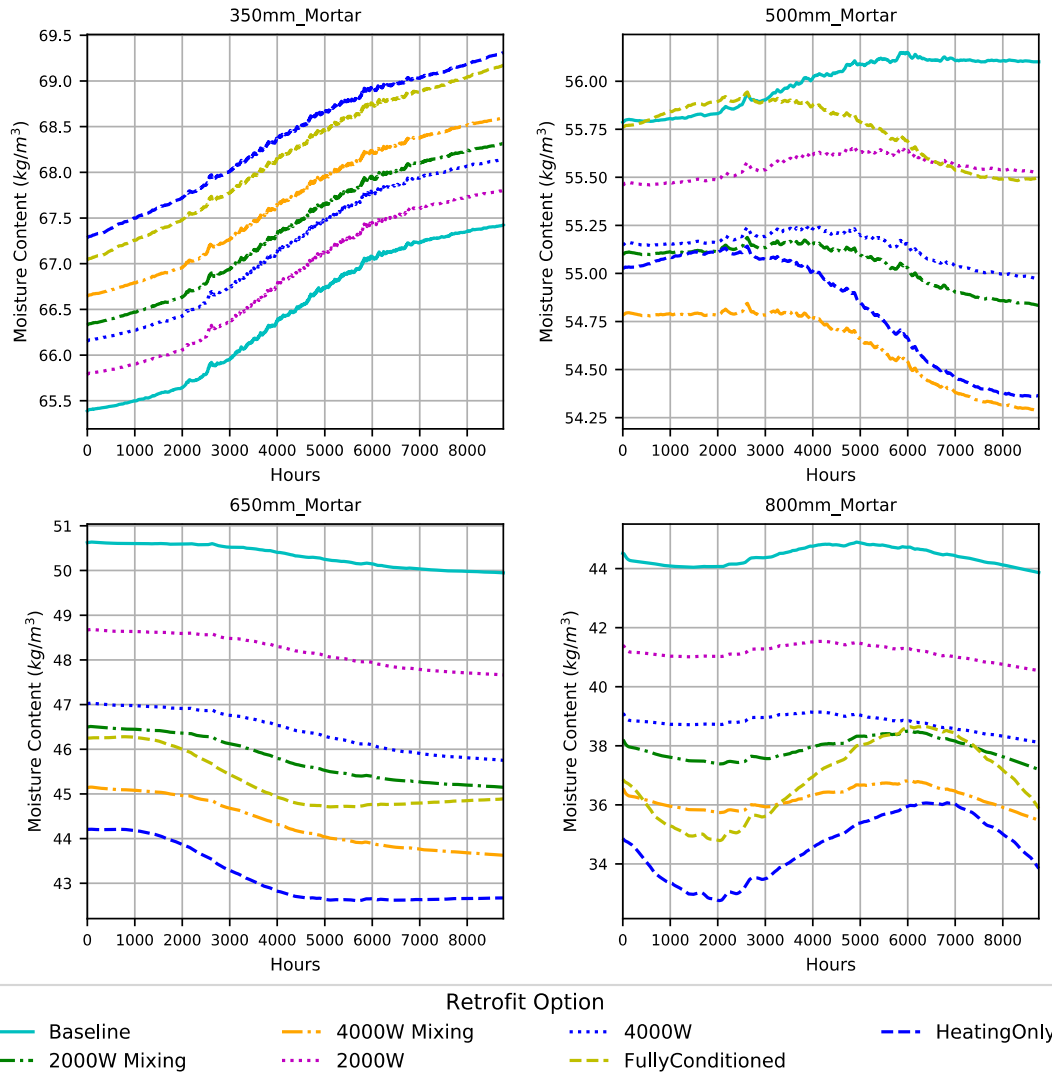


**Figure 3-12: Moisture Content versus Time for the sixth floor wall under low moisture conditions**

The same general trend can be seen under high moisture loading conditions where the retrofits are reducing moisture content and initiating drying closer to

the interior face of the wall. Once again there is an inversion toward the exterior face where the retrofits are predicted to performing marginally worse.

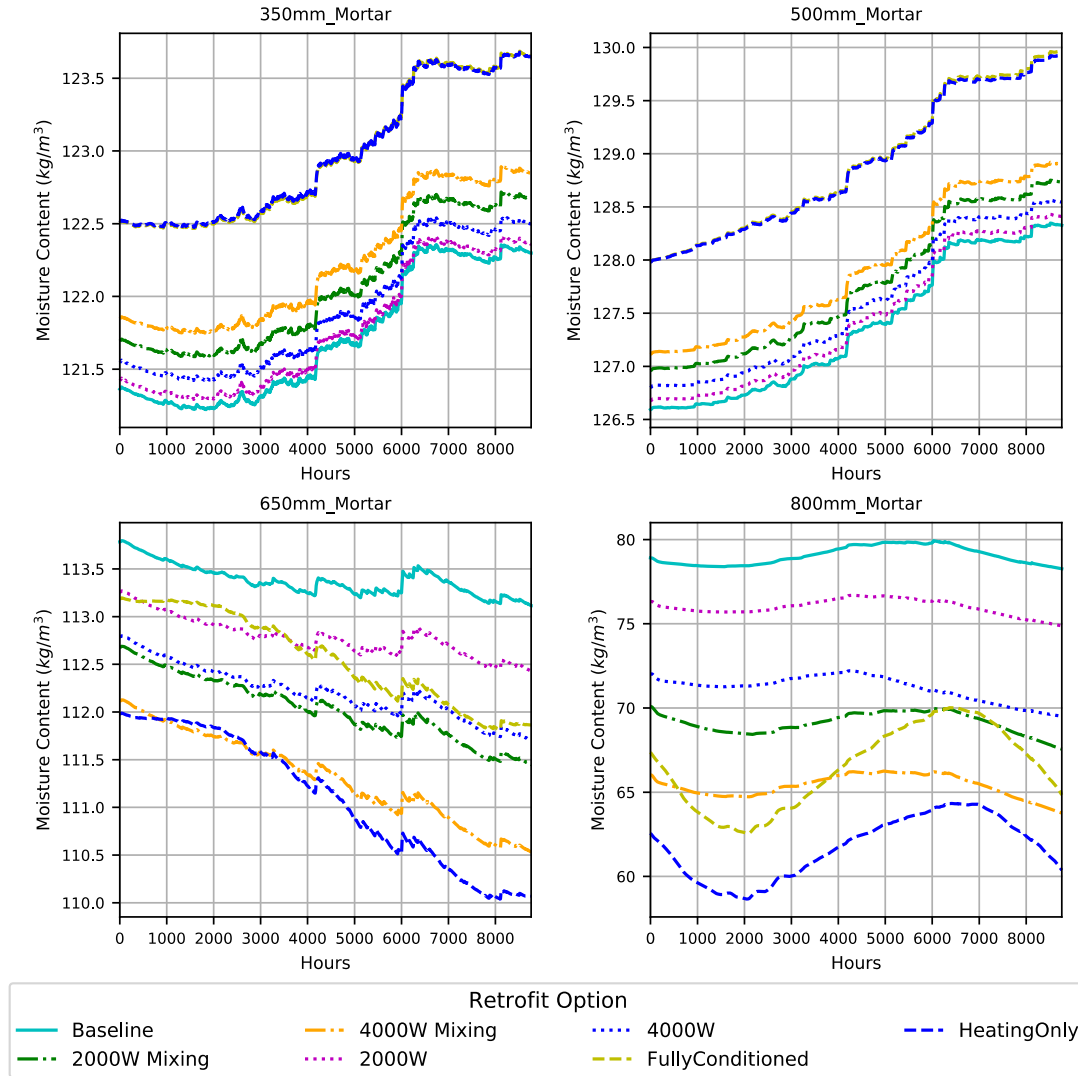


**Figure 3-13: moisture content versus time for the sixth floor wall under high moisture conditions**

While only, the sixth-floor South façade results are presented in the graphs, the same general trends can be found in the results for the West facades and the fourth floor. There was no significant difference in moisture through the core, when taking from the mortar line or next to the stone. As evident from the difference in moisture content between low and high moisture loadings, rain infiltration and adhering fraction of rain play a more significant role than interior conditions.

### **3.6.3.3 Discussion**

The influence of interior climate appears to extend only to the inner half of the wall at best, while the exterior climate influences the outer part. The outer half of the wall is where we expect the moisture-related damage to occur as evidenced by the freeze-thaw cycle graphs in Figure 3-10 - Figure 3-11. Because the drying effect cannot extend to the exterior portions of the wall, the benefit to the durability of the walls is not as clear-cut.

One possible cause for the inversion in the predicted moisture content relative to the baseline in the outer portion of the masonry is because of moisture drive in the vapour phase. Because the retrofits cause higher temperatures, there is a higher vapour gradient between inside and outside. This leads to vapour travelling from inside to outside being absorbed later in the wall.

The retrofits which are predicted to perform best are the heating only option, followed by the high-density installation with increased flow rate (4000W with mixing) followed by a fully-conditioned tower. The heating only option is predicted to cut the moisture content 800 mm from the exterior by roughly 25% after 5 years. The heating only option performs better than the 4000W with mixing option because it can guarantee warmer conditions, while the fully conditioned option performs slightly worse because higher interior temperatures are suppressed, and a certain minimum RH is maintained which will inhibit desorption from the masonry.

The hygrothermal simulations were done only with the typical weather file repeated every year. A wider cross-section of historical or predicted weather data that encompass drier, wetter, colder or hotter years, may provide different conclusion.

These are very thick walls. If this same study were to be done on thinner stone walls (600-700mm) or a multi-wythe brick wall, the conclusion may be different. The interior climate may be able to influence drying of the wall more thoroughly. A wall with different material properties or geometry may also produce different results.

The recommended retrofit would be to re-install the electronic equipment in the

fourth floor and increase the exhaust flow rate up the tower. This retrofit will warm the upper portions of the tower, keep the RH suppressed as the air rises in the tower and will also reduce the risk of condensation and frost forming on windows and the interior surfaces, remembering that RH has been recorded above 90% in the sixth floor. This retrofit also uses waste heat from another process to accomplish this and requires minimal additional energy consumption other than fan energy compared to a dedicated heating and cooling system.

### **3.7 Conclusion**

This paper demonstrates a procedure used to develop a calibrated energy model on a heritage designated structure with the purpose of assessing durability concerns related to moisture-related damage. The interior ambient RH and T were monitored beginning in September 2017 on the first, fourth, fifth and sixth floors of the tower. From this data, a calibrated energy model was created that could predict the temperatures in the tower. The calibration was done using GenOpt optimization software and went through two evolutions. The final calibrated energy model was able to achieve an overall RMSE for all 4 measured zones of 1.040°C for the period between 1 September to 2 August.

Using the calibrated energy model as a baseline, six possible retrofits that would alter the ambient temperature profile inside the tower were modelled. These six retrofits were to reinstall electronic equipment on the fourth floor that was

removed in both a smaller and larger installation configuration, both with the current exhaust flow rate and increased one; a fully conditioned HVAC system and a heating only system for the upper parts of the tower. The resulting modelled ambient RH and temperatures from these retrofits were fed into a Delphin hygrothermal model of a typical masonry cross-section on both the fourth and sixth floors. The wall was modelled in a low moisture loading and high moisture loading configuration. The number of freeze-thaw cycles and moisture contents for each retrofit were recorded.

The results of the hygrothermal models showed that the benefits to drying the masonry wall were localized to the interior half of the wall. In the exterior portion of the wall, the predicted effect of these retrofits was marginal and were in cases worse than the baseline condition. This is important because the exterior is the place where we would expect most moisture-related damage to freeze-thaw action to occur. The retrofits reduced the number of hours that the wall was subjected to conditions below 0°C but the reduction in freeze-thaw cycling was not significant.

The recommended retrofit would be to re-install the electronic equipment in the fourth floor and increase the exhaust flow rate up the tower. This will keep the upper portions of the tower warmer, reduces risk of condensation on windows

and surfaces and requires minimal additional energy compared to a dedicated heating and cooling system.

Future studies include further calibration of the energy model. 17 months of data were collected in total where a full annual cycle can be analysed. Ultimately, the end goal is to create calibrated hygrothermal models using a similar procedure. This would be based on interstitial RH or MC sensors. The goal would be to understand uncertain hygrothermal parameters such as sorption and liquid suction curves in-situ.

## **4. Calibrated Envelope Modelling**

This section contains content published in and presented at:

Gutland, Michael, Mario Santana Quintero, and Scott Bucking. 2019. "Calibration of an Historic Masonry Building Using Measured Temperature and Heat Flux Data." In Proceedings of Building Simulation 2019: 16th Conference of IBPSA. Rome, Italy.

Some sections from the conference paper have been removed because they are duplicated content from Section 3..

### **4.1 Wall Calibration**

The theme of calibration was extended to analysis of individual walls by comparing measured heat flux, surface temperatures and interstitial temperatures. This will help to verify some of the wall's thermal properties from the EnergyPlus calibration.

Two wall sections were studied; the fourth-floor south façade and the sixth-floor south façade. Both walls had Type T thermocouples and Omega HSF-4 Thin Film Heat Flux Sensors (OMEGA Engineering, n.d.) affixed to the interior surface (the sixth floor heat flux sensor debonded from the wall midway through the experiment and its results are not discussed further). Interstitial temperatures

were recorded via Vaisala RH Sensors (Vaisala, 2011) on the sixth floor and by SMT Embedded Moisture Sensors (EMS) on the fourth floor (SMT Research, n.d.). These sensors were installed to monitor hygrothermal conditions over time and were staggered at different depths. The heat flux sensors have an uncertainty of  $\pm 10\%$  W/m<sup>2</sup> and the Type T thermocouples have an uncertainty of  $\pm 0.5$  °C.

Two types of calibration metrics were used. The first was to perform a calibration based on measured temperatures. The second was to calibrate against measured heat flux.

Delphin 6.0 was chosen for the calibration of the wall because of the flexibility it offers with regard to temperature and moisture-dependent conduction and has two-dimensional capabilities (Bauklimatik Dresden, 2018).

The model was a simple two-dimensional wall shown in Figure 4-1. The model was separated into two material types (Sandstone and Mortar/Core). The two materials were thought to have different thermal properties, especially the sandstone having a much higher conductivity than the mortar/core.

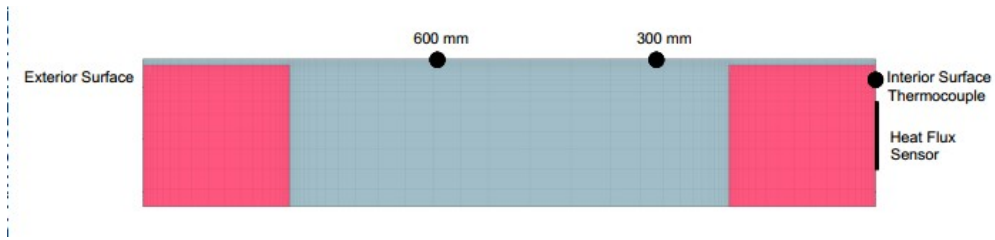


**Figure 4-1: Delphin 6.0 model used for calibration of wall thermal properties. Red = sandstone, grey = mortar**

Delphin allows for exterior convection coefficients to vary based on wind velocity. A correlation based on Nusselt and Jurges (1922) was used but with a variable constant term ( $x$ ) to go with the fixed linear term (*EnergyPlus*, 2017b).

$$h_e = x + 3.94 V_z \quad (4-1)$$

- $h_e$  = exterior convection coefficient [W/m<sup>2</sup>-K]
- $x$  is a variable constant
- $V_z$  = local wind speed [m/s].

Interior convection was specified at a fixed value. Delphin does not have an adaptive algorithm for interior convection like *EnergyPlus* does. However, it is expected this value remains relatively stable.

Because conductivity is a function of moisture-content in porous media the fraction of absorbing rain and initial RH was modified depending on which wall

was being simulated. modified depending on which wall was being simulated. The 4th floor walls were giving higher values to represent its known moisture issued (and theoretically higher conductivity). The default moisture and temperature dependent formulas was used (Vogelsang et al., 2018). A list of the input parameters is shown in Table 4-1.

**Table 4-1: Parameters for wall calibration**

	Range		Interval	Calibration Results	
	Min	Max		Temperature (6 <sup>th</sup> floor)	Heat Flux (4th floor)
Conductivity Sandstone (W/m-K)	1.0	2.5	0.25	1.0	2.0
Conductivity Core (W/m-K)	0.7	1.1	0.1	0.7	1.1
Capacity Sandstone (W/m-K)	550	1150	100	550	550
Capacity Core (W/m-K)	550	1150	100	1050	1150
Interior Convection Coefficient (W/m2-K)	6	10	1	10	6
Exterior Convection Coefficient (W/m2-K)	4	8	1	8	4
Solar Absorption Coefficient (-)	0.5	0.9	0.1	0.9	0.9

The calibration was again performed with GenOpt using the Particle Swarm Algorithm. The timeframe began on 15 September and lasted for 270 days (9 months) for the sixth floor. It began on 1 February and lasted for 180 days (6 months) on the fourth floor.

#### **4.1.1 Calibration against measured temperatures**

The results for the calibrated model of the 6th floor are summarized in Figure 4-2. In general, the RMSE for each sentinel are better toward the interior than the exterior. The RMSE for the surface temperature have a good correlation to

measured values.

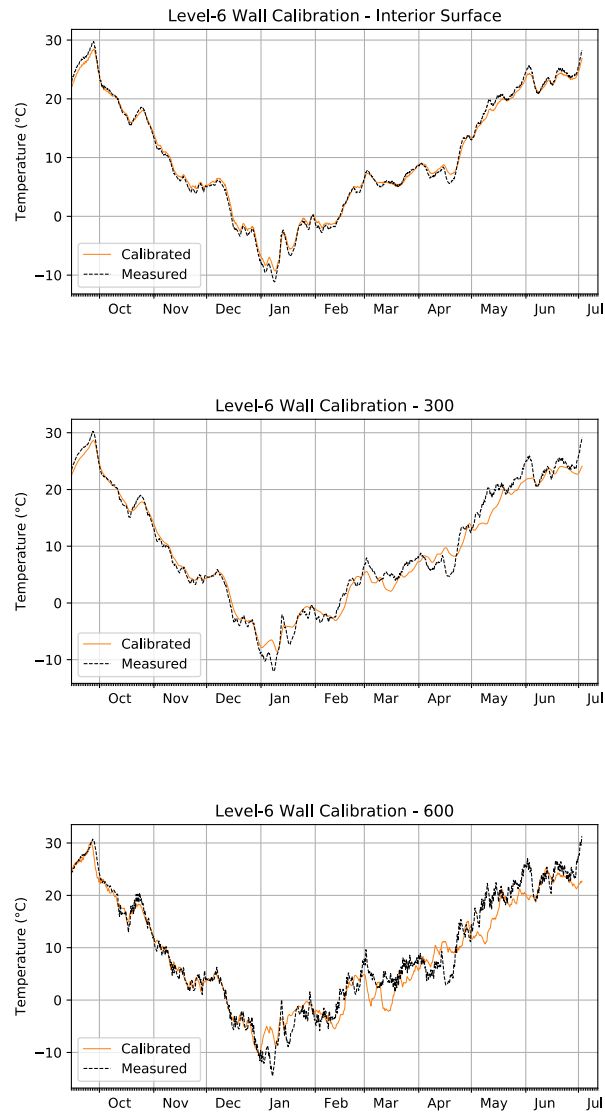


**Figure 4-2: Calibrated v. Measured data for the wall temperature calibration along the interior surface, 300mm and 600mm depths.**

The calibrated model of the 6th floor lead to some surprising and noteworthy results: The results of the calibration pointed toward the thermal conductivity of the sandstone being much lower than initially thought ( $<1.0 \text{ W/m}^2\text{-K}$ ). This could have been influenced by the presence of voids acting as insulating layers. This result needs to be inferred as an effective conductivity averaged throughout the layer and not as an inherent material property.

The second surprising outcome was that the interior convection coefficient was at the high end of the anticipated range ( $>10 \text{ W/m}^2\text{-K}$ ). This indicates one of 2 things. First there is sufficient air movement in the tower (either through buoyant or force convective loops); or that there is a small measurement bias in the surface mounted thermocouple that infers higher convection coefficients.

The next noticeable result was that the calibrated model tended toward unusually high solar absorption coefficients ( $\alpha > 0.9$ ). Coefficients this high are typical of black coloured materials. The masonry has endured significant soiling which has turned the stone a much darker colour.

The results were much better for the first 3 months than the rest of the calibration period. After this there are several anomalies which are not easily explained. In general, the temperatures are underestimated in the calibrated model.

The calibration to the interior surface is good, but as we move toward the exterior, the RMSEs get progressively worse (Table 4-2). Because the interior boundary condition had a good correlation, the fact that the correlation of the model decays as we go toward the exterior indicates an uncertainty with the exterior boundary condition, either with the weather file, solar absorption coefficients or exterior convection coefficients.

**Table 4-2: Wall calibration results**

Model	Sentinel	RMSE
Temperature (6th floor)	Overall	1.928°C
	Interior Surface	0.678°C
	300 mm from interior	1.657°C
	600 mm from interior	2.818°C
Heat Flux (4th floor)	Interior surface	5.150 W/m <sup>2</sup>

#### 4.1.2 Calibration against measured heat flux

The results for the calibrated model of the 6th floor are summarized in Figure 4-3. Positive heat flux is energy flowing out of the zone and negative is heat flowing toward the interior on warm days. An RMSE of 5.150 W/m<sup>2</sup> was achieved for the 6-month time period. There are some noticeable weak points in the model, where there is poor correlation. In February when heat transfer is near its peak, there is a consistent difference of approximately 5 W/m<sup>2</sup>. This is echoed from the calibration of the tower where it was difficult to model in winter. There is a strong

anomaly in April and in July there is a large discrepancy where the sensor is reading significant heat gain into the space, whereas the model never registers significant heat gain into the space.

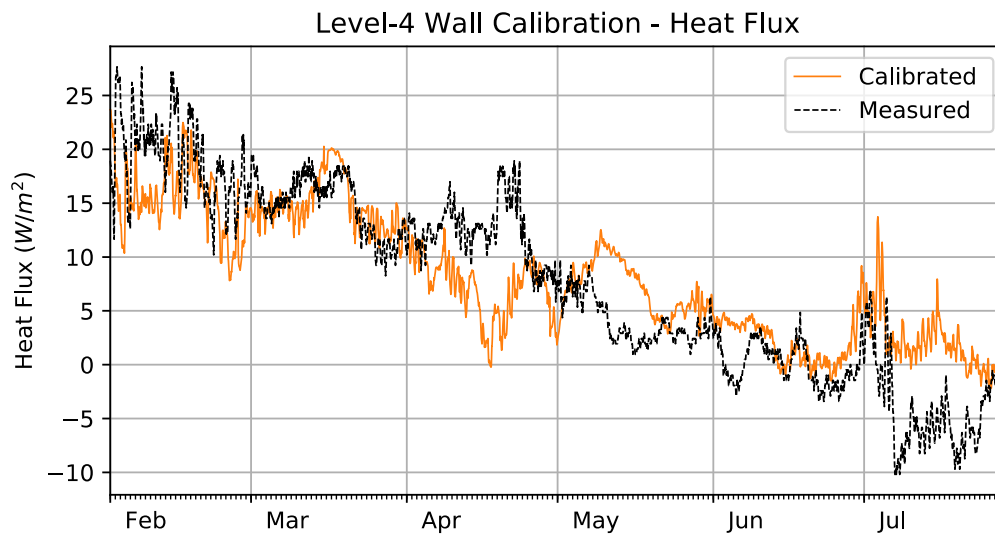


**Figure 4-3: Measured v. Calibrated surface heat flux for the fourth-floor South facade.**

While the calibrated model was not always able to achieve comparable magnitudes throughout, the amplitude of the diurnal amplitude was well represented. For example, in early February and in July, where there were prominent oscillations in the measured heat flux and the model was able to replicate this. Similarly, in May where there are relatively stable diurnal effects, the model is able to replicate this. The results returned an effective U-value of  $1.38 \text{ W/m}^2\text{-K}$ . This comparable to previous in-situ studies of historic masonry by

Lucchi (2017) and Baker (2011), with consideration that this wall is much thicker, has a very dense sandstone and is at a critical level of saturation.

The heat flux calibration returned both similar and contradictory findings to the wall temperature calibration. This model shared a tendency toward very high solar absorptivity and lower heat capacities. This indicates the wall has much more thermal dynamism than expected. The two factors lead to the fact there may be less thermal mass in the wall and that the numerous voids in the wall may be a contributor. This can also explain why we do not see the measured minimum and maximum heat fluxes as shown in Figure 4-3. The high solar absorbance may be attributed to the knuckled texture of the stone which gives more surface area than a flat planar surface.

The calibrated heat flux model does not share the calibrated wall temperature model's trend toward low thermal conductivity. Part of the difference between the two may be attributed to the 4th floor wall being saturated and the 6th floor being dry. The thermal conductivity for sandstone is more representative of what was found in the EnergyPlus calibration of the whole tower. The heat flux calibration returned interior convection coefficients that were much lower.

Between the two methods presented here for calibrating a wall, the heat flux method appears more trustworthy. It returns parameter values which are more plausible, especially for thermal conductivity. The fact that the wall studied is

essentially symmetrical and the relatively similar conductivity between materials makes it difficult to ascertain conductivity. The interstitial temperature profile is essentially linear between the exterior and interior surface temperatures, no matter what value is selected for conductivity. This also gives too much weight to both the interior and exterior coefficients.

#### **4.1.3 Conclusions**

Calibrated energy models of the Southwest Tower of the East Block building were performed against ambient air temperatures and surface heat flux measurements beginning in September 2017. Two types of calibrated model were developed; an EnergyPlus model of the entire tower and two-dimensional finite element models of a corresponding masonry wall assembly. The goal of this process is to both characterize the building's performance in its current state and to help define the thermal properties of the mass masonry walls in-situ.

An EnergyPlus model of the tower was created and the model was calibrated using GenOpt. The calibrated model for the entire tower achieved an RMSE of 1.040°C for the period between 1 September to 2 August across all 4 measured zones. Modelling parameters which had the greatest influence on the model were those regarding air transfer and mixing between zones. Air infiltration, and

thermal properties of the masonry envelope had a moderate influence, while glazing and optical properties had negligible impact.

Calibrated models of wall assemblies were developed using Delphin 6.0. Interstitial temperatures and interior surface heat flux were used as metrics for the calibration.

An overall RMSE of 1.928 °C was achieved for the sixth-floor wall using temperatures. A good RMSE was achieved for interior surface temperatures, but the quality of the calibration as you progress towards the exterior. An RMSE of 5.150 W/m<sup>2</sup> was achieved for the fourth-floor wall using measured heat flux to calibrate against. The parameters from these models trended toward higher solar absorption and lower heat capacities than default assumptions. This leads to assume that the wall has a more dynamic thermal response. Between the two methods of calibrating the wall, the heat flux sensor was deemed more reliable.

## 5. Masonry Interface Modelling

This section contains content published in:

Gutland, M., Bucking, S., & Santana Quintero, M. (2021). A methodology for hygrothermal modelling of imperfect masonry interfaces. *Journal of Building Physics*, 44(6), 485–509. <https://doi.org/10.1177/1744259121989388>

### 5.1 Abstract

Hygrothermal models are important tools for assessing the risk of moisture-related decay mechanisms which can compromise structural integrity, loss of architectural features and material. There are several sources of uncertainty when modelling masonry, related to material properties, boundary conditions, quality of construction and two-dimensional interactions between mortar and unit. This paper examines the uncertainty at the mortar-unit interface with imperfections such as hairline cracks or imperfect contact conditions. These imperfections will alter the rate of liquid transport into and out of the wall and impede the liquid transport between mortar and masonry unit. This means that the effective liquid transport of the wall system will be different than if only properties of the bulk material were modelled.

A detailed methodology for modelling this interface as a fracture is presented including definition of material properties for the fracture. The modelling methodology considers the combined effect of both the interface resistance across the mortar-unit interface and increase liquid transport in parallel to the interface, and is generalizable to various combinations of materials, geometries and fracture apertures. Two-dimensional Delphin models of a clay brick/cement-mortar masonry wall were created to simulate this interaction. The models were exposed to different boundary conditions to simulate wetting, drying and natural cyclic weather conditions. The results of these simulations were compared to a baseline model where the fracture model was not included.

The presence of fractures increased the rate of absorption in the wetting phase and an increased rate of desorption in the drying phase. Under cyclic conditions, the result was higher peak moisture contents after rain events compared to baseline and lower moisture contents after long periods of drying. This demonstrated that detailed modelling of imperfections at the mortar-unit interface can have a definitive influence on results and conclusions from hygrothermal simulations.

## 5.2 Introduction

Hygrothermal models are important tools for assessing durability risks in building envelopes, such as biological growth (mould and wood rot fungi), corrosion and freeze-thaw action in masonry. These pathological conditions can compromise structural integrity, affect the health and wellness of occupants and lead to irreversible loss of architectural material and features; some which may have historical significance.

Hygrothermal modelling is known to have numerous weaknesses and gaps in our understanding. First, there are significant uncertainties relating to model inputs including material properties, boundary conditions, quality of construction and two-dimensional interactions between adjacent materials. Second, it is difficult to calibrate predicted model performance to that which is measured in the field. Part of this relates to the previously mentioned uncertainties and to difficulties obtaining accurate in-situ moisture measurements. Third, two and three-dimensional interactions are poorly understood and are rarely modelled in practice. The presence of these gaps can reduce our confidence in the model's ability to accurately capture the true extent of moisture issues in an assembly.

It is common procedure to make the following assumptions for hygrothermal modelling:

1. Materials are homogeneous. There are no localized variations in pore structure, physical properties or chemical composition.
2. Adjacent materials are in perfect contact with each other.
3. There are no imperfections in the materials or assembly.

For masonry walls, these assumptions are not always valid. This is most apparent at the interface between the mortar and the unit where there are imperfections such as cracks or imperfect contact conditions between adjacent materials. An example of this is shown in Figure 5-1. On this heritage sandstone building, a combination of stone displacement, shrinkage and repointing of varying composition and quality have led to physical separations between mortar and unit. This is evident in several ways from an open joint, hairline crack or an imperfect contact between the two. Intuitively, it is reasonable to assume this would lead to an increase of liquid water absorption into the wall from wind-driven rain. Many experienced masons and conservation professionals will say this a gateway for water to penetrate into the wall. The question is to what extent will absorption into the wall change, and is there a risk for increased moisture-related damage?

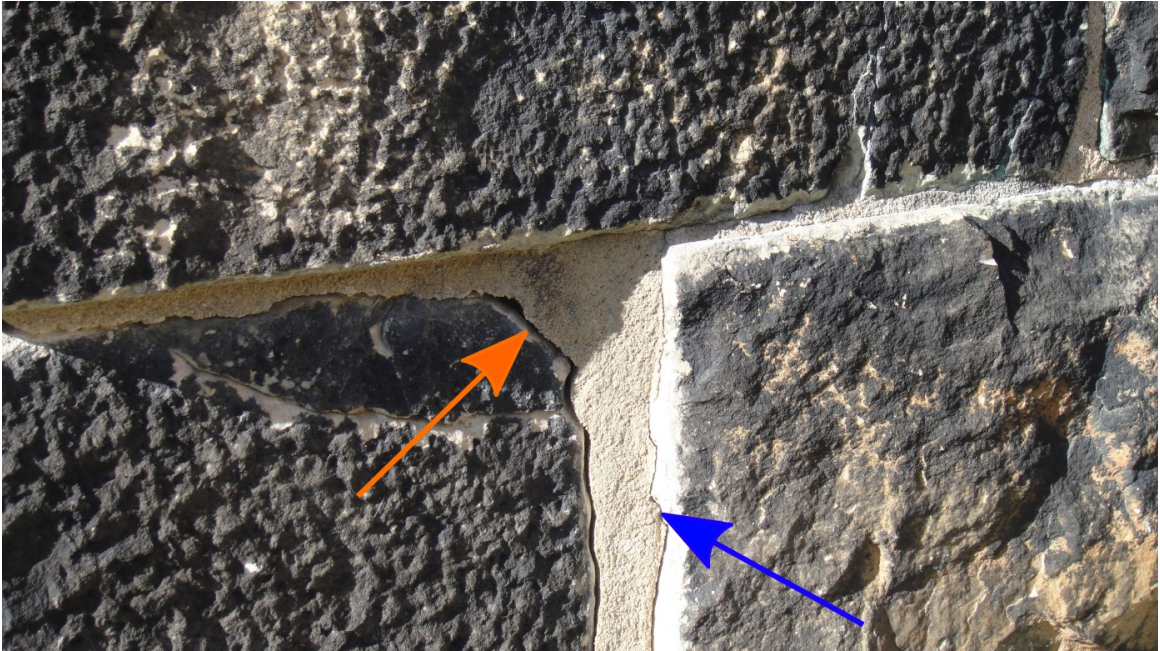


***Figure 5-1: Sandstone masonry wall with open joint (Orange) and hairline crack (dark blue) between stone and mortar***

This paper outlines a generalizable method for modelling these imperfections by introducing a fracture interface into a hygrothermal model. This model combines two different phenomena which are often modelled in isolation; interface resistances and increased fluid flow through fractures. Different size fractures (apertures) were modelled between unit and mortar, with and without an interface resistance in between. Simulations were performed under absorption, drying and natural (cyclic) conditions. The latter two are often neglected in studies and should be considered because masonry is often under drying conditions. The

change in moisture content over time was compared to a baseline scenario without the fracture and perfect contact is assumed.

### **5.3 Literature Review**

The mortar-unit interface is a complex area in the context of moisture transfer, especially considering when there are imperfect contacts, cracks or other damages. Many studies have examined the presence of an interface resistance which slows the liquid transport from mortar to unit or vice versa. The interface resistance affects transport perpendicular to the interface and not parallel to the interface. Moisture transport should also be considered parallel to the unit interface. Several studies have examined moisture transport in fractured building materials, and the absorption rate when exposed to liquid water. Often, the fractures are in a homogeneous material such as concrete and the presence of fractures and required detailed geometric mapping.

Both of these phenomena are often studied in isolation, and not in tandem. There isn't a simple and generalizable modelling method developed which connects the magnitudes of the interface resistance, and increased liquid flow via the fracture. By generalizable method, we are referring to a model which is based on one or two observable parameters and utilizes a more upscaled approach. In this case the parameters are the visible level of damage, or more specifically the assumed

aperture of the fracture. Furthermore, these studies often focus only on the wetting phase and do not consider the drying phase, or the transient cyclic weather conditions a building envelope will experience.

### **5.3.1 Mortar – Unit Interface Resistance**

Previous studies have demonstrated that there is an interface resistance ( $R_{IF}$ ) between the mortar and unit which inhibits liquid moisture transport across the interface. This is caused by two reasons. The first reason is there are gaps between the two materials which formed either immediately after curing or by cracking/displacement over time. Water lacks the capillary traction forces to efficiently traverse the gap and needs to travel across the gap via vapour diffusion instead of through quicker capillary action. The nature of the gap may be inconsistent along the interface ranging from a perfect contact to an open fracture (Figure 5-2). The second reason is migration of fine particles toward the mortar joint during the curing stages (Brocken, 1998). The fine particles form smaller pores near the interface and this reduces liquid flow. The interface resistance can be modelled in several ways. It can be modelled with as an explicit infinitesimal layer analogous to contact resistances in heat transfer (Calle et al., 2019; Derluyn et al., 2011; Janssen et al., 2012; Qiu et al., 2003); or as an air layer between materials as in Equation 5-1 (Brocken, 1998).

$$R_{IF} = \frac{h}{\delta_a} \frac{\Delta P_c}{\Delta P_v} \quad (5-1)$$

- $h$  = height of air layer [m]
- $\delta_a$  = vapour diffusion coefficient for still air [s]
- $P_c$  = Capillary Pressure [Pa]
- $P_v$  = Vapour Pressure [Pa]

Laboratory tests have measured the interface resistance between  $1.0E08$  and  $1.0E12$  m/s (Calle et al., 2019; Derluyn et al., 2011; Qiu et al., 2003). These values changed depending on the combination of materials, whether the mortar was dry or wet cured and whether the joints were oriented vertically or horizontally. Simulations have also demonstrated the effect that the interface resistance has on moisture absorption when exposed to realistic wind-driven rain and rising damp conditions (Vereecken & Roels, 2013; Zhou et al., 2018). A different laboratory test performed by Zhou et al (2020) designed to measure water uptake while considered interface resistances found a noticeably quicker advance in the wetting front adjacent to an interface with a visible crack. The authors noted a need for an absorption model for masonry with cracks at the interface.

The interface resistance is assumed to be a constant value in simulation and laboratory tests. It is possible that this is not true, and it changes depending on degree of saturation. If the case of a fracture is considered, as the moisture front approaches and the fracture is wetted, water would be able to bridge across the upper and lower surfaces of the fracture, and the resistance will diminish. As simulation study by Alfaiate (2010) indicates that the interface resistance may be moisture-dependant. Here a fracture was modelled with a fixed boundary condition, next to the porous media and separated by a surface transfer coefficient. This value was estimated to be in the range of  $10^6$  m/s and is several orders of magnitude lower than what was found by laboratory tests. The possibility of a non-constant interface resistance would be important if both drying and wetting cycles are considered; or if water is coming parallel to the interface. Because the fracture is more likely to be dry under natural cyclic conditions,  $R_{IF}$  will be assumed to be constant for the simulations in this paper and calculated from Equation 5-1.

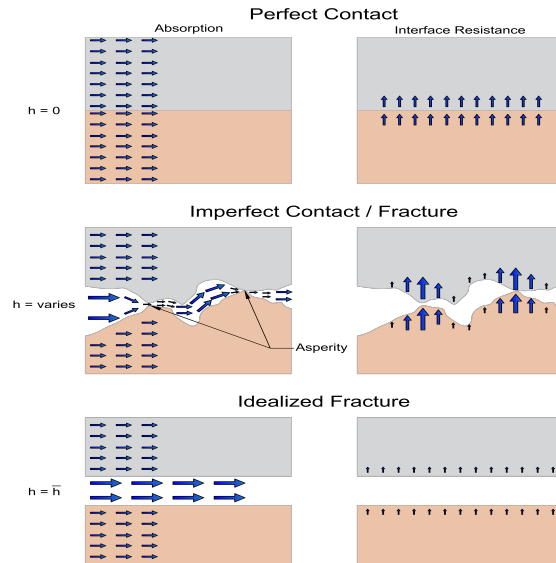


**Figure 5-2: Illustration of various contact conditions and how it affects moisture transfer in the interface.**

### 5.3.2 Fracture Modelling

The interface resistance does not explicitly consider transport parallel to the interface. Water absorption in fractured materials (brick and concrete) has been studied by Roels and Rouchier in 2D (Rouchier, 2012; Vereecken & Roels, 2013) and by Li and Smyl in 3D (Li et al., 2018; Smyl et al., 2016). In all scenarios, the rate of water absorption increased through the porous media. These studies had a few procedural weaknesses in their applicability to masonry. First the fractures required detailed geometric analysis and discretization into a finite-volume grid. This requires increased effort and computational costs and is difficult to

generalize for large sections of wall or the variety of crack patterns which could be encountered. The second is that the testing and simulations were done on homogeneous materials, meaning that the material was the same either side of the fracture. In a masonry interface this is not true as the hygroscopic properties of the two adjacent materials may be quite different. And third, these studies primarily focused on the wetting phase only. Considering these weaknesses, a simplified model is proposed where cracks at the mortar-unit interface are explicitly modelled as fractures.

Liquid water transport in fractures is similar but distinct to that of traditional capillary mechanics in porous media (bundle of capillaries model). Fluid flow in fractures is bounded only on two sides, whereas in capillaries it is bound in all directions. A fracture will also have fewer obstructions than the bundle of capillaries model and have less resistance to moisture flow.

To calculate the hygric properties of a fracture, we start with the Navier-Stokes equation and the assumption that the fracture be modelled as two smooth parallel plates. If external forces are neglected, one-dimensional flow and steady-state conditions are assumed, then the Navier-Stokes equation can be transformed into the Cubic Law which calculates mass flow rate across the width of the fracture.

$$Q = \frac{-\rho w h^3}{12\mu} \nabla P_c \quad (5-2)$$

- $Q$  = mass flow rate of liquid [kg/-s]
- $\rho$  = density [kg/m<sup>3</sup>]
- $w$  = width of fracture [m]
- $h$  = aperture [m]
- $\nabla P_c$  = capillary pressure gradient [Pa]
- $\mu$  = dynamic viscosity [kg/m-s]

This can also be expressed on a per area basis by dividing by the width and aperture ( $w/h$ ):

$$\dot{m}_l = \frac{-\rho h^2}{12\mu} \nabla P_c \quad (5-3)$$

The first term of Equation 5-3 is the liquid conductivity of the fracture and is similar in form to the Hagen-Poiseuille equation for liquid flow through tubes. The difference between the two is the denominator being 12 instead of 8, and that aperture is used instead of the capillary radius.

The aperture is the distance between the upper and lower boundary surfaces of a fracture. One assumption for the Cubic Law is that the aperture remains constant throughout the fracture. In reality, fractures are non-uniform; the aperture widens and contracts, changes direction, and generally follows a tortuous path as fluid travels along its length (Figure 5-2). This means that the aperture is difficult to quantify at all points along the fracture length, and an alternative and simpler method is required.

Two methods are to use the average aperture height of the fracture ( $\bar{h}$ ), or to use what is known as the hydraulic aperture ( $h_H$ ). The hydraulic aperture is the value of  $h$  which would make the cubic-law true for the bulk media in question (Zimmerman & Bodvarsson, 1994). A literature review on the subject provides numerous expressions to arrive at a value for  $h_H$  (Zimmerman & Bodvarsson, 1994). Other models of fractures have been developed which consider the micro-scale aberrations and tortuosity of the flow path (Brown, 1987; Ge, 1997). This however increases model complexity and is difficult to generalize for this application.

Asperities also effect the flow path in a fracture. Asperities are points where the upper and lower walls of the fracture are in contact with another and the aperture height effectively becomes zero. In the context of masonry, these are the points where mortar and unit bond and transmit normal forces to one another (See

imperfect contact in Figure 5-2). There have been many models and formulas developed to calculate the effect of asperity that depend on the size, shape and distribution of the asperities. Kirkpatrick (1973) developed a theory on how asperity changes hydraulic aperture and therefore conductivity by the use of effective medium theory. From this method, the following equation predicts that:

$$h_H^3 = h_0^3(1 - 2c) \quad (5-4)$$

- $h_H$  = hydraulic aperture [m]
- $h_0$  = average aperture [m]
- $c$  = contact area or concentration of asperities [--]

The greater the number of asperities, the lower the effective hydraulic aperture will be and therefore reduced liquid transport. More complex equations have been proposed and it has been found that in some cases, using the above equation with asperities considered, versus only using only the mean aperture, resulted in differences in hydraulic conductivity of more than an order of magnitude (Zimmerman & Bodvarsson, 1994). The difference between mean aperture and hydraulic aperture has been reported to be a factor of between 1.1 and 1.7 (Hakami, 1995). Typical apertures in subterranean rock are reported to be in the 1-100 $\mu$ m magnitude range (Pyrack-Nolte et al., 1987) and fractures in

building materials range are in a similar range (Roels et al., 2003; Rouchier, 2012). Anything much smaller than this and liquid transport is greatly reduced.

The advantage of using hydraulic aperture over the mean aperture is that it avoids investigating and describing the complex geometry of the fractures. For the remainder of this article when using the term aperture or the symbol ( $h$ ), we are referring to the hydraulic aperture.

### **5.3.3 Hygrothermal Simulation Tools**

A two-dimensional finite volume software is required for simulation of fractured material of this type. Commercially available hygrothermal software which can handle this type of problem include WUFI 2D (Fraunhofer Institute for Building Physics, 2019b) and Delphin (Bauklimatik Dresden, 2018). Other software such as COMSOL or hydrogeological modelling software could also be used for this problem, but lacks the set-up for hygrothermal problems. A custom finite-element code a la Roels (2003) was not considered practical to develop. Delphin was chosen because it has the ability to easily model contact resistances and can handle very small ( $< \mu\text{m}$ ) grid elements needed for the fracture models.

### **5.3.4 Synthesis**

There have been many studies of the interface in masonry which focus on moisture transport in only one direction; either parallel or perpendicular to the

interface, but not both. These studies primarily focus on the absorption phase and little attention is given to the drying phase or exposure to realistic boundary conditions. The methods and results can also be difficult to generalize for various cracking patterns, crack widths and states of decay.

This paper proposes a generalized methodology for modelling the mortar-unit interface by idealizing the system as a fracture. The method simultaneously considers transport both parallel and perpendicular to the fracture and examines the absorption, drying phases and natural cyclic weather conditions. The models use a simplified geometry and can be transferred to any combination of material properties and dimensions of mortar and unit. The hygric properties of the fractures and adjacent materials can be determined from basic principles.

#### **5.4 Methodology**

A series of two-dimensional hygrothermal models were created which explicitly modelled the mortar-unit interface as a fracture. The wall typology simulated is an uninsulated double-wythe brick masonry wall with cement-based mortars. The fracture was modelled with different size apertures ranging from 1  $\mu\text{m}$  to 500  $\mu\text{m}$ .

Five distinct models were created, which included three different interface models and three different boundary conditions:

1. Absorption: Fracture without interface resistance

2. Absorption: Interface resistance only
3. Absorption: Fracture with interface resistance
4. Drying: Fracture with interface resistance
5. Cyclical: Fracture with interface resistance

Models 1-3 examine the absorption phase only. They are intended to mimic a water absorption test held at a constant boundary condition. Three different ways of modelling the interface were tried combining the fracture model and interface resistance model together and in isolation. Model 4 examines the drying phase to examine how the fracture may help or hinder drying from near-saturation conditions. Model 5 represents a simple double-wythe wall assembly exposed to realistic exterior and interior boundary conditions, to examine its behaviour under cyclic wetting and drying periods.

#### **5.4.1 Delphin Model**

Delphin 6.0 was chosen to perform the simulations (Bauklimatik Dresden, 2018). The model was kept geometrically simple, consisting of three materials: mortar, interface and clay brick Figure 5-3. The interface's height and properties change depending on the aperture chosen. The dimensions of the brick were based on standard North American sizes.

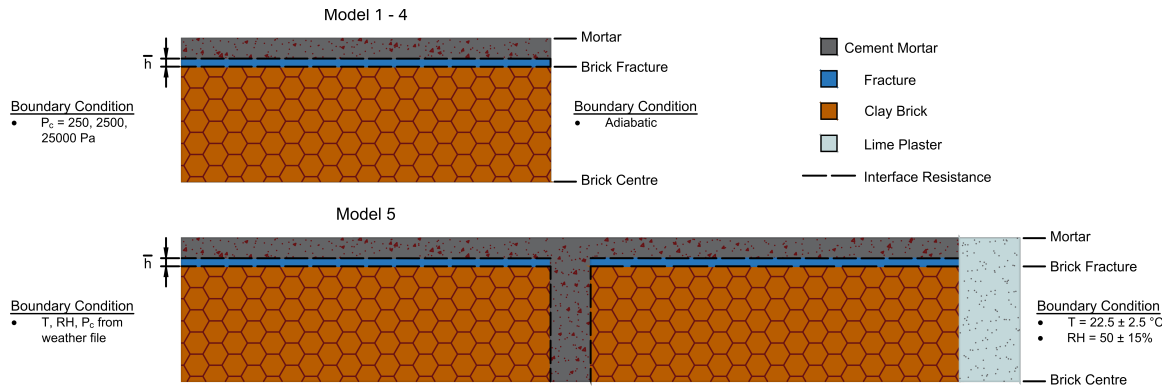


**Figure 5-3: Geometries used in the Delphin simulations**

Adiabatic and impermeable (zero-gradient) boundary conditions were assumed on the top and bottom taking advantage of symmetry. For the absorption models (Models 1-3), the exterior boundary condition was held at a fixed capillary suction pressure. Three levels of capillary pressure were used (250 Pa, 2500 Pa, 25000 Pa) to simulate three different degrees of wetting. The 250 Pa boundary condition was used to simulate immersion in water. Ideally this would be set to 0 Pa (the transition point from hydrostatic pressures) if a water absorption experiment were simulated. However, some numerical stability issues were encountered at very low suction pressures. Trial simulations below 250 Pa did not produce substantially different outcomes. The 2500 Pa boundary condition was used to simulate a heavy rain event and the 25000 Pa boundary condition was used to simulate a light to moderate rainfall event. The interior was modelled with zero-gradient boundary conditions. The initial RH of the three materials was set to 50% and heat transfer was not modelled.

Model 4 (drying) had the same geometry and material properties as the absorption models. The initial MC was set at near saturation. The ambient boundary condition was set to RH = 50%. The vapour convection coefficient was set to  $3 \times 10^8$  s/m. Again, the interior was modelled with zero-gradient boundary conditions and heat transfer was not considered.

For Model 5 (cyclical), the exterior boundary condition was determined from the 1 in 10 year weather year for the Ottawa International Airport using the RHT method (Zhou et al., 2016). This weather file had an average temperature of 7.6 °C, average RH of 73.0% and annual precipitation of 945mm. The interior boundary conditions were based on annual sine curves:  $T = 22.5^\circ\text{C} \pm 2.5^\circ\text{C}$  and  $\text{RH} = 50\% \pm 15\%$ . In general, the default model parameters in Delphin such as convection coefficients and solar absorption coefficients were used. The only exception being the rain exposure coefficient being increased to  $F_D F_L = 1.0$  to put more stress on the wall assembly (ASHRAE, 2016).

Care was needed when defining the finite-volume grid. Because of the sub-millimetre height of the aperture layer, individual grids in the y-direction are very small. A smooth transition between neighbouring elements is needed and a relatively large number of grids were required. An expansion ratio of 1.2 was used throughout with grids concentrated around the wetting boundary condition and fracture. The mass balance absolute tolerance was set to  $5 \times 10^{-5}$  kg at each

timestep. Delphin's solver parameters were adjusted based on the needs of each simulations.

## 5.4.2 Material Properties

### 5.4.2.1 Bulk Materials

The hygrothermal properties of the clay brick and the mortar are shown in Table 5-1. They were determined by taking the median values of all similar types of materials in the Delphin library. The moisture retention curves and liquid conductivity curves were calculated using single-mode Van Genuchten curves (van Genuchten, 1980). For each database material, the  $n$  and  $\alpha$  parameters were calculated via least-squares regression. The median values of  $n$  and  $\alpha$  were then used to generate the moisture retention curve for the clay brick and cement mortar. The material property curves are shown in Figure 5-4.

$$P_c = \frac{1}{\alpha} \left[ S_{eff}^{-\left(\frac{n}{n-1}\right)} - 1 \right]^{\frac{1}{n}} \quad (5-5)$$

Van Genuchten Equation where

- $P_c$  = capillary pressure [Pa],
- $S_{eff}$  = effective saturation [-],

- $n$  = material-specific fitting parameter [--],
- $\alpha$  = material-specific fitting parameter [ $\text{Pa}^{-1}$ ].

**Table 5-1: Bulk material properties used in Delphin simulations**

	Clay Brick	Cement Mortar
$\theta$ [--]	0.294	0.230
$\lambda$ [W/m-K]	0.682	0.723
$\mu$ [--]	20.2	25.6
$k_{l, \text{eff}}$ [s]	2.21E-09	9.05E-12
$n$ [--]	1.55	1.45
$\alpha$ [1/kPa]	0.1	0.02

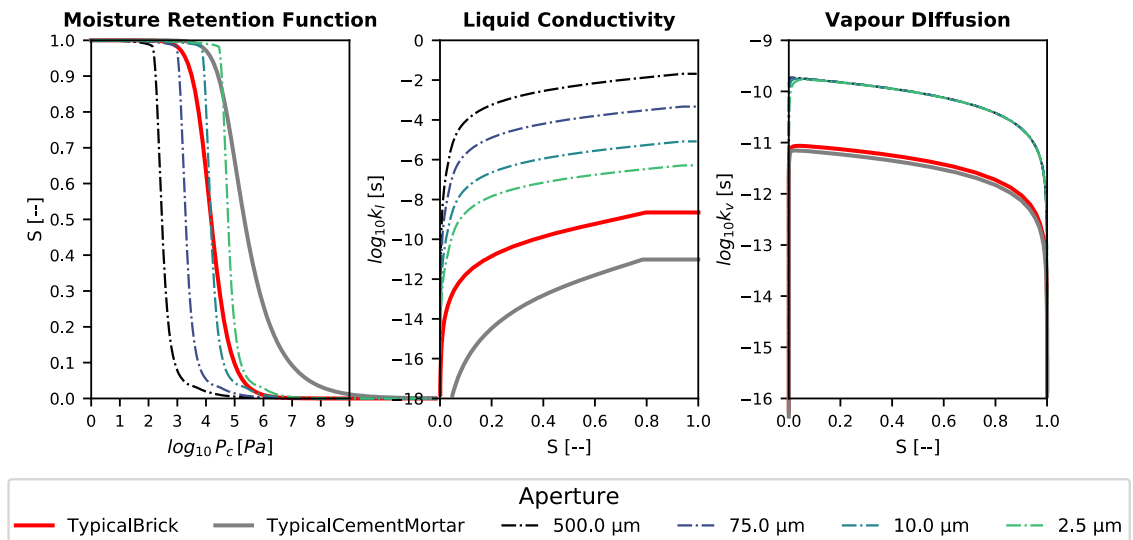


**Figure 5-4: Material property curves used in simulation**

The approach for liquid conductivity was to use the theoretical Van Genuchten curves and the Hagen-Poiseuille equation to create the moisture-dependent curve ( $k_l(\theta)$ ). The pore size distribution can be inferred through the Young-

Laplace equation which equates capillary pressure ( $P_c$ ) into capillary radius ( $r$ ). The liquid conductivity through a capillary can be calculated using the Hagen-Poiseuille equation. At low degrees of saturation, only the small capillaries are filled and available for liquid transport. As the media becomes more saturated the liquid conductivity increases as the more open and freer flowing pores become active. Integrating over the range of active capillaries yields the following equation (Burdine, 1953; Scheffler et al., 2004):

$$k_l(\theta_l) = \frac{\rho}{\tau} \int_{R_{min}}^R \frac{\pi r^4}{8 \mu_l} \frac{dn}{dr} dr \quad (5-6)$$

- $k_l(\theta_l)$  = moisture-dependent liquid conductivity [S]
- $\rho$  = density [kg/m<sup>3</sup>]
- $\tau$  = tortuosity [--]
- $r$  = capillary radius [m]
- $\mu$  = Dynamic viscosity [kg/m-s]
- $n$  = number of capillaries of that size.

This equation was reduced by a tortuosity factor ( $\tau$ ) which was determined by scaling the liquid conductivity to the effective liquid conductivity at saturation ( $k_{l,eff}$ ).

$$\tau = \frac{k_l(\theta_{cap})}{k_{l,eff}} \quad (5-7)$$

- $k_l(\theta_{cap})$  = liquid conductivity at capillary saturation from Equation 5-6
- $k_{l,eff}$  = effective liquid conductivity obtained from physical testing in the Delphin library.

The vapour diffusion coefficients were calculated using the following equation:

$$k_v(\theta_l) = \frac{\delta_a}{\mu} (1 - S_{eff}) \quad (5-8)$$

- $k_v(\theta_l)$  = moisture-dependent vapour permeability [s]
- $\delta_a$  = Vapour diffusion coefficient for still air [s]
- $\mu$  = Vapour Resistance Factor [--]
- $S_{eff}$  = Degree of Saturation [--]

#### 5.4.2.2 Fractures

The hygric properties of the fractures can also be calculated using (Equation 5-6 to 5-8). The main difference is that the capillary radius ( $r$ ) is substituted for the aperture ( $h_H$ ). Capillary media has a pore radius distribution whereas the fracture is idealized as having a constant aperture. This leads to issues when defining the moisture retention curve as it turns into a step function with an abrupt transition from fully saturated to bone dry. This will lead to numerical issues in the

simulation program. To counter this, the fracture apertures were modelled as a normal distribution with mean ( $h$ ) and standard deviation ( $h/2$ ) which gives an aperture size distribution. This improves the numerical issues and is more representative of the geometry of an actual fracture.

The aperture distribution was translated into a moisture retention curve using the Young-Laplace equation. On the moisture retention curve (Figure 5-4), the larger apertures are located toward the left (low capillary suction) while the smaller apertures are shifted toward the right and resemble more traditional curves for porous media. Larger fractures require lower capillary suction pressure to fill and activate the fracture for liquid flow while smaller fractures become active at more common capillary suction pressures.

With the aperture distribution determined, the moisture-dependent liquid conductivity curve can be calculated using Equation 5-7 and the moisture-dependent vapour permeability curve can be conducted using Equation 5-8. Larger apertures allow for higher liquid conductivity than smaller fractures but require low capillary suction to become fully active. As seen in Figure 5-4, the liquid conductivity of the fractures are several orders of magnitude greater than the brick and mortar. Even though the exposed area of the fracture is small it can contribute to an increase in overall moisture transport.

The fractures were assumed to be fully open ( $\theta = 0.99$ ) and vapour resistance factor ( $\mu$ ) equal to 1.0. As a result, the vapour diffusivity in the fractures is considerably higher than the bulk material.

Models 2-5 have an interface resistance included. The interface resistance was calculated using Equation 1.  $R_{IF}$  ranged from  $3.0 \times 10^{-8}$  ( $1 \mu\text{m}$ ) to  $1.5 \times 10^{-11}$  m/s ( $500 \mu\text{m}$ ) which fits in the range given by literature values. Model 1 is assumed to have an  $R_{IF} = 0$ .

Model 2 does not include the aperture and one resistance was included in the model equal to  $R_{IF}$ . Models 3-5 have two resistances either side of the aperture equal to  $R_{IF}/2$ . In Model 5, an interface resistance was included between the centre mortar and two brick wythes. An explicitly modelled fracture was not modelled at these interfaces. The capillary pressure differential is not as great along this direction as it is into and out of the wall and therefore liquid transport would not be as great. Adding this would also increase the size and complexity of the grid.

## **5.5 Results and Discussion**

Results are presented for the five models. Nine monitoring positions were selected for presentation (Figure 5-3). The 'Mortar' line was taken at the upper most row of the finite-volume grid (centre of mortar considering symmetry); the

'Brick Fracture' line was taken just below the fracture; and the 'Brick Centre' line was taken at the lowest row of the grid (centre of brick considering symmetry). Each of the three lines were monitored at 20 mm, 50mm, and 80 mm from the exterior boundary conditions.

#### **5.5.1 Model 1 – Absorption: Fracture without interface resistance**

The results for Model 1 at the 250 Pa boundary condition are shown in Figure 5-5. The results show a significant increase in moisture content at all nine monitoring locations compared to the baseline. The larger fractures saw the most significant increase in moisture content while smaller fractures saw a less significant increase. The relationship between aperture and maximum moisture content is monotonically increasing. Higher moisture contents were achieved at all locations and they were achieved much quicker. This was most noticeable in the mortar and at the centre of the brick. Fractures as small as 5  $\mu\text{m}$  led to a measurable increase throughout the mortar, while fractures as large as 25  $\mu\text{m}$  caused the mortar to approach saturation after 5 hours, whereas previously the moisture content had barely increased at this time. At the centre of the brick, saturation levels were achieved after less than 2 hours of wetting for the larger fractures. This was in part contributed to the geometry of the brick. The larger fractures are efficient at transporting water and effectively recreates the 250 Pa wetting boundary condition inside the fracture. Instead of the distance from the

boundary condition being 50mm or 80mm, the distance to the boundary condition becomes 28.5 mm.

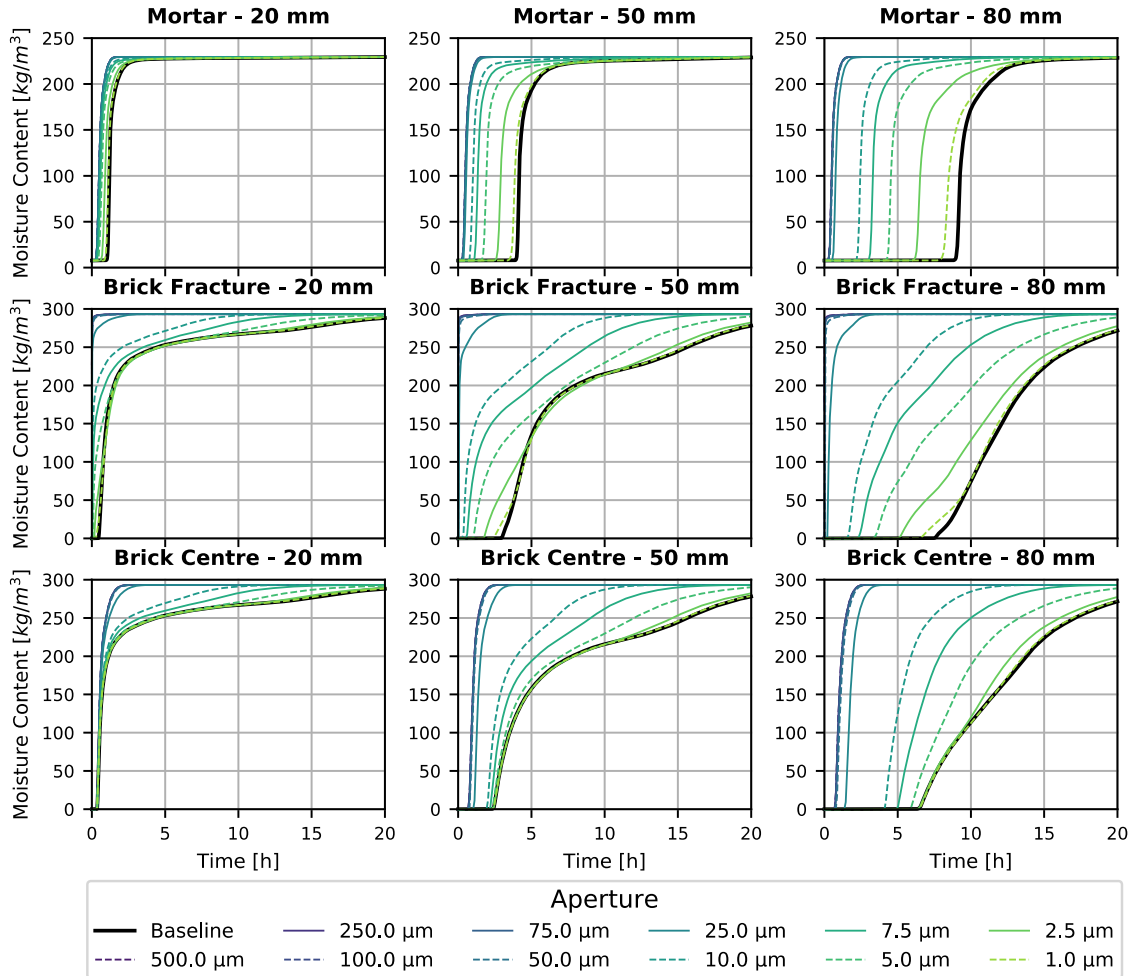


**Figure 5-5: Moisture content comparison for Model 1 (250 Pa)**

When this model is run with different boundary conditions, a few things of note happen. First, the maximum moisture contents are lower in both the brick and mortar, and it takes more time to obtain those moisture contents. This was

expected because there is less wetting at the boundary condition. The second thing of note is that the relationship between aperture and maximum moisture content is no longer monotonically increasing. This is shown in Figure 5-6.

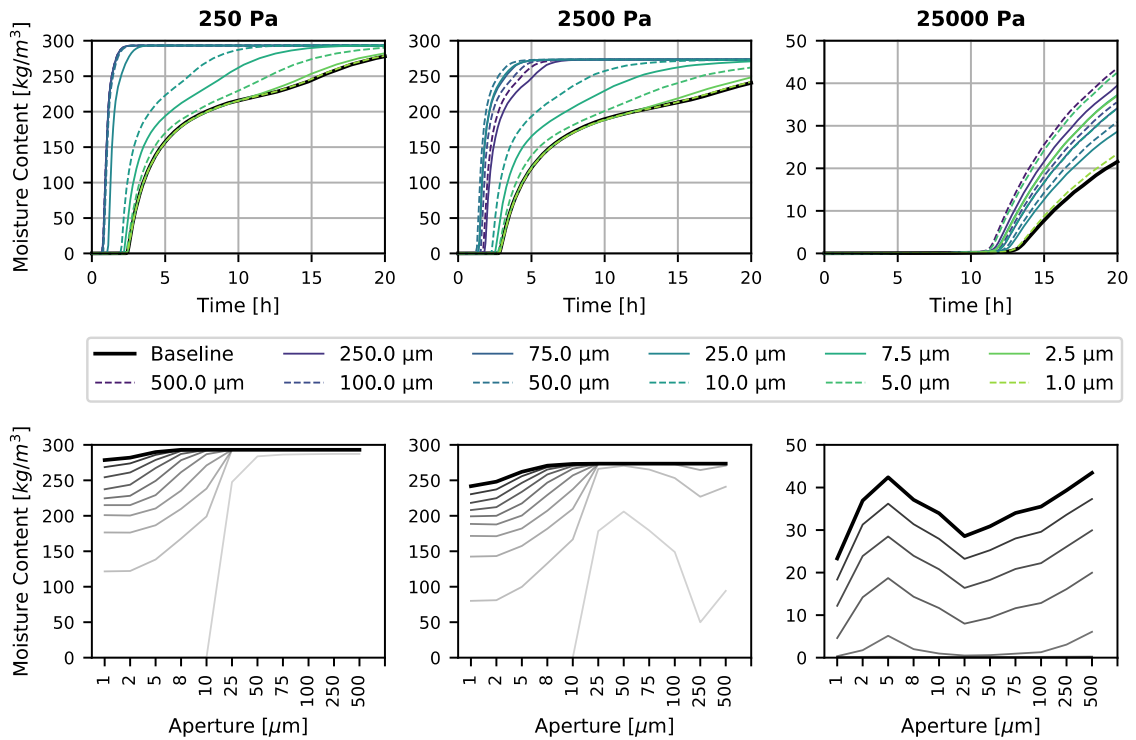


**Figure 5-6: Moisture content at Centre Brick – 50mm for three different boundary conditions. The bottom graphs illustrate the moisture contents from  $t=0$  (light gray) to  $t=24$  h (black). Note that there are different y-axis scales.**

At 2500 Pa, the maximum absorption occurs in the 25 – 75  $\mu\text{m}$  aperture range. Apertures smaller than this show a relatively similar pattern to the 250 Pa

simulation. The larger apertures are unable to fill to the same degree at this capillary pressure and therefore have a reduced liquid conductivity.

At 25000 Pa, the monotonically increasing relationship begins to break down further. At various points in the model, the 5 – 10  $\mu\text{m}$  aperture range has the maximum moisture content, while in other areas, the largest apertures have the maximum. Universally, the 25 – 75  $\mu\text{m}$  range had one of the lowest moisture contents, opposite to what was found in the 2500 Pa simulations.

It is difficult to put numbers to the difference in moisture content between the baseline model or other size apertures because it is very location and time dependent. Consider the Centre Brick – 80 mm graph in Figure 5-5 for example. The relative difference between the 500  $\mu\text{m}$  and 5  $\mu\text{m}$  are quite extreme after a few hours, but after the 24-hour simulation period, the lines begin to converge. The difference is less pronounced if we consider moisture at shallower depths into the wall. Generally, with the increase in capillary pressure, the variation in moisture content between the various apertures decreases compared to the 250 Pa model. The duration of the wetting event will have a significant effect on water absorbed, with the larger fractures still able to transport water deep into the assembly under brief rain events.

### **5.5.2 Model 2 – Absorption: Interface resistance only**

The results for Model 3 at the 250 Pa boundary condition are shown in Figure 5-7. The biggest change from the baseline model was in the mortar. When the interface resistance is included in the model, the moisture content in the mortar over time decreases proportionately to the aperture size. The decrease is indicative that moisture was being transferred from the brick into the mortar in the baseline model.

As can be seen in Figure 5-7, there is little change throughout the brick from the baseline or different size apertures. The moisture that got prevented from entering into the mortar from the brick by the interface remained in the brick. There was a very small increase in moisture content in the brick (difficult to see in graphs), with the larger apertures having a slightly greater increase than the smaller apertures. Overall, a nearly identical quantity of water was being absorbed into the assembly between the baseline and various sized apertures. This was not the case in Model 1, where there was a significant increase in the total amount of water absorbed. Results were similar for the 2500 Pa and 25000 Pa simulations.

In isolation, the effect of the interface resistance appeared to have minimal impact on absorption into and out of the wall.

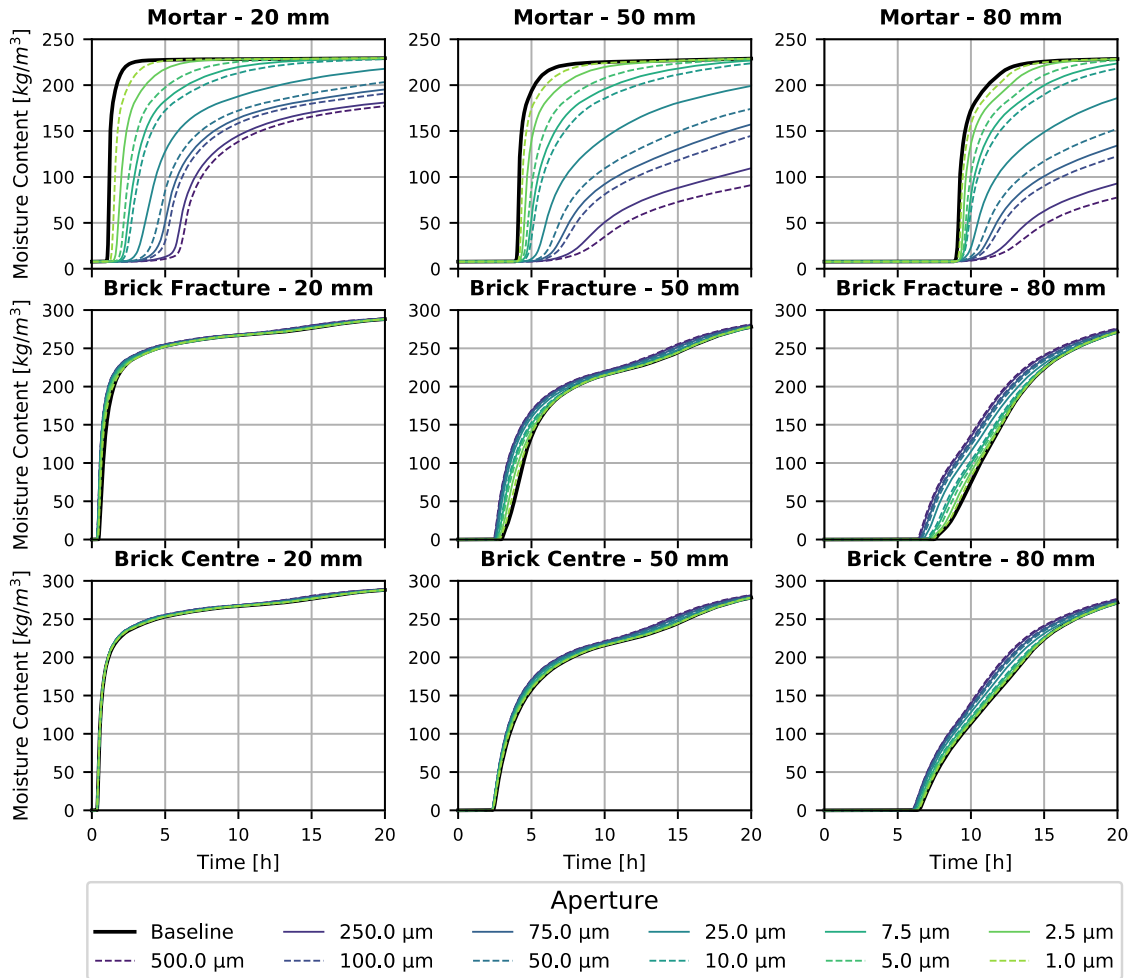


**Figure 5-7: Moisture content comparison for Model 2 (250 Pa)**

### 5.5.3 Model 3 – Absorption: Fracture with interface resistance

The results for Model 3 at the 250 Pa boundary condition are shown in Figure 5-8. The difference compared to the baseline is not as great as Model 1. The presence of an interface resistance has dampened the increases in moisture of the open fracture.

The moisture content of the mortar nearer the exterior tends to be lower than the baseline. A similar effect was noted in Model 2. However, this effect begins to be negated as we go deeper into the assembly and the moisture content becomes greater than the baseline for some apertures. This is because the fracture is filled and there is a larger capillary pressure gradient to overcome the interface resistance. The larger fractures exhibit some interesting behaviour. There is a relatively fast advancement of the wetting front followed by a gradual square-root-of-time wetting pattern. This is the influence of the interface resistance and a larger percentage of the moisture in these fractures is arriving parallel to the fracture.

Like the mortar, the increases in moisture content in the brick are not as significant as with Model 1. Near the fracture, there isn't as sharp, or as immediate an increase in moisture content, especially for the larger fractures. There is a significant increase in moisture content near the fracture in the early moments of the simulation once the fracture quickly fills toward saturation and causes a large pressure gradient. Apart from that mentioned, the lines in Figure 5-8 generally follow a similar curve to that of the baseline.

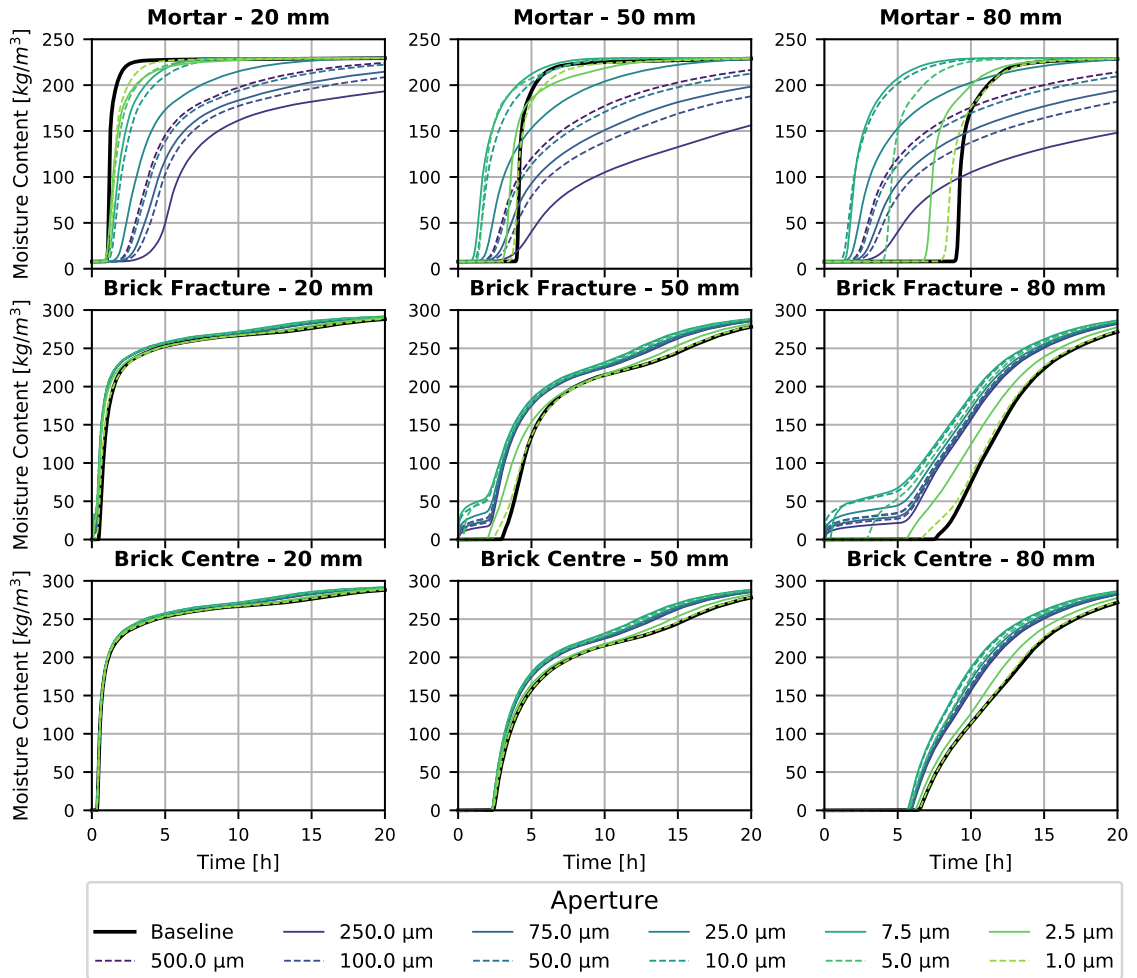


**Figure 5-8: Moisture content comparison for Model 3 (250 Pa)**

Figure 5-9 shows the moisture content relative to aperture size at three different capillary pressures. At 250 and 2500 Pa, the moisture contents at each time interval are relatively flat, with an apparent maximum around 5  $\mu\text{m}$ . At 25000 Pa, the lines are no longer flat, and a pattern similar to Model 1 (Figure 5-6) begins to show with a maximum around 5  $\mu\text{m}$  and minimum around 25  $\mu\text{m}$ . At 25000 Pa,

the moisture content curves for all monitoring points starts to approach the curves in Model 1 with the same boundary condition. This is not true at the other capillary pressures modelled.

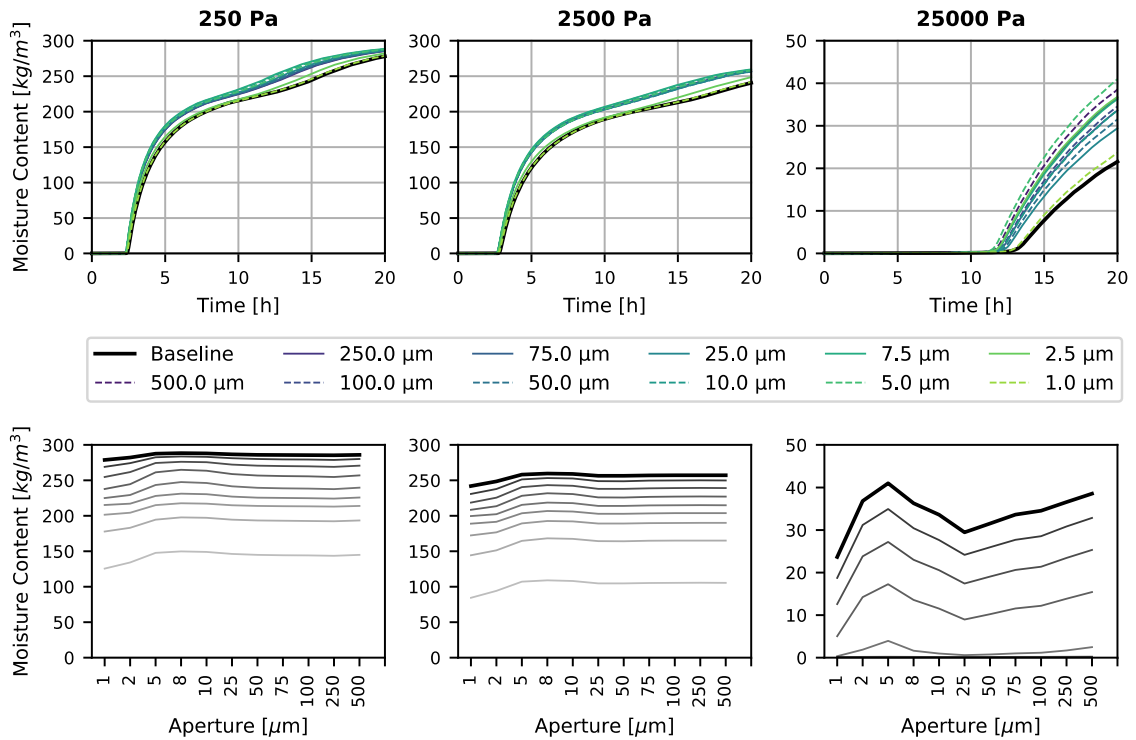


**Figure 5-9: Moisture content at Centre Brick – 50mm for three different boundary conditions. The bottom graphs illustrate the moisture contents from  $t=0$  (light gray) to  $t=24$  h (Black). Note that there are different y-axis scales.**

#### 5.5.4 Model 4 – Drying: Fracture with interface resistance

Results for Model 4 are shown in Figure 5-10. All nine monitoring position demonstrated a similar pattern to that showed in Figure 5-10. The important

takeaway is that the fracture encourages drying of the material, and the larger the fracture, the quicker it dries. The potential magnitude of this effect was surprising at first. However, a material with efficient transport properties in one direction (absorption) will also be efficient at transport when the sign of the differential is switched (drying).

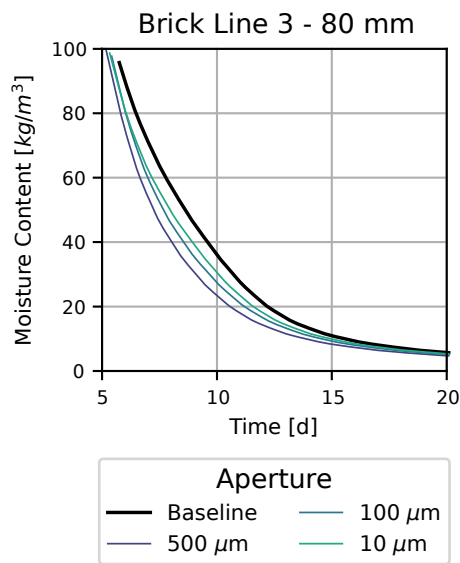


**Figure 5-10: Moisture Content comparison for Model 4.**

During, the first phase of the simulation (partially cropped in Figure 5-10), the simulations closely match the baseline model and dries at a constant rate. In this early stage, the flow rate is largely governed by the vapour convection coefficient which dominates mass transfer resistance and is the controlling layer. The high liquid conductivity of the fractures offers little resistance and has negligible impact

on transport when combined with the convection coefficient. As the assembly dries, the rate of drying decreases and we reach an apex in the curve. This is caused by a combination of reduced vapour pressure differential which slows the transfer to the ambient air (vapour convection); and the liquid conductivity of both bulk material and the fractures diminish adding resistance to the system.

However, the liquid conductivity of the larger fractures doesn't diminish to the point where their resistance is significant in relation to the system and mass transfer continues at a rate similar to the first phase of the simulation for a longer period of time. It should be noted that if a higher vapour convection coefficient (typical of exterior conditions) were used the slope in the first phase of the simulation will be steeper and the behaviour at the apex may change.

Some drying simulations were performed with different values of  $\mu$  for the fractures. It was found that the vapour diffusion through the fracture had minimal impact and that the effect seen was driven primarily by transfer in the liquid phase. The model does not consider hysteresis in the moisture retention curve. Hysteresis causes porous media to release moisture at slower rate than it is absorbed. This may lessen the increased drying rate if modelled.

The results indicate that drying may have a significant contribution in the cyclic model, especially if wetting brings the moisture content in the apex range of the drying curve.

### 5.5.5 Model 5 – Cyclical: Fracture with interface resistance

The results for Model 5 are shown in Figure 5-11 for one calendar year. The results are presented for the centre of the exterior brick.

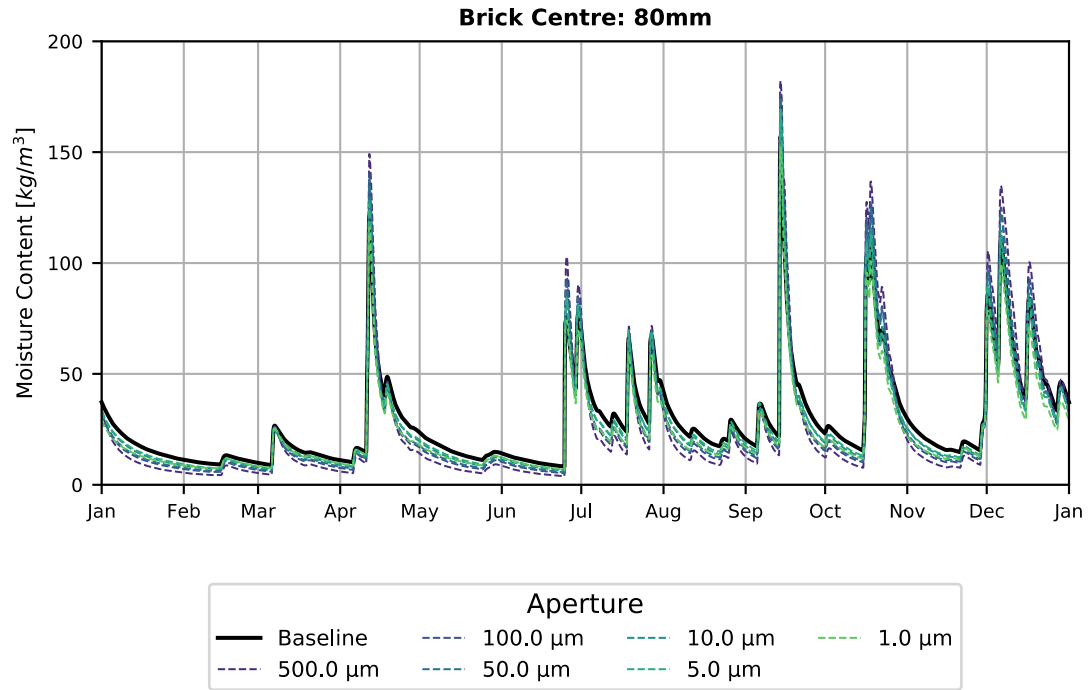


**Figure 5-11: Annual MC for the baseline model and select apertures**

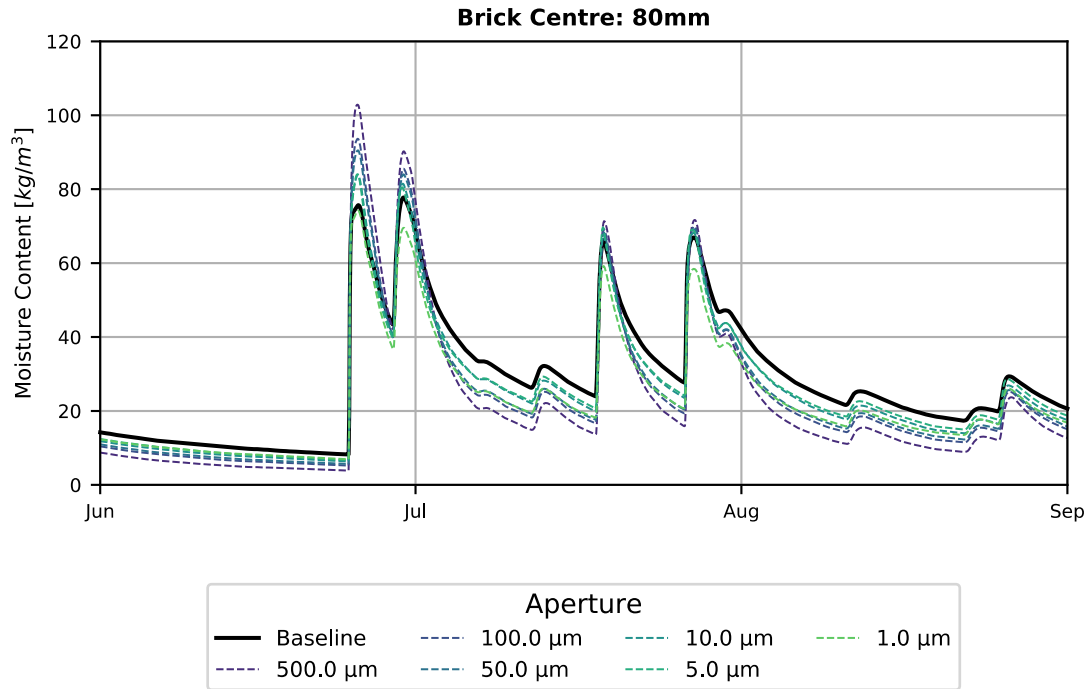


**Figure 5-12: Moisture content for the baseline model and select apertures during the summer months**

Figure 5-11 shows that there are several significant wetting events which caused a spike in moisture content over the course of the year. Figure 5-12 shows the same data zoomed in for the summer months. During each wetting event, the fractures are able to absorb more moisture than the baseline model can. Depending on a combination of factors such as wind-driven rain intensity, duration or relative difference in moisture content at the beginning of wetting, the moisture content may exceed the baseline model. The wetting phase is succeeded by a drying phase, and the assembly begins to dry quicker than the

baseline. The drying is enhanced because we are often in the apex region described in the discussion of Model 4. Drying periods occur more often than wetting periods which means that drying behaviour is more dominant than absorption behaviour under realistic weather conditions. As a result, the fracture model tends to reduce the moisture content in the masonry over the long term. For the larger apertures, the drying is more pronounced than the smaller fractures, where it is not as definitive whether moisture content is reduced.

Throughout the first wythe of brick, the shape of the curves follows a similar pattern to Figure 5-11 regardless of material or depth. The results in the second wythe followed a different pattern largely because an interface resistance was placed in between slowing absorption into this region of the wall. Here the moisture content is lower than the outer wythe and the wetting spikes are not as pronounced, but a similar story occurs. There is a decrease in moisture content relative to baseline and the larger the aperture, the lower the moisture content.

It is important to note that the significance of the results shown in Figure 5-11 and Figure 5-12 will be dependent on climate and material properties. Even with a relatively high rain exposure and deposition factor, the walls were not able to continuously reach the types of capillary pressures that would allow for the increased absorption rates shown in Model 1 and Model 3 at very low capillary pressures (Figure 5-5 and Figure 5-8). The highest intensity rainstorms had short

durations (<5 hours) and not enough liquid water can be absorbed to fully activate the larger fractures.

Material properties such as the moisture retention curve and liquid conductivity curve can also affect the behaviour under cyclic conditions. If materials with comparatively low pore size distribution (high residual moisture content) are used for either the mortar or unit, the relative difference in MC between the baseline and different sized fractures decreases. This is partly because we begin at higher points in the liquid conductivity curve than a low residual moisture content material and water can be more readily absorbed into the materials and not penetrate as deep into the fracture. Materials with lower liquid conductivities will siphon less liquid water as it travels in the fracture allowing it to fill more and penetrate further along the fracture.

#### **5.5.6 Additional Notes**

Other geometries and combinations of materials may produce different results than presented here for the clay brick and cement mortar. Some simulations were run for a sandstone – lime mortar combination comprising of larger stones than the bricks. Here the effect in the absorption phase was not as pronounced, especially at the centre of the unit. This is because the fractures have more

material to transfer water into and that the bulk materials used were better liquid conductors than the clay brick and cement mortar.

This model has applications other than vertical walls exposed to wind-driven rain. One application is at foundation level where contact with damp soils leading to rising damp. Here the boundary conditions will be similar to the absorption simulations in Models 1-3 and its appropriate to model with a capillary suction pressure. The degree of wetting will be greater and more constant than what was used in Model 5 and there will be reduced time in the drying phase. Here, we may see that moisture contents increase under realistic conditions. Gravity was not considered in this model, but the fracture model could be utilized to estimate direct leaks from above into the assembly. The model would be applicable to other combinations of hygroscopic materials in building envelopes with imperfect contact conditions, not just masonry. It may also be able to be utilized with non-hygroscopic materials such as junctions between flashing and masonry.

Future applications for this work including determining an 'effective' liquid absorption coefficient which can account for the degree of decay in a wall and can be plugged into either 2D or 1D hygrothermal models. Determining what the hydraulic aperture should be for an actual masonry wall is another challenge that needs to be addressed. This would be dependent on many things including the techniques and skill of the mason (e.g., do they wet the stone), level of

deterioration (good, fair, bad) and types of materials used and specification of the mortar mix. As mentioned, determining what the effects of a possible moisture-dependent interface resistance are is another challenge that needs to be addressed.

The results from this proposed model still require experimental validation. It will be a challenge to create reliable and replicable test specimens with fractures of varying width. Mortar segments can be cast separately from the brick and then spaced a set distance apart, or the fracture can be closed using compression forces. The specimens should be evaluated under both absorption and drying conditions.

## **5.6 Conclusion**

The results of the Delphin simulations show that modelling imperfections at the masonry unit-mortar interface as fractures can affect simulation results when compared to the baseline model which only used bulk material properties. Simulations were performed for a clay brick/cement mortar assembly with an explicitly modelled fracture interface. Hygrothermal properties for the bulk materials and fracture were built from fundamental principles. Five sets of simulations were performed which assessed the effect of the various sized apertures under absorption, drying and cyclic boundary conditions.

The simulation results showed that the inclusion of a fracture model had a significant impact. The rate of absorption increased, but this was countered with an increased rate of drying. Under cyclic conditions the drying effect of the fracture outweighed the increased absorption during wetting events. This led to the wall being drier than the baseline model over the long-term.

## 6. Spatially-stochastic geometry in masonry-walls

This section contains content published in:

Gutland, M., Bucking, S., & Santana Quintero, M. (2022). Hygrothermal modelling of historic rubble masonry walls: Accounting for geometric and compositional variability. *Journal of Building Engineering*, 48, 103929.

<https://doi.org/10.1016/j.jobbe.2021.103929>

### 6.1 Abstract

An established issue when assessing the hygrothermal performance of heritage buildings is the correlation between measured data and model outputs. This can be attributed to many factors including climate data and hygrothermal material property data. Two overlooked factors are the variation in geometry and level of decay in the structure. This can be true for several historic wall assemblies with irregular geometries and elevated levels of decay. There is a lack of guidance on how and when to incorporate this into a hygrothermal model. The goal of this paper is to examine how this variability in geometry and composition may affect model outcomes using a simulation approach with stochastic methods for a sample rubble core masonry wall.

Geometrically stochastic models were generated from a script accounting for varying levels of air voids in the wall and irregular stone patterns. The presence of voids alters heat, capillary and vapour transport. This was combined with hygrothermally dissimilar mortar and stone units. Simulations were performed under four boundary conditions: heat, drying, wetting and actual weather data. The results showed that geometric stochasticity can lead to a large variation of results. The presence of voids in the wall also led to a reduction in heat and moisture transport in the assemblies. The results of the stochastic simulations were then compared to a set of simplified one and two-dimensional models to judge their appropriateness. It was found that 2-D parallel like models that account for the mortar joint in some fashion are most appropriate.

## **6.2 Introduction**

There is an increasing pressure to make historic buildings more energy-efficient to combat climate change and reduce their carbon footprint. Energy-efficient measures may be applied to the building's HVAC and lighting systems as well as the building envelope with interior thermal insulation being a common proposal. Before considering any retrofits, it is best practice to investigate the current physical performance, understand its dynamics and establish a dependable baseline model of the building. With a dependable baseline model, it is possible

to confidently project the positive and negative effects of various proposed retrofit options in terms of energy performance, occupant comfort or durability risk.

Historic buildings whether masonry, wood, concrete etc., have many non-contemporary, unique, or nuanced construction methods, materials which can complicate the process of establishing a baseline of the hygrothermal performance of the building envelope. This can be further complicated by a lack of published data for these systems. For example, determining an effective U-value of the wall is necessary for energy models. U-values are often estimated from literature or standards and without the aid of in-situ monitoring or testing (e.g., heat flux plate). Complicating factors in estimating the U-value of an historic wall assembly include the natural variability in thermal conductivity and heat capacities of the building materials, dampness of the assembly, and uncertainty in the construction, composition, and dimensions behind what we can observe on the interior and exterior surfaces. All these factors can influence the effective U-value of the wall compared to what is estimated when referring to values in standards and literature.

Estimating the hygrothermal moisture response of a wall to boundary stimuli (rain absorption, drying) has similar complications to that of estimating the U-value.

There can be large variability in the hygroscopic properties in the same material or a combination of materials, and there is also the uncertainty of what lies

behind the surfaces of the wall. Verifying the hygrothermal response through in-situ monitoring can be challenging because of technical challenges related to the sensors and the temporal scale needed compared to heat transfer only. The accumulated effects of damage, defect and decay can compound the challenge of knowing what lies behind the surfaces of the wall. These are often neglected from consideration when calculating the U-value or hygrothermal responses in assemblies.

In this paper we will focus on how the uncertainty in geometry, composition, and level of decay can affect heat transfer and hygrothermal response in an assembly. An example of a rubble core masonry wall is used which has an outer sandstone wythe with an irregular stone pattern and varying thicknesses (Figure 6-1). The core of the wall is a mixture of smaller stones of varying sizes and a poured lime mortar grout. The inner sandstone wythe has a more regular pattern. Previous investigations into the wall have shown that there has been considerable decay over time and that a substantial number of voids (air cavities) have formed behind the outer wythe over time.



**Figure 6-1: Example drawing of rubble core wall and voids (blue)**

Walls of this type and with known levels of decay can be difficult, costly, or impractical to recreate in laboratory settings, and can also be challenging to instrument and monitor in-situ for long-term hygrothermal performance.

Considering this, simulation can be a useful and practical tool for analyzing the hygrothermal behaviour of these walls, especially when existing decay, damage or defects need to be considered. Simulation can also be viable when there are non-existent data or ground truth for a particular scenario.

The inconsistent geometries and presence of voids makes it difficult to abstract geometry and this can lead to a degree of inherent uncertainty with the hygrothermal models. The presence of voids can alter heat, vapour, and liquid transfer in the wall. The relatively still air in the voids will have a lower thermal conductivity than the sandstone, and the voids can behave like mini-rainscreens

causing capillary breaks and reducing vapour resistance. The stone and the mortar have significantly different hygroscopic properties which can exaggerate thermal bridges and preferential moisture transfer paths through mortar joints etc.

The goal of this project is to understand how the variability in the wall composition may affect the U-value and moisture response using a combination of complex high resolution geometric models and simplified models. A series of hygrothermal simulations were performed using a variety of wall geometries and four different sets of boundary conditions. The geometry of the walls was stochastically generated based on parameters of the masonry wall such as the stone and mortar joint dimensions, and void ratio. A script was written to randomly position stones and mortar in the wythes and core in a way that mimics how they were placed during construction. A set of simplified geometries were then compared to the stochastically generated geometries to compare their appropriateness in terms of heat and moisture transfer. The results of both the stochastic and simplified models were analyzed to understand how viewing the wall's composition and level of decay stochastically can result in statistical variance, which can influence conclusions on the wall's baseline performance and durability risk.

## **6.3 Literature Review**

### **6.3.1 Heat Transfer and U-values**

Creating a valid performance model for historic buildings can be a challenging process with nuances different to that of contemporary construction (Hansen & Møller, 2018; Huerto-Cardenas et al., 2020; Webb, 2017). Establishing an accurate effective U-value is an important first step and there are several ways of doing this for historic masonry. These include hand calculations, finite-element modelling techniques, heat flux measurements, infrared techniques and through calibrated energy models. Non-destructive in-situ measurements are often done using heat flux meters or infrared thermography. Both methods are imperfect for measuring U-values. Both methods require consistent climatic conditions (temperature, minimal wind, solar radiation, moisture) which are not always achievable (Nardi et al., 2018). Heat flux meters can be connected to a datalogger. Combined with surface temperature measurements and weather data, the U-value can be calibrated for. Thermography can be executed quickly and can survey a large surface area, but are generally one-time measurements and its difficult to discern the effects of the weather preceding the measurement. Previous studies have shown that there is often a discrepancy between calculated U-values and those measured in-situ in historic masonry and there are

several plausible reasons for this discrepancy. A technical paper by Baker (2011) examined a variety of walls (including rubble core and cavity-wall construction) under real-world and laboratory conditions. It was found that software techniques tended to overestimate the measured U-values and that discrepancies between the two values may be caused by lack-of knowledge of the actual construction and the thermal properties of the historic materials. The simulation models were two layers representing the stone and the mortar. A survey by Lucchi (2017) came to similar conclusions to Baker and that the ratio of stone, mortar and void had a definite impact on the measured U-value. Other examples of in-situ measurements of historic masonry include (Rye & Scott, 2012).

Litti et al. (2015) measured heat flux in a historic brick building and found that the measured U-value could vary as much as a factor of three. This was attributed to high moisture in certain areas. A previous hygrothermal study on a different part of this case study building used model calibration techniques to infer the thermal conductivity of the stone and mortar (Gutland, Santana Quintero, et al., 2019). It was found that the thermal conductivity was close to twice as high in a section of wall with high moisture than low moisture and that the thermal response was different between the two sections.

Heat transfer simulations were performed in support of some of these measured findings taking different approaches to abstracting the complicated and random

geometry of rubble core walls ranging from 1-D series constructions to 2-D of varying complexity (Baker, 2011; Little et al., 2015; Pascucci & Lucchi, 2016). The geometry used tended to be regular shapes and highly symmetrical not accounting for clusters of stone and mortar. The presence of air in the assembly can complicate heat transfer calculations, whether intentionally placed such as rainscreen or hollow block, or unintentional through the effects of decay or defect. These effects are often not considered in hygrothermal simulations of masonry (Kersten & van Schnijdel, 2013; Kočí et al., 2018; Nagy & Tóth, 2016).

### **6.3.2 Hygrothermal simulations including moisture transfer**

Previous simulation studies of masonry walls which included moisture transport have compared 2-D constructions versus simplified 1-D series constructions (Bottino-Leone et al., 2021; Little et al., 2015; Nagy, 2019). Their consensus was that 2-D simulations produce better results if the material properties of the mortar, stone or other materials in the assembly have dissimilar hygrothermal properties.

2-D simulations however have drawbacks like increased model complexity, computational time and data storage and processing. It is appealing to keep the models in 1-D and accept the shortcomings regarding the influence of mortar.

Bottino-Leone et al. calls this simplification the Stone/Brick layer and examined the difference between 1-D and 2-D simulations of a brick wall. For the 1-D

simulations a Homogenized Porous Material (HPM) was calculated from the weighted average of brick and mortar and later optimized. Other times where 2-D simulations are warranted are when embedded wood or metallic elements are included (Harrestrup & Svendsen, 2016; Iodice et al., 2016; Morelli & Svendsen, 2013).

### **6.3.3 Spatially stochastic masonry models**

In practice, a deterministic approach to hygrothermal modelling is used. This technique is limited, especially if knowledge of hygroscopic properties is low or could be highly variable. One method around this is to interchange use similar library of the same class into the model and the worst-case scenario being used as a basis (Browne, 2012). The problem with this approach is that it is inherently too conservative.

Stochastic modelling techniques have been previously used in hygrothermal models as first outlined by Salonvaara (2001) for contemporary construction. Probabilistic values are assigned to key material properties and the results are presented within a probabilistic framework. Further examples of stochastic hygrothermal models have been performed often with a view toward calibration (Akkurt et al., 2020; Freudenberg et al., 2017; Goffart et al., 2017; Gutland, Santana Quintero, et al., 2019; Vereecken et al., 2015; Zhao et al., 2011). Some

obstacles to stochastic hygrothermal modelling in practice, include the increased time and lack of easy-to-use software that can handle this problem.

Most stochastic models focus only on the hygroscopic material properties and have fixed geometry, neglecting variances in the wall's geometry, composition or the interfaces between stone and mortar. Models which consider these are called spatially-stochastic and can be more representative of masonry where there may be localized variations in material properties between units, and varying levels of workmanship, damage, and decay. This approach to stochastic modelling has begun to be implemented in the structural analysis of historic masonry (Pulatsu et al., 2021). Here, the researchers have assigned probabilistic values to the mechanical properties of the units and mortar (e.g., compression strength), but also mechanical properties of the unit-mortar interfaces (e.g., stiffness, bond tensile strength, cohesion etc.). They were then assigned non-uniformly to each unit and joint in the discrete-element model. It was found that the spatially-stochastic models produced more consistent results with less scatter between the upper and lower bounds compared to non spatially-stochastic models. This concept has not been explored in depth in hygrothermal analysis.

## **6.4 Methodology**

### **6.4.1 Case Study**

The case study is a heritage-designated masonry building in Ottawa, Canada constructed between 1859-1867 and is in the process of being rehabilitated. The rehabilitation includes examining the energy and hygrothermal performance of the envelope and retrofits are being considered to reduce energy consumption and greenhouse gas emissions.

The stone masonry consists of snecked rough-faced outer sandstone wythe and an undressed random-coursed inner wythe sandwiching a rubble core. The rubble core consists of smaller stones shards of various sizes which was then grouted with poured mortar. The rough dimensions of the wall vary throughout the building. Previous documentation had indicated that the typical above-grade rubble wall is approximately 530 mm (21 in.) thick, but investigations show that this wall could be up to 600mm thick. In parts of the building the inner wythe is exposed and other areas it is finished with plaster. Typical foundation and plinth-level walls are up to 1200 mm thick. Other areas of the building such as towers and around pilasters have thicker cross-sections and detailed ornamentation. As a result, it is challenging to define a clear-field assembly that is suitable to all elevations and levels of the building.

The building is known to have chronic moisture issues from poor water shedding features and irregular maintenance, both exacerbated by the harsh Ottawa climate. This has been corroborated by previous and current hygrothermal monitoring of the buildings, and is visibly evident from the exterior in open mortar joints, material loss in the stone, staining and efflorescence. Previous inspection reports, localized dismantling of the wall and previous Ground Penetrating Radar (GPR) surveys have also shown decay in the core of the wall with the presence of a significant number of voids. The voids are caused by two reasons. First the binder in the mortar has been washed away after decades of exposure to high moisture contents from various sources. The second is that the core was incompletely filled at the time of construction. From recent visual inspection of the typical above-ground walls, it was estimated that the voiding was as high as 30% in some walls. GPR studies in the building's towers showed that up to 85% of those walls contained voids. This was corroborated when drilling into the masonry walls to install sensors. The drill would often be met with no resistance beyond the sandstone wythes.

Previous and ongoing hygrothermal monitoring has shown highly variable moisture contents from one location to another, with only tenuous correlation in moisture contents between elevation, storey, wall type or occupancy. Some walls appear to be in a healthy state and some appear to be critically wet. There are

many possible reasons for this variance including exposure to wind-driven rain and run-off from the roofs, previous damages, leaks etc. It has also been theorized that the geometry of the wall could be responsible for the relative health (especially on interior surfaces) of some walls relative to others because of the theorized rain-screen effect from the voids, and/or placing a sensor nearer a location with more densely spaced mortar joints.

A previous project on hygrothermal calibration from the monitoring data was not successful. Two of the three stations monitored were extremely saturated ( $RH > 99\%$ ), and it was a moot exercise to calibrate this data set. The other station was relatively dry even though it was thought to be a candidate for high moisture based on its exposure. The calibration results were inconclusive, and it was thought the known voids and air exchange at this station were a contributing factor.

#### **6.4.2 Building Geometry**

The finite-volume hygrothermal simulation software Delphin 6.1 was used for the simulations (Bauklimatik Dresden, 2020). The software has been validated to solve the coupled transient heat and moisture transport equations, distinguishing between transport in the vapour and liquid phases. Simulations were performed

for a typical bare wall assembly with no interior finishes and a 600mm thickness.

The simulations were performed in 2-D.

The rubble core exterior walls of this building have a seemingly random construction which makes it difficult to generalize one set of model geometry. Stones of different sizes (height and width planar to the wall, thickness into the wall) were used in both the inner and outer wythes. This results in mortar joints being more densely packed in certain regions than others. This can result in pockets of high or low resistance in the clear-field assembly. To counteract this, a stochastic approach to defining the geometries was developed.

The dimension of the sandstone wythes, mortar joints and rubble core were estimated with the aid of some scaled and rectified photogrammetric images of partially dismantled walls from the building. A distribution of dimension was recorded and given in Table 6-1:

**Table 6-1: Dimensions [mm] used to create geometry in hygrothermal models**

		Mean	Standard Deviation	Min	Max
Outer Wythe	Height	135	57	52	254
	Thickness	213	17	190	240
Inner Wythe	Height	137.6	27	100	200
	Thickness	219	17	200	240
Mortar Joint	Height	8.6	2	6	15
Core Stone	Thickness	55	25	None	None

The mean dimensions of the inner and outer wythe are similar, but the outer wythe has a wider variation due to the aesthetic bond pattern used. The thickness of the stones ranges from 190mm to 240mm to help with structural keying into the wall. The height of the mortar joints was difficult to estimate because in many instances replacement mortar was smeared over the weathered arrises (edges) of the stone appearing wider at the surface than a further depth.

The dimensions of the infill stones in the core were difficult to estimate from images because they are partially enclosed in mortar. What could be ascertained was that there seemed to be a wide distribution of sizes and that there was a combination of square/spherical stones and more elongated stones. This could be characterized using an aspect ratio. Infill stones also tended to be laying flat and not tipped at a large angle ( $<30^\circ$ ).

### **6.4.3 3.3. Model Geometry**

A Python script stochastically creates wall segments using the stone dimensions in Table 6-1. The script was designed to mimic how the rubble stones would have been placed in construction – by dropping them from above and settling into place. The general procedure is as follows:

1. A list of inner and outer stones was created each with a height, thickness and stone height and mortar width taken randomly from a Gaussian distribution.
2. A list of rectangular rubble stones was created with a height, width, rotation and vertical and horizontal spacing from neighbouring stones. The heights and widths were randomly chosen from a Gaussian distribution. The rotation and spacings were randomly chosen from a uniform distribution ( $-30^\circ$  to  $30^\circ$  respectively).
3. A list of rectangular voids was created similar to that of the rubble stones with a height, width and rotation
4. The inner and outer wythes were constructed using the thickness and spacing from the mortar joint list.
5. The rubble stones were placed sequentially beginning with the bottom left corner. Subsequent rubble stones were placed at the lowest available point while respecting the spacing from neighbouring rubble and wythe stones. The four coordinates were recorded for each stone. The process was continued until reaching the target height.
6. If voids were included, then each void rectangle created was sequentially placed at random coordinates within the core. This process was repeated

until the percentage of matrix coordinates reached a pre-determined target percentage of the core.

7. The dimensions of the wythes and the core were translated into a pixel matrix based on a given scale (one grid = 0.5 mm, 1.0 mm, 1.5 mm etc.) The mortar, stone, and air were assigned unique numbers in the matrix.
8. The tops and bottoms of the pixel matrix were trimmed to minimize the bias of the first stone laid and emptiness when the top is reached. As a result of trimming, there is a deviation from the target void percentage.
9. The matrix was then translated into Delphin's XML input file format.

In the process writing the geometry into the input file, junctions between materials were noted. An interface resistance ( $R_{IF}$ ) of  $1.0 \cdot 10^{10}$  m/s was inserted between stone and mortar (Calle et al., 2019; Derluyn et al., 2011; Qiu et al., 2003). When an air gap neighbored either stone or mortar no interface resistance was inserted. For each void, along each grid line in the y-direction, the horizontal dimension was recorded, and a bespoke air gap material file was assigned (See Section 6.4.5.2).

Sets of models were created with to represent five different degrees of voiding ( $V$ ) of different severity ranging from a perfect wall ( $V = 0\%$ ) to an extremely decayed wall ( $V = 20\%$ ). The same geometric models were used with the same boundary

conditions. Examples of the models are shown in Figure 6-2. The random nature of the grid generation results in walls with wider or narrow cores, collections of smaller or larger stones and different mortar joint sizes and spacings. The walls were 500 mm tall to ensure multiple mortar joints in each model. It was decided to keep the thickness of the walls fixed at 600 mm to reduce the scope of the problem, though this parameter also has a degree of stochasticity.

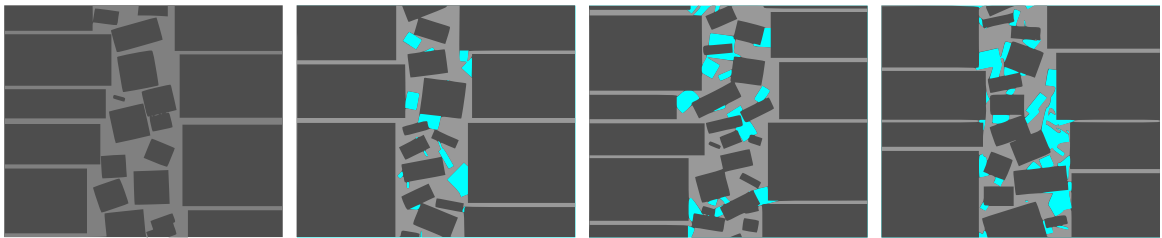


**Figure 6-2: A sample of stochastically generated grids with  $V=0\%$  on the left and  $V=15\%$  on the right.**

A sensitivity analysis was performed to determine an appropriate mesh density which balances simulation accuracy and computational effort and time.

Geometries were created with the same dimensions and placement of stone, mortar, and void (10%) but with meshes of different densities. The densities simulated ranged from 2mm/element to 0.25mm/element. The grid sensitivity analyses were performed under steady-state and transient conditions.

It was decided that the ideal mesh density was 1.5mm/element. All grids in the y-direction were 1.5mm. In the x-direction, the core had uniform grids of 1.5 mm,

while the wythes utilized an expansion ration of 1.2 to reduce the total number of elements.

#### **6.4.4 Simplified Models**

A series of simplified models were created for comparison to the stochastically generated models. The goal of the simplified models is to have geometry that is convenient for a modeller to generate, be computed more efficiently and still have an acceptable accuracy. A collection of 1-D and 2-D models of varying complexity were generated (Figure 6-3) with and without voids. The 1-D models can generally be described as elements oriented in series and are the simplest to generate and are the most computationally efficient to solve. This advantageous if numerous variations are to be run as part of hygrothermal analysis. Some of the 1-D models have blended materials properties (hatched) which have been weight averaged between stone, mortar, and void (see section 6.4.5.3). This is often done as a means to include the 2-D effects of the mortar while preserving the simpler 1-D geometry.

The 2-D models have elements oriented in parallel and explicitly includes a mortar joint and bridging can occur. The two models contain more finite grids and take measurably longer to solve. While more complex than 1-D, they are much simpler, regular, and smaller than the explicitly modelled walls.

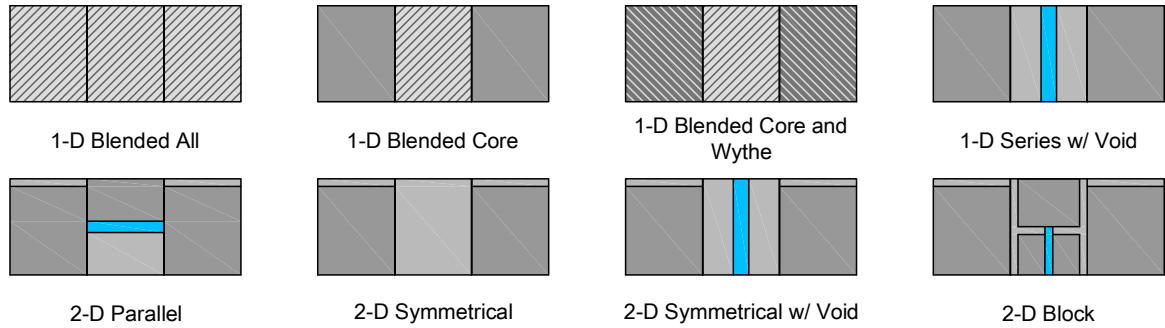


**Figure 6-3: Simplified geometric representations of rubble core walls**

The dimensions of the simplified were based on the mean dimensions from Table 6-1. The height was reduced to one half stone plus one half mortar joint (71.8 mm). The placement is shown in the centre of the core. Models were also created where the void was placed at the extremity of the core (e.g. next to the outer or inner wythe). Under most circumstances there were not substantial differences in results between the placement of the void for a model type. In the results, it is assumed that the void is placed in the centre unless noted.

Two versions of the 1-D series and 2-D parallel models were made. The first assumes that the wythes thicknesses are from the mean thicknesses from Table 6-1. The second assumes an increased wythe thickness based on the correct ratio of stone for the whole assembly.

## **6.4.5 Material Properties**

### **6.4.5.1 Sandstone and Mortar**

The primary type of stone used in the clear-field walls is Nepean Sandstone. The Nepean is extremely dense and has a low porosity for a sandstone. As a result, it has low absorption and a high vapour resistance for natural stone. It has endured well over time. The original mortar and core grout were lime based. Over time, different formulations (Portland and Roman cement) have been used sporadically as repair and repointing mortar. Decay of both the original and repointing mortar has been a persistent issue. A mortar representative of the original mortar is assumed for the simulations.

The material properties used in the simulation are shown in Table 6-2. Most of the properties were based on values from laboratory testing, with the exception of the thermal conductivities and heat capacities which were estimated or inferred from previous studies (Gutland, Santana Quintero, et al., 2019). Moisture – dependent thermal conductivity and vapour permeability was assumed using Delphin's default model.

**Table 6-2: Hygrothermal properties of sandstone and mortar used in Delphin simulations**

	Nepean Sandstone	Heritage Mortar
$\lambda_{dry}$ [W/m-K]	2.5 (Assumed)	0.9 (Assumed)
$C_p$ [J/kg-K]	850 (Assumed)	1050 (Assumed)
$\theta_{eff}$ [--]	0.098	0.246
$\theta_{cap}$ [--]	0.069	0.197
$\rho$ [kg/m <sup>3</sup> ]	2550	1890
$A_w$ [kg/m <sup>2</sup> -√s]	0.00649	0.059
$\mu_{dry}$ [--]	166	32

The moisture retention curves and transport curves were not able to be lab tested. They were modified from the Delphin library materials Sandstone Oberkirchner and Red Lime Plaster (Figure 6-4). These materials most closely matched the known porosity, pore distribution and absorption characteristics of the Nepean sandstone and mortar.

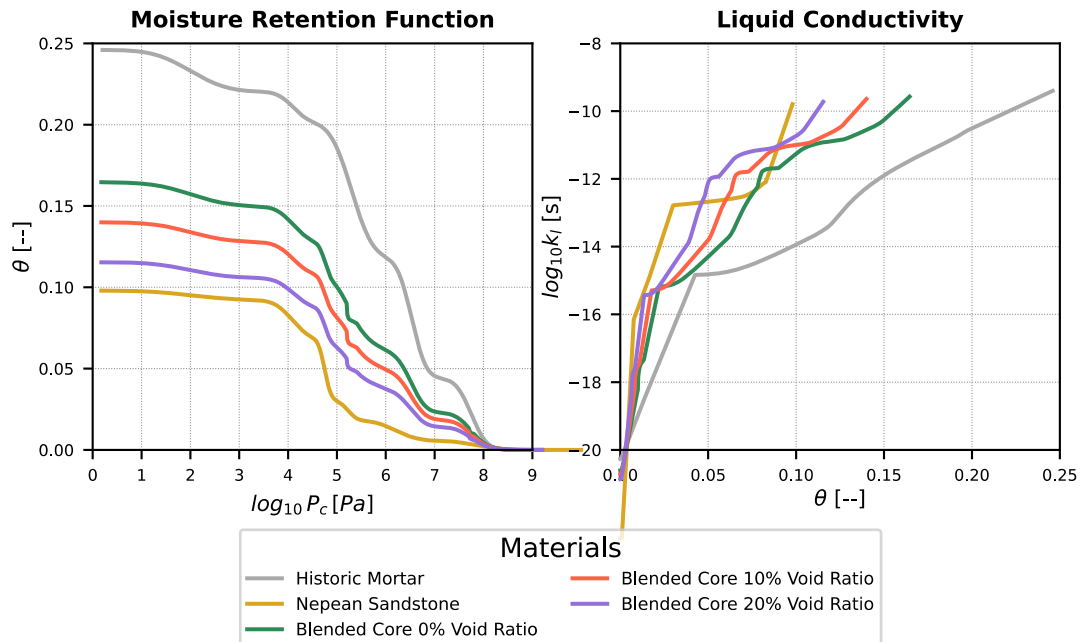


**Figure 6-4: Hygroscopic material properties of materials used in the simulations including some blended material properties.**

The sandstone and mortar have quite different material properties in terms of thermal conductivity, A-value, and dry-cup vapour diffusion. This could lead to minor thermal bridges and preferential moisture paths through the core and mortar joints. This is exaggerated when there are air voids present.

#### 6.4.5.2 Air Properties and Longwave Radiation

Heat transfer in the voids is modelled via conduction and longwave radiation. The thermal resistance of an unventilated air gap ( $R_a$ ) is a function of its width and is given by ISO 6946 Annex D (2017).

$$R_a = \frac{1}{h_a + h_r} \quad (6-1)$$

- $h_a$  is the combined conduction/convection coefficient [W/m<sup>2</sup>-K]
- $h_r$  is the radiative coefficient [W/m<sup>2</sup>-K]

$h_a$  is a function of the thickness of the cavity ( $d$ ) in the direction of heat flow and was converted into an equivalent thermal conductivity for a given sized air gap.

$$h_a = \max(0.025d, 1.25) \quad (6-2)$$

There is a range of air cavity thickness in the x-direction in the models. Unique material files were created for each thickness of air gap. Because heat transfer primarily occurs in only the x-direction, anisotropic thermal conductivity was not considered for oblong cavities.

For conductive and convective heat transfer, the voids were considered as unventilated air layers according to ISO 6946. It could be argued that these should be considered as slightly ventilated air layers because they may be connected to the exterior environment via open mortar joints or other forms of deterioration. Though the voids are unventilated, they still have an air exchange occurring. An air exchange of 1.0 1/h was assumed in the voids. There isn't any

published data on irregular voids or cavities of this type. This value was based on engineering judgment based on previous calibrated modelling attempts on this building which suggested that air exchange played a significant factor.

The longwave radiation was handled using Delphin's "longwave radiation exchange in cavity" model. The emissivity of each surface was 0.85 and reflections were accounted for.

#### **6.4.5.3 Blended Materials**

Some of the simplified models use blended material properties in lieu of detailed geometry. This is an approach used in practice for modelling stone/mortar layers. Constant hygrothermal properties such as thermal conductivity, porosity or heat capacity were calculated by simple weighted averages, for example using thermal conductivity:

$$\lambda_{Blended} = \chi_{Stone} \lambda_{Stone} + \chi_{Mortar} \lambda_{Mortar} + \chi_{Air} \lambda_{air} \quad (6-3)$$

The rubble core was assumed to be 55% stone and the remaining 45% a combination of mortar and air depending on the void ratio (V). The wythes were assumed to be 6% mortar and 94% stone and zero voids. For the blended all model the stone was assumed to be 83% and the rest a combination of mortar and air.

**Table 6-3: Blended material properties used in Delphin simulations**

	Blended Wythe	Blended Core (V=0)	Blended Core (V = 10)	Blended All (V = 0)	Blended All (V = 10)
$\chi$ [Stone: Mortar: Air]	94:6:0	55:45:0	55:35:10	83:17:0	83:14.2:2.8
$\lambda_{dry}$ [W/m-K]	2.40	1.78	1.69	2.23	2.20
$C_p$ [J/kg-K]	862	940	940	884	884
$\theta_{eff}$ [--]	0.107	0.165	0.240	0.123	0.144
$\theta_{cap}$ [--]	0.0767	0.127	0.107	0.091	0.085
$\rho$ [kg/m <sup>3</sup> ]	2508	2252	2063	2436	2383
$A_w$ [kg/m <sup>2</sup> -√s]	0.0096	0.0301	0.0242	0.0154	0.0138

Non-linear properties including the moisture retention curve and liquid conductivity curve were calculated by weighted superposition. In the weighting, the voids were considered to have minimum liquid conductivity, maximum vapour permeability and have very large pores in the moisture retention curve. Refer to Figure 6-4 for their moisture retention and liquid conductivity curves.

#### **6.4.6 Boundary Conditions**

Each set of models were simulated under four distinct boundary conditions.

1. **Steady-state heat transfer** – Imposed surface temperatures of  $T_{out} = 1^\circ\text{C}$  and  $T_{in} = 0^\circ\text{C}$  (no surface convection or radiation). Moisture transport not modelled. Duration = 120 h to establish equilibrium.
2. **Drying** – Initial RH = 99%,  $RH_{out} = RH_{in} = 50\%$ . Heat transport not modelled. Duration = 120 days to allow for measurable drying in the core.

3. **Wetting** – Initial RH = 50%, Pulsed rain load of 1 kg/m<sup>2</sup>h on exterior face for 8 hours every day for a duration of 120 days to allow adequate penetration of the moisture front past the outer wythe. Heat transport not modelled.
4. **Actual Weather Years** – 2 years of real weather data from the Ottawa International Airport.

The first three sets of boundary conditions were intended to isolate phases of a wall's cycle from a noisy full-year simulation results for direct comparison. Standard constant heat and mass transfer convection coefficients were used for Boundary Conditions 2 and 3. For Boundary Condition 4, actual weather data was used including hourly temperature, RH, wind velocity, precipitation, shortwave and longwave radiation (*Environment and Climate Change Canada*, 2020; Saha et al., 2011).

For Boundary Condition 4. the wind-driven rain exposure was assumed to have an  $F_E F_D$  of 1.0 indicating relatively high moisture loadings (ASHRAE, 2016). Interior conditions were modelled according to ASHRAE 160 simplified method. Wind-dependent convection coefficients were used on the exterior while they remained constant on the interior. No moisture sources or leaks were included in the models.

The relevant state variables ( $T$ ,  $RH$ ,  $Q_{\text{heat}}$ ,  $Q_w$ ) were recorded at pre-determined depths (output lines) in the model at 1.5 h intervals. The total moisture content (MC integral) of the assembly was also recorded for Boundary Conditions 2-4.

The damage functions RHT Index and freeze-thaw cycles were also calculated. The RHT Index was calculated on an hourly basis with thresholds of  $RH = 80\%$  and  $T = 5^\circ\text{C}$  (Kumaran et al., 2010).

$$RHT = \sum (RH - 80) * (T - 5) \text{ if } RH > 80 \text{ and } T > 5 \quad (6-4)$$

Freeze-thaw performance was evaluated in terms of number of critical freeze-thaw cycles assuming both  $S_{\text{crit}}$  of 0.5 and 0.75 to represent mortar and stone. The number of cycles were counted at depths from 5mm to 25mm. A critical cycle was counted every time the moisture content exceeded  $S_{\text{crit}}$  when the temperature cycled below  $0^\circ\text{C}$ .

## 6.5 Results

### 6.5.1 Steady State Heat Transfer

The results of the steady-state heat transfer simulations are shown in the violin plots of Figure 6-5.

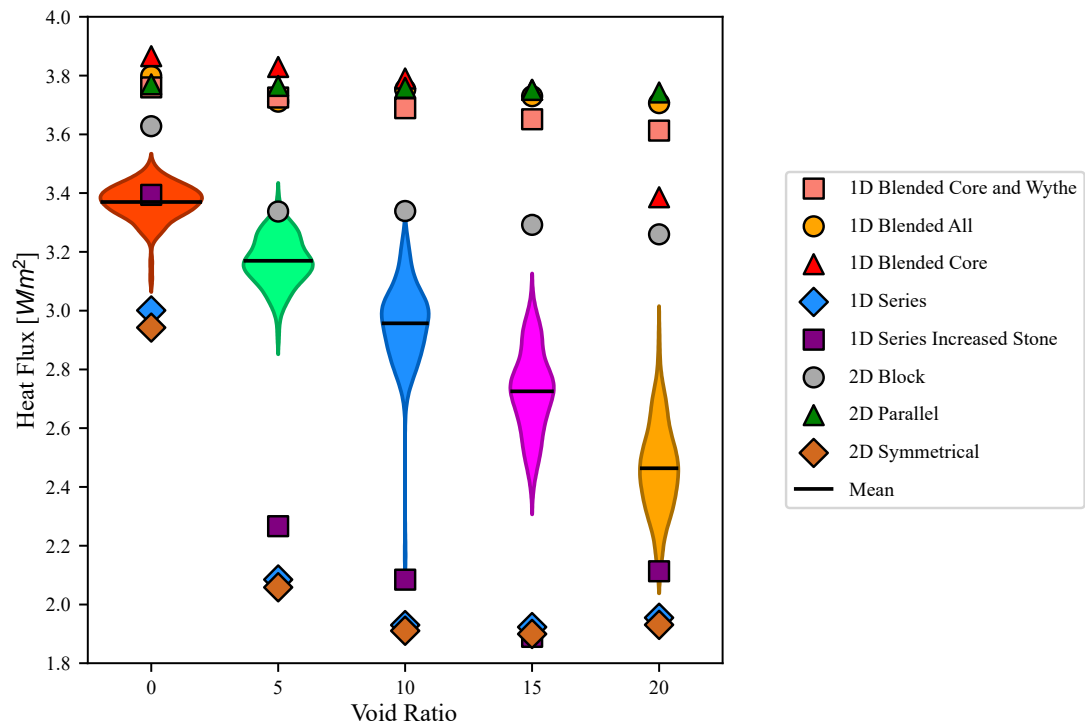


**Figure 6-5: Results of the steady-state heat transfer simulations. The reported values are taken at the exterior surface. The violin plots are created from the mean values from each simulation with 95% confidence intervals. [Note the heat flux is not equivalent to the U-value because surface resistance was not considered].**

There is a definitive decrease in the mean heat flux as the presence of voids increases which corresponds with expectations. There is also an increase in the variation in the mean heat flux between simulations as void ratio increases. The standard deviation of the means increases from  $0.059 W/m^2$  for zero voids to  $0.160 W/m^2$  with  $V=20\%$ . The increasing spread in simulation results can be

largely attributed to the presence of voids. As Figure 6-6 shows with zero voids, the mean heat flux is largely a function of the total stone/mortar ratio of the wall with an  $R^2 = 0.88$ . With the presence of only 5% voids, the quality of the fit diminishes to  $R^2 = 0.41$  and diminishes further with increased void ratio. When there are void present, the most dominant geometric factor becomes the void content of the core, however this correlation is weak with  $R^2$  ranging from 0.37 to 0.39.

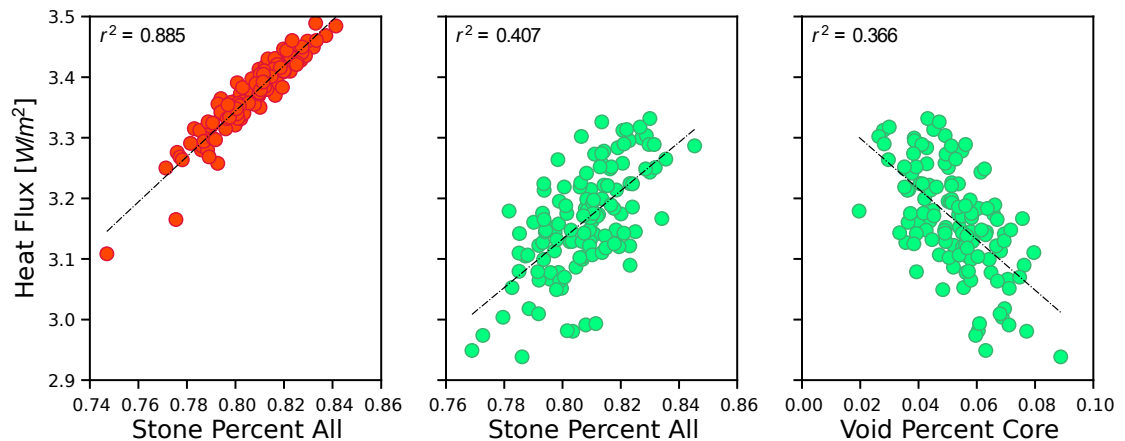


**Figure 6-6: Scatter plot of grid variables and their effect on heat transfer. Red = zero voids, Green = 5% Voids.**

Comparing the stochastically generated models to the simplified models, the blended and parallel models tend to overestimate the heat flux, while the series models tend to underestimate the heat flux.

The 1-D model with the correct stone ratio was accurate when there were no voids included, as corroborated in Figure 6-6 where the percent of stone had a very strong correlation. When voids were included, its accuracy quickly diminished. The parabolic shape of the series models is due to the width and effective R-value of the modelled air gap being non-linear above 25mm (The air gap is equal to 25.2 mm in the V=15 scenario). The inclusion of a highly resistive layer in series is not suitable in this scenario.

The blended and parallel models did not deviate much as voids increased and consistently overestimate heat transfer relative to the stochastic models. One reason for this is that longwave radiation is not factored in the property definition. This emphasizes that neither the series nor parallel heat transfer calculation methods are completely appropriate for estimating the U-value. A hybrid of the two methods is required.

The 2-D block model was the best if voids were included in the model, but still overestimated the heat flux relative to the stochastic models slightly. This model had the same stone/mortar ratio as the 1-D series model with the correct stone ratio (83%). The void in this model was placed somewhat in the centre of the core and as one. If the void were separated, staggered, or repositioned to behave more in series than in parallel, better results could have been achieved but this would be at the expense of the simplicity of the geometry.

Simulation runs were also made with transient exterior temperatures based on a sine curve to investigate if there was a thermal mass effect. The heat flux was integrated over a 24-hour period. There were no substantial changes to conclusion gained from the steady-state models in terms of the effect of voids, variance, and relationship to the simplified models.

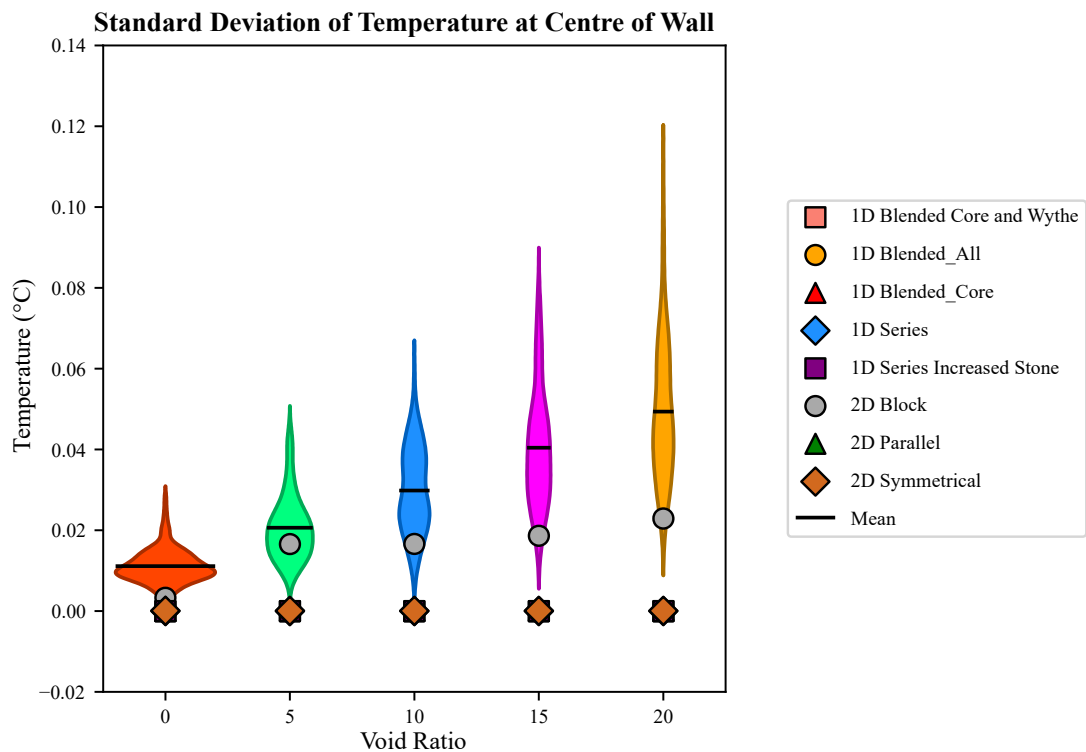


**Figure 6-7: Violin plot of standard deviation in temperature at the centre line of the wall. The y-axis scale is normalized to a 1.0 °C temperature gradient.**

Another product of the stochastically generated models is the variance in temperature at depths towards the centre of the wall. Figure 6-7 shows the

standard deviation in temperature at the centre of the wall for different void ratios. With the solid walls the deviation is less than 2% of the temperature gradient and increases up to a mean of 5% of the temperature gradient for the high void models. This may have consequences for the assessment of decay mechanisms at specific if they have temperature dependency such as freeze-thaw, corrosion, and biological growth if those elements are embedded.

### **6.5.2 Drying**

The total moisture content of the whole assembly was recorded throughout the drying and wetting simulation. Because of the different ratios of materials and their moisture retention properties, the models did not have an equal starting total moisture content. The best method for characterising the drying capabilities was to report the total moisture lost at the end of 120 days. This includes moisture transfer at the boundary conditions and via air exchange within the voids.

Generally, the models followed an asymptotic exponential decay with moisture flux at the surfaces high at the beginning and then tapering toward the end. The results of the steady-state heat transfer simulations are shown in the violin plots in Figure 6-8.

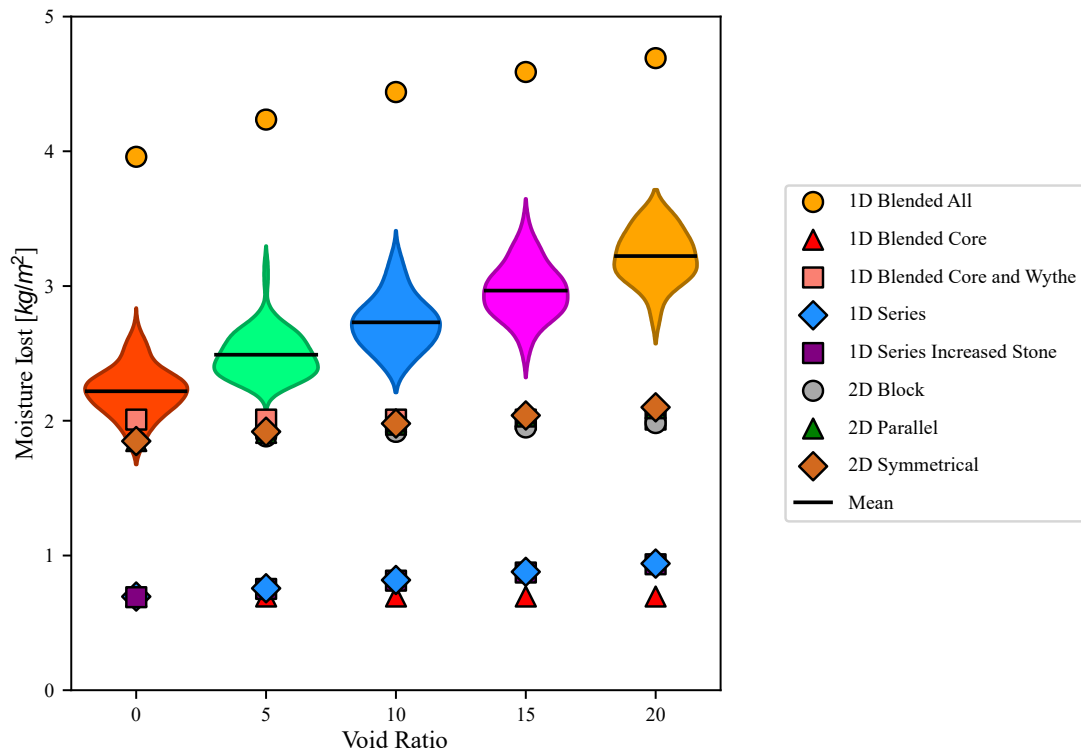


**Figure 6-8: Results of the drying moisture transfer simulations in terms of the amount of moisture lost per wall area**

The amount of drying increases roughly linearly with the void ratio as expected. The increase is mostly attributable to the air exchange in the system because the moisture flux at both the interior and exterior surfaces were relatively constant no matter what the void ratio was. It is noted that the moisture removed by air exchange if it connected to unfavourably cold or humid conditions. The standard deviation in the means also increases with void ratio.

Relative humidity was fairly constant along output lines throughout the assembly except for the centre of the outer wythe. Large variations up to 10% RH began to show as moisture was more tightly held inside the stone than the mortar. Similar to the variability in temperature, this may have consequences for the assessment of decay mechanisms at specific depths if they have RH or moisture dependency such as freeze-thaw or corrosion.

The grid variable which had the greatest influence on the wall performance was the fraction of mortar in the outer wythe (Figure 6-9). With zero voids present there was a strong correlation ( $R^2 = 0.797$ ) between the fraction of mortar in the outer wythe and the amount of moisture lost. This attests to the importance of vapour open mortars in evacuating water from the walls. The outer wythe had a much stronger correlation than the inner wythe possibly to the effect of the stronger convection coefficient on the exterior side. As the amount of voids the strength of the correlation diminished ( $R^2 < 0.40$ ). and the influence of the voids became much greater. The correlation between the fraction of mortar in the outer wythe and the moisture flux was very strong ( $R^2 > 0.99$ ).

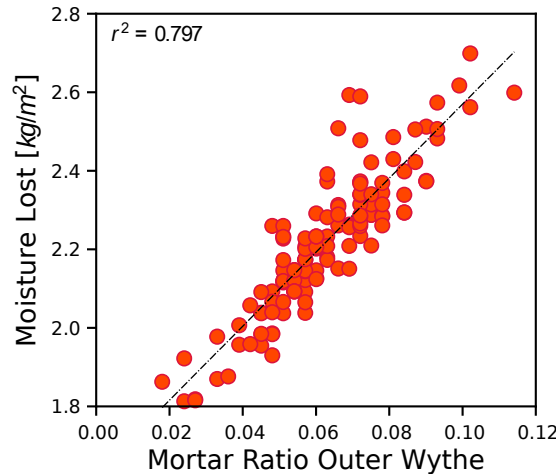


**Figure 6-9: Correlation between mortar ratio and moisture lost during drying simulation.**

Of the simplified models the best options were the Blended Core and Wythe, 2D Parallel and 2D Block models. These models all incorporate the exterior mortar joint in some fashion. This is corroborated by the fact that there was a very close relationship between moisture flux and the fraction of mortar in the outer wythe.

The Blended All model overestimates the drying effect significantly relative to the stochastic models. This is because the effective vapour resistance of the wythes is much lower compared to the Blended Core and Wythe, 2D Parallel or 2D Block models. The series models underestimate the moisture flux significantly (<38%). This is because only the highly resistive Nepean Sandstone is present at the boundary conditions.

The simplified models demonstrated a slight linear increase in drying as a function of void ratio but is significantly smaller relative to the stochastically generated models. This is thought to be attributable to the increased surface area found in the stochastic models than the simplified ones. There was no correlation between the initial moisture content and the fraction of moisture lost.

### **6.5.3 Wetting**

Wetting simulations were performed for 120 days to ensure sufficient penetration of a wetting front. The best method for characterizing the absorption capabilities was to report the total moisture gained at the end of the simulation period. Models followed an asymptotic exponential increase in moisture over the duration of the simulations.

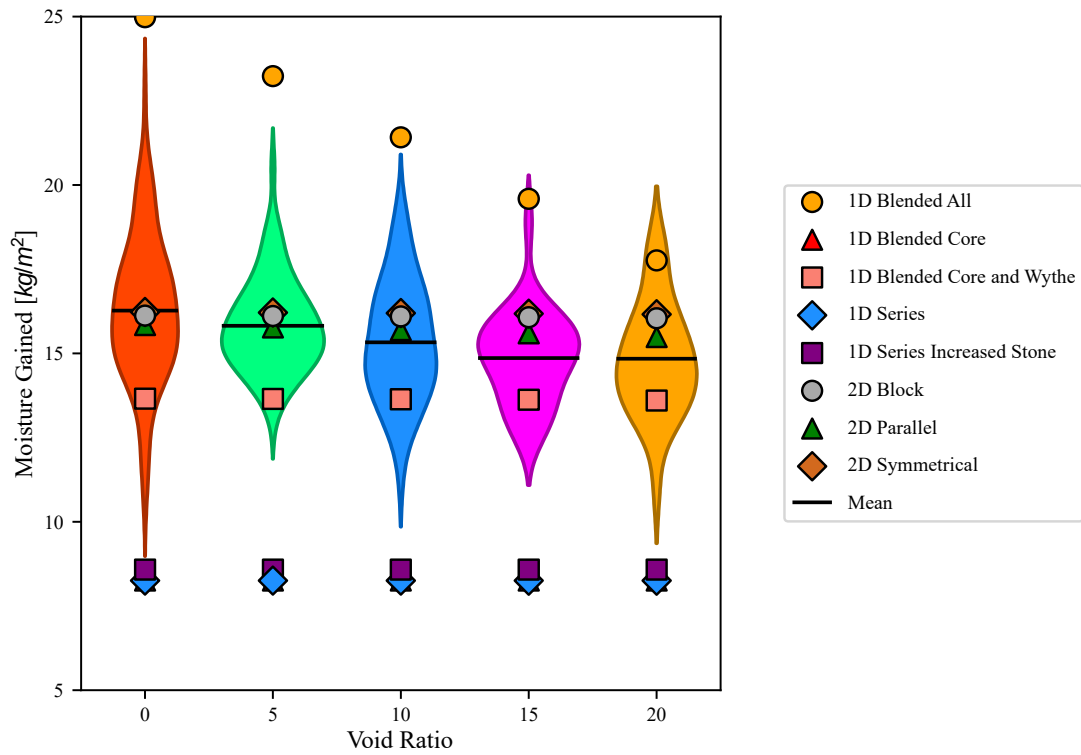


**Figure 6-10: Results of the wetting moisture transfer simulations in terms of the amount of moisture gained per wall area**

The wetting simulations are not as dependent on void ratio as the heat transfer or drying simulations. There is a small linear decrease in the amount of moisture gained with increasing void ratio. This is most likely attributable to voids or stone immediately behind the mortar joints, either slowing absorption or acting like capillary breaks.

The variable with the strongest correlation with wetting is fraction of mortar in the outer wythe. With zero voids present, the correlation is very strong ( $R^2 = 0.99$ ).

When voids are present this correlation begins to diminish but remains strong, falling to a minimum of  $R^2 = 0.843$  when  $V=15\%$ . The correlation between void ratio and absorption is very minimal which suggest that the location of the voids is just as significant as quantity. The high tail on the 0% void ratio violin is due to a geometric outlier with many densely spaced mortar joints.

Similar to the drying simulations, the simplified models which performed best were ones which included the mortar joint either explicitly or as a blended material. The 2D block and symmetrical models are the best models followed by the Blended Core and Wythe. The results for these models in Figure 6-10 are with the void placed centrally. For the 2D symmetrical model, if the void is placed next to the outer wythe (effectively turning the outer wythe into a rainscreen) there wasn't much difference in total moisture gained. However, there was an increase in MC in the stone and inward of the void was drier. This only became pronounced after about 30 days of the wetting cycle when the wetting front reached the back of the wythe. This further supports the hypothesis that the placement of what is behind the wythe can change hygrothermal performance.

Again, the Blended All and 1-D Series models proved unsuitable. The blended all model overestimates absorption relative to the stochastic models because of the high proportion of mortar being included at the wetting boundary. The decline in absorption with void ratio is because of zero liquid conductivity air being factored

into the weighted averaging. The 1-D Series models underestimate absorption relative to the stochastic models by as much as 50%, which indicates that the mortar contributes an equivalent portion to absorption into the wall. The small increase in absorption between the 1-D series models and the one with the increased stone ratio can be attributed to the interface resistance between the outer wythe and core being at a further depth.

#### **6.5.4 Actual Weather Years**

Results for the simulations with Actual Weather Years for Ottawa are reported for the final year of simulation. The results were also assessed in terms of state variables such as RH, temperature, and fluxes, and also damage functions such as the RHT Index and freeze-thaw susceptibility.

The net integrated heat flux over the year produced a similar pattern to that of the steady-state heat transfer simulations (Figure 6-5) for both stochastic and simplified models. There was only noticeable difference was a slight reduction in the variance between models. This means that the findings from the steady-state heat simulations can be extrapolated to transient models.

In terms of RH and moisture transfer, there were some interesting takeaways. The total moisture absorbed over the duration of the simulation decreased with increasing V (Figure 6-11).

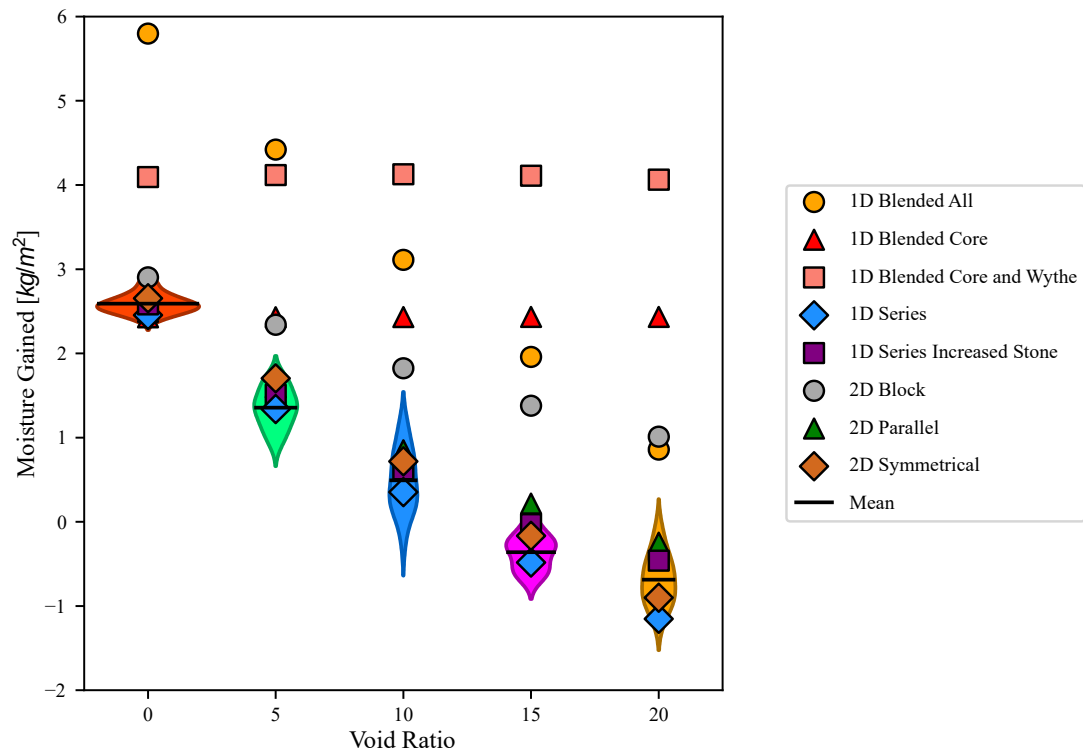


**Figure 6-11: Results of the actual weather year simulations in terms of the amount of moisture gained per wall area**

Walls with  $V < 10$  gain moisture relative to  $t=0$  while walls with  $V > 10$  lose moisture. Again, this is attributable to increased air exchange and blocking of capillary action. The 2D parallel models match best with the stochastic models and interestingly the 1D – series models perform well by this metric too despite not performing well in the drying and wetting simulations. These models tended to absorb slower and release slower. The net result has however proved similar to those models which have a more dynamic response.

When examining the RH, a trend of increasing variability and decreasing RH was observed at monitoring positions. Figure 6-12 shows the variability inherent in the models. These graphs were constructed by combining all the data from each simulation – for each grid at a given output position. The median and  $2\sigma$  quantiles were recorded for each timestep. With zero voids, there is a smaller total variance of between 3 and 5%, tightening at higher RH. As voids are introduced the variance begins to increase greatly and the mean RH begins to drop. This variance was reflected in the simplified models with the 1-D series models being at or below the lower threshold and the 2-D parallel models being at the top of the range. Previous monitoring on a section of this building with major voids also had unexpectedly low RH in the core.

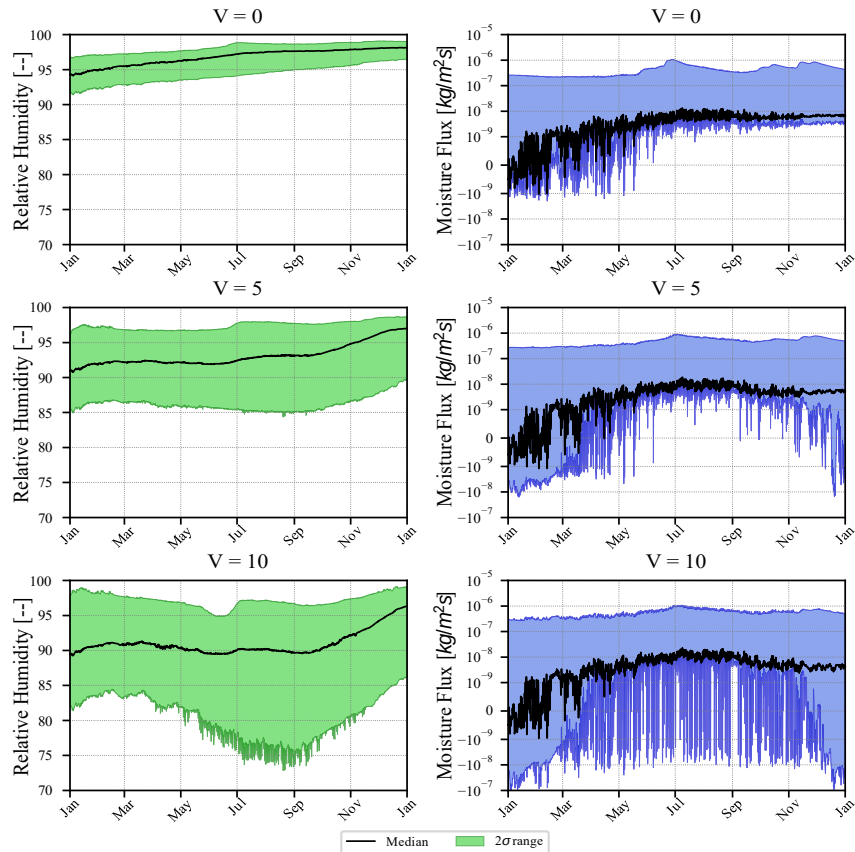


**Figure 6-12: RH and Moisture Flux behind the outer wythe of stone. Positive moisture flux are inward and negative fluxes are outward.**

The moisture flux graphs reflect this variability too. The inward fluxes do not change much, but outward fluxes become more pronounced. The frequency with which inward and outward fluxes are predicted increases through moisture being carried out of the system through voids.

The RHT Index results are shown in Figure 6-13. There is a prominent decline in RHT Index with increasing void ratio and approaches 0 as  $V \geq 15$ . This is

attributable to air exchange drying out the core and if there is enough exchange it can reduce the RH to below levels of concern. There is also a significant variance between simulations as indicated by the long, thin shape of the violins. There was a minor tendency for RHT Index to be worse in the mortar than the stone, but this did not always hold true.

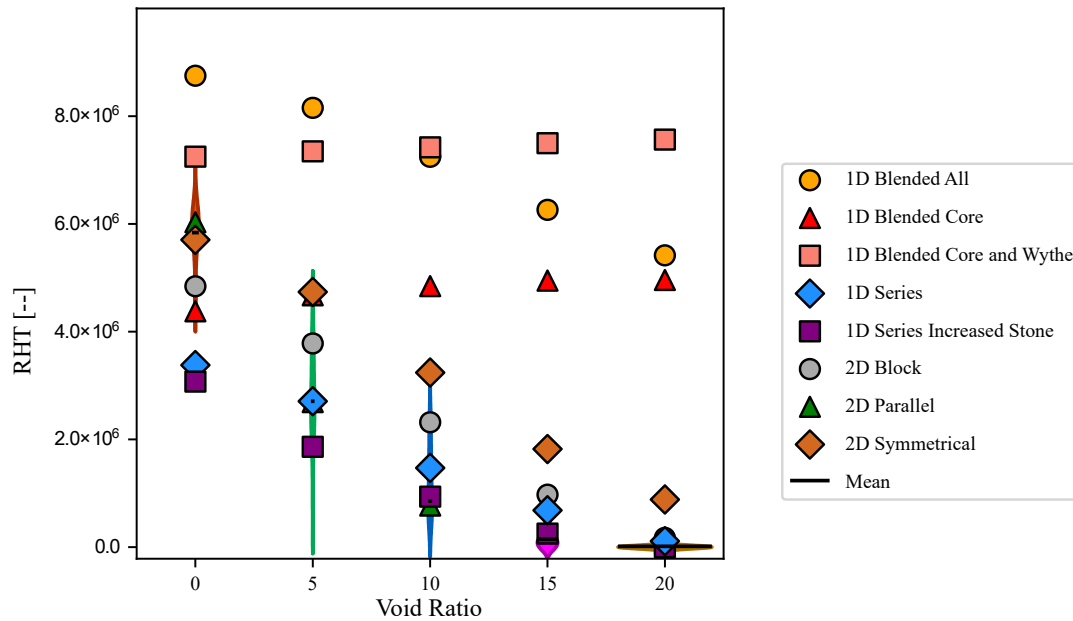


**Figure 6-13: RHT Index for the actual weather year simulations. Results are taken at the middle of the rubble core wall.**

Amongst the simplified models, the 2D parallel models correlated best at V=0, but this did not hold with increasing V. This can be attributed to the surface area of the simplified models being less. At higher values of V, the 1D series started to

perform better relative to the 2D parallel models. The blended models which did not account for air exchange behaved the worst.

In terms of freeze-thaw, there was very little differentiation in performance as a function of void ratio, or the stochastic vs. the simplified models. There was however a difference in the number of critical freeze cycles in the mortar and the stone. The mortar was slightly worse than the stone at 5mm, but the difference increased with depth into the wall where the mortar was projected to be under more stress and the stone was projected to be under none (Figure 6-14). This difference is not something that would have been observed if a 1-D model was used and should not be neglected.

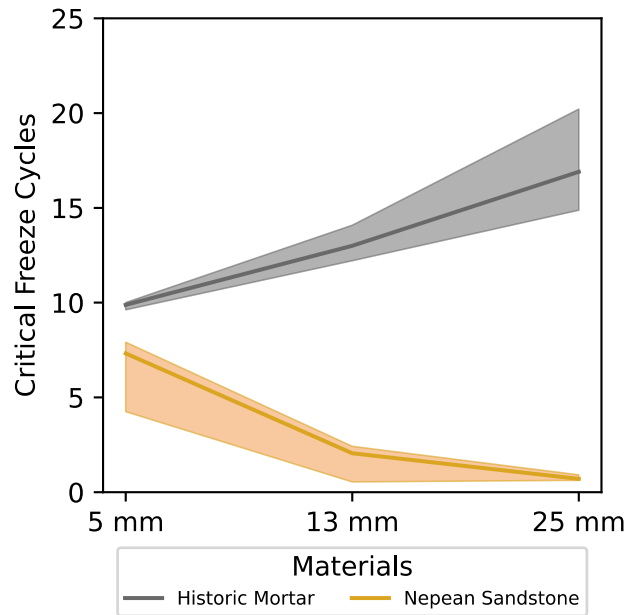


**Figure 6-14: Critical Freeze Thaw Cycles as a function of depth and their maximum and minimum extents. ( $T = 0^{\circ}\text{C}$  ,  $S_{\text{Crit}} = 50\%$ )**

## 6.6 Discussion

The results show the difficulty in abstracting geometry in rubble core masonry walls and how much the normal variations in geometry and composition can alter the perception of a walls performance. Under all four sets of boundary conditions there was a significant variation in outcome between walls generated from the pre-defined stochastic geometric parameters. This variation is comparable to what previous papers have found when using stochastically assigned material properties.

It is evident that the presence of voids can reduce heat transport, vapour transport through increased drying from air exchange and liquid transport once the moisture front reaches deep into the wall. The stochastically generated models are more influenced by this than the simplified models where the effects of voids are difficult to capture. Air exchange was shown to have an influence on drying. It is possible that the estimated 1.0 1/h was too high, but there isn't published data for an unintentional and non-planar air cavity.

The 1-D series models are the least appropriate for this type of wall under heat, and the wetting and drying cycle. The 1-D models tend to have more inertia and resistance in the system, being slower to absorb and slower to release moisture. The 2-D Parallel models were the best models often fitting within the range of the stochastic models (with the exception of heat transfer). The blended material models were not appropriate. The Blended Core and Wythe model was decent under wetting and drying but failed under actual weather conditions. The performance of these models could be improved with optimization, not using a pure weighted average.

The hygroscopic properties of the mortar and the stone were dissimilar. If the properties are comparably similar to each other in either heat, vapour, or liquid transport, then the results between the simplified models and the spread in the stochastic models will be reduced. Likewise, if the geometry is more regular,

there will be less variance. Leaks/water sources were not considered. It is arguable that the likelihood of water leaks increases if voids are present and this could negate the drying trend observed with increasing voids.

While the highly detailed stochastic models provide much more accurate models and allow insight into the effects of the natural variability of the geometry, they are not viable for everyday engineering practice. The set-up time and simulation time is prohibitive. Due to the randomized nature of the geometric grid, there is an increased chance of creating an ill-conditioned finite-volume grid. This chance increases when voids are present. As a result, some simulations have a propensity to 'stall' and take an extremely long time to complete (>7 days/simulation year). The number of finite elements used in these models could exceed 64000. Cutting the size of the grid to reduce the computational effort did not fully improve this problem.

Though not part of the scope of this paper, spatially stochastic material properties can also be incorporated into this model. For example, laboratory tests have shown that the Nepean Sandstone has a fairly wide distribution in its hygroscopic properties. Each stone in the model can be given randomly chosen properties. This concept could be expanded to different bedding, pointing or repair mortar mixes, different interface resistances, air exchanges, and water sources if voids are present.

## 6.7 Conclusion

A series of hygrothermal simulations using Delphin 6.1 were performed for rubble core walls with irregular geometry and which had considerable damage in the form of voids. A Python script was developed to stochastically create the geometry of the walls, based on Gaussian distributions of key dimensions. Simulations were performed under four sets of boundary conditions: heat transfer only, drying, wetting and actual weather years. The results of the stochastically generated geometries were compared to a set of simplified geometries to see which are most suitable.

It was found that the degree of voids had an impact on the simulated heat transfer, drying and to a lesser degree wetting. Using an actual weather year, a significant variation in state variables, heat and moisture fluxes and damage functions could be found between stochastically generated geometry in the mortar joints and in the rubble core. Stochastically generated geometries are challenging to produce and can take a lot of time to simulate. When compared to simplified models, it was found that 2-D Parallel models which accounted for the mortar joint were the most appropriate for this type of wall but struggled to accurately account for voids. 1-D Series models were found to be unsuitable for modelling this type of wall. Future work will include expanding on how spatially stochastic material properties will affect hygrothermal outcomes. Further

experimental or in-situ monitoring work will be required to validate the simulation work.

## 7. Conclusion

The projects demonstrated in this integrated thesis examined several ways in which uncertainty can play a role in our understanding of the hygrothermal performance of historic masonry wall assemblies. The projects used a combination of field study and simulation to explore and advance our understanding of the discrepancy between often found between observed conditions and what is modelled.

The first project on the Southwest Tower of the East Block began as a monitoring program with an eye to developing a methodology for calibrating hygrothermal models of the mass masonry walls. This effort was not successful due to a combination of the extreme moisture conditions and uncertainty with regards to airflow and physical composition of the walls. From the data collected, it was noticed that a unique interior climate was present, that had recently been altered. A new research question was then asked about how the interior conditions impact the durability risk which was solved with the support of a calibrated baseline energy model of the tower. The energy model of the tower was calibrated using measured RH and temperature data from the first, fourth, fifth and sixth floors of the tower.

The calibrated energy model was used as a basis for models of retrofits which could impact the interior conditions of the building. These new interior conditions could be fed to a hygrothermal model and the impact on the hygrothermal performance analysed. It was recommended to revert the tower to its previous configuration with the re-installation of heat generating equipment at the fourth floor with an increased exhaust flow rate up the tower.

The second project examined the impacts of imperfections in masonry, specifically imperfect contacts or hairline cracks between mortar and unit. Often imperfections are not considered in practice and there is minimal guidance on how to incorporate these into hygrothermal models. A generalizable method was sought to characterize the changes in moisture transport these imperfections had by modelling the interface with a known aperture ( $h$ ). Moisture transfer perpendicular to the mortar-unit interface (interface resistance) and parallel to the interface was simulated under wetting, drying and cyclic conditions.

The simulation results showed that the inclusion of a fracture model had a significant impact. The rate of absorption increased, but this was countered with an increased rate of drying. Under cyclic conditions the drying effect of the fracture outweighed the increased absorption during wetting events. This led to the wall being drier than the baseline model over the long-term.

The third project began the exploration of spatial and geometrically stochastic techniques in hygrothermal modelling. The rubble-core masonry walls of the East Block with irregular geometry and a considerable number of voids was used as an inspiration. The irregular geometry was thought to create preferential heat and moisture paths and the voids were hypothesized to act like rainscreens, altering heat and moisture transport.

A Python script was created to stochastically generate wall sections based on observed geometric parameters and degree of voids. These stochastic models were then compared to a set of simplified models to see which were most suitable.

It was found that the degree of voids had an impact on the simulated heat transfer, drying and to a lesser degree wetting. Using an actual weather year, a significant variation in state variables, heat and moisture fluxes and damage functions could be found between stochastically generated geometry in the mortar joints and in the rubble core. When compared to simplified models, it was found that 2-D Parallel models which accounted for the mortar joint were the most appropriate for this type of wall but struggled to accurately account for voids. 1-D Series models were found to be unsuitable for modelling this type of wall.

## 7.1 Contributions

This research contributes to the fields of building science, hygrothermal simulation and heritage conservation. The goal of this research was to develop methodologies to improve the process of hygrothermal modelling of masonry walls by examining sources of uncertainty in greater detail. Three research objectives were established:

1. Understanding the correlation between hygrothermal models and in-situ field measurements inside the masonry.
2. Understand how the inclusion of two-dimensional interactions and imperfections in hygrothermal models of masonry may effect results compared to when these details are omitted
3. Understand how the inherent uncertainty in hygrothermal material properties, boundary conditions and quality of construction effects hygrothermal outcomes and how this can be incorporated into practice.

Each of the published articles addresses one or more of these research objectives. Specific contributions from the articles include:

- Development of an integrated methodology for energy and hygrothermal modelling of heritage structures with unique ambient conditions.

- Applying model calibration techniques using GenOpt optimization software to energy and hygrothermal models for the purposes of assessing durability.
- Expanding the idea that imperfections and natural decay should be considered when performing hygrothermal with the specific examples.
- Introducing the concept of fractures to describe the mortar-unit interface and how this may impact moisture transport under both wetting and drying conditions. This ties into the concept of material resistance factors for use in the limit-states analog for hygrothermal assessment.
- Introducing the concept of spatially-stochastic geometry and material properties into hygrothermal modelling.
- Demonstrating the limitations of simplified 1D and 2D hygrothermal models when simulating complex masonry wall assemblies.

These contributions can be further developed and incorporated into practical design and retrofit guidelines for heritage masonry. This guidance would allow practitioners to more accurately and realistically model heritage masonry walls and how and when to consider various sources of uncertainty. While the application of the term 'heritage' implies an importance or significance to the building, the points discussed in this thesis could be equally applied to non-

designated buildings, buildings which are not yet seen as heritage by the general public, or contemporary masonry construction (eg. rainscreen cladding) which require hygrothermal analysis.

## **7.2 Future Work**

There are several avenues in which the concepts discussed in this thesis can be explored further. Presently, I am undertaking work on spatially-stochastic material properties for rubble-core masonry walls using a similar modelling process as used in Section 6.. This idea was inspired by the wide variation in material properties observed from samples of Nepean Sandstone, mortar and other building materials taken from buildings in Ottawa. The concept of stochastic material properties had been explored before in hygrothermal models. However, it is expected that the spatially-stochastic process will demonstrate a narrower confidence interval than the conventional stochastic process. The spatially-stochastic method can account for the fact that there is a reduced likelihood of materials on the extreme end of the material property distribution (eg.  $A_w$ ,  $\mu$ ,  $\lambda$ ) being adjacent to one another. This should dilute the influence of extreme results when calculating the statistics.

The spatially-stochastic methodology can also be applied at a more granular level. One example being studying the behaviour of deteriorated or repointed

mortar joints, where different mortar mixes may have been used and the quality of the repointing may vary. This also ties into the theme of considering decay when performing hygrothermal modelling of masonry.

Much of the work that I have performed focuses on sandstone and rubble-core masonry because most of the projects I have worked on have been walls of this type. The explored concepts are applicable to brick masonry as well of which there are more of than stone buildings in Canada. The geometry of brick is much more regular than that of rubble-core stone walls, but some geometric irregularity can be found (thickness of joints, bond pattern to some degree). Spatially-stochastic material properties can also apply to historic brick where quality control was not as tight as modern brick.

Eventually, I would like to apply these concepts to other envelope materials and contemporary construction, not just historic masonry. The concept of including imperfections into hygrothermal models could extend to many scenarios. For example the imperfect environmental barriers that have deteriorated, damaged or installed imperfectly. This could cause points of increased water, vapour, heat and air flow into an assembly. Are there ways this can be explicitly simulated compared to some of the cruder methods in standards (ie ASHRAE 160 §4.6.1 stating that default value for water penetrating the exterior surface shall be 1% of the water reaching that surface) and accounting for different levels of decay?

Things like flaws in continuous air or moisture barriers and their effects on moisture risk could be simulated with spatially-stochastic concepts too. I would like to develop these topics into more informative practical design and retrofit guidelines for heritage masonry. This would be in combination with Python data analysis tools to aide practitioners analysis and visualize results, as well as setting parallel runs for efficient parametric analysis or stochastic analysis.

Another topic for further consideration is the development of more accurate moisture sensors for masonry that can better address the correlation issue between measured and modelled data. Long-term monitoring of masonry is an increasingly common activity in heritage buildings, especially when there are valid durability concerns and thermal retrofits are on the table. There is a gap in the academic research on the accuracy, appropriateness and data analysis of long-term moisture monitoring. This would include the installation of more monitoring sensors in buildings to better understand the moisture response of building in situ, and under a variety of climate exposures.

## 8. References

- Agliata, R., Mollo, L., & Greco, R. (2018). Moisture measurements in heritage masonries: A review of current methods. *Materials Evaluation*, 76, 1468–1477.
- Ahlström, J. (2014). *Corrosion of steel in concrete at various moisture and chloride levels*. Energiforsk AB.
- Akkurt, G. G., Aste, N., Borderon, J., Buda, A., Calzolari, M., Chung, D., Costanzo, V., Del Pero, C., Evola, G., Huerto-Cardenas, H. E., Leonforte, F., Lo Faro, A., Lucchi, E., Marletta, L., Nocera, F., Pracchi, V., & Turhan, C. (2020). Dynamic thermal and hygrometric simulation of historical buildings: Critical factors and possible solutions. *Renewable and Sustainable Energy Reviews*, 118, 109509.  
<https://doi.org/10.1016/j.rser.2019.109509>
- Alfaiate, J., Moonen, P., Sluys, L. J., & Carmeliet, J. (2010). On the use of strong discontinuity formulations for the modeling of preferential moisture uptake in fractured porous media. *Computer Methods in Applied Mechanics and Engineering*, 199(45–48), 2828–2839.  
<https://doi.org/10.1016/j.cma.2010.05.004>
- Antretter, F., Sauer, F., Schöpfer, T., & Holm, A. (2011). Validation of a hygrothermal whole building simulation software. *Proceedings of Building Simulation 2011: 12th Conference of International Building Performance Simulation Association*, 1694–1701.
- ASHRAE. (2009). *ASHRAE Standard 160-2009, Criteria for Moisture-Control Design Analysis in Buildings*. American Society of Heating, Refrigerating and Air-Conditioning Engineers.

- ASHRAE. (2013a). Chapter 25: Heat, Air and Moisture Control in Building Assemblies—Fundamentals. In *2013 ASHRAE Handbook—Fundamentals*. American Society of Heating, Refrigerating and Air-Conditioning Engineers.
- ASHRAE. (2013b). Chapter 26: Heat, Air and Moisture Control in Building Assemblies—Material Properties. In *2013 ASHRAE Handbook—Fundamentals*. American Society of Heating, Refrigerating and Air-Conditioning Engineers.
- ASHRAE. (2013c). Chapter 27: Heat, Air and Moisture Control in Building Assemblies—Examples. In *2013 ASHRAE Handbook—Fundamentals*. American Society of Heating, Refrigerating and Air-Conditioning Engineers.
- ASHRAE. (2014). *ASHRAE Guideline 14-2014—Measurement of Energy, Demand, and Water Savings*. American Society of Heating, Refrigerating and Air-Conditioning Engineers.
- ASHRAE. (2016). *ASHRAE Standard 160-2016, Criteria for Moisture-Control Design Analysis in Buildings*. American Society of Heating, Refrigerating and Air-Conditioning Engineers.
- ASHRAE. (2017). *ASHRAE Standard 140-2017, Standard Method of Test for the Evaluation of Building Energy Analysis Computer Programs*. American Society of Heating, Refrigerating and Air-Conditioning Engineers.
- ASHRAE. (2019). *ASHRAE Guideline 34-2019—Energy Guideline for Historic Buildings*. American Society of Heating, Refrigerating and Air-Conditioning Engineers.
- Ashurst, J. (1977). *Departmental Buildings, Eastern Block, Parliament Hill*. Ottawa.

- ASTM C20-00(2015), Standard Test Methods for Apparent Porosity, Water Absorption, Apparent Specific Gravity, and Bulk Density of Burned Refractory Brick and Shapes by Boiling Water.* (2015). ASTM International.
- ASTM C830-00(2016), Standard Test Methods for Apparent Porosity, Liquid Absorption, Apparent Specific Gravity, and Bulk Density of Refractory Shapes by Vacuum Pressure.* (2016a). ASTM International.
- ASTM C1498-04a(2016), Standard Test Method for Hygroscopic Sorption Isotherms of Building Materials.* (2016b). ASTM International.
- ASTM C1713-17 Standard Specification for Mortars for the Repair of Historic Masonry.* (2017). ASTM International.
- ASTM C1794-19 Standard Test Methods for Determination of the Water Absorption Coefficient by Partial Immersion.* (2019). ASTM International.
- ASTM E96/ E96M-16, Standard Test Methods for Water Vapor Transmission of Materials.* (2016c). ASTM International.
- Baker, P. (2011). *U-values and traditional buildings—In situ measurements and their comparisons to calculated values* (Technical Paper 10). Historic Scotland.
- Bauklimatik Dresden. (2018). *DELPHIN 6.0* (6.0.18) [Computer software].  
<https://bauklimatik-dresden.de/delphin/index.php?aLa=en>
- Bauklimatik Dresden. (2020). *DELPHIN 6.1* (6.1.0) [Computer software].  
<https://bauklimatik-dresden.de/delphin/index.php?aLa=en>
- Benchmark test of EN 15026.* (2020). Fraunhofer Institute for Building Physics.  
<https://wufi.de/en/2015/04/09/benchmark-test-of-en-15026/>
- Berger, J., Orlande, H. R. B., Mendes, N., & Guernouti, S. (2016). Bayesian inference for estimating thermal properties of a historic building wall.

- Building and Environment*, 106, 327–339.  
<https://doi.org/10.1016/j.buildenv.2016.06.037>
- Best practice guide, wood frame envelopes*. (1999). Canada Mortgage and Housing Corporation.
- Blocken, B., & Carmeliet, J. (2006). On the validity of the cosine projection in wind-driven rain calculations on buildings. *Building and Environment*, 41(9), 1182–1189. <https://doi.org/10.1016/j.buildenv.2005.05.002>
- Blocken, B., & Carmeliet, J. (2007). Validation of CFD simulations of wind-driven rain on a low-rise building facade. *Building and Environment*, 42(7), 2530–2548. <https://doi.org/10.1016/j.buildenv.2006.07.032>
- Blocken, B., & Carmeliet, J. (2012). A simplified numerical model for rainwater runoff on building facades: Possibilities and limitations. *Building and Environment*, 53, 59–73. <https://doi.org/10.1016/j.buildenv.2012.01.010>
- Blocken, B., Derome, D., & Carmeliet, J. (2013). Rainwater runoff from building facades: A review. *Building and Environment*, 60, 339–361.  
<https://doi.org/10.1016/j.buildenv.2012.10.008>
- Blümich, B., Casanova, F., Perlo, J., Presciutti, F., Anselmi, C., & Doherty, B. (2010). Noninvasive Testing of Art and Cultural Heritage by Mobile NMR. *Accounts of Chemical Research*, 43(6), 761–770.  
<https://doi.org/10.1021/ar900277h>
- Bottino-Leone, D., Larcher, M., Troi, A., & Grunewald, J. (2021). Hygrothermal characterization of a fictitious homogenized porous material to describe multiphase heat and moisture transport in massive historic walls. *Construction and Building Materials*, 266, 121497.  
<https://doi.org/10.1016/j.conbuildmat.2020.121497>
- Brocken, H. J. P. (1998). *Moisture transport in brick masonry: The grey area between bricks* [Dissertation]. Technische Universiteit Eindhoven.

- Brown, S. R. (1987). Fluid flow through rock joints: The effect of surface roughness. *Journal of Geophysical Research: Solid Earth*, 92(B2), 1337–1347. <https://doi.org/10.1029/JB092iB02p01337>
- Browne, D. (2012). *The SPAB Research Report 3: The SPAB Hygrothermal Modelling*. Society for Protection of Ancient Buildings.
- Burdine, N. T. (1953). Relative Permeability Calculations From Pore Size Distribution Data. *SPE-225-G*, 5(03), 71–78. <https://doi.org/10.2118/225-G>
- Busser, T., Berger, J., Piot, A., Pailha, M., & Woloszyn, M. (2018). *Experimental validation of hygrothermal models for building materials and walls: An analysis of recent trends*. HAL Archives. <https://hal.archives-ouvertes.fr/hal-01678857>
- Calle, K., De Kock, T., Cnudde, V., & Van den Bossche, N. (2019). Liquid moisture transport in combined ceramic brick and natural hydraulic lime mortar samples: Does the hygric interface resistance dominate the moisture transport? *Journal of Building Physics*, 43(3), 208–228. <https://doi.org/10.1177/1744259119857762>
- Cammalleri, V., & Lagus, P. L. (2009). Moisture Techniques and Instrumentation: The Key Factor in Mold Prevention. In *Moisture Control in Buildings* (2nd ed., pp. 139–159). American Society for Testing and Materials.
- Canadian Climate Normals 1981-2010 Station Data*. (2017). Environment and Climate Change Canada. [http://climate.weather.gc.ca/climate\\_normals/index\\_e.html#1981](http://climate.weather.gc.ca/climate_normals/index_e.html#1981)
- Carmeliet, J., Descamps, F., & Houvenaghel, G. (1999). A Multiscale Network Model for Simulating Moisture Transfer Properties of Porous Media. *Transport in Porous Media*, 35(1), 67–88. <https://doi.org/10.1023/A:1006500716417>

- Carmeliet, J., & Roels, S. (2002). Determination of the Moisture Capacity of Porous Building Materials. *Journal of Thermal Envelope and Building Science*, 25(3), 209–237. <https://doi.org/10.1106/109719602022835>
- Carsana, M., Marra, E., & Bertolini, L. (2015). Corrosion behaviour of metal inserts in simulated ancient masonry mortars. *Construction and Building Materials*, 95, 457–466. <https://doi.org/10.1016/j.conbuildmat.2015.07.110>
- CEN. (2017). *EN 16883:2017—Conservation of cultural heritage—Guidelines for improving the energy performance of historic buildings*. European Committee for Standardization.
- Černý, R. (2009). Time-domain reflectometry method and its application for measuring moisture content in porous materials: A review. *Measurement*, 42(3), 329–336. <https://doi.org/10.1016/j.measurement.2008.08.011>
- Charola, A. E. (1995). Water-Repellent Treatments for Building Stones: A Practical Overview. *APT Bulletin: The Journal of Preservation Technology*, 26(2/3), 10–17. JSTOR. <https://doi.org/10.2307/1504480>
- Charola, A. E. (1998). *Review of the Literature on the Topic of Acidic Deposition on Stone*. The National Center for Preservation Technology and Training.
- Charola, A. E., Pühringer, J., & Steiger, M. (2007). Gypsum: A review of its role in the deterioration of building materials. *Environmental Geology*, 52(2), 339–352. <https://doi.org/10.1007/s00254-006-0566-9>
- Clarke, J. (2013). Moisture flow modelling within the ESP-r integrated building performance simulation system. *Journal of Building Performance Simulation*, 6(5), 385–399. <https://doi.org/10.1080/19401493.2013.777117>
- Clarke, J. A., Johnstone, C. M., Kelly, N. J., McLean, R. C., Anderson, J. A., Rowan, N. J., & Smith, J. E. (1999). A technique for the prediction of the conditions leading to mould growth in buildings. *Building and Environment*, 34(4), 515–521. [https://doi.org/10.1016/S0360-1323\(98\)00023-7](https://doi.org/10.1016/S0360-1323(98)00023-7)

- CSA. (2014a). *CAN/CSA-A179-14—Mortar and grout for unit masonry*. CSA Group.
- CSA. (2014b). *CSA-S304-14—Design of masonry structures*. CSA Group.
- CUAHSI HIS Hydroclient. (2020). Consortium of Universities for the Advancement of Hydrologic Science, Inc. <http://data.cuahsi.org/>
- De Freitas, V. P., Abrantes, V., & Crausse, P. (1996). Moisture migration in building walls—Analysis of the interface phenomena. *Building and Environment*, 31(2), 99–108. [https://doi.org/10.1016/0360-1323\(95\)00027-5](https://doi.org/10.1016/0360-1323(95)00027-5)
- De Rose, D., Pearson, N., Mensinga, P., & Straube, J. (2014). Towards a Limit States Approach to Insulating Solid Masonry Walls in a Cold Climate. *Buildings for Tomorrow*, 521–530.
- Defo, M., Lacasse, M., & Laouadi, A. (2021). A comparison of hygrothermal simulation results derived from four simulation tools. *Journal of Building Physics*, 174425912098876. <https://doi.org/10.1177/1744259120988760>
- Delgado, J. M. P. Q., Ramos, N. M. M., Barreira, E., & de Freitas, V. P. (2010). A critical review of hygrothermal models used in porous building materials. *Journal of Porous Media*, 13(3), 221–234. <https://doi.org/10.1615/JPorMedia.v13.i3.30>
- Derluyn, H., Derome, D., Carmeliet, J., Stora, E., & Barbarulo, R. (2012). Hysteretic moisture behavior of concrete: Modeling and analysis. *Cement and Concrete Research*, 42(10), 1379–1388. <https://doi.org/10.1016/j.cemconres.2012.06.010>
- Derluyn, H., Janssen, H., & Carmeliet, J. (2011). Influence of the nature of interfaces on the capillary transport in layered materials. *Construction and Building Materials*, 25(9), 3685–3693. <https://doi.org/10.1016/j.conbuildmat.2011.03.063>

- Di Tullio, V., Proietti, N., Gentile, G., Giani, E., Poggi, D., & Capitani, D. (2012). Unilateral NMR: a Noninvasive Tool for Monitoring In Situ the Effectiveness of Intervention to Reduce the Capillary Raise of Water in an Ancient Deteriorated Wall Painting. *International Journal of Spectroscopy*, 2012, 494301. <https://doi.org/10.1155/2012/494301>
- DIN EN 12087:2013—Thermal Insulating Products For Building Applications—Determination Of Long Term Water Absorption By Immersion*. (2013). Deutsches Institut für Normung.
- Drysdale, R. G. (2012). Masonry engineering in Canada past current and future developments. *Proceedings of the 15th International Brick and Block Masonry Conference*. 15th International Brick and Block Masonry Conference, Florianópolis.
- Durner, W. (1994). Hydraulic conductivity estimation for soils with heterogeneous pore structure. *Water Resources Research*, 30(2), 211–223. <https://doi.org/10.1029/93WR02676>
- Eklund, J. A., Zhang, H., Viles, H. A., & Curteis, T. (2013). Using Handheld Moisture Meters on Limestone: Factors Affecting Performance and Guidelines for Best Practice. *International Journal of Architectural Heritage*, 7(2), 207–224. <https://doi.org/10.1080/15583058.2011.626491>
- EN 15026: Hygrothermal performance of building components and building elements. Assessment of moisture transfer by numerical simulation*. (2007). European Committee for Standardization.
- EnergyPlus Version 8-8-0 Documentation—Auxillary Programs*. (2017a). U.S. Department of Energy. <https://energyplus.net/documentation>
- EnergyPlus Version 8-8-0 Documentation—Engineering Reference*. (2017b). U.S. Department of Energy. <https://energyplus.net/documentation>

- EnergyPlus Version 9-0-1 Documentation—Engineering Reference*. (2018). U.S. Department of Energy. <https://energyplus.net/documentation>
- Fagerlund, G. (1977). RILEM Recommendation: The critical degree of saturation method of assessing the freeze/thaw resistance of concrete. *Materials and Structures*, 10(58), 217–229.
- Forster, A. (2007). Binder loss in traditional mass masonry: A cause for concern? *Structural Survey*, 25(2), 148–170.  
<https://doi.org/10.1108/02630800710747717>
- Fraunhofer Institute for Building Physics. (2019a). *WUFI* (6.3) [Computer software]. <https://wufi.de/en/software/wufi-pro/>
- Fraunhofer Institute for Building Physics. (2019b). *WUFI 2D* (4.2) [Computer software]. <https://wufi.de/en/software/wufi-2d/>
- Fraunhofer Institute for Building Physics. (2019c). *WUFI Plus* (3.2) [Computer software]. <https://wufi.de/en/software/wufi-plus/>
- Freudenberg, P., Ruisinger, U., & Stöcker, E. (2017). Calibration of Hygrothermal Simulations by the Help of a Generic Optimization Tool. *Energy Procedia*, 132, 405–410. <https://doi.org/10.1016/j.egypro.2017.09.645>
- Galambos, T. V. (1981). Load and Resistance Factor Design. *Engineering Journal*, 18, 74–82.
- Gaur, A., Lacasse, M., & Armstrong, M. (2019). Climate Data to Undertake Hygrothermal and Whole Building Simulations Under Projected Climate Change Influences for 11 Canadian Cities. *Data*, 4(2).  
<https://doi.org/10.3390/data4020072>
- Ge, S. (1997). A governing equation for fluid flow in rough fractures. *Water Resources Research*, 33(1), 53–61.
- Giuliani, M., Henze, G. P., & Florita, A. R. (2016). Modelling and calibration of a high-mass historic building for reducing the prebound effect in energy

- assessment. *Energy and Buildings*, 116, 434–448.  
<https://doi.org/10.1016/j.enbuild.2016.01.034>
- Glazer, R. (2013). *Hygrothermal Monitoring of Southwest Tower, East Block, Parliament Hill* (No. A1-002613-02.1). National Research Council.
- Goffart, J., Rabouille, M., & Mendes, N. (2017). Uncertainty and sensitivity analysis applied to hygrothermal simulation of a brick building in a hot and humid climate. *Journal of Building Performance Simulation*, 10(1), 37–57.  
<https://doi.org/10.1080/19401493.2015.1112430>
- Grunewald, J., Häupl, P., & Bomberg, M. (2003). Towards an Engineering Model of Material Characteristics for Input to Ham Transport Simulations—Part 1: An Approach. *Journal of Thermal Envelope and Building Science*, 26(4), 343–366. <https://doi.org/10.1177/1097196303026004002>
- Gutland, M., Bucking, S., & Santana Quintero, M. (2019). Assessing Durability of Historic Masonry Walls with Calibrated Energy Models and Hygrothermal Modeling. *International Journal of Architectural Heritage*, 1–17.  
<https://doi.org/10.1080/15583058.2019.1618976>
- Gutland, M., Santana Quintero, M., & Bucking, S. (2019, September). Calibration of an historic masonry building using measured temperature and heat flux data. *Proceedings of Building Simulation 2019: 16th Conference of IBPSA*. Building Simulation 2019, Rome, Italy.
- Hakami, E. (1995). *Aperture Distribution of Rock Fractures* [Ph.D]. Royal Institute of Technology.
- Hall, C., & Kalimeris, A. N. (1982). Water movement in porous building materials—V. Absorption and shedding of rain by building surfaces. *Building and Environment*, 17(4), 257–262. [https://doi.org/10.1016/0360-1323\(82\)90018-X](https://doi.org/10.1016/0360-1323(82)90018-X)

- HAMSTAD—Determination of liquid water transfer properties of porous building materials and development of numerical assessment methods.* (2002). Chalmers University of Technology.
- Hansen, E. J. de P., & Møller, E. B. (2018). How to estimate material properties for external walls in historic buildings before applying internal insulation. *Energy Efficiency in Historic Buildings*, 41–49.
- Harrestrup, M., & Svendsen, S. (2016). Internal insulation applied in heritage multi-storey buildings with wooden beams embedded in solid masonry brick façades. *Building and Environment*, 99, 59–72.  
<https://doi.org/10.1016/j.buildenv.2016.01.019>
- Hens, H. (1990). *Guidelines & practice. International Energy Agency Annex XIV.* International Energy Agency.
- Hens, H. (1999). Fungal Defacement in Buildings: A Performance Related Approach. *HVAC&R Research*, 5(3), 265–280.  
<https://doi.org/10.1080/10789669.1999.10391237>
- Heritage Character Statement—East Block Parliament Hill.* (1987). Federal Heritage Buildings Review Office.
- Herrera-Avellanosa, D., Haas, F., Leijonhufvud, G., Brostrom, T., Buda, A., Pracchi, V., Webb, A. L., Hüttler, W., & Troi, A. (2019). Deep renovation of historic buildings: The IEA-SHC Task 59 path towards the lowest possible energy demand and CO<sub>2</sub> emissions. *International Journal of Building Pathology and Adaptation*, ahead-of-print(ahead-of-print).  
<https://doi.org/10.1108/IJBPA-12-2018-0102>
- Historical Data.* (2020). Environment and Climate Change Canada.  
[http://climate.weather.gc.ca/historical\\_data/search\\_historic\\_data\\_e.html](http://climate.weather.gc.ca/historical_data/search_historic_data_e.html)

- Hoffman, D., & Niesel, K. (2008). *Effect of air pollutants on renderings and moisture-transport phenomena in masonry*. Bundesanstalt für Materialforschung und -prüfung.
- Huerto-Cardenas, H. E., Leonforte, F., Aste, N., Del Pero, C., Evola, G., Costanzo, V., & Lucchi, E. (2020). Validation of dynamic hygrothermal simulation models for historical buildings: State of the art, research challenges and recommendations. *Building and Environment*, 180, 107081. <https://doi.org/10.1016/j.buildenv.2020.107081>
- Iodice, P., Massarotti, N., & Mauro, A. (2016). Effects of Inhomogeneities on Heat and Mass Transport Phenomena in Thermal Bridges. *Energies*, 9(3), 126. <https://doi.org/10.3390/en9030126>
- ISO. (2005). *ISO 15927-4: Hygrothermal performance of buildings—Calculation and presentation of climatic data—Part 4: Hourly data for assessing the annual energy use for heating and cooling*. International Organization for Standardization.
- ISO. (2009). *ISO 15927-3: Hygrothermal performance of buildings—Calculation and presentation of climatic data—Part 3: Calculation of a driving rain index for vertical surfaces from hourly wind and rain data*. International Organization for Standardization.
- ISO. (2012a). *ISO 9223:2012—Corrosion of metals and alloys—Corrosivity of atmospheres—Classification, determination and estimation*. International Organization for Standardization.
- ISO. (2012b). *ISO 13788: Hygrothermal performance of building components and building elements — Internal surface temperature to avoid critical surface humidity and interstitial condensation — Calculation methods*. International Organization for Standardization.

- ISO. (2017). *ISO 6946:2017 Building components and building elements—Thermal resistance and thermal transmittance—Calculation method*. International Organization for Standardization.
- Janssen, H., Derluyn, H., & Carmeliet, J. (2012). Moisture transfer through mortar joints: A sharp-front analysis. *Cement and Concrete Research*, 42(8), 1105–1112. <https://doi.org/10.1016/j.cemconres.2012.05.004>
- Jokilehto, J. (1986). *A History of Architectural Conservation: The Contribution of English, French, German and Italian Thought towards an International Approach to the Conservation of Cultural Property* [Ph.D]. University of York.
- Karoglou, M., Moropoulou, A., Maroulis, Z. B., & Krokida, M. K. (2005). Water Sorption Isotherms of Some Building Materials. *Drying Technology*, 23(1–2), 289–303. <https://doi.org/10.1081/DRT-200047948>
- Kersten, B., & van Schnijdel, J. (2013). Modeling the Heat Exchange in Cavities of Building Constructions using Comsol. *Proceedings of the 2013 COMSOL Conference*. COMSOL Conference 2013 Rotterdam, Rotterdam, Nederland.
- Khalilzadeh, A., Ge, H., & Dick Ng, H. (2016). CFD modelling of wind-driven rain wetting of building facade. *ESIM 2016 Conference Proceedings*. eSIM 2016, Hamilton, Canada.
- Kirkpatrick, S. (1973). Percolation and Conduction. *Reviews of Modern Physics*, 45(4), 574–588. <https://doi.org/10.1103/RevModPhys.45.574>
- Klůšeiko, P., Arumägi, E., & Kalamees, T. (2015). Hygrothermal performance of internally insulated brick wall in cold climate: A case study in a historical school building. *Journal of Building Physics*, 38(5), 444–464. <https://doi.org/10.1177/1744259114532609>

- Knarud, J., & Geving, S. (2015). Implementation and Benchmarking of a 3D Hygrothermal Model in the COMSOL Multiphysics Software. *Energy Procedia*, 78, 3440–3445. <https://doi.org/10.1016/j.egypro.2015.12.327>
- Knarud, J. I., & Geving, S. (2017). Comparative study of hygrothermal simulations of a masonry wall. *Energy Procedia*, 132, 771–776. <https://doi.org/10.1016/j.egypro.2017.10.027>
- Kočí, V., Čáchová, M., Koňáková, D., Vejmelková, E., Jerman, M., Keppert, M., Maděra, J., & Černý, R. (2018). Heat and Moisture Transport and Storage Parameters of Bricks Affected by the Environment. *International Journal of Thermophysics*, 39(5), 63. <https://doi.org/10.1007/s10765-018-2383-2>
- Krus, M. (1996). *Moisture Transport and Storage Coefficients of Porous Mineral Building Materials*. Fraunhofer Institute for Building Physics. <https://wufi.de/literatur/Krus%201996%20-%20Moisture%20Transport%20and%20Storage%20Coefficients.pdf>
- Kubičár, L., Vretenár, V., Štofanič, V., & Boháč, V. (2010). Hot-Ball Method for Measuring Thermal Conductivity. *International Journal of Thermophysics*, 31(10), 1904–1918. <https://doi.org/10.1007/s10765-008-0544-4>
- Kubilay, A., Carmeliet, J., & Derome, D. (2017). Computational fluid dynamics simulations of wind-driven rain on a mid-rise residential building with various types of facade details. *Journal of Building Performance Simulation*, 10(2), 125–143. <https://doi.org/10.1080/19401493.2016.1152304>
- Kubilay, A., Derome, D., & Carmeliet, J. (2018). Coupling of physical phenomena in urban microclimate: A model integrating air flow, wind-driven rain, radiation and transport in building materials. *Urban Climate*, 24, 398–418. <https://doi.org/10.1016/j.uclim.2017.04.012>

- Kumaran, M. K., & Bomberg, M. (1985). A Gamma-spectrometer for determination of density distribution and moisture distribution in building materials. *Proceedings of the International Symposium on Moisture and Humidity*, 485–490.
- Kumaran, M. K., Mukhopadhyaya, P., Cornick, S. M., Lacasse, M. A., Meref, W., Rousseau, M. Z., Nofal, M., Quirt, J. D., & Dalglish, W. A. (2010). A Methodology to develop moisture management strategies for wood-frame walls in North America: Application to stucco-clad walls. *Proceedings of the 6th Symposium on Building Physics in the Nordic Countries. Trondheim*, 651–658.
- Künzel, H. M. (1994). *One and Two Dimensional Calculation of the Simultaneous Heat and Moisture Transport in Building Components, Using Simple Parameters* [Dissertation]. Fraunhofer Institute for Building Physics.
- Künzel, H. M., & Holm, A. (2009, March). Moisture Control and Problem Analysis of Heritage Constructions. *PATORREB 2009 Conference*. PATORREB 2009, Porto, Portugal.
- Lacasse, M. A., Gaur, A., & Moore, T. V. (2020). Durability and Climate Change—Implications for Service Life Prediction and the Maintainability of Buildings. *Buildings*, 10(3). <https://doi.org/10.3390/buildings10030053>
- Lacy, R. E. (1965). Driving rain maps and the onslaught of rain on buildings. *RILEM/ CIB Symposium on Moisture Problems in Buildings Rain Penetration*, 3, 3–4.
- Lawton, M. D., & Hoffman, S. P. (1998). Decision Making on the Indoor Environment and Building Envelope of Canada's Library of Parliament. *Thermal Performance of the Exterior Envelopes of Buildings VII*. Thermal performance of the exterior envelopes of buildings VII, Clearwater Beach.

- Lehmann, F. (2018). *Instrumented monitoring of moisture and salt by electrical impedance measurements* [Ph.D]. University of Stuttgart.
- Li, X., Chen, S., Xu, Q., & Xu, Y. (2018). Modeling Capillary Water Absorption in Concrete with Discrete Crack Network. *Journal of Materials in Civil Engineering*, 30(1), 04017263. [https://doi.org/10.1061/\(ASCE\)MT.1943-5533.0002122](https://doi.org/10.1061/(ASCE)MT.1943-5533.0002122)
- Libralato, M., Angelis, A., D'Agaro, P., Cortella, G., & Saro, O. (2021). Multiyear hygrothermal performance simulation of historic building envelopes. *IOP Conference Series: Earth and Environmental Science*, 863, 012045. <https://doi.org/10.1088/1755-1315/863/1/012045>
- Libralato, M., Murano, G., De Angelis, A., Saro, O., & Corrado, V. (2018, September 23). Hygrothermal modelling of building enclosures: Reference year design for moisture accumulation and condensation risk assessment. *Proceedings of the 7th International Building Physics Conference*. 7th International Building Physics Conference, Syracuse. <https://doi.org/10.14305/ibpc.2018.ps19>
- Libralato, M., Pernigotto, G., Prada, A., De Angelis, A., Saro, O., & Gasparella, A. (2020, August 31). Design and Evaluation of Extreme Moisture Reference Years for Moisture-Related Risk Assessments. *Building Simulation Applications BSA 2019*. 4th IBPSA-Italy Conference, Bolzano.
- Likos, W. J., Lu, N., & Godt, J. W. (2014). Hysteresis and Uncertainty in Soil Water-Retention Curve Parameters. *Journal of Geotechnical and Geoenvironmental Engineering*, 140(4), 04013050. [https://doi.org/10.1061/\(ASCE\)GT.1943-5606.0001071](https://doi.org/10.1061/(ASCE)GT.1943-5606.0001071)
- Litti, G., Khoshdel, S., Audenaert, A., & Braet, J. (2015). Hygrothermal performance evaluation of traditional brick masonry in historic buildings.

- Energy and Buildings*, 105, 393–411.  
<https://doi.org/10.1016/j.enbuild.2015.07.049>
- Little, J., Ferraro, C., & Arregi, B. (2015). *Historic Environment Scotland Technical Paper 15—Assessing risks in insulation retrofits using hygrothermal software tools*. Historic Environment Scotland.
- Lucchi, E. (2017). Thermal transmittance of historical stone masonries: A comparison among standard, calculated and measured data. *Energy and Buildings*, 151, 393–405. <https://doi.org/10.1016/j.enbuild.2017.07.002>
- Marra, E., Zirkelbach, D., & Künzle, H. M. (2015). Prediction of Steel Corrosion in Porous Building Materials by Means of a New Hygrothermal Model. *Energy Procedia*, 78, 1299–1304.  
<https://doi.org/10.1016/j.egypro.2015.11.144>
- Maxwell, E. L. (1987). *A Quasi-Physical Model for Converting Hourly Global Horizontal to Direct Normal Insolation*. Solar Energy Research Institute.
- Mensinga, P. (2009). *Determining the Critical Degree of Saturation of Brick Using Frost Dilatometry* [Thesis]. University of Waterloo.
- Morelli, M., & Svendsen, S. (2013). Investigation of interior post-insulated masonry walls with wooden beam ends. *Journal of Building Physics*, 36(3), 265–293. <https://doi.org/10.1177/1744259112447928>
- Morris, P. I. (1998). *Understanding Biodeterioration of Wood in Structures*. British Columbia Building Envelope Council.  
<https://cwc.ca/wp-content/uploads/aboutdecay-biodeterioration.pdf>
- Nagy, B. (2019). Designing insulation filled masonry blocks against hygrothermal deterioration. *Engineering Failure Analysis*, 103, 144–157.  
<https://doi.org/10.1016/j.engfailanal.2019.05.005>

- Nagy, B., & Tóth, E. (2016, August 22). *Hygrothermal behaviour of hollow and filled ceramic masonry blocks*. International RILEM Conference on Materials, Systems and Structures in Civil Engineering, Lyngby, Denmark.
- Napp, M., & Kalamees, T. (2015). Energy use and indoor climate of conservation heating, dehumidification and adaptive ventilation for the climate control of a mediaeval church in a cold climate. *Energy and Buildings*, *108*, 61–71. <https://doi.org/10.1016/j.enbuild.2015.08.013>
- Napp, M., Wessberg, M., Kalamees, T., & Broström, T. (2016). Adaptive ventilation for climate control in a medieval church in cold climate. *International Journal of Ventilation*, *15*(1), 1–14. <https://doi.org/10.1080/14733315.2016.1173289>
- Nardi, I., Lucchi, E., de Rubeis, T., & Ambrosini, D. (2018). Quantification of heat energy losses through the building envelope: A state-of-the-art analysis with critical and comprehensive review on infrared thermography. *Building and Environment*, *146*, 190–205. <https://doi.org/10.1016/j.buildenv.2018.09.050>
- National Energy Code of Canada for Buildings 2015*. (2015). National Research Council of Canada.
- Nicolai, A. (2008). *Modeling and Numerical Simulation of Salt Transport and Phase Transitions in Unsaturated Porous Building Materials* [Ph.D Dissertation]. Syracuse University.
- Ojanen, T., Viitanen, H., Peuhkuri, R., Lähdesmäki, K., Vinha, J., & Salminen, K. (2010). Mold Growth Modeling of Building Structures Using Sensitivity Classes of Materials. *Thermal Performance of the Exterior Envelopes of Whole Buildings XI International Conference*, *10*.

- Oligschläger, D., Waldow, S., Haber, A., Zia, W., & Blümich, B. (2015). Moisture dynamics in wall paintings monitored by single-sided NMR. *Magnetic Resonance in Chemistry*, 53(1), 48–57. <https://doi.org/10.1002/mrc.4153>
- OMEGA Engineering. (n.d.). *HFS-3, HFS-4 Thin-Film Heat Flux Sensors*. OMEGA Engineering. <https://assets.omega.com/manuals/M1844.pdf>
- Orr, S. A., Young, M., Stelfox, D., Curran, J., & Viles, H. (2018). Wind-driven rain and future risk to built heritage in the United Kingdom: Novel metrics for characterising rain spells. *Science of The Total Environment*, 640–641, 1098–1111. <https://doi.org/10.1016/j.scitotenv.2018.05.354>
- Pascucci, M., & Lucchi, E. (2016). 2D-Hygrothermal simulation of historical solid walls. *Proceedings International Conference on Computer Aided Architectural Design*. CAADence in Architecture, Budapest, Hungary.
- Patera, A., Derome, D., Griffa, M., & Carmeliet, J. (2013). Hysteresis in swelling and in sorption of wood tissue. *Journal of Structural Biology*, 182(3), 226–234. <https://doi.org/10.1016/j.jsb.2013.03.003>
- Pechinig, R., Mottaghy, D., Koch, A., Jorand, R., & Clauser, C. (2007, June). Prediction of Thermal Properties for Mesozoic Rocks of Southern Germany. *European Geothermal Congress 2007*. European Geothermal Congress 2007, Unterhaching, Germany.
- Perez, R., Ineichen, P., Maxwell, E. L., Seals, R. D., & Zelenka, A. (1992). Dynamic global-to-direct irradiance conversion models. *ASHRAE Transactions*, 98, 354–369.
- Pernetti, R., Prada, A., & Baggio, P. (2013). On the influence of several parameters in energy model calibration: The case of a historical building. *Conference: 1st IBPSA Italy Conference*, 10.
- Phillipson, M. C., Baker, P. H., Davies, M., Ye, Z., McNaughtan, A., Galbraith, G. H., & McLean, R. C. (2007). Moisture measurement in building materials:

An overview of current methods and new approaches. *Building Services Engineering Research and Technology*, 28(4), 303–316.

<https://doi.org/10.1177/0143624407084184>

Plagge, R., Scheffler, G., & Nicolai, A. (2007). Experimental Methods to Derive Hygrothermal Material Functions for Numerical Simulation Tools. *Thermal Performance of the Exterior Envelopes of Whole Buildings X International Conference, Clearwater*.

Pollock, M. D., O'Donnell, G., Quinn, P., Dutton, M., Black, A., Wilkinson, M. E., Colli, M., Stagnaro, M., Lanza, L. G., Lewis, E., Kilsby, C. G., & O'Connell, P. E. (2018). Quantifying and Mitigating Wind-Induced Undercatch in Rainfall Measurements. *Water Resources Research*, 54(6), 3863–3875.

<https://doi.org/10.1029/2017WR022421>

Proietti, N., Calicchia, P., Colao, F., De Simone, S., Di Tullio, V., Luvidi, L., Prestileo, F., Romani, M., & Tatì, A. (2021). Moisture Damage in Ancient Masonry: A Multidisciplinary Approach for In Situ Diagnostics. *Minerals*, 11(4), 406. <https://doi.org/10.3390/min11040406>

Province of Canada. (1861). *Contract, Specifications and Schedule of Prices of Departmental Buildings, Ottawa City, C. W.*

Pulatsu, B., Gonen, S., Erdogmus, E., Lourenço, P. B., Lemos, J. V., & Prakash, R. (2021). In-plane structural performance of dry-joint stone masonry Walls: A spatial and non-spatial stochastic discontinuum analysis.

*Engineering Structures*, 242, 112620.

<https://doi.org/10.1016/j.engstruct.2021.112620>

Pyrack-Nolte, L. J., Myer, L. R., Cook, N. G. W., & Witherspoon, P. A. (1987, January 1). *Hydraulic and mechanical properties of natural fractures in low-permeability rock*. <https://www.osti.gov/servlets/purl/6406367>

- Qiu, X., Haghghat, F., & Kumaran, M. (2003). Moisture Transport Across Interfaces Between Autoclaved Aerated Concrete and Mortar. *Journal of Building Physics*, 26, 213–236. <https://doi.org/10.1177/109719603032804>
- Raftery, P., Keane, M., & Costa, A. (2011). Calibrating whole building energy models: Detailed case study using hourly measured data. *Energy and Buildings*, 43(12), 3666–3679. <https://doi.org/10.1016/j.enbuild.2011.09.039>
- Reginato, L., & Handegord, G. (1990). Procedure for Estimating the Moisture Performance of Building Envelopes. *Proceedings of Fifth Conference on Building Science and Technology*, 123–132.
- RiBuild—Robust internal thermal insulation of historic buildings*. (2020). <https://www.ribuild.eu>
- Ridout, B., & McCaig, I. (2016). *Measuring Moisture Content in Historic Building Materials*. Historic England.
- Roberti, F., Oberegger, U. F., & Gasparella, A. (2015). Calibrating historic building energy models to hourly indoor air and surface temperatures: Methodology and case study. *Energy and Buildings*, 108, 236–243. <https://doi.org/10.1016/j.enbuild.2015.09.010>
- Roels, S., & Carmeliet, J. (2006). Analysis of moisture flow in porous materials using microfocus X-ray radiography. *International Journal of Heat and Mass Transfer*, 49(25–26), 4762–4772. <https://doi.org/10.1016/j.ijheatmasstransfer.2006.06.035>
- Roels, S., Vandersteen, K., & Carmeliet, J. (2003). Measuring and simulating moisture uptake in a fractured porous medium. *Advances in Water Resources*, 26(3), 237–246. [https://doi.org/10.1016/S0309-1708\(02\)00185-9](https://doi.org/10.1016/S0309-1708(02)00185-9)

- Rouchier, S. (2012). *Hygrothermal performance assessment of damaged building materials* [Doctorate, Université de Lyon].  
<https://doi.org/10.13140/rg.2.1.1532.4561>
- Rye, C., & Scott, C. (2012). *The SPAB Research Report 1. U-Value Report*. Society for the Protection of Ancient Buildings.
- Saha, S., Moorthi, S., Wu, X., Wang, J., Nadiga, S., Tripp, P., Behringer, D., Hou, Y.-T., Chuang, H., Iredell, M., Ek, M., Meng, J., Yang, R., Mendez, M. P., van den Dool, H., Zhang, Q., Wang, W., Chen, M., & Becker, E. (2011). *NCEP Climate Forecast System Version 2 (CFSv2) Selected Hourly Time-Series Products*. Research Data Archive at the National Center for Atmospheric Research, Computational and Information Systems Laboratory. <https://doi.org/10.5065/D6N877VB>
- Sahyoun, S., Wang, L., Ge, H., Defo, M., & Lacasse, M. (2020). Durability of Internally Insulated Historical Solid Masonry Under Future Climates: A Stochastic Approach. *XV International Conference on Durability of Building Materials and Components. EBook of Proceedings. XV International Conference on Durability of Building Materials and Components*. <https://doi.org/10.23967/dbmc.2020.044>
- Salonvaara, M. (2010). *ASHRAE RP-1325—Environmental Weather Loads for Hygrothermal Analysis and Design of Buildings*. American Society of Heating, Refrigerating and Air-Conditioning Engineers.
- Salonvaara, M., Karagiozis, A., & Holm, A. (2001). Stochastic Building Envelope Modeling—The Influence of Material Properties. *Buildings VIII Proceedings*, 8.
- Scheffler, G., Grunewald, J., & Häupl, P. (2004). Calibration of an engineering model of hygrothermal material characterisation. *Council for Research and Innovation in Building and Construction W40 Meeting*.

- Schroeter, H. (2007). *Meteorological Data Missing-Value Fill-in Study for Ontario* [Memo]. Schroeter & Associates.
- Sedlbauer, K. (2001). *Prediction of mould fungus formation on the surface of and inside building components*. Fraunhofer Institute for Building Physics.
- SMT Research. (n.d.). *Embedded Moisture sensor Product Datasheet*. Structural Monitoring Technology. [http://docs.smtresearch.ca/EMS\\_Datasheet.pdf](http://docs.smtresearch.ca/EMS_Datasheet.pdf)
- Smyl, D., Hallaji, M., Seppänen, A., & Pour-Ghaz, M. (2016). Three dimensional electrical imaging of moisture ingress in mortar. *American Concrete Institute, ACI Special Publication, 2016-January, 27–48*. [www.scopus.com](http://www.scopus.com)
- Sontag, L., Nicolai, A., & Vogelsang, S. (2013). *Validierung der Solverimplementierung des hygrothermischen Simulationsprogramms Delphin*. Institut für Bauklimatik, Technische Universität Dresden.
- Soulios, V., Jan de Place Hansen, E., & Peuhkuri, R. (2021). Hygrothermal performance of hydrophobized and internally insulated masonry walls— Simulating the impact of hydrophobization based on experimental results. *Building and Environment, 187*, 107410. <https://doi.org/10.1016/j.buildenv.2020.107410>
- Standards and Guidelines for the Conservation of Historic Places in Canada* (Second Edition). (2010). Canada's Historic Places.
- Straube, J., & Burnett, E. (2000). Simplified prediction of driving rain deposition. *Proceedings of the International Building Physics Conference, 375–382*.
- Straube, J., & Burnett, E. (2001). Overview of Hygrothermal (HAM) Analysis Methods. In *Moisture Analysis and Condensation Control in Building Envelopes* (pp. 81–89). American Society for Testing and Materials.
- Straube, J., Ueno, K., & Schumacher, C. (2011). *Internal Insulation of Masonry Walls: Final Measure Guideline* (Building America Report-1105). Building Science Corporation.

- Structural Commentaries (User's Guide – NBC 2015: Part 4 of Division B)*.  
(2017). National Research Council of Canada.
- TenWolde, A. (1985). Steady-State One-Dimensional Water Vapour Movement by Diffusion and Convection in a Multi-layer Wall. *ASHRAE Transactions*, 91(1), 322–342.
- Thomson, D. J., Zhao, J., & Murison, E. R. (2013). *Calibration of capacitance sensors for use in wireless data logging systems for moisture measurement in building stones*. ISIS Canada Resource Centre, University of Manitoba.
- Trechsel, H. R. (2001). *Moisture Analysis and Condensation Control in Building Envelopes*. American Society for Testing and Materials.
- Urbandale Centre for Home Energy Research. (2017). Carleton University.  
<https://carleton.ca/bprc/people/cher-house/>
- Vaisala. (2011). *Vaisala INTERCAP® Humidity and Temperature Probe HMP60 Technical Data*. Vaisala.
- van Genuchten, Martinus. Th. (1980). A Closed-form Equation for Predicting the Hydraulic Conductivity of Unsaturated Soils<sup>1</sup>. *Soil Science Society of America Journal*, 44(5), 892.  
<https://doi.org/10.2136/sssaj1980.03615995004400050002x>
- van Schijndel, J., Goesten, S., & Schellen, H. L. (2016, October 12). HAMSTAD Benchmarks using Comsol revisited. *Excerpt from the Proceedings of the 2016 COMSOL Conference in Munich*.
- Vandemeulebroucke, I., Caluwaerts, S., & Bossche, N. (2020). Freeze-Thaw Risk in Solid Masonry: Are 'Hygrothermal Response Based' Analyses Mandatory when Studying the Sensitivity of Building Envelopes to Climate Change? *XV International Conference on Durability of Building Materials and Components. EBook of Proceedings*. XV International Conference on

Durability of Building Materials and Components.

<https://doi.org/10.23967/dbmc.2020.070>

Vereecken, E., & Roels, S. (2013). Hygric performance of a massive masonry wall: How do the mortar joints influence the moisture flux? *Construction and Building Materials*, 41, 697–707.

<https://doi.org/10.1016/j.conbuildmat.2012.12.024>

Vereecken, E., & Roels, S. (2021). Hygrothermal performance of internally insulated masonry walls with embedded wooden beam heads: A field study on the impact of hydrophobisation. *Journal of Physics: Conference Series*, 2069(1), 012019. <https://doi.org/10.1088/1742-6596/2069/1/012019>

Vereecken, E., Van Gelder, L., Janssen, H., & Roels, S. (2015). Interior insulation for wall retrofitting – A probabilistic analysis of energy savings and hygrothermal risks. *Energy and Buildings*, 89, 231–244.

<https://doi.org/10.1016/j.enbuild.2014.12.031>

Vogelsang, S., Fechner, H., & Nicolai, A. (2018). *Delphin 6 Material File Specification, Version 6.0*. Institut für Bauklimatik.

Walker, R., Pavía, S., & Dalton, M. (2016). Measurement of moisture content in solid brick walls using timber dowel. *Materials and Structures*, 49(7), 2549–2561. <https://doi.org/10.1617/s11527-015-0667-6>

Webb, A. L. (2017). Energy retrofits in historic and traditional buildings: A review of problems and methods. *Renewable and Sustainable Energy Reviews*, 77, 748–759. <https://doi.org/10.1016/j.rser.2017.01.145>

Weritz, F., Kruschwitz, S., Maierhofer, C., & Wendrich, A. (2009). Assessment of Moisture and Salt Contents in Brick Masonry with Microwave Transmission, Spectral-Induced Polarization, and Laser-Induced

- Breakdown Spectroscopy. *International Journal of Architectural Heritage*, 3(2), 126–144. <https://doi.org/10.1080/15583050802278992>
- Wetter, M. (2016). *GenOpt—Generic Optimization Program (3.1.1)* [Computer software]. Lawrence Berkeley National Laboratory. <https://simulationresearch.lbl.gov/GO/>
- WINDOW (7.3). (2015). [Computer software]. Lawrence Berkeley National Laboratory. <https://windows.lbl.gov/>
- Zhao, J., Plagge, R., Nicolai, A., Grunewald, J., & Zhang, J. S. (2011). Stochastic study of hygrothermal performance of a wall assembly—The influence of material properties and boundary coefficients. *HVAC&R Research*, 17(4), 591–601. <https://doi.org/10.1080/10789669.2011.585421>
- Zhou, X., Derome, D., & Carmeliet, J. (2016). Robust moisture reference year methodology for hygrothermal simulations. *Building and Environment*, 110, 23–35. <https://doi.org/10.1016/j.buildenv.2016.09.021>
- Zhou, X., Derome, D., & Carmeliet, J. (2017). Hygrothermal modeling and evaluation of freeze-thaw damage risk of masonry walls retrofitted with internal insulation. *Building and Environment*, 125, 285–298. <https://doi.org/10.1016/j.buildenv.2017.08.001>
- Zhou, X., Desmarais, G., Vontobel, P., Carmeliet, J., & Derome, D. (2018). Water uptake in masonry: Effect of brick/mortar interface. *7th International Building Physics Conference Proceedings*, 103–108.
- Zhou, X., Desmarais, G., Vontobel, P., Carmeliet, J., & Derome, D. (2020). Masonry brick–cement mortar interface resistance to water transport determined with neutron radiography and numerical modeling. *Journal of Building Physics*, 44(3), 251–271. <https://doi.org/10.1177/1744259120908967>

Zimmerman, R. W., & Bodvarsson, G. S. (1994). *Hydraulic Conductivity of Rock Fractures*. Lawrence Berkley Laboratory.